Application of a mass balance partitioning model of Ra-226, Pb-210 and Po-210 to freshwater lakes and streams

Submitted by: Kevin John Britton

Thesis submitted to the
Faculty of Graduate and Postdoctoral Studies
in partial fulfillment of the requirements for the
Master of Science degree specialization in Chemical and Environmental Toxicology
(Earth Sciences)

Department of Earth Sciences

Faculty of Science

University of Ottawa

Supervisors:

Robert Jack Cornett[†] (Department of Earth Sciences)

Ian D Clark (Department of Earth Sciences)

Co-Supervisors:

Trevor J Stocki (Department of Earth Sciences)

Adrienne LM Ethier (Department of Earth Sciences)

Thesis Committee:

Clément Bataille

Laurel Sinclair

2018 November 15

Abstract

The objectives of this thesis were: (1) to develop a mass balance partitioning model of the natural uranium-238 series comprising radium-226, lead-210 and polonium-210 and (2) to apply the model to estimate the source and fate of these radionuclides in freshwater lakes and streams. Samples were collected from Ottawa River watershed tributaries and measured for lead-210 and polonium-210 content to determine the water concentrations that were input to the model.

The radium-226 partitioning model was developed by reconstructing and analyzing Quantitative Water, Air, Sediment Interaction (QWASI) models of lead for Lake Ontario and Hamilton Harbour and selecting parameters for an updated QWASI model of lead for a Lake Ontario basin. This study gave insight about model basis definition, and partition coefficient and sediment particle constraint. The radium-226 series model was formulated by connecting separate QWASI modules for radium-226, lead-210 and polonium-210 with decay and ingrowth terms. The radium-226 model was applied to studies of Crystal Lake, Wisconsin; Bickford Pond, Massachusetts; and Clinton River, Michigan, using parameters reported in these and other studies. Model error was evident in the applications to Crystal Lake due to underlying lake heterogeneity, to Bickford Pond due to unidentified sources of lead-210 from sediment diffusion or watershed runoff, and to Clinton River from watershed runoff.

The model was applied to seven Laurentian Shield lakes in the Ottawa River watershed using the sample measurements as the basis for water concentration inputs. The application showed that hydrologic flushing rate may be a factor in the proportion of watershed atmospheric deposition and overall Pb-210 input to the water. Laurentian Shield Lakes with the lowest hydrologic flushing rates ($<3\ a^{-1}$) had proportions of Pb-210 losses to sediment greater than 85%. In another application to Judge Sissons Lake, Nunavut, the model indicated that the watershed was the source of about 85% of Pb-210 and 98% of Po-210 input to the water, and that a significant geologic component of Pb-210 input to the lake was likely. The model indicated that most of the Pb-210 in Judge Sissons Lake was lost to outflow, and that most of the Po-210 was lost to sediment.

The model showed that sedimentation is a better proxy measurement for atmospheric deposition of Pb-210 to the Laurentian lakes than originally estimated. The model also showed that watershed contributions to Judge Sissons Lake could explain the observed background concentrations of Pb-210 and Po-210.

Acknowledgements

I would like to acknowledge and thank Adrienne Ethier and Canadian Nuclear Laboratories (CNL) for initiating this research into adaptation of the HERMES model to uranium series radionuclides. Adrienne provided the original HERMES model, hosted me in the Environmental Protection Branch at CNL, and assisted with manuscript review. I would also like to thank Marilyne Stuart for assuming the role as CNL liaison.

I would like to thank Diane Martens at AREVA (Orano) Resources Canada for providing the Kiggavik study data reports.

I am most grateful to Jack Cornett at the University of Ottawa who enabled this thesis. I was fortunate for the time he shared with me. He is missed by many students. I would like to thank the staff and students of A. E. Lalonde Laboratory, particularly Barbara Francisco, Soroush Fard and Cole MacDonald.

I would like to acknowledge and thank Trevor Stocki at Health Canada. Trevor assumed the role of supervisor after Jack. He gave many detailed reviews during manuscript writing. I would like to express special thanks to Ian Clark for bridging the gap at the University of Ottawa as official supervisor in these final months. Both made completion of this project possible.

I would like to acknowledge and thank Jack Cornett and Canadian Nuclear Laboratories for funding this project.

Statement of Originality

Chapter 2

I studied the QWASI aquivalence model for lead in Lake Ontario and Hamilton Harbour developed by Dr. Donald Mackay *et al* to identify challenges to the planned extension to the Ra-226 series nuclides. I expected that the QWASI aquivalence model applications would be internally and mutually consistent. I studied the model partly by verifying and adapting the HERMES mercury model developed by Dr. Adrienne Ethier *et al*. to the QWASI lead formulation. I reproduced QWASI aquivalence model applications and confirmed the sources for the parameters cited. I found no unexpected inconsistencies among the QWASI aquivalence model applications, but two of the three did not constrain particle flux for molar conservation. Further, I found that input and output concentrations were not consistent, which I addressed with a modification of the basic QWASI aquivalence model to differentiate between diffusion from water to sediment and from sediment to water. I implemented the diffusion modification and particle conservation constraint to the existing applications. I applied the updated model of lead in Lake Ontario using some parameters from a rate constant study, and to a Lake Ontario basin using a combination of parameters representing a new application.

Chapter 3

The updated QWASI aquivalence model was applicable to lead but needed to be further developed for the Ra-226 series, and a method was required to fit parameters for specific applications. I expected that the model would be applicable to Pb-210 using many of the existing parameters and could be extended to Ra-226 and Po-210 by selection of appropriate parameters from existing studies and the literature. I expected that the separate modules could be connected by terms for decay and ingrowth. I developed the Ra-226 model by linking the updated QWASI modules with terms for loss and ingrowth by decay for Ra-226, Pb-210 and Po-210. I assigned parameters to this model from previously published studies of Crystal Lake, Wisconsin; Bickford Pond, Massachusetts; and Clinton River, Michigan; and other sources, and adjusted the parameters in an optimization process developed from the Chapter 2 study. The results indicated that the model was extendable to each of the selected Ra-226 nuclides, and that modules could be linked to account for radioactive decay and ingrowth. The developed method was effective in adjusting parameters to the data in the original studies. Comparison of the Ra-226 model to the original dynamic study models revealed discrepancies, attributed either to the original models missing episodic events, and / or to the inability of the steady-state Ra-226 model to represent the effects of parameter variation by single expected values.

Chapter 4

Two hypotheses were investigated in Chapter 4 with the Ra-226 series model developed in Chapter 3. The first question was whether the sedimentation

proportion of Pb-210 losses from the water in a set of Laurentian lakes was as low as estimated in a previous study **(CORNETT, 1984)**. The second question was whether water and sediment measurements of Judge Sissons Lake at the proposed Nunavut mine site **(GUERIN, 2012)** indicated a watershed contribution to Pb-210 and Po-210 concentrations. I augmented the Laurentian lakes study data with measurements of water from local streams. I selected sample locations, collected samples and with Soroush Fard I performed wet chemistry operations in the A. E. Lalonde actinide laboratory at the University of Ottawa under the direction of Dr. Robert Cornett. Dr. Cornett performed the alpha spectrometry measurements and Cole MacDonald and Dr. Barbara Francisco performed the Inductively-Coupled Plasma Source Mass Spectrometry (ICP-MS) measurements. I applied the Ra-226 model to the original studies using data from these and other sources. I used the Ra-226 model to estimate lake process rates in the original studies. The sedimentation rates in the Laurentian lakes were concluded to be higher than originally estimated: above 85% in five of the seven lakes. I concluded that the watershed was the source of most of the Pb-210 and Po-210 in Judge Sissons Lake water and sediment, and further that a significant proportion from the watershed may originate in the ground.

Contents

TABLES

FIGURES

APPENDIX TABLES

APPENDIX FIGURES

Abbreviations

CIC	Constant Initial Concentration
CRS	Constant Rate of Supply
DI	De-Ionized
HERMES	Hg Environmental Ratios Multimedia Ecosystem Sources
ICP-MS	Inductively-Coupled Plasma Source Mass Spectrometry
NORM	Naturally Occurring Radioactive Material
PAN	PolyAcrylNitrile
PCB	PolyChlorinated Biphenyl
QWASI	Quantitative Water, Air, Sediment Interaction
SPM	Suspended Particulate Matter
TENORM	Technologically Enhanced Naturally Occurring Radioactive Material

A list of symbols is found in Appendix L.

1 Introduction

Naturally occurring radioactive material (NORM) occurs in all media and includes radionuclides of the U-238 decay series **(RPB, 2011)**. Natural uranium is 99.3% U-238 **(MEIJA, 2016)**. Uranium occurs in a variety of igneous, metamorphic and sedimentary rock, and at concentrations greater than 1 ppm in phosphate minerals, shale, granite, and coal **(IAEA, 2003)**. The earth's crust contains about 2.7 ppm uranium on average **(RUDNICK, 2014)**, corresponding to a U-238 concentration of 33 Bq/kg in secular (long-term) equilibrium with the nuclides of its decay series in unweathered rocks **(IAEA, 2017)**. As such, uranium ores contain about 0.5 g of Ra-226 and 0.1 mg of Po-210 per ton of U-238 **(BAGNALL, 1962)**. Radionuclides of the U-238 series can become concentrated by industrial extraction and processing of uranium ore, metals, fossil fuels, phosphates and rare earths **(IAEA, 2003)** as Technologically Enhanced NORM (TENORM) **(RPB, 2011)**. Radium is identified as a significant industrial pollutant in soil and water **(IAEA, 1990)**.

This thesis concerns the transport of Ra-226, Pb-210 and Po-210 in dissolved, SPM and sediment phases into, through and out of freshwater bodies. A partitioning mass balance model was adapted and applied to account for inputs from the atmosphere and watershed of lakes and streams to water outflow and sediment. Partitioning is the process by which a molecule or element changes phase among gas, liquid and solid. The original partitioning model had been applied to the base metal lead. Those parameters and applications were considered for relevance to the isotope Pb-210. The model was extended further to the semimetal polonium represented by Po-210, and to the alkaline earth radium represented by Ra-226. The three modules were linked by terms representing radioactive decay and ingrowth.

1.1 RA-226 SERIES

The Ra-226 series, neglecting intermediate products of Rn-222 having half-lives less than one day represented by "⇒", is **(IAEA, 2017)**:

$$^{226}Ra \xrightarrow{1602a} {}^{222}Rn \overset{3.82d}{\Longrightarrow} {}^{210}Pb \xrightarrow{22.2a} {}^{210}Bi \xrightarrow{5.01d} {}^{210}Po \xrightarrow{138d} {}^{206}Pb \qquad (1)$$

Several processes can separate the nuclides of the Ra-226 series and create conditions of disequilibria (unequal rates of radioactive decay), among them: migration of Rn-222 (a noble gas) into water and vapour phases, solid phase adsorption, and biota uptake **(IAEA, 2017)**.

Bi-210 reaches equilibrium with Pb-210 over a much shorter interval than Po-210, so that a disequilibrium resulting from a deficit of Bi-210 has little effect on the evolution of Po-210 **(IAEA, 2017)**. Bi-210 is disregarded in this thesis.

The exhalation of Rn-222 from soil results in a deficiency of Pb-210 relative to Ra-226. Atmospheric deposition of Pb-210 creates excess in oceans, from which the exhalation rate of Rn-222 is orders of magnitude lower **(IAEA, 2017)**. The

mean residence time of air masses in the troposphere (the lowest several kilometers of the atmosphere where weather occurs) is about 20 days, resulting in secular equilibrium of the intermediate products of Rn-222 decaying to Pb-210 **(BURTON, 1960)**. In the atmosphere, these nuclides become associated with aerosols that are subject to removal primarily by scavenging wet deposition and rain washout, and secondarily by dry deposition **(IAEA, 2017)**. Rn-222 is disregarded in this thesis.

Knowledge of the behavior of Pb-210 is needed to assess its significance in the effluent from uranium mine tailings **(CORNETT, 1984)**. The transport of nuclides in freshwater systems is influenced by sorption onto solids. Contaminant loading to a lake from discharges due to industrial activity can be moderated by suspended particulate matter (SPM) sorption and extended by desorption and diffusion from sediment **(MCKEE, 1987)**. Mine effluent and other industrial sources can increase the concentration of Po-210, which is a significant natural source of human ingestion doses and of total dose among certain populations and species **(UNSCEAR, 2000)**[1].

Pb-210 is often used to establish chronologies in lake sediments **(CORNETT, 1984)**. The literature is lacking studies of both Pb-210 and Po-210 in the phases of a freshwater system: dissolved, colloidal, suspended particulate, settling particulate, sediment and porewater **(CHAI, 2004)**. Knowledge of the distribution of Pb-210 and Po-210 in freshwater systems is sparse relative to the ocean **(MUDBIDRE, 2014)**. This study can contribute to that knowledge.

1.2 PB-210 TRACER

Pb-210 is an established geochronological sediment tracer. Although it is natural and ubiquitous, the experimenter must determine the rate of supply. Pb-210 is used first in studies of Greenland snow accumulation **(GOLDBERG, 1963)** and subsequently of freshwater sedimentation **(KRISHNASWAMY, 1971)**. These studies assume that the Pb-210 inputs are entirely atmospheric and constant.

The source of Great Lakes Pb-210 in sediment is discerned between the atmosphere and lateral redistribution only by extensive measurements over the sediment area **(ROBBINS, 1975)**. Atmospheric and terrigenous sources of Pb-210 for dating are also confounded by source regional variability, aquatic residence time, sedimentation processes and compaction **(EDGINGTON, 1976)**. The sediment dating method can account for changing rates of Pb-210 accumulation over time with a constant initial concentration (CIC) model, or with a constant rate of supply (CRS) of model if the rate of sedimentation over time can be estimated **(APPLEBY, 1978)(CORNETT, 1992)**. Any given lake will fall somewhere between the models, depending on the total pool of lake water Pb-210, partitioning of Pb-210 between

[1] Annex B

dissolved and SPM-adsorbed forms, bulk sedimentation rate, and hydrologic flushing rate **(BINFORD, 1990)**.

The study of Pb-210 sedimentation is relevant to sediment dating and sedimentation rate studies, and to assimilation of other contaminants. A known, constant supply of atmospheric Pb-210 is assumed to determine Pb, Zn, As, and Cd accumulation in Adirondack region lake sediments **(KADA, 1992)**. Watershed contribution is controlled in a Belgian study by measuring sediment from standing ponds **(PETIT, 1984)**.

There are lakes for which neither the water residence time nor the ratio of watershed to lake area are related to the sediment lead concentration. In these cases the only source of lead to the lake surface is the atmosphere **(DILLON, 1982)**. Conversely in the study of Pb-210 in Laurentian lakes sediment, a significant portion of the total inputs are concluded to be lost to outflow. The most important factor in the calculation of atmospheric deposition sediment measurements is the sedimentation proportion **(CORNETT, 1984)**. A study of 51 North American lakes confirms that the hydrologic flushing rate is a significant factor in the initial (sediment deposition) concentration of Pb-210. This initial concentration is a key parameter in Pb-210 sedimentation models. A divergence between correlation of initial concentration with water residence time and no correlation is shown at a water residence time of about 2 years. At the lower water residence times where the correlation exists, the CIC model may be better because sedimentation efficiency is limited. For residence times longer than 2 years, and more likely in seepage than drainage lakes, the CRS model may better reflect complete sedimentation. The significance of the hydrologic flushing rate, and other factors including sediment mixing, acidification, resuspension and diffusion differ among lakes **(BINFORD, 1993)**.

Estimation of atmospheric deposition of Pb-210 by freshwater sedimentation has advantages over precipitation sample collection. Although precipitation is the primary atmospheric removal mechanism, measurement of collected samples is challenged by seasons, wind direction, and local variation. Where measurements involve stable lead, dry collectors are also required, particularly near urban areas. Stable lead and Pb-210 measurements of freshwater samples can have significant uncertainty that is not associated with sediment samples **(EVANS, 1986)**.

1.3 STUDY LAKES

Lakes and streams were selected for Ra-226 model application based on criteria to achieve two objectives. The Chapter 3 lakes were considered suitable to test the adapted QWASI aquivalence model and parameter fitting method. Crystal Lake, Wisconsin is without tributaries or outflow, limiting the main processes controlling lake concentrations of the Ra-226 series to atmospheric deposition, sedimentation, and perhaps groundwater seepage or watershed runoff. Studies provide detailed measurements of Pb-210 and Po-210 in the water and adsorbed to SPM, and of

atmospheric deposition and sedimentation of Pb-210. **(TALBOT, 1983)(TALBOT, 1984)**, Bickford Pond, Massachusetts is a lake similar to Crystal Lake in area and depth but has tributaries and outflow. Studies report measurements very similar to Crystal Lake **(BENOIT, 1987)(BENOIT, 1990)**. Both Crystal Lake and Bickford Pond studies include detailed dynamic models that availed comparison with the Ra-226 model. A study of Clinton River, Michigan reports measurements of Pb-210 and Po-210 in the water and adsorbed to SPM from samples taken along several kilometers of its course. The study provided a contrast to Crystal Lake since it was dominated by inflow and outflow **(MUDBIDRE, 2014)**.

The updated partitioning model was applied to the Laurentian lakes study of seven lakes in the Ottawa River watershed. In the original study, lake sediment is measured to estimate sedimentation rates, and soil is measured to estimate atmospheric deposition rates. A constant proportion of atmospheric deposition to each watershed area is assumed as the component of runoff to the lakes. Random samples from 25 locations at each lake establish that there is little focusing (redistribution after sedimentation). Pb-210 sedimentation rates, lake area and depth, watershed area, and estimated flow rate are reported for each lake **(CORNETT, 1984)**. The Ra-226 model was applied to this data, and to Pb-210 and Po-210 concentrations derived from measurements of samples from nearby lakes. The application was used to review the study finding that significant proportions of the Pb-210 inputs are lost to outflow. The result is relevant to studies that use Pb-210 as a tracer to determine the historical flux of contaminants to surface waters.

The partitioning model was applied to the Kiggavik site in Nunavut. The site is subject to an extensive study that supported an application for approval of a uranium mine in 2012. Four open pit and one subterranean mine had been proposed at locations about 80 km wet of Baker Lake. The studies report measurements of water and sediment samples from a network of lakes and streams in the watersheds of the proposed mine sites. Regional air concentrations are reported **(GUERIN, 2012)**. The Ra-226 model was applied to Judge Sissons Lake, the largest in the Kiggavik drainage region (96 km^2 area). The application was used to determine the watershed proportion of Pb-210 and Po-210 inputs. The result is relevant to understanding transport of the Ra-226 series in a watershed under natural conditions that contains locations which may be developed by the mining industry.

1.4 PARTITIONING MODEL

The fugacity concept is a simplification of gas behavior under ideal conditions **(LEWIS, 1901)**. Fugacity measures the escaping tendency from a phase, and was applied to chemical processing **(MACKAY, 1982)** and is used to evaluate equations of state in the laboratory. It is an alternative to chemical potential for quantifying the transport of partitioning pollutants where concentration data are available in several phases **(MACKAY, 1979)**.

Motivated by measurements of mercury in a river, the fugacity approach is developed as the Quantitative Water, Air, Sediment Interaction (QWASI) model **(MACKAY, 1983)**. QWASI is adapted for lead as a non-volatile species in Lake Ontario by reformulating the model using an equivalent aqueous ("aquivalent") basis instead of fugacity and neglecting the vapour phase **(MACKAY, 1989)**. The aquivalent form is applied to a controlled study of lake enclosures spiked with radioisotope tracers to investigate water-sediment transfer dynamics **(DIAMOND, 1990)**. A QWASI aquivalence calibration is developed for lead at Hamilton Harbour in Lake Ontario **(LING, 1993)(DIAMOND, 1996)**.

An aquivalence model is extended to interconverting chemical species **(DIAMOND, 1992)** and formulated as an extension of the QWASI aquivalence model for three chemical forms of mercury using proportions of measured media concentrations **(DIAMOND, 1999)**. An innovation of the aquivalence interconversion model is to introduce a single key species and define other species by a "multiplier", enabled in those phases where relative concentrations are constant **(TOOSE, 2004)**. The QWASI aquivalence mercury model is applied to Big Dam West, Nova Scotia using the "multiplier" method as Hg Environmental Ratios Multimedia Ecosystem Sources (HERMES) **(ETHIER, 2008)(ETHIER, 2009)**. The HERMES model is further developed as a research tool by calibrating it to predict of mercury concentrations in Lake Ontario water and sediment **(ETHIER, 2012)**.

QWASI aquivalence applications to Lake Ontario that vary under limited hydrogeologic conditions were reproduced and analyzed. An updated model was developed comprising modules for Ra-226, Pb-210 and Po-210.

The QWASI model represents equilibrium conditions **(MACKAY, 1983)** formulated at steady-state (unchanging with time) **(MACKAY, 2001)**. The equilibrium condition is a result of the formulation of flow processes for only the water medium in a steady-state model. Equilibrium is defined by phase concentrations that correspond to fixed distribution (partition) coefficients. The QWASI model uses solid to liquid distribution coefficients, one for sediment (K_d) and another for SPM (K_p) **(MACKAY, 1983)**. In the original QWASI aquivalence application, the distribution coefficients are inputs **(MACKAY, 1989)**, but they could also be calculated from concentrations.

The QWASI model is designed to predict water and sediment concentrations from parameters and processes of specific lakes and streams **(MACKAY, 1983)**. Each Ra-226 model application in this thesis comprised a unique combination of parameter inputs that included in some cases concentrations. Priority in input selection was given to available data the subject study. Judgement was applied to select values from other studies and the literature review where specific study values were not available. Parameter sources and adjustments are documented to describe how the model was fit for each application.

A characteristic of temperate lakes is spatial and temporal variation in concentration are driven by changes in process rates, much of which is associated with annual cycles. The concentrations and process variables assumed or

calculated from study data or otherwise from the literature were intended to represent these ranges with single values. Taken together, these assumed "expected values" (average or median) are unlikely to represent any instantaneous condition. This discrepancy is a source of error beyond the scope of this thesis and is a limitation of the model. Error is considered further in Chapter 2.

1.5 THESIS OUTLINE

This work is significant because it demonstrates development and application of a versatile partitioning mass balance model to provide insight to separate questions pertaining to sedimentation and watershed input of the key Ra-226 series.

Thesis elements were developed in three chapters in a paper-based format. The conclusion is presented in Chapter 5.

1.5.1 LEAD PARTITIONING MODEL

In Chapter 2 the study of the QWASI aquivalence multimedia partitioning model of lead in lakes is presented. The original QWASI aquivalence application to Lake Ontario and subsequent applications to Hamilton Harbour **(LING, 1993)(DIAMOND, 1996)** were reproduced, analyzed and updated. The updated model was applied to a related rate constant model of Lake Ontario **(THOMPSON, 1999)** and to a Lake Ontario basin in a new scenario. The model updates and constraints were analyzed, and significant processes were identified in preparation for development of the Ra-226 model.

1.5.2 RADIUM SERIES MODEL

In Chapter 3 the development of the Ra-226 model is presented. Chapter 3 details the extension of the updated lead model to Pb-210, and in separate modules to Ra-226 and Po-210 connected by decay and ingrowth terms. The Ra-226 model was applied to studies of the temperate Crystal Lake **(TALBOT, 1984)**, Bickford Pond **(BENOIT, 1987)** and Clinton River **(MUDBIDRE, 2014)**. The method for selection and adjustment of parameters was developed and documented. Potential sources of error and dominant processes for each application were identified.

1.5.3 RADIUM SERIES IN FRESHWATER

In Chapter 4 the Ra-226 model developed in Chapter 3 was applied to investigate two hypotheses:

1. The proportions of Pb-210 input lost to the sediment of the Laurentian study lakes are as determined in the original study **(CORNETT, 1984)**.

2. The watershed contributes to Pb-210 and Po-210 in the water and sediment of Judge Sissons Lake **(GUERIN, 2012)**.

2 Lead partitioning model

2.1 INTRODUCTION

QWASI is motivated by an interest in the recovery time (the time to return to natural conditions) for areas which have been contaminated by past emissions and are now experiencing concentration reductions due to transport, reaction or burial in sediments **(MACKAY, 1983)**. The aquivalence version of QWASI is demonstrated with lead to describe the processes of water and particle advection, wet and dry deposition, rainfall, sediment diffusion, and particle deposition, resuspension and burial **(MACKAY, 1989)**. Fugacity models can be customized by media and process for particular applications **(MACKAY, 2001)**.

The goal of Chapter 2 was to identify challenges to the planned development of the QWASI aquivalence model for the Ra-226 series. The expectation was to find that the applications, as objectives, were correct and mutually consistent.

The original QWASI aquivalence model and a variant that layered the water medium were reproduced and applications of them studied. The original QWASI aquivalence application to polychlorinated biphenyl (PCB) and lead in Lake Ontario demonstrates capability to represent volatile chemical and heavy metal species **(MACKAY, 1989)**. Two studies report intermediate parameters that provide model insight: the original QWASI aquivalence application **(MACKAY, 1989)**, and a study of Hamilton Harbour using a two-compartment QWASI aquivalence variant **(LING, 1993)**. A second Hamilton Harbour study updates the original with revised input assumptions **(DIAMOND, 1996)**.

The QWASI aquivalence lead model was updated with a modification and new constraints were introduced for the applications. The updated QWASI aquivalence lead model was applied to another study of Lake Ontario lead (that uses a similar process rate constant model with common inputs) **(THOMPSON, 1999)** and to a new scenario representing the Lake Ontario Mississauga Basin.

The geochemistry of lead in Lake Ontario is complicated by large and variable industrial, municipal and natural inputs, and by intensified and temporally variable interactions with sediments and biota **(COALE, 1989)**. This variable component of model error was considered further in section 2.1.3.

2.1.1 THE AQUIVALENCE MODEL

QWASI is formulated from fugacity **(MACKAY, 1983)**. Fugacity is defined by making four assumptions **(LEWIS, 1901)**:

- a closed system (1st Law of Thermodynamics)
- reversible phase changes (2nd Law of Thermodynamics)
- the Ideal Gas Law equation of state
- an internal energy datum (Gibbs free energy)

Fugacity capacity is formulated separately for gas, liquid and solid phases. QWASI models use fugacity as the controlling variable instead of concentration, defined with the conjugate fugacity capacity as **(MACKAY, 1989)**:

$$C = \text{f}Z \tag{2}$$

where

C = concentration [$M \cdot L^{-3}$]

f = fugacity [$M \cdot L^{-1} \cdot T^{-2}$]

Z = fugacity capacity [$T^2 \cdot L^{-2}$]

The ideal gas law equation of state, $PV = nRT$, is derived from kinetic theory by disregarding molecular interactions. For an ideal gas, vapour pressure $P \rightarrow f$, and the fugacity capacity of the gas phase Z_A is a function of temperature:

$$\frac{n}{PV} = \frac{1}{RT} \tag{3}$$

$$Z_A = \frac{C_A}{f} = \frac{1}{RT} \tag{4}$$

where

P = pressure [$M \cdot L \cdot T^{-2}$]

V = volume [L^3]

n = mols [N]

R = ideal gas law constant [$M \cdot L^2 \cdot N^{-1} \cdot T^{-2} \cdot \theta^{-1}$]

T = temperature [θ]

For a liquid phase with a solute sufficiently dilute at equilibrium that chemical interaction can be neglected, Henry's Law is an expression equivalent to the fugacity capacity of the liquid phase Z_W:

$$H = \frac{P_V}{S} \tag{5}$$

$$Z_W = \frac{C_W}{f} = \frac{S}{P_V} = \frac{1}{H} \tag{6}$$

where

H = Henry's law (mass) solubility constant [$L^2 \cdot T^{-2}$]

S = chemical solubility [$M \cdot L^{-3}$]

P_V = liquid vapour pressure [$M \cdot L^{-1} \cdot T^{-2}$]

The fugacity capacity of the solid phase is expressed by the linear sorption isotherm definition (that assumes a constant concentration ratio between solid and aqueous phases) for the sediment distribution (partition) coefficient K_d:

$$K_d = \frac{C_S}{C_W \rho_S} \tag{7}$$

$$Z_S = \frac{C_S}{f} = \frac{C_W K_d \rho_S}{f} = \frac{S K_d \rho_S}{P_V} \tag{8}$$

where

ρ_S = sediment density [M·L^{-3}]

The fugacity capacity is characteristic of the chemical species, medium, and temperature. The fugacity formulation is not feasible for metals, organometals, ionic compounds and some organics that have a low or unknown liquid vapour pressure P_V, since it leads to arbitrarily large water and solid fugacity capacities. Chemical solubility S may be unknown or uncertain as well. These situations can be overcome by factoring out P_V and S from the fugacity capacities and neglecting the air vapour phase. This is the key feature of the QWASI aquivalence models. By this factoring, instead of the fugacity capacity, a dimensionless *aquivalence capacity*, $\mathbb{Z}$, having a unit value for the liquid phase, and aquivalence, $\mathbb{A}$, having concentration units. Table 1 summarizes the fugacity and aquivalence formulations and dimensions **(MACKAY, 1989)**.

Table 1. Fugacity and aquivalence formulations and dimensions

Quantity	Unit	Symbol	Air	Water	Solid
Fugacity capacity	$\frac{T^2}{L^2}$	Z	$\frac{1}{RT}$	$\frac{S}{P_V}$	$\frac{SK_d\rho_S}{P_V}$
Fugacity	$\frac{M}{LT^2}$	f	$C_A(RT)$	$C_W\frac{P_V}{S}$	$C_S\frac{P_V}{SK_d\rho_S}$
Aquivalence capacity	-	$\mathbb{Z}$	$\frac{P_V}{S(RT)}$	1	$K_d\rho_S$
Aquivalence	$\frac{M}{L^3}$	$\mathbb{A}$	$C_A(RT)\frac{S}{P_V}$	C_W	$\frac{C_S}{K_d\rho_S}$

Aquivalence capacity expressions are further defined for particle / water partitioning $\mathbb{Z}_P$ and aerosol dry particle / water partitioning $\mathbb{Z}_Q$:

air	$\mathbb{Z}_A = \frac{P_V}{SRT_W}$	(9)
water	$\mathbb{Z}_W = 1$	(10)
solid	$\mathbb{Z}_S = K_d \rho_S$	(11)
SPM	$\mathbb{Z}_P = K_p \rho_W$	(12)
aerosol	$\mathbb{Z}_Q = 1E + 8$ [2]	(13)

where:

K_d distribution coefficient, sediment [L^3 M]

K_p distribution coefficient, particle [L^3 M]

ρ_W density of SPM [$M \cdot L^{-3}$]

T_W temperature of water [θ]

Appendix A details further the QWASI aquivalence model **(MACKAY, 1989)**.

2.1.2 LEAD

2.1.2.1 *CHEMICAL PROPERTIES*

Lead is a (carbon) group 14 element, the chemical family which also includes Sn, Si, and C. Aqueous lead has only the +2 oxidation state, reducing the significance of redox reactions; lead sulfide has very low solubility: K_{sp} = 3.4E-28 **(GIBSON, 1961)**. The least soluble forms of lead are in oxidizing water carbonate $PbCO_3$, hydroxide $Pb(OH)_2$, and hydroxycarbonate $Pb_3(OH)_2(CO_3)_2$, and in reducing systems galena PbS **(HEM, 1973)**. These species limit the concentrations of lead in the pH of natural waters, commonly <10 $\mu g \cdot L^{-1}$ **(HEM, 1976A)**, having solubilities and exhibiting rate kinetics that result in precipitation. The phase distribution of lead may be calculated from equations representing major ions, cation exchange capacity, pH, anion complexation, and ionic strength. Transport may be predominated by SPM adsorption **(HEM, 1976B)** and manganese dioxide co-precipitation **(BROWN, 2015)**. Phosphates may control lead solubility in some natural water systems, being the least soluble minerals under aerobic conditions **(SAUVÉ, 1998)**. Lead(II) exists in of low alkaline, acidic water **(BROWN, 2015)**.

2.1.2.2 *CONCENTRATION IN MEDIA*

Atmospheric aerosol and rain concentrations of Pb may be influenced locally by anthropogenic sources. Aerosol samples indicate Pb concentrations ranging from

[2] A value of $\mathbb{Z}_Q$ = 1E+5 was suggested to address the lack of published air/aerosol partitioning ratios, and 1E+8 used in the original **(MACKAY, 1989)** and subsequent models.

0.4 $\mu g \cdot m^{-3}$ in rural Tuxedo, New York to 4 $\mu g \cdot m^{-3}$ in New York City, but Pb-210 concentrations at these locations are consistent with each other at about 3E-10 $\mu g \cdot m^{-3}$ (1 $mBq \cdot m^{-3}$) **(KNEIP, 1970)**. Measurements supporting a study of Crystal Lake, Wisconsin (section 3.2.1) indicate a weighted mean rain concentration of 8 $mg \cdot m^{-3}$, including an August peak of 20 $mg \cdot m^{-3}$ that may represent releases from leaded gasoline of local automobile traffic **(TALBOT, 1983)**. Lead in rainwater is associated with sub-micron particles **(BENOIT, 1987)**.

Freshwater concentrations of lead are relatively low. Lead is complexed in stream water by dissolved organic compounds **(BENOIT, 1987)**. The concentration of Pb in rivers worldwide ranges from 4 to 400 $ng \cdot L^{-1}$, and is rarely above 2 $\mu g \cdot L^{-1}$ **(GAILLARDET, 2014)**.

2.1.2.3 *PROCESSES*

Processes significant to lead transport in lakes are atmospheric deposition, sedimentation and diffusion.

Lead is released from pollution sources primarily as a volatile compound and aerosolize with the products of photolytic reactions similarly to Pb-210 **(TUREKIAN, 2014)**. The anthropogenic contribution to the flow of lead into the atmosphere is estimated at 10% **(KOWNACKA, 1990)**, a result which would suggest that industrial source forms are preferentially removed over natural forms.

A global study determines Pb precipitation flux by indexing to Pb-210 measurements, which is found to range from 4 $ng \cdot cm^{-2} \cdot a^{-1}$ for remote Tahiti, isolated from industrial emissions, to 390 $ng \cdot cm^{-2} \cdot a^{-1}$ in the Sargasso Sea, influenced by North American emissions **(SETTLE, 1982)**.

The mean annual wet deposition flux is calculated for Pb to be 600 $ng \cdot cm^{-2} \cdot a^{-1}$ in the supporting Crystal Lake study (section 3.2.1). Volumetric washout ratios (section 3.1.2.4) are found to range from 1.9E+05 to 1.6E+06 (n = 6), and are suspected to be biased high by up to a factor of 2 due to the summer concentration peak. The mean annual flux with dry particles is estimated in summer to be at least 200 $ng \cdot cm^{-2} \cdot a^{-1}$ **(TALBOT, 1983)**.

The anthropogenic lead flux to Lake Michigan sediment is determined in 1972 to be 130 $mg \cdot m^{-2} \cdot a^{-1}$, and the natural background flux is estimated to be 16 $mg \cdot m^{-2} \cdot a^{-1}$ **(EDGINGTON, 1976)**. Sediment cores of Bob Lake, Ontario indicate a total anthropogenic lead accumulation rate of 820 $mg \cdot m^{-2} \cdot a^{-1}$ (from both inflow and atmospheric deposition, corrected for an estimate of background contributions) **(EVANS, 1980)**.

Fick's First Law of diffusion is applied to pore and river water concentration measurements. In an urban and agricultural basin in Spain, the formula suggests fluxes at three locations from the sediment to water ranging 0-580 $mg \cdot m^{-2} \cdot a^{-1}$ (n = 12), having median 24 $mg \cdot m^{-2} \cdot a^{-1}$ **(CAMPANHA, 2012)**. At Lake Taihu, China,

measurements indicate, according to Fick's First Law, an average flux from sediment of 2850 $mg \cdot m^{-2} \cdot a^{-1}$ (n = 12) **(LEI, 2016)**.

2.1.3 MODEL UNCERTAINTY

Model uncertainty may be analyzed by a differential sensitivity method. The derivation of this method was reviewed, and the method was considered for application to the original QWASI lead model reproductions and updates and to the Ra-226 model development.

The uncertainty in a model involves an "aleatory" component due to stochastic variability, comprising parameter heterogeneity and measurement precision, and an "epistemic" component due to lack of knowledge about items that are invariant **(MCKONE, 1996)(HOFFMAN, 1994)** (model infidelity). The aleatory components can be treated separately when propagating uncertainty **(MCKONE, 1996)**, or together in a complete preliminary analysis of variable sensitivity by assuming that the model is unbiased (disregarding the epistemic uncertainty) **(MACLEOD, 2002)**.

Differential analysis is a sensitivity method which identifies important contributors to uncertainty in a model predictor variable. Other methods for this purpose are response surface replacement and a form of Monte Carlo analysis. The differential method can be applied generally with partial derivatives using series expansion. It provides good local information about input variables, but it can be challenging to implement and to interpret globally **(IMAN, 1988)**. Estimating a model's variance with a Taylor series requires that the model is linear. If variables X_i are lognormally distributed and the model expresses the variables as products and powers a_i, a lognormal transformation results in a normally distributed model predictor Y as a linear combination of normally distributed variables **(SLOB, 1994)**:

$$Y = \prod_i X_i^{a_i} \tag{14}$$

$$\ln Y = \sum_i a_i \ln X_i \tag{15}$$

For uncorrelated random variables (having pair covariances of 0), the variance of a lognormal distribution **(MOOD, 1973)** is from Equation 15:

$$\sigma_{\ln Y}{}^2 = \sum_i a_i{}^2 \sigma_{\ln X_i}{}^2 \tag{16}$$

A coefficient a_i can be interpreted as a sensitivity factor $\mathcal{S}$, which is defined as the partial derivative of the model output O to an input I, normalized by the reciprocal of those values, and as the ratio of the standard deviations **(MACLEOD, 2002)**:

$$|\mathcal{S}| = \left|\frac{\partial O}{\partial I}\frac{I}{O}\right| = \frac{\sigma_O}{\sigma_I} \tag{17}$$

The method assigns a confidence factor of 1 arbitrarily to 2σ representing 95% of the distribution. In this way each ∂I is set so that $\partial I/I$ is consistent for every input variable, and the contribution to overall variance is scaled by the confidence factor that corresponds to the estimate of the variable standard deviation **(MACLEOD, 2002)**. The output variance σ_O^2 was understood to represent the independent component of a total output variance. Following from Equation 17:

$$a_i' = |\mathcal{S}_i| = \left| \frac{\delta Y_i / Y}{\delta X_i / X_i} \right| = \frac{\sigma'_{\ln Y_i}}{\sigma_{\ln X_i}} \tag{18}$$

The QWASI aquivalence models are not entirely multiplicative. The molar rate balance terms of the aquivalence $\mathcal{A}$ and transport parameter *D* products are solved for water and sediment from the original QWASI model formulation by Equations A.9 and A.10 and for epilimnion, hypolimnion and sediment from the layered model formulation variant by Equations B.8, B.7 and B.9. These formulas are products and sums of the transport parameters, in contrast to the form of Equation 14. Further the transport parameters are not independent, having common constituent variables (clear by inspection of Table A-2 and Table A-3). An aquivalence model may be pseudo-linear in this sense over some intervals of the input variables, but nonlinear over transition ranges between dominant terms. Results of this lognormal differential sensitivity analysis method may still be valid for a specific set of inputs, but not generally for a comparison of the relative importance of variables between different applications.

Being steady state and phenomenological, the Pb model uncertainty was considered dominated by epistemic error, and a parameter sensitivity method was deemed not crucial to the thesis. As a tool to investigate aleatory error, Monte Carlo analysis is unconstrained by the type of model that can be analyzed or the selection of input distributions **(SLOB, 1994)(MACLEOD, 2002)**. Monte Carlo analysis is conducted using a Markov Chain method to a water and sediment pesticide transport model **(BOULANGE, 2017)**. The method would be useful for partitioning models with greater aleatory than epistemic error.

2.2 METHOD

The model applications were reproduced and developed in a spreadsheet with scaling factors **(SOUTHWOOD, 1989)(MACKAY, 2001)** to adjust input variables and examine the relative effects on parameters and outputs. The original QWASI **(MACKAY, 1989)** and Hamilton Harbour two-layer variants **(LING, 1993)(DIAMOND, 1996)** applications were reproduced and updated with a modification and new constraints as detailed below. The updated QWASI model was applied to the inputs used in a related rate constant model for Lake Ontario lead that has common processes and parameters **(THOMPSON, 1999)**. A new application of the updated QWASI model was made for Lake Ontario in the Mississauga Basin.

2.2.1 QWASI AQUIVALENCE MODEL

The original QWASI aquivalence lead model reports aquivalence capacities, transport parameters, process rates and concentrations **(MACKAY, 1989)**. Appendix A contains the original QWASI formulation, and the reported inputs, intermediated parameters and outputs to verify the reproduced model.

The original QWASI data represent consensus estimates from a workshop of subject matter experts **(STRACHAN, 1987)(MACKAY, 1989)**. Values for the particle settling, resuspension and sediment burial flux F_S, F_R and F_B are not reported **(MACKAY, 1989)**, but were understood to be adjusted to optimize the output concentrations. However, the particle flux values were found to not satisfy the Equation A.27 particle balance. Case 1 was constructed by decreasing the particle resuspension flux F_R to satisfy particle conservation by Equation A.27.

The original QWASI model output sediment and water concentrations imply a sediment distribution coefficient $K_d{}' = 5.34E+05$ L·kg^{-1}, in contrast to the $K_d = 3.33E+05$ L·kg^{-1} corresponding to the input (observed) concentrations **(MACKAY, 1989)**, as confirmed in the reproduced model (Appendix A). Case 2 was constructed by increasing the particle resuspension flux F_R, and Case 3 by increasing the sediment burial flux F_B so that the output water and sediment concentrations were consistent with the input $K_d = 3.33E+05$ L·kg^{-1}.

Another option to constrain the output concentrations to the input sediment distribution coefficient K_d was to specify a separate upward mass transfer coefficient for diffusion k_{TW}, and from it create a second volumetric flow rate for diffusion out of the sediment Q_{TW}, and transport parameter D_{TW}:

$$Q_{TW} = k_{TW} A_{SE} \tag{19}$$

$$D_{TW} = Q_{TW} \mathbb{Z}_W \tag{20}$$

The constraint required revisions to the Equation A.9 water aquivalence, Equation A.10 sediment aquivalence, and Equation A.21 process rate formulas (specifying D_T as D_{TS} specifically for water-sediment diffusion):

$$\mathbb{A}_W = \frac{E_w + (D_I + D_X)\mathbb{A}_{WI} + \left(D_V + D_M + D_C + D_Q\right)\mathbb{A}_A}{D_{TS} + D_D + D_V + D_J + D_Y - (D_{TW} + D_R)\frac{D_{TS} + D_D}{D_B + D_{TW} + D_R}} \tag{21}$$

$$\mathbb{A}_S = \frac{D_{TS} + D_D}{D_B + D_{TW} + D_R}\mathbb{A}_W \tag{22}$$

$$q_{TW} = D_{TW}\mathbb{A}_S \tag{23}$$

Case 4 was constructed by setting k_{TW} to constrain the output water and sediment concentrations to the same sediment distribution coefficient K_d as the inputs.

The base and alternate cases were:

- Base: optimized to report observations by adjusting unreported particle settling flux values F_S, F_R and F_B
- Case 1: Equation A.27 particle conservation by reduced particle resuspension flux F_R
- Case 2: K_d alignment by particle resuspension flux F_R increase
- Case 3: K_d alignment by sediment burial flux F_B increase
- Case 4: K_d alignment by sediment-water diffusion coefficient k_{TW} increase

2.2.2 HAMILTON HARBOUR

The original QWASI model is applied to stable lead in Hamilton Harbour, an enclosed water body at the western end of Lake Ontario. The accuracy of the inputs is not a priority for the study **(LING, 1993)**, but the inputs were confirmed from the cited sources. The report contains a comprehensive set of inputs for elevated particulate and lead concentrations and reports interim parameters **(LING, 1993)**. The interim parameters enabled the reproduction to confirm the original study formulation. The original QWASI model two-layer variant is implemented with separate water compartments, one for the upper epilimnion and another for the lower hypolimnion. The reproduced model documented in Appendix B neglects the insignificant volatilization and decay processes.

Distribution coefficients K_d and K_p are the values calculated **(LING, 1993)** from the assumed observation concentrations in the original aquivalence model **(MACKAY, 1989)**.

Particle flux is ambiguous in the original QWASI model scenario (section 2.2.1), but specific data are applied in the Hamilton Harbour study. Sediment burial flux is cited to range from 410 to 1590 $g \cdot m^{-2} \cdot a^{-1}$ (from 1.12 to 4.36 $g \cdot m^{-2} \cdot d^{-1}$) **(LING, 1993)**. The fluxes are determined from Pb-210 dating, interpreted as sedimentation, the lower most recently and the upper from the pre-dredging era **(NRIAGU, 1983)**. Unpublished sediment trap data are reported as a harbour deposition rate of 6.5 $g \cdot m^{-2} \cdot d^{-1}$; present resuspension is judged to range from 1.3 to 2.0 $g \cdot m^{-2} \cdot d^{-1}$ **(LING, 1993)**. The burial rate is set to 4.36 $g \cdot m^{-2} \cdot d^{-1}$ and the model optimized through another contaminant application by adjusting the deposition rate to 6.0 $g \cdot m^{-2} \cdot d^{-1}$ and the resuspension rate to 1.63 $g \cdot m^{-2} \cdot d^{-1}$ **(LING, 1993)**. This set of particle fluxes satisfies particle conservation Equation A.27 and were applied to the reproduced model.

Sediment concentrations are reported to range from 34 to 690 $\mu g \cdot g^{-1}$ **(LING, 1993)**. Ten reported sediment measurements from this era have a geometric mean of about 300 $\mu g \cdot g^{-1}$ **(OME, 1992A)(OME, 1992C)**. Water concentration is tabled as <3 $\mu g \cdot L^{-1}$ **(LING, 1993)** consistent with the source measurement

detection limit **(OME, 1992c)**. Among the scenario variations, the no-thermocline variant (section B.2: equal diffusion between hypolimnion and epilimnion) is established by increasing the layer diffusion mass transfer coefficient by a factor of 1000 from k_{HE} = 0.4 to 400 m·d^{-1} as implemented in the original study model **(LING, 1993)**.

The parameter adjustments made in the reproduction of the original QWASI scenario (section 2.2.1) were applied to the no-thermocline scenario variant to constrain the output water and sediment concentrations to a sediment distribution coefficient K_d consistent with the inputs. The base and alternate cases were:

- Base: thermocline, $A_H > A_E$
- Case 1: no thermocline, $A_H = A_E$
- Case 2: no thermocline, K_d alignment by particle resuspension flux F_R increase
- Case 3: no thermocline, K_d alignment by sediment burial flux F_B increase
- Case 4: no thermocline, K_d alignment by sediment-water diffusion coefficient k_{TW} increase

2.2.3 HAMILTON HARBOUR II

The two-layer model Hamilton Harbour model **(LING, 1993)** with updated parameter values **(DIAMOND, 1996)** was reproduced as described in Appendix C.

Distribution coefficients are decreased based on measurements, for sediment K_d = 9.55E+04 L·kg^{-1} **(OME, 1992a)** and for SPM K_p = 1.10E+05 L·kg^{-1} (OME unpublished data)**(DIAMOND, 1996)**.

Particle flux values are updated: particle resuspension flux F_R is increased from 1.63 to 2.5 g·m^{-2}·d^{-1} using a calibration of the model applied to phosphorus, and sediment burial flux is reduced from 4.4 to 3.0 g·m^{-2}·d^{-1} as a representative rate **(DIAMOND, 1996)**. Other input changes are a lower particle mass rate from land to the harbour, a higher particle mass rate from the harbour to Lake Ontario, a lower particle concentration in the harbour, and higher lead emission by including municipal sources **(DIAMOND, 1996)**.

The no-thermocline variant is established by increasing the epilimnion/hypolimnion diffusion mass transfer coefficient by a factor of 1000 from k_{HE} = 0.4 to 400 m·d^{-1} as implemented in the Hamilton Harbour scenario (section 2.2.2).

The parameter adjustments made in the reproduction of the original QWASI scenario (section 2.2.1) and the Hamilton Harbour study (section 2.2.2) were applied to the no-thermocline scenario variant to constrain the output water and sediment concentrations to a sediment distribution coefficient K_d consistent with the inputs.

The base and alternate cases were:

- Base: thermocline, $A_H > A_E$
- Case 1: no thermocline, $A_H = A_E$
- Case 2: no thermocline, K_d alignment by particle resuspension flux F_R increase
- Case 3: no thermocline, K_d alignment by sediment burial flux F_B increase
- Case 4: no thermocline, K_d alignment by sediment-water diffusion coefficient k_{TW} increase

2.2.4 LAKE ONTARIO RATE CONSTANT STUDY

The original QWASI model described in Appendix A was applied using parameters from a rate constant study of Great Lakes toxic pollutant reduction that includes stable lead in Lake Ontario **(THOMPSON, 1999)**, as documented in Appendix D.

Distribution coefficients were calculated from particle density and the fraction dissolved in water and sediment (section D.1), giving sediment K_d = 1.08E+04 $L \cdot kg^{-1}$ and SPM K_p = 1E+06 $L \cdot kg^{-1}$. Particle flux values were assumed from the Appendix C Hamilton Harbour II scenario for settling, resuspension and burial: F_S = 6.0 $g \cdot m^{-2} \cdot d^{-1}$, F_R = 2.5 $g \cdot m^{-2} \cdot d^{-1}$ and F_B = 3.0 $g \cdot m^{-2} \cdot d^{-1}$ **(DIAMOND, 1996)**. These were adjusted by trial-and-error, while monitoring and comparing with the reported **(THOMPSON, 1999)** process rates of deposition, resuspension and burial, and concentrations of total water and sediment. The particle flux values were constrained by Equation A.27 to reflect no net change in particle sediment inventory.

The parameter adjustments made in the reproduction of the original QWASI scenario (section 2.2.1) and the Hamilton Harbour studies I and II (sections 2.2.2 and 2.2.3) were applied to the no-thermocline scenario variant to constrain the output water and sediment concentrations to a sediment distribution coefficient K_d consistent with the inputs. The base and alternate cases were:

- Base: optimized by particle flux adjustment
- Case 1: K_d alignment by particle resuspension flux F_R increase
- Case 2: K_d alignment by sediment burial flux F_B increase
- Case 3: K_d alignment by sediment-water diffusion coefficient k_{TW} increase

2.2.5 MISSISSAUGA BASIN

The aquivalence model was applied to data representing a location in the Mississauga Basin of Lake Ontario, as detailed in Appendix E. Sediment trap data constrained the particle fluxes to relatively low values **(MARVIN, 2007)**.

Atmospheric deposition of stable lead has decreased in the Lake Ontario region since 1978 **(WATMOUGH, 2017)** and emissions to the lake have declined. The Niagara River is the largest tributary input at the western end of the lake, but a significant proportion of the lead it carries is deposited in nearby sediments. While the case variables correspond to the full extent of the lake, the full proportion of emission and inflow inventory of lead was not expected to reach the bottom of the central basin.

Background estimates of lead in Lake Ontario sediments less than 30 $\mu g \cdot g^{-1}$ **(KEMP, 1976)(MUDROCH, 1988)** enabled a second case representing pre-industrial conditions. Reduced atmospheric deposition was represented by measurements at Plastic Lake in Haliburton, Ontario **(WATMOUGH, 2017)**.

The two scenario variants were optimized by setting the emissions $E_W = 0$, assuming elimination occurs by deposition close to source or by outflow and does not reach the Mississauga Basin (section E.2). The other parameters adjusted to optimize the base scenario were:

- Q_I/Q_J inflow / outflow
- k_{TS} water-sediment diffusion coefficient

The alternate scenario assumed $Q_I/Q_J = 1$ as found in the base scenario since the effective flow through the basin was assumed to be unchanged over time. The other parameters adjusted to optimize the alternate scenario were:

- k_{TW} sediment-water diffusion coefficient
- C_{OI} inflow concentration

2.3 RESULTS

2.3.1 QWASI AQUIVALENCE MODEL

The Figure A-2 process diagram shows that the proportion of atmospheric deposition to water input was 55% in the reproduced model. This result is consistent with the estimated 50% contribution of atmospheric deposition to Lake Ontario inputs **(STRACHAN, 1987)**.

As shown in Table A-8, the estimated sediment concentration coincides with the input value of 100 $\mu g \cdot g^{-1}$, but the water and SPM concentrations were underestimates of the observations **(MACKAY, 1989)**. Particle flux values were adjusted by trial-and-error using the scaling factors to make the water, SPM, and sediment lead concentrations consistent with the input values, but could only be aligned with the estimates of the original model. The final particle flux values shown in Table A-7 were likely the one that the reported model uses **(MACKAY, 1989)** since they gave corresponding transport parameter values.

The particle flux values were found not to satisfy the Equation A.27 particle balance, implying a net erosion of sediments at 0.34 $g \cdot m^{-2} \cdot h^{-1}$. The alternate Case 1 was made by reducing the particle resuspension flux by this amount, from 1.16 to 0.82 $g \cdot m^{-2} \cdot h^{-1}$. Figure A-3 depicts the process diagram for Case 1. The result was little change to the sediment concentration, from 99 to 101 $\mu g \cdot g^{-1}$, but a significant decrease in the total water concentration from 247 to 204 $ng \cdot L^{-1}$, a departure from the reported model estimate **(MACKAY, 1989)**.

The remaining cases were to constrain the output sediment and water concentrations to the sediment distribution coefficient K_d corresponding to that assumed from the reported input concentrations. The case 2 process diagram is shown in Figure A-4, in which net sediment erosion was increased by the resuspension flux F_R. The case 3 process diagram is shown in Figure A-5, in which the sediment burial flux F_B was set greater than the particle settling flux F_S. Both cases depart further from the Equation A.27 particle balance. Case 2 features a total water concentration of 371 $ng \cdot L^{-1}$ and sediment concentration of 93 $\mu g \cdot g^{-1}$. Case 3 features lower total water concentration at 148 $ng \cdot L^{-1}$ and sediment concentration at 37 $\mu g \cdot g^{-1}$. The case 4 process diagram is shown in Figure A-6, depicting the total water concentration consistent with the base scenario, but lower sediment concentration at 62 $\mu g \cdot g^{-1}$. Table 2 shows the adjusted variables, water and sediment concentrations, and sediment distribution coefficient for each case.

Table 2. Original QWASI model scenario variations

Parameter	Unit	Base	Case			
			1 (F_R)	2 (F_R)	3 (F_B)	4 (k_{TW})
F_R (flux on SPM, settling)	$g \cdot m^{-2} \cdot h^{-1}$	1.16	0.82	2.23	1.16	1.16
F_B (flux on SPM, burial)	$g \cdot m^{-2} \cdot h^{-1}$	0.59	0.59	0.59	1.66	0.59
k_{TW} (diff. coeff., sed.-water)	$m \cdot h^{-1}$	0.0004	0.0004	0.0004	0.0004	0.0152
C_W (concentration, water)	$ng \cdot L^{-1}$	247	204	370	148	247
C_S (concentration, sediment)	$\mu g \cdot g^{-1}$	99	101	93	37	62
K_d (dist. Coeff., sediment)	$L \cdot kg^{-1}$	5.3E+5	6.6E+5	3.3E+5	3.3E+5	3.3E+5

The water and air volatilization processes were demonstrated to be insignificant. Using the approximations for lead vapour pressure P_V and chemical solubility S in Lake Ontario, the volatilization process rate from water to air was about 1E-19 $mol \cdot h^{-1}$ and from air to water was about 1E-20 $mol \cdot h^{-1}$. The next least significant process was rain at 0.34 $mol \cdot h^{-1}$, and the most was significant was particle deposition at 680 $mol \cdot h^{-1}$.

2.3.2 HAMILTON HARBOUR

The process diagrams are depicted for the base scenario with thermocline in Figure B-2 for case 1 with no thermocline in Figure B-3. The thermocline variant had higher concentrations in the hypolimnion, but there was no significant difference in sediment concentrations between the two cases.

As with the original QWASI scenario (section 2.3.1), the sediment and water concentrations output imply a sediment distribution coefficient $K_d' = 6.67E+05$ L·kg^{-1}, in contrast to the $K_d = 3.33E+05$ L·kg^{-1} input. Case 2 is depicted in Figure B-4, featuring much higher epilimnion and hypolimnion concentrations, and marginally lower sediment concentration. Case 3 is depicted in Figure B-5, having lower concentrations in both compartments, and less than half the concentration in sediment relative to the base case. Case 4 is depicted in Figure B-6, having concentrations nearly identical to case 2. Table 3 summarizes the adjusted variables, the water and sediment concentrations, and the sediment distribution coefficients for each case.

Table 3. Hamilton Harbour scenario variations

Parameter	Unit	Base	Case			
			1*	2* (F_R)	3* (F_B)	4* (k_{TW})
F_R (flux on SPM, settling)	g·m^{-2}·h^{-1}	1.63	1.63	7.66	1.63	1.63
F_B (flux on SPM, burial)	g·m^{-2}·h^{-1}	4.36	4.36	4.36	10.4	4.36
k_{TW} (diff. coeff., sed.-water)	m·h^{-1}	0.0004	0.0004	0.0004	0.0004	0.0840
C_E (concentration, epilimnion)	ng·L^{-1}	2163	2487	4359	2139	4358
C_H (concentration, hypolimnion)	ng·L^{-1}	2543	2491	4382	2140	4380
C_S (concentration, sediment)	µg·g^{-1}	221	216	190	93	190
K_d (dist. Coeff., sediment)	L·kg^{-1}	6.7E+5	6.7E+5	3.3E+5	3.3E+5	3.3E+5

* no thermocline

2.3.3 HAMILTON HARBOUR II

The process diagrams are depicted for the base scenario with thermocline in Figure C-1 and for case 1 with no thermocline in Figure C-2. The thermocline variant features higher concentrations in the hypolimnion and sediment in the thermocline variant, both about double the differences in the Hamilton Harbour application (section 2.2.2).

As with the original QWASI (section 2.3.1) and Hamilton Harbour (section 2.2.2) scenarios, the sediment and water concentrations outputs imply a sediment distribution coefficient that is not consistent with the input concentrations. The thermocline variant gave $K_d' = 1.20E+05$ L·kg^{-1}, in contrast to $K_d = 9.55E+04$ L·kg^{-1} for the input concentrations.

Case 2 is depicted in Figure C-3, featuring marginally higher epilimnion and hypolimnion concentrations, and marginally lower sediment concentration. Case 3 is depicted in Figure C-4, having lower concentrations in both compartments, and about two-thirds the concentration in sediment versus the base case. Case 4 is depicted in Figure C-5, having concentrations nearly identical to case 2. Table 4 summarizes the adjusted variables, the water and sediment concentrations, and the sediment distribution coefficients for each scenario variant.

Table 4. Hamilton Harbour II scenario variations

Parameter	Unit	Base	Case			
			1*	2* (F_R)	3* (F_B)	4* (k_{TW})
F_R (flux on SPM, settling)	$g \cdot m^{-2} \cdot h^{-1}$	2.50	2.50	3.90	2.50	2.50
F_B (flux on SPM, burial)	$g \cdot m^{-2} \cdot h^{-1}$	3.00	3.00	3.00	4.41	3.00
k_{TW} (diff. coeff., sed.-water)	$m \cdot h^{-1}$	0.0004	0.0004	0.0004	0.0004	0.0060
C_E (concentration, epilimnion)	$ng \cdot L^{-1}$	2541	3040	3448	2755	3450
C_H (concentration, hypolimnion)	$ng \cdot L^{-1}$	3385	3042	3451	2757	3453
C_S (concentration, sediment)	$\mu g \cdot g^{-1}$	249	224	203	162	203
K_d (dist. Coeff., sediment)	$L \cdot kg^{-1}$	1.2E+5	1.2E+5	9.6E+4	9.6E+4	9.6E+4

* no thermocline

2.3.4 LAKE ONTARIO RATE CONSTANT STUDY

Table D-5 shows that the fitted aquivalence model application water and sediment rate constants were consistent with the reported rate constant model. The base scenario particle flux values were close to the original QWASI scenario case 1 (Table 2) values adjusted for particle conservation by Equation A.27. The Lake Ontario Rate Constant Study scenario has a particle settling flux F_S = 1.27 $g \cdot m^{-2} \cdot d^{-1}$, versus 1.41 $g \cdot m^{-2} \cdot d^{-1}$ for the original QWASI scenario, and particle resuspension to sediment burial flux ratio of 0.55/0.72 versus 0.82/0.59 for the original QWASI scenario.

As with the original QWASI scenario (section 2.2.1) and the Hamilton Harbour studies I and II (sections 2.2.2 and 2.2.3), alternate cases were constructed to constrain the input and model output sediment and water concentrations to a consistent sediment distribution coefficient K_d. The distribution coefficient calculated from the output concentrations was K_d' = 8.53E+05 $L \cdot kg^{-1}$ in contrast to the K_d = 1.08E+04 $L \cdot kg^{-1}$ calculated from the input concentrations.

The process diagrams are shown for case 1 in Figure D-2, in which the particle resuspension flux F_R was increased, and for case 2 in Figure D-3, in which the sediment burial flux F_B was increased. As with the original QWASI scenario, both variants depart further from the Equation A.27 particle balance. However, very large (unrealistic) values were required. They implied sediment concentrations small fractions of the base scenario, and a tripling and halving of the water concentration, respectively. The case 3 process diagram is shown in Figure D-4, depicting the total water concentration consistent with the base scenario, but also with a drastically lower sediment concentration. Table 5 summarizes the adjusted variables, the water and sediment concentrations, and the sediment distribution coefficient for each scenario variant.

Table 5. Lake Ontario Rate Constant Study scenario variations

Parameter	Unit	Base	Case		
			1 (F_R)	2 (F_B)	3 (k_{TW})
F_R (flux on SPM, settling)	$g \cdot m^{-2} \cdot h^{-1}$	0.55	116.6	0.55	0.55
F_B (flux on SPM, burial)	$g \cdot m^{-2} \cdot h^{-1}$	0.72	0.72	116.6	0.72
k_{TW} (diff. coeff., sed.-water)	$m \cdot h^{-1}$	0.0004	0.0004	0.0004	0.0526
C_W (concentration, water)	$ng \cdot L^{-1}$	571	1693	334	571
C_S (concentration, sediment)	$\mu g \cdot g^{-1}$	97	4	1	1
K_d (dist. Coeff., sediment)	$L \cdot kg^{-1}$	8.5E+5	1.1E+4	1.1E+4	1.1E+4

2.3.5 MISSISSAUGA BASIN

Figure E-1 shows the process diagram for the case optimized by eliminating emission, reducing the rate of inflow / outflow, and increasing the water-sediment diffusion coefficient. Using the flowrate found in the base scenario variant, the alternate scenario was created by increasing instead the sediment-water diffusion coefficient, and decreasing the inflow concentration, for which the process diagram is shown in Figure E-2. Table 6 summarizes the adjusted variables, and sediment concentration for base and alternate cases.

Table 6. Mississauga Basin scenario variations

Parameter	Unit	Base	Alternate
E_W (emission to water)	$kg \cdot h^{-1}$	0	0
Q_I / Q_J (vol. rate, in/out)	$m^3 \cdot h^{-1}$	1.83E+07	1.83E+07
k_{TS} (diff. coeff., water-sed.)	$m \cdot h^{-1}$	0.0474	0.0004
k_{TW} (diff. coeff., sed.-water)	$m \cdot h^{-1}$	0.0004	0.0924
C_{OI} (concentration, inflow)	$ng \cdot L^{-1}$	888	842
C_S (concentration, sediment)	$\mu g \cdot g^{-1}$	75	25

2.4 DISCUSSION

The construction of each scenario variation demonstrated that the input concentrations used to define the sediment distribution coefficients and the water and sediment output concentrations **(MACKAY, 1989)** did not correspond. The scenarios also demonstrated that particle conservation may not be satisfied. The model was analyzed to understand the method constraints applied to address these observations.

The output concentrations were determined according to the model by Equation A.12 for lead dissolved in water C_W, by Equation A.13 for lead adsorbed to SPM C_P, and by Equation A.14 for lead adsorbed to sediment solids C_S. Through the model, these equations rely on the input distribution coefficients for lead adsorbed to sediment K_d and adsorbed to SPM K_p, which are themselves defined from the corresponding input concentrations C_{OW}, C_{OP}, and C_{OS} by Equations A.33 and A.34. The distribution coefficients enter the model in the definitions for aquivalence capacity of sediment solid $\mathbb{Z}_S$ by Equation 11 for K_d and of water SPM $\mathbb{Z}_P$ by Equation

12 for K_p. Although the SPM distribution coefficients K_p determined by the input and output concentrations were always consistent, the sediment distribution coefficients K_d were not. The scenario variants for the original QWASI, Hamilton Harbour and Lake Ontario Rate Constant Study studies were constructed to address the alignment of the input and output K_d.

The input SPM distribution coefficient K_p can be compared with the output SPM distribution coefficient K_p' from Equation A.34:

$$K_p = K_p' \tag{24}$$

$$K_p = \frac{C_P}{C_W C_{PL}} \tag{25}$$

Substituting concentrations C_W and C_P from Equations A.12 and A.13:

$$K_p = \frac{f_{WV}\mathbb{Z}_P\mathbb{A}_W}{(1-f_{WV})\mathbb{Z}_W\mathbb{A}_W C_{PL}} \tag{26}$$

Substituting the expressions for $\mathbb{Z}_P$ by Equation 12 and for C_{PL} by Equation A.31:

$$\mathbb{Z}_W' = \frac{1}{1-f_{WV}} \tag{27}$$

The result reveals an inconsistency between the definition of the water aquivalence capacity, $\mathbb{Z}_W = 1$ shown in Table 1, and the water concentration definition given by Equation A.12. Water concentration is commonly understood to represent bulk volume, and K_p is defined assuming that C_p and C_W have a common volumetric basis. The error is small since $f_{WV} << 1$ but could be resolved by adopting Equation 27 as a definition. Otherwise since the result is valid for any inputs, it demonstrates how K_P is always consistent.

The inconsistency of the sediment distribution coefficient K_d was demonstrated by equating with the output K_d' defined from the output concentrations similarly to Equation A.33:

$$K_d = K_d' \tag{28}$$

$$K_d = \frac{C_S}{C_W} \tag{29}$$

Substituting concentrations C_W and C_S from Equations A.12 and A.14:

$$K_d = \frac{\mathbb{Z}_S\mathbb{A}_S}{\rho_S(1-f_{WV})\mathbb{Z}_W\mathbb{A}_W} \tag{30}$$

Substituting the expressions for $\mathbb{Z}_S$ by Equation 22 and for $\mathbb{A}_S$ by Equation A.10:

$$(1-f_{WV})\mathbb{Z}_W = \frac{D_{TS}+D_D}{D_B+D_R+D_{TW}} \tag{31}$$

Equation A.10 resolves to unity, so that imposing Equation 28 results in equivalence of the water and sediment aquivalence, $\mathbb{A}_S = \mathbb{A}_W$.

Substituting expressions for process rate D from Table A-2 and for volumetric rate Q from Table A-3, applying D_T, Q_T and k_T specifically to water-sediment diffusion D_{TS}, Q_{TS} and k_{TS}, and the definitions from Equations 20 and 19 for D_{TW} and Q_{TW} and simplifying:

$$1 \approx (1 - f_{WV})\mathbb{Z}_W = \frac{k_{TS}\mathbb{Z}_W + F_S K_p}{k_{TW}\mathbb{Z}_W + (F_B + F_R)K_d} \tag{32}$$

Only specific values of particle flux for settling F_S, resuspension F_R and sediment burial F_B and diffusion coefficients k_{TS} and k_{TW} meeting Equation 32 result in a consistent sediment distribution coefficient K_d. If one of the input concentrations C_{OW} or C_{OS} are uncertain, they could also be adjusted to meet Equation 32 by manipulating K_d through Equation A.33.

Solutions could be constrained further by imposing particle conservation according to Equation A.27:

$$1 = \frac{F_S}{F_B + F_R} \tag{33}$$

The Equation A.27 constraint was applied to the final scenario variants of the original QWASI, Hamilton Harbour, Hamilton Harbour II, and Lake Ontario Rate Constant Study applications where one of the diffusion coefficients was adjusted to make the K_d consistent, effectively solving Equation 32. The implication of not meeting Equation A.27 is that the effective "modelled" sediment layer is either shrinking or growing. While meeting Equation A.27, net sedimentation can be expressed by $F_B > 0$, and net erosion by $F_R > F_S$. Equation A.27 is not met in the original QWASI **(MACKAY, 1989)** and Hamilton Harbour **(LING, 1993)** studies.

The introduction of separate diffusion coefficients k_{TS} and k_{TW} for water-sediment and sediment-water was made to circumvent the control by aquivalence (either $\mathbb{A}_W$ or $\mathbb{A}_S$) over net diffusion (Table A-2). A phenomenological consideration of sediment diffusion is beyond the scope of this thesis. Diffusion has been measured and explained by Fick's First Law from freshwater **(CAMPANHA, 2012)(LEI, 2016)** and estuary sediment **(KALNEJAIS, 2015)**. Hypolimnion stratification that becomes anoxic leads to increased lead sorption by organic complexes and colloids **(LING, 1993)**; specifically mineralization of organic carbon and scavenging by iron and manganese oxyhydroxides **(KALNEJAIS, 2015)**. These and other mechanisms may control the net diffusion of a freshwater-sediment system. The coarser and greater abundance of bed than suspended sediment **(IAEA, 2001)** may result in SPM-adsorbed lead settling into sediment and diffusing out under some reducing conditions.

Each of the original QWASI, Hamilton Harbour, Hamilton Harbour II, and Lake Ontario Rate Constant Study applications required a sediment-water diffusion

coefficient k_{TW} to satisfy Equation 32 under the Equation A.27 particle conservation constraint. The Mississauga Basic application alternate scenario in contrast required a water-sediment coefficient k_{TS}. This reflected lead water concentrations that were too high for the assumed background sediment concentration. Table 7 summarizes fluxes for the diffusion coefficient scenario variants and those reported in recent studies.

Table 7. Model and study sediment-water diffusion flux

Flux ($\mu g \cdot m^{-2} \cdot d^{-1}$)	Scenario / study
10	Lake Windermere, England **(HAMILTON-TAYLOR, 1979)**
0-1600	Turvo/Grande basin, Brazil **(CAMPANHA, 2012)**
4.5±5.6	Hingham Bay **(KALNEJAIS, 2015)**
1.1±2.2	Massachusetts Bay **(KALNEJAIS, 2015)**
8	Taihu Lake, China **(LEI, 2016)**
7-19	Ziya River system, China **(ZHU, 2016)**
5	Lake Ontario original QWASI (section 2.3.1)
500	Hamilton Harbour (section 2.3.2)
36	Hamilton Harbour II (section 2.3.3)
19	Lake Ontario Rate Constant Study (section 2.3.4)
33	Mississauga Basin (section 2.3.5)

The most significant difference between the original QWASI case 4 (section 2.3.1) and Rate Constant Study case 3 (section 2.3.4) scenarios, adjusted by diffusion coefficient to satisfy Equation 32 and Equation A.27, is the particle settling rate D_D. The Rate Constant Study scenario settling rate was lower due to the effective lake sediment area A_{SE} assumed to be 60% (Table D-1) of the lake area assumed in the original QWASI scenario (Table A-6). The difference overcomes a greater divergence between the original QWASI and Rate Constant Study scenarios in the particle outflow rate D_Y, due mainly to the 8-fold higher particle concentration C_{PL} in the Rate Constant Study scenario, because particle settling was a greater proportion of the total water debits.

Aquivalences of the original QWASI case 4 and Mississauga Basin case 3 (section 2.3.5) scenarios, adjusted by diffusion coefficient to satisfy Equation 32 and Equation A.27, differ by an order of magnitude. The Basin scenario aquivalences were about an order of magnitude lower than those of the original QWASI application, due in equal parts to lower inputs and higher outputs, each by a factor of about 3. The lower Basin inputs result mainly from the much lower aerosol concentration adjusted for atmospheric deposition to match the pre-industrial estimate. The higher Basin output results from the higher ratio of input concentrations of lead on SPM (C_{OP}) to lead dissolved (C_{OW}) through the SPM distribution coefficient and settling flux.

The Hamilton Harbour case 4 scenarios were adjusted by sediment-water diffusion coefficient k_{TW} to satisfy Equation 32 and Equation A.27. They differ most

significantly due to the Harbour II scenario (section 2.3.2) particle distribution coefficient K_p, which was assumed from measurements to be lower than the value in the Harbour scenario (section 2.3.3) by a factor of 6. Diffusion was the dominant process as imposed by a large epilimnion/hypolimnion diffusion coefficient k_{HE} in the no-thermocline variant, but it created equal aquivalences and therefore diffusion between the compartments. The decreased transport of lead adsorbed to settling particles from the epilimnion and hypolimnion, and from the hypolimnion to sediment drives higher aquivalences by a factor of nearly 4. The effect of lower K_p was attenuated by flow processes. The Hamilton Harbour scenarios demonstrated how a steady state aquivalence model can be constructed with a consistent sediment distribution coefficient K_d while enabling separate aquivalence values.

Another significant difference was evident from the Table 7 sediment-water diffusion fluxes. They were higher in the Harbour scenario by a factor of 14 due to a 50% higher particle resuspension flux F_R in the Harbour II scenario, and a net accumulation of 0.5 $g \cdot m^{-2} \cdot d^{-1}$ by the assumed particle flux values in the study report **(DIAMOND, 1996)** (which from Table C-1 do not satisfy particle conservation by Equation A.27). The result demonstrated that lead transport by adsorbed particle flux was the dominant transport mechanism between water and sediment, and that a large diffusion flux could result (from an overestimate of it) relative to the published values summarized in Table 7.

2.5 CONCLUSION

Constraining the output water and sediment concentrations to be consistent with the input sediment distribution coefficient results in equivalent water and sediment aquivalences in a coherent steady-state model formulation.

Particle flux conservation should be imposed among the settling, resuspension and burial components. Both net sedimentation and net erosion can be represented within the constraint.

The basis water aquivalence can be made internally consistent with the definitions of concentration and distribution coefficients by accounting for the volume fraction of particles using the factor $1/(1–f_{WV})$.

Particle adsorption and flux are the most significant processes controlling lead in Lake Ontario and Hamilton Harbour.

2.6 FUTURE WORK

Monte Carlo methods such as the Markov Chain applied to a water and sediment transport model **(BOULANGE, 2017)** could be considered for future development of the aquivalence models.

3 Radium series model

3.1 Introduction

Chapter 1 documented the rationale for selecting Ra-226, Pb-210 and Po-210 among the Ra-226 series for extension of the model. These are natural radionuclides significant to mining and other industries, tracer studies and radiological exposures. They can represent the Ra-226 series in partitioning model of freshwater lakes and streams. Figure 1 shows these nuclides within this span of the U-238 series.

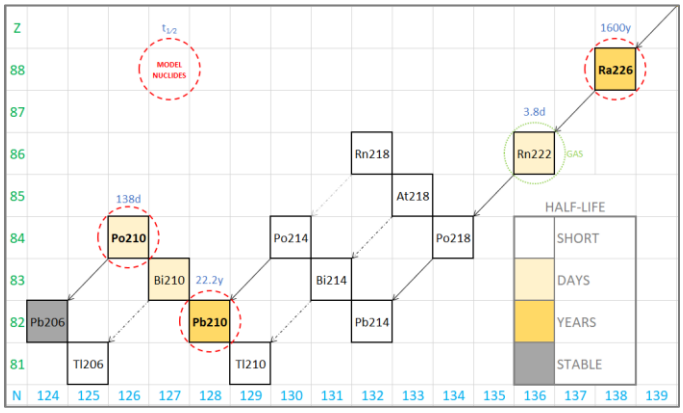

Figure 1. Ra-226 series and model radionuclides

Chapter 2 documented the reproduction, update and analysis of the QWASI aquivalence model of lead in three existing applications and two new applications. A modification was made to incorporate separate water to sediment and sediment to water diffusion coefficients. Additional constraints were implemented to impose equilibrium between water and sediment concentrations and particle conservation. The updated model and constraints were the basis for development of the Ra-226 model.

The behaviour of Pb-210 should be very similar to stable lead **(Cornett, 1984)**. A literature review was conducted to investigate the occurrence and process characteristics of each of the model nuclides. The review included nuclide properties, atmospheric deposition, aqueous and sediment concentrations, and sedimentation. The review provided concentrations and process variables to the model applications, and context for the fitting procedure.

The Ra-226 model was created by writing decay terms for the molar balance of the water and sediment media for each of the nuclides to represent decay, and for Pb-210 and Po210 to represent ingrowth. Volatilization of stable lead, concluded in Chapter 2 to be many orders of magnitude lower than the next least significant process (rain scavenging), was considered further for each nuclide.

Two lakes and a river were selected from the literature to test and analyze the Ra-226 model. Crystal Lake, Wisconsin is a seepage lake without inflow or outflow that undergoes annual intervals of stratification. This lake provided a controlled study limited to atmospheric deposition and sedimentation **(Talbot, 1984)**. Bickford Pond, Massachusetts is a lake draining a hilly watershed fed and drained by streams **(Benoit, 1987)**. Dissolved and SPM-adsorbed Pb-210 and Po-210 are measured by depth and at times representing spring, summer and autumn seasons for both studies. A third application of the model was made to Clinton River,

Michigan where dissolved and SPM-adsorbed Pb-210 and Po-210 is measured along the course through a suburban environment. The study provided insight into the influence of a watershed **(MUDBIDRE, 2014)**.

3.1.1 NUCLIDE PROPERTIES

Ra-226, Pb-210 and Po-210 are classified among the radionuclides with high radiotoxicity **(IAEA, 1963)**.

3.1.1.1 *RADIUM-226*

Radium is a group 2 alkaline earth metal element, the chemical family which also includes Ba, Sr, and Ca. Radium exists naturally in only the +2 valence state, invariant under anoxic conditions **(HESSLEIN, 1984)**. It tends to form ions as simple salts instead of as complexes. Although radium forms the most soluble alkaline earth hydroxide as $Ra(OH)_2$, the salts $RaSO_4$ and $RaCO_3$ have low solubility. Radium has similar chemical properties to barium and often coprecipitates with it **(KIRBY, 1964)**. The most important radium coprecipitants are barium sulphate and ferric hydroxide. Ferric hydroxide adsorption depends strongly on pH over the range of natural waters, 6-8. Generally interaction with sediments is significantly affected by water composition **(BENEŠ, 1982)**. Radium is most likely to be adsorbed to manganese oxides. The reduced form Mn(II) prevails in natural water even with low levels of oxygen, releasing radium from sediment **(HESSLEIN, 1984)**. In water with high sulphate content, the neutral ion pair $RaSO_4$ may be a significant carrier **(BENEŠ, 1982)**. Radium is typically at such low concentrations that precipitation is rarely important, but can occur by coprecipitation as sulphates and carbonates **(IAEA, 1990)**.

Ra-226 transforms by α decay with a half-life of 1600 y **(NNDC, 2018)**, the longest among the four naturally occurring radium isotopes (with Ra-223, Ra-224 and Ra-228), all of which are radioactive **(IAEA, 2014)**.

3.1.1.2 *LEAD-210*

Differentiation in occurrence and form between stable lead (Pb-204, Pb-206, Pb-207 and Pb-208) and Pb-210 due to differences in atmospheric origin are detailed in section 3.1.2.2. The Pb-210 content in water depends significantly on pH, and at lower pH may be associated predominantly with SPM and microbes **(CHAU, 2001)**. Pb(II) exists under conditions of low alkalinity where there is little carbonate buffering capacity **(BROWN, 2015)**.

Pb-210 transforms by β/γ decay (β_o=64 keV, γ_o=47 keV) with a half-life of 22.2 y **(NNDC, 2018)**, one of eight naturally occurring lead isotopes, and the only one of four of those that are radioactive with a half-life longer than 11 h **(PETERSON, 2007)**.

3.1.1.3 *POLONIUM-210*

The chemical properties of Po are similar to Te as a Group VI **(MOYER, 1956)** (group 16 or chalcogen) element, the chemical family which also includes S, Se and Te. Po chemistry is similar to Te, and valences of +2 (II) and +4 (IV) are well established **(BAGNALL, 1957)**. Po(IV) exists in solution, has been shown to form the hydroxide $PoO(OH)_2$ **(FIGGINS, 1961)**, and may exist environmentally in this form and as Na_2PoCl_6 and reduce to the more mobile Po(II) **(BRUNSKILL, 1987)**. The principle seawater species is $Po(OH)_4$ **(HARADA, 1989)**, which has a solubility product 1E-37 **(FIGGINS, 1961)**. Freshwater solubility likely is enhanced by tetravalent complexing with dissolved oxygen **(BENOIT, 1990)**, where between pH 5 and 8.5 the predominant species is $Po(IV)O_2$, although Po(II) can exist under reducing conditions **(HUSSAIN, 1995)**. A small region in the plot of Eh versus pH features insoluble PoS (K_{SP} = 5.5E-29) in sulfidic waters. At natural concentrations ranging 10^{-20}-10^{-16} M (from 0.35 to 3500 $mBq \cdot L^{-1}$), polonide compounds are not formed **(BROOKINS, 1988)**. Po-210 is a "particle reactive" species which adsorbs to negatively charged particles **(HARADA, 1989)**.

Po-210 transforms by α-decay with a half-life of 138 d **(NNDC, 2018)**, one of seven naturally occurring polonium isotopes, and the only with a half-life longer than 186 s **(PETERSON, 2007)**. There are no polonium isotopes in nature of greater abundance available for study.

3.1.2 ATMOSPHERIC MEDIUM

The mean atmospheric concentration of Rn-222 over continents is 4 $mBq \cdot m^{-3}$ **(ISRAEL, 1951)**, supported by average release of 8 $mBq \cdot m^{-2} \cdot s^{-1}$ (lognormal mean, n = 27) from soil at locations across the globe **(TUREKIAN, 1977)**, and of up to 40 $mBq \cdot m^{-2} \cdot s^{-1}$ from US soils **(TUREKIAN, 2014)**. Pb-210 and short-lived precursors decayed from Rn-222 become attached to aerosols and are swept from the atmosphere by precipitation and dry fallout with an atmospheric residence time of less than a week **(POET, 1972)**. Rn-222 measurements in the air at 78 communities across Canada indicate little correlation with ground uranium concentration, but instead with occurrence of dry conditions and glacial lake clays which coincide in central Canada **(GRASTY, 1994)**.

Volatilization processes were neglected as detailed in this section.

3.1.2.1 *RADIUM-226*

The vapor pressure of radium is extrapolated from other alkaline earth metals to be on the order of 4E-19 Pa at 298 K **(ALCOCK, 1984)**, and is likely much lower in chemical forms in the environment. The anthropogenic contribution to the flow of Ra-226 on aerosol into the atmosphere is estimated at 4% **(KOWNACKA, 1990)**, attributed to phosphate fertilizer and cement production, dwarfing the natural contribution from volcanoes, forest fires and erosion **(JAWOROWSKI, 1976)**.

Reference atmospheric concentration is established for Ra-226 at 1 $\mu Bq \cdot m^{-3}$, **(UNSCEAR, 2000)**[3]. Radium is present in air in resuspended soil particles; an aerosol concentration of 50 $\mu g \cdot m^{-3}$ is assumed typically for inhalation pathway evaluation, which at the global average soil concentration of 32 $Bq \cdot kg^{-1}$ corresponds to 1.5 $\mu Bq \cdot m^{-3}$ **(IAEA, 2014)**. Measurements of air sampled in the western United States indicate a bulk aerosol concentration of 10.7 ± 7.5 $\mu g \cdot m^{-3}$ and corresponding concentration of Ra-226 on aerosol of 0.73 ± 0.42 $\mu Bq \cdot m^{-3}$ (n = 13) **(MOORE, 1976)**.

3.1.2.2 *LEAD-210*

Applications of the Lake Ontario lead model in Chapter 2 demonstrated that, among the modelled processes, the contribution of volatilization to the transport of lead was insignificant. The molar rate of volatilization to air, relative to rain, the next least significant process, was 1E–16 or less for all scenarios.

Measurements of Pb-210 on aerosol samples collected from New York City and upstate New York were consistent at about 0.8 $mBq \cdot m^{-3}$, in contrast to total lead concentrations in the city, which are higher by up to an order of magnitude **(KNEIP, 1970)**. The Crystal Lake, Wisconsin study (section 3.2.1) shows similar overall deposition rates for stable lead and Pb-210. However, the result is due to the concentration of Pb-210 in precipitation being about half that of lead, and conversely the scavenging ratio of Pb-210 being about double that of lead. The differences are attributed to variation in lead sources and aerosol size associations **(TALBOT, 1983)**.

Ground level Pb-210 measurements of dust samples in the United Kingdom range from 0.16 to 0.41 $mBq \cdot m^{-3}$ **(PEIRSON, 1966)**. A global database of atmospheric Pb-210 indicates concentrations ranging from 0.9 $mBq \cdot m^{-3}$ at 90°W to 0.6 $mBq \cdot m^{-3}$ at 70°W between 30°N and 60°N; and an average deposition velocity of 0.58 $cm \cdot s^{-1}$ **(PREISS, 1996)**. Stable lead in rainwater is associated with sub-micron particles, and Pb-210 may have similar association **(BENOIT, 1987)**.

The anthropogenic contribution to the input of Pb-210 into the atmosphere is estimated at 0.3% **(KOWNACKA, 1990)**.

Table 8 shows measurements of atmospheric concentrations of Pb-210 and Po-210 from various studies using the "$\pm$" notation for arithmetic means and standard deviations and the "$*$" notation for geometric means and standard deviations **(KIRKWOOD, 1979)(LIMPERT, 2001)**.

[3] *Annex B Table 14* **(UNSCEAR, 2000)** relying heavily on data for northern temperate latitudes in *Annex A Table 11* **(UNSCEAR, 1993)**

Table 8. Pb-210 and Po-210 concentration in the atmosphere near ground level

Concentration $mBq \cdot m^{-3}$		Location	Source
Pb-210	Po-210		
0.14	≤0.012	England (estimated)	**(BURTON, 1960)**
0.11	0.010	global (mean)	**(MARSDEN, 1964)**
0.41±0.20	0.023∗15	Colorado (n=20)	**(POET, 1972)**
0.2-0.7	0.003-0.08	western USA (n=12)	**(MOORE, 1973)**
0.11±0.05	0.030±0.011	Wisconsin (n=8)	**(TALBOT, 1983)**
0.50[3]	0.050[3,4]	reference	**(UNSCEAR, 2000)**
0.42∗1.5	NA	Ottawa (n=373)	**(RPB, 2017)**

3.1.2.3 *POLONIUM-210*

Early measurements found that polonium is considerably more volatile than originally predicted from Group VI (16) properties **(MOYER, 1956)**. More recent measurements revise the value for the monatomic vapour pressure to 4E-22 Pa at 298 K **(EICHLER, 2002)**, attributing the difference to energetic decay of Po-210 in the apparatus of the experiments **(MAUGERI, 2014)**.

Polonium may be volatile in some environments by biological metabolism and release of alkyl polonides. The ocean surface is recognized as a potential source of Rn-222 decay products, including Po-210 **(TUREKIAN, 1977)**. Tracer scale studies provide evidence for the formation of dialkyl and diaryl polonides analogous to the behavior of selenium and tellurium **(BAGNALL, 1983)**. Polonium is processed as an analogue of sulfur, taken up rapidly by cell walls, cytoplasm and high molecular weight proteins of bacteria **(CHERRIER, 1995)**. Sea and air measurements of Rn-222, Pb-210 and Po-210 in the air and sea of the North Atlantic suggest volatility of alkylated polonium species **(HUSSAIN, 1998)**. Biologically mediated emission of polonium is observed from laboratory cultures of sea sediment **(MOMOSHIMA, 2001)** and freshwater involving distinct phylologenies **(MOMOSHIMA, 2002)**. The coupling of osmoregulation with uptake of Po-210 by marine phytoplankton and negligible release of freshwater dimethyl sulfide are presented as evidence against metabolism of Po-210 by freshwater plankton **(CHAI, 2004)**. The volatility of polonium may due to the most reduced form, H_2Po **(ANSOBORLO, 2012)**. The existence and activity of microbes capable of mobilizing Po-210 from low-oxygen lake bottom environments is unclear **(NELSON, 2017)**.

The removal activity ratio Po-210 / Pb-210 is estimated at 0.1 **(BURTON, 1960)**, which at the reference concentrations given in Table 8 **(UNSCEAR, 2000)** would imply equal removal efficiency. Atmospheric concentrations of Pb-210 and Po-210 are variable by season **(MARSDEN, 1964)**, having Po-210 / Pb-210 ratios ranging from 0.08 to 0.35 **(PEIRSON, 1966)**. Ground-level concentrations of Pb-210 and Po-210 are shown to be moderately correlated (r = 0.68) **(POET, 1972)**. Observed

[4] *Annex A Table 10* **(UNSCEAR, 1988)**

atmospheric excess Po-210 relative to aerosol residence time are suggested to result from stratospheric input **(GAVINI, 1974)** or biochemical volatilization of polonium from oceans **(HUSSAIN, 1995)**.

The concentration of Po-210 and airborne particulate is observed to be correlated ($r = 0.70$) at Crystal Lake (section 3.2.1); the airborne particulate ranges from 7 $\mu g \cdot m^{-3}$ in winter to 35 $\mu g \cdot m^{-3}$ in summer, suggesting a significant local snow-free contribution **(TALBOT, 1983)**.

3.1.2.4 *DEPOSITION*

Pb-210 associates with aerosols in the from 0.1 to 0.5 μm range, large enough for Brownian motion diffusion and small enough for gravitational settling both to be low, such that precipitation scavenging is the primary atmospheric removal mechanism **(TUREKIAN, 2014)**. The concept of deposition velocity is proposed to relate dry deposition to the concentration in air at some reference point above the surface **(CHAMBERLAIN, 1960)**. The definition is extended by some authors to include net removal from the atmosphere by all processes, including wet and dry deposition **(PREISS, 1996)**. Washout ratios are species-specific, and are reported on a volume or mass basis distinguished by the density of standard air at about 0.0012 $kg \cdot L^{-1}$ **(ENGELMANN, 1971)**. Mixed units represent the activity scavenged from 1 m^3 of air by 1 kg of precipitation **(HUSSAIN, 1998)**. The scavenging ratio is affected by: particle size and aerosol hygroscopicity, which itself depends on chemical speciation and atmospheric history; and cloud type and precipitation intensity **(ENCINAS, 2004)**. Scavenging refers specifically to the removal of aerosol activity ("wet deposition") from the atmosphere by rain, and washout to the removal from the atmosphere by both wet deposition and rain **(MACKAY, 2001)**. Studies in the literature typically measure and report washout, while in fugacity models, washout is the effect (Equation A.11) of both partitioning by the aquivalence (fugacity) capacity and wet deposition by the scavenging ratio (Table A-3).

Washout ratios from Pb-210 measurements in England are found to range from 600 to 800 on a mass basis, attributed to regional variation in radon and climate **(PEIRSON, 1966)**. Wide ranges of washout ratios are observed near Crystal Lake, Wisconsin, being on a volume basis for lead from 1.9E+05 to 1.6E+06; for Pb-210 from 4.9E+05 to 1.5E+06; and for Po-210 from 5E+04 to 1.1E+06, attributing the wider lead range to greater continental source variation, and the wider Po-210 range to sporadic entrainment of soil particles and varying atmospheric residence time **(TALBOT, 1983)**. Precipitation and air sampled in the western United States measured for Ra-226 suggest a washout ratio of 974 on a mass basis **(MOORE, 1976)**. The scavenging ratio W_g was formulated on a volume basis in the Ra-226 model (Table F-2, Table G-2, Table H-2).

Table 9 shows measurements of rain concentrations of Pb-210 and Po-210 from various studies.

Table 9. Pb-210 and Po-210 concentration in rain

Concentration mean±SD mBq·L^{-1}		Location	Source
Pb-210	Po-210		
83	8.5	England	**(BURTON, 1960)**
54±56	NA	western US (n=3)	**(RAMA, 1961)**
80⁎7.4	NA	global (n=76)	**(PEIRSON, 1966)**
185±53	11⁎4.1	Colorado (n=7)	**(POET, 1972)**
108±2	14.5±2.1	Arkansas (n=71)	**(GAVINI, 1974)**
290	22	Wisconsin (time-weighted)	**(TALBOT, 1983)**
153±4.6	NA	Ontario (n=8)	**(BRUNSKILL, 1987)**
80	NA	Massachusetts (volume-weighted)	**(BENOIT, 1987)**
260±140	41±59	India (n=25)	**(PILLAI, 1988)**

Global measurements of Pb-210 and Po-210 in rain indicate higher concentrations at continental locations **(PEIRSON, 1966)**. Measurements in Arkansas show that the ratio of Po-210 to Pb-210 concentrations was 0.14⁎5.5 (n=71) and are correlated (r = 0.67); variation in the ratio is attributed to episodic rainfall events and air mass lifetimes **(GAVINI, 1974)**.

Precipitation and air sampled in the western United States are measured for Ra-226, indicating rain concentrations 58±33 mBq·L^{-1} (n = 17) **(MOORE, 1976)**. Measurements of Ra-226 in rain water in India show concentrations of 33±44 mBq·L^{-1} (n=25) **(PILLAI, 1988)**. Rainwater samples from southern Spain show Ra-226 concentrations 6.9⁎5.0 mBq·L^{-1} (n=18) **(MARTÍNEZ-AGUIRRE, 1991)**.

Atmospheric fallout of Pb-210 varies little geographically integrated over a year or more, while fallout of Po-210 varies by an order of magnitude geographically. Pb-210 concentrations over northern latitudes are reduced by snow and ice cover. **(PERSSON, 2011)**. Table 10 shows measurements of atmospheric deposition of Pb-210 and Po-210 from various studies.

Table 10. Atmospheric deposition of Pb-210 and Po-210

Deposition ($Bq \cdot m^{-2} \cdot a^{-1}$)		Location	Source
Pb-210	Po-210		
61	NA	England (rain, mean)	**(BURTON, 1960)**
73	NA	global (rain, annual)	**(PEIRSON, 1966)**
100	NA	North Atlantic (total, estimate)	**(BACON, 1976)**
70∗6.7	NA	global (n=38)	**(TUREKIAN, 1977)**
233	19	Wisconsin (wet, estimate)	**(TALBOT, 1983)**
26	1.85	Wisconsin (dry, estimate)	**(TALBOT, 1983)**
96	NA	Massachusetts (wet, mean)	**(BENOIT, 1987)**
80	NA	Ontario (total, mean)	**(BRUNSKILL, 1987)**
18	7.3	Australia (dry, mean)	**(PETTERSSON, 1991)**

The dry deposition fluxes shown in Table 10 representing the Ranger Mine, Australia are measured by horizontal plane deposition 100 km from the open pit. The technique also indicates Ra-226 deposition of about 6 $Bq \cdot m^{-2} \cdot a^{-1}$ (mean) **(PETTERSSON, 1991)**.

A study near Crystal Lake (section 3.2.1) shows that most activity is carried on sub-micron particles but deposited in association with particles of diameter >1 μm **(TALBOT, 1983)**.

Table 11 shows some reported dry deposition velocities calculated from measurements of Pb-210.

Table 11. Dry deposition velocities for Pb-210

Deposition velocity ($cm \cdot s^{-1}$)	Application	Source
0.43-1.33	UK, US, Australia	**(TUREKIAN, 1977)**
0.3	particulate air ingrowth of Rn-222 daughters (estimated ∅=0.003 μm)	**(USNRC, 1980)** **(THOMAS, 2000)**
0.25±0.15	Australia (estimate)	**(PETTERSSON, 1991)**

3.1.3 AQUEOUS MEDIUM

SPM in Lake 239 of the Experimental Lakes Area is measured to range <1-10 $mg \cdot L^{-1}$ normally and reach 30 $mg \cdot L^{-1}$ in association with the ascending limb of rainstorm hydrographs **(BRUNSKILL, 1987)**. Rivers have the capacity to carry higher SPM concentrations than freshwater lakes due to the force of flowing water **(MUDBIDRE, 2014)**.

3.1.3.1 *Radium-226*

Measurements of Ra-226 in samples from Great Slave Lake, Northwest Territories show dissolved concentrations ranging from 0.8 to 2.8 $mBq \cdot L^{-1}$, and no detectable concentrations in association with SPM **(Elliott, 1981)**. Measurements of surface samples from background condition Experimental Lakes Area lakes show Ra-226 concentrations ranging from 0.4 to 3.0 $mBq \cdot L^{-1}$ **(Hesslein, 1984)** and from 5.7 to 8.8 $mBq \cdot L^{-1}$ **(Clulow, 1998b)**. Measurement of water sampled through the depth of the Bickford Pond (section 3.3.4) shows the concentration of Ra-226 at <0.17 $mBq \cdot L^{-1}$ **(Benoit, 1987)**. An Ottawa River study shows that 99% of the Ra-226 is transported in the dissolved phase at an average concentration of 5.1 $mBq \cdot L^{-1}$ **(Joshi, 1990)**. Ra-226 concentrations in freshwater are low and lie in a narrow range, generally from 0.5 to 20 $mBq \cdot L^{-1}$, but are measured up to 3 $Bq \cdot L^{-1}$ in mining areas **(IAEA, 1990)**. Decreasing sulphate concentrations in two Serpent River watershed lakes near Elliot Lake, Ontario affected by past mining activity are expected to indicate release of barium sulphate and associated radium, elevating the concentration of Ra-226 **(Russel, 2011)**.

3.1.3.2 *Lead-210 & Polonium-210*

Figure 2 shows concentrations determined for samples taken at Crystal Lake, Wisconsin. The measurements are of samples collected between May and October in 1979/80 over the range of lake depth, from 1 to 20 m **(Talbot, 1984)**. Figure 3 shows concentrations determined for samples taken at Bickford Pond, Massachusetts in 1982/83 **(Benoit, 1987)**.

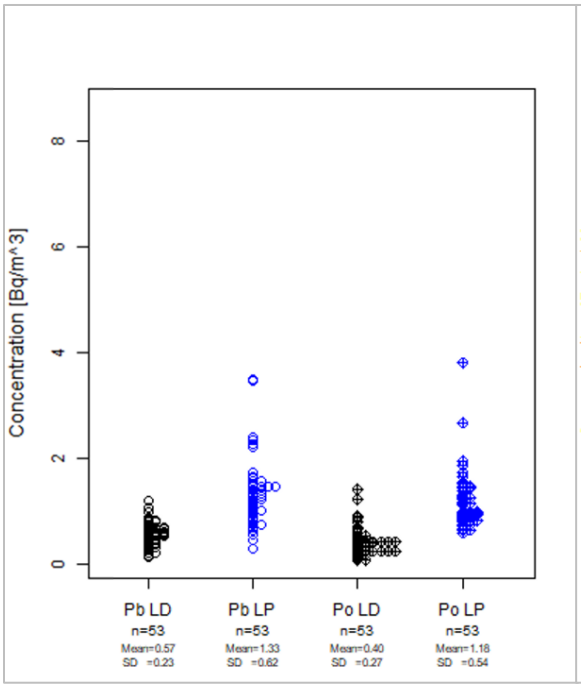

Figure 2. Crystal Lake concentrations

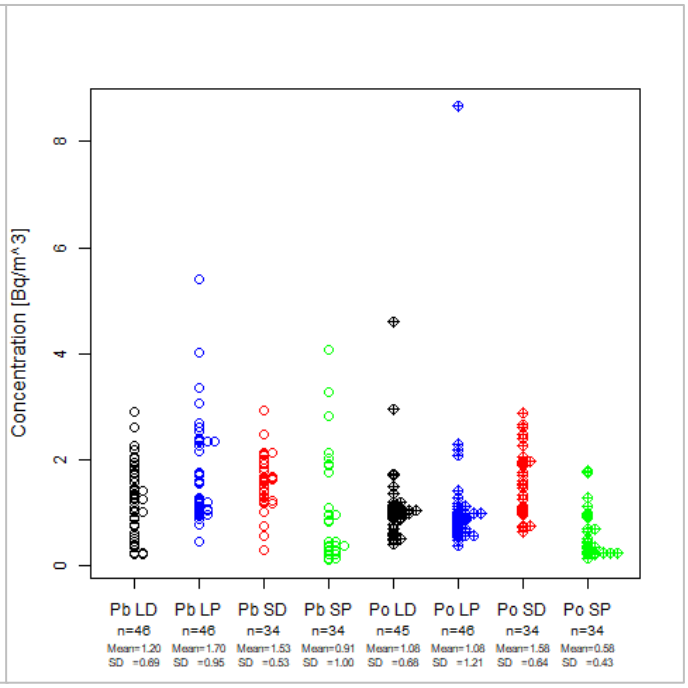

Figure 3. Bickford Pond concentrations

lake (L), stream (S), dissolved (D), particulate (P)

Table 12 shows mean concentrations determined for samples taken at Bickford Pond between June and October 1985 **(BENOIT, 1990)**. The higher concentrations of both nuclides at 12 m depth nearest the sediment vary seasonally and peak in late September.

Table 12. Bickford Pond Pb-210, Po-210 concentrations in 1985

		Concentration (mean±SD)			
($Bq \cdot m^{-3}$)	n	Pb-210		Po-210	
		dissolved	particulate	dissolved	particulate
1 m depth	7	0.71±0.31	1.42±0.32	0.62±0.29	0.66±0.14
12 m depth	12	4.7±4.0	4.1±2.1	3.7±2.0	7.5±4.9

Table 13 indicates the Clinton River concentrations measured at four locations along a 25 km length over four months **(MUDBIDRE, 2014)**.

Table 13. Clinton River Pb-210, Po-210 concentrations

($Bq \cdot m^{-3}$)	Pb-210		Po-210	
	dissolved	particulate	dissolved	particulate
n	13	16	13	13
range	0.8-9.0	0.2-9.8	1.0-5.3	0.5-2.7
geometric mean	3.3	2.3	2.3	1.3

Concentrations vary seasonally and by SPM association. Higher winter than summer concentrations are observed in samples from two unaffected lakes near Elliott Lake measured for Pb-210, ranging from 1 to 14 $mBq \cdot L^{-1}$ **(CLULOW, 1998A)**, and from Odra River and tributaries in Poland measured for Po-210 **(SKWARZEC, 2008)**. In the Rhone watershed, Switzerland, 85% of the activity is exported from the watershed adsorbed to SPM, represented by a total activity of about 8 $mBq \cdot L^{-1}$ in July and August and 2 $mBq \cdot L^{-1}$ in other months **(DOMINIK, 1987)**. An Ottawa River study shows that 77% of the Pb-210 is transported in the dissolved phase from a relatively steady total average concentration of about 4 $mBq \cdot L^{-1}$ **(JOSHI, 1990)**. In seawater, iron oxides scavenge Pb-210 and Po-210, and concentration ratios of the nuclides are affected by biological activity **(BACON, 1976)**. Biological uptake and recycling governs marine concentrations of Po-210 significantly, but nonbiogenic particles and dissolved organic carbon likely limit the effect in temperate freshwater **(BENOIT, 1990)**. In freshwater, Pb-210 is more particle reactive than Po-210, a reversal of marine observations **(CHAI, 2004)**. Stable lead is complexed in stream water by dissolved organic compounds, and Pb-210 may have similar association **(BENOIT, 1987)**. Po-210 concentration in freshwater is strongly correlated with silicon, total organic carbon, sulfate, and temperature **(NELSON, 2017)**. Average concentrations of Po-210 are higher in seasonally anoxic freshwater **(KIM, 2011)**, correlated with the release of Fe and Mn oxides and oxyhydroxides from sediment **(BENOIT, 1990)(KIM, 2005)**. Pb-210 may be more closely associated with iron, and Po-210 with manganese, while both nuclides are influenced by sulfur cycling **(BALISTRIERI, 1995)**.

3.1.4 SEDIMENT MEDIUM

A sedimentation rate of 1E-03 $m \cdot a^{-1}$ is given for Canadian Shield lakes among guidelines for deriving release limits of radionuclides **(CSA, 2014)**. The rate is based on measurements of fossil diatom and pollen in sediment cores from Quirke Lake, Ontario in the uranium mining district of Elliot Lake, which indicate settling from 96 to 185 $g \cdot m^{-2} \cdot a^{-1}$ in the post mining period and from 34 to 64 $g \cdot m^{-2} \cdot a^{-1}$ in the pre-mining period **(MCKEE, 1987)**. Table 14 shows sedimentation rates from study data.

Table 14. Study sedimentation rates

Sedimentation rate ($Bq \cdot m^{-2} \cdot d^{-1}$)			Source
Ra-226	Pb-210	Po-210	
NA	0.80	NA	Crystal Lake **(TALBOT, 1984)**
NA	0.20-0.56	NA	Rhone watershed, Switzerland **(DOMINIK, 1987)**
0.93-4.3	3.3-7.1	3.8-8.8	Quirke Lake, Ontario **(MCKEE, 1987)**

The Quirke Lake sedimentation rates, affected by mining activity, is estimated to be about 2 orders of magnitude greater than the pre-mining period, and from 1 to 3 times greater than uncontaminated arctic lakes **(MCKEE, 1987)**. The range of Quirke Lake Pb-210 sedimentation rates are about one order of magnitude above the value determined for Crystal Lake and the range determined in the Rhone watershed. Table 15 shows sediment concentrations from study data.

Table 15. Study sediment concentrations

Sediment concentration ($Bq \cdot g^{-1}$)			Source
Ra-226	Pb-210	Po-210	
0.002-0.056	NA	NA	sandy - organic, Lake 224 **(HESSLEIN, 1984)**
2-17	8-23	8-23	Quirke Lake, 1984 **(MCKEE, 1987)**
NA	0.5	NA	unaffected lakes, Elliot Lake **(CLULOW, 1998A)**
0.007-0.34	NA	NA	unaffected lakes, Elliot Lake **(CLULOW, 1998B)**
0.37-2.2	0.31-2.5	0.27-2.6	Experimental Lakes Area **(HART, 2011)**
2.2	2.3	2.6	Quirke Lake, 2009 **(HART, 2011)**

Distribution of a chemical species between a solution and a solid by adsorption can under certain circumstances obey a simple distribution law:

$$C_S = \mathrm{K} \cdot \mathrm{C} \tag{34}$$

where C is the concentration in solution and C_S is the concentration on the solid **(LERMAN, 1979)**. The factor K is the distribution coefficient, given for sediment K_d by Equation A.33 and by extension for SPM K_p by Equation A.34. The factor K is a function of temperature, solution composition, and the nature of the solid substrate, and is applicable to dilute solutions where concentration can be used instead of thermodynamic activity **(LERMAN, 1979)**.

3.1.4.1 *RADIUM-226*

The limited data for radium adsorption on sediment indicates that it decreases with increasing ionic strength, being the most strongly adsorbed alkaline earth metal by ion exchange on clay minerals **(WILHELM, 2004)**.

The Langmuir adsorption model accounts for site-limited adsorption **(LANGMUIR, 1918)**; a modified distribution coefficient of that form was suggested on the basis

of measurements of 25 river sediments[5] **(BENEŠ, 1982)**. A strong correlation is reported between depth and sediment content of Ra-226 ($r=0.95$, $p<0.01$) **(HESSLEIN, 1984)**. In one of a set of compiled studies **(CIFFROY, 2009)(IAEA, 2009B)**, laboratory measurements of sediments from the Ploucnice River, Czech Republic yield data for the radium adsorption fraction, showing significant variation as a function of pH, ionic strength, calcium and sulphate concentration **(BENEŠ, 1986)**.

Table 16 lists Ra-226 distribution coefficients compiled from study data.

Table 16. Ra-226 distribution coefficients from study data

K_d or K_p ($L \cdot kg^{-1}$)	Source
3.6E+02	sediment, 25 rivers (low) **(BENEŠ, 1982)**
1.7E+04	sediment, 25 rivers (high) **(BENEŠ, 1982)**
5.4E+03	sediment, Danube River **(SZTANYIK, 1984)**
3.0E+02	sediment, River Paka, Slovenia **(MLJAČ, 1996)**[6]
2.0E+04	SPM, Lake 239, Ont. (low) **(BRUNSKILL, 1987)**
2.0E+05	SPM, Lake 239, Ont. (high) **(BRUNSKILL, 1987)**
7.8E+03	SPM, Ottawa River **(JOSHI, 1990)**
1.4E+04	SPM, Jucar River, Spain **(SANCHEZ, 1999)**[7]
1.3E+03	sediment & SPM, 5th percentile of 7 studies **(CIFFROY, 2009)**
5.0E+04	sediment & SPM, 95th percentile of 7 studies **(CIFFROY, 2009)**
7.4E+03	sediment & SPM, geometric mean of 7 studies **(IAEA, 2009B)**

3.1.4.2 *LEAD-210 & POLONIUM-210*

A Black Sea study suggests that dissolved organic carbon rather than inorganic SPM are the major carriers of Po-210, and that release from sediments can result in Po-210 excess above equilibrium with Pb-210 in water **(WEI, 1994)**. Sediment concentrations of Pb-210 and Po-210 are shown to be significantly higher than equilibrium with Ra-226, and suggest that mechanisms may support concentrations of Po-210 marginally higher than equilibrium with Pb-210 **(NELSON, 2017)**.

An inverse relationship between solid concentration and distribution coefficient, the particle concentration effect **(O'CONNOR, 1980)**, is observed from Pb-210 measurements of the Rhone watershed, Switzerland **(DOMINIK, 1987)**, Perch Lake and Maskinonge Lake **(WANG, 1993)** and New England rivers, and is suggested to be due to colloids and large diameter SPM **(BENOIT, 1999)**. This explanation would

[5] Mansfeld A, Hanslík E (1980) The Effect of Mining Radioactive Raw Materials on the Quality of Surface Waters. Prague, Water Research Institute, Final Report C16–331-112-03-04.
[6] Lower range of compilation **(CIFFROY, 2009)(IAEA, 2009B)**
[7] Upper range of compilation **(CIFFROY, 2009)(IAEA, 2009B)**

be amenable to the steady-state model (section 3.3) which does not account for particle size.

Table 17 lists distribution coefficients of Pb-210 and Po-210 calculated from study measurements. Perch Lake and Maskinonge Lake demonstrate much higher SPM than sediment distribution coefficients **(WANG, 1993)**. In freshwater, Pb-210 is more particle reactive than Po-210, reflected in marginally higher distribution coefficients, a reversal of marine observations **(CHAI, 2004)**. Distribution coefficients lower by about two orders of magnitude are measured in the Clinton River (section 3.2.3) **(MUDBIDRE, 2014)**. Lower distribution coefficients are posited for acid mine drainage conditions **(BLASCO, 2016)**.

Table 17. Pb-210 and Po-210 distribution coefficients from study data

K_d or K_p ($L \cdot kg^{-1}$)		Source
Pb-210	Po-210	
5.0E+04		particle, Lake 239, Ontario (low) **(BRUNSKILL, 1987)**
3.3E+05		particle, Lake 239, Ontario (high) **(BRUNSKILL, 1987)**
1.9E+05	NA	particle, Ottawa River **(JOSHI, 1990)**
6.4E+06	1.7E+06	particle, Lake Sammamish, Wash. **(BALISTRIERI, 1995)**
1.2E+07	1.1E+07	particle, Lake Superior **(CHAI, 2004)**
8.0E+04	7.0E+04	particle, Clinton River, Michigan **(MUDBIDRE, 2014)**
NA	2.5E+05	particle, Huelva, Spain **(BLASCO, 2016)**
5.4E+05	6.8E+05	particle, Chalk River, Ontario[8] (low) **(WANG, 1993)**
5.6E+06	6.1E+06	particle, Chalk River, Ontario[8] (high) **(WANG, 1993)**
6.7E+05	1.3E+05	sediment[9], Chalk River, Ontario[8] (low) **(WANG, 1993)**
1.3E+04	3.8E+05	sediment[9], Chalk River, Ontario[8] (high) **(WANG, 1993)**

3.2 FRESHWATER STUDIES

3.2.1 CRYSTAL LAKE

Crystal Lake, Wisconsin is a 31 ha lake of maximum depth 21 m and average depth 10.4 m without inflow or outflow, and with little groundwater interaction **(TALBOT, 1984)**. The body is a seepage lake with a residence time of about 20 a **(BENOIT, 1987)**. The surrounding soils are sandy and permeable, minimizing runoff. The water is low in carbonate, phosphorus and silica. Thermal stratification occurs during the summer, and the authors speculate that reduced conditions developed near the sediment interface by fall turnover. Sediment consists of a significant

[8] Perch & Maskinonge Lake
[9] top 2 cm

proportion of diatom frustules and pollen grains. Water and SPM-adsorbed Pb-210 and Po-210 are measured over depths for a year in 1979/80, as summarized in Figure 3. SPM-adsorbed Pb-210 is found to be highly correlated with biological activity, but also turnover events. Concentrations peak during spring bloom and decrease by an order of magnitude over the stratification interval. The annual average SPM concentration of 0.5 $mg \cdot L^{-1}$ spikes to 1 $mg \cdot L^{-1}$ during the summer plankton bloom. Dissolved Po-210 is in deficit relative to Pb-210 overall, and there are more cases of SPM-adsorbed excess, and these cases are positively correlated with depth. Dissolved and SPM phases are separated by 0.45 μm filters **(TALBOT, 1984)**.

3.2.2 BICKFORD POND

Bickford Pond, Massachusetts is a 60 ha lake of maximum depth 13 m and average depth 5.7 m fed by two streams that regularly drain a 760 ha watershed, and overflow from a 770 ha catchment. Runoff flow is 1.37E+07 $m^3 \cdot a^{-1}$, and rainfall 7E+05 $m^3 \cdot a^{-1}$. The water is of low ionic strength and dissolved solids content. Water and particulate Pb-210 and Po-210 in the tributaries and lake are summarized in Figure 2. Dissolved and particle phases ware separated by 0.45 μm filters **(BENOIT, 1987)**.

3.2.3 CLINTON RIVER

Clinton River, Michigan drains 1980 km^2 of the northern suburbs of Detroit and travels about 125 km to drain into Lake St. Clair. The concentration of SPM was measured to range from 4.2 to 15.2 $mg \cdot L^{-1}$, which is higher than freshwater lakes, but typical of rivers. The SPM-adsorbed concentrations of Pb-210 and Po-210 are low relative to the Crystal Lake and Bickford Pond studies. Coloured water samples after 0.5 μm filtration are attributed to macromolecular colloidal material, which would skew the phase balance towards the dissolved fraction. Dissolved and SPM phases are separated by 0.4 μm filters **(MUDBIDRE, 2014)**.

3.3 METHOD

3.3.1 RA-226 MODEL

A radioactive series (Ra-226) model was constructed by linking separate modules with first order decay processes in the water and sediment media. Figure 1 shows the intermediary nuclides with short half-lives that reach equilibrium with parent nuclides quickly. The longest lived is Bi-210, which has a half-life of five days.

The Table A-2 processes were extended to include radioactive decay of nuclides in water $q_{\lambda W}$, and sediment $q_{\lambda S}$:

$$q_{\lambda W} = D_{\lambda W} \mathbb{A}_W \tag{35}$$

$$q_{\lambda S} = D_{\lambda S} \mathbb{A}_S \tag{36}$$

The Table A-2 transport parameters were extended to include radioactive decay of nuclides in water $D_{\lambda W}$ and sediment $D_{\lambda S}$:

$$D_{\lambda W} = Q_{\lambda W}\mathbb{Z}_{WT} \quad (37)$$

$$D_{\lambda S} = Q_{\lambda S}\mathbb{Z}_{ST} \quad (38)$$

Volumetric decay in water $Q_{\lambda W}$ and sediment $Q_{\lambda S}$ were formulated as:

$$Q_{\lambda W} = A_{LA}d_{LA}\lambda \quad (39)$$

$$Q_{\lambda S} = A_{SE}d_{SE}\lambda \quad (40)$$

These expressions introduce new variables to the model:

d_{LA} depth of water body [L]

d_{SE} depth of sediment [L]

λ radioactive decay constant [T^{-1}]

The decay constant is defined for the first order radioactive transformation as:

$$\lambda = \frac{\ln 2}{t_{1/2}} \quad (41)$$

where

$t_{1/2}$ radioactive half life [T]

The decay process must be incorporated into a model with appropriate units. The SI unit for decay is the becquerel (Bq) defined as the number of disintegrations per second s^{-1}, or $atoms{\cdot}s^{-1}$. Since the model balance was expressed in amount and time bases of *mols* and *hours*, the decay constant was converted to these units:

$$\lambda_h = \frac{\ln 2}{t_{1/2}}\frac{1}{N_A}\frac{3600s}{h} \quad (42)$$

where

N_A Avogadro's number, 6.02E-23 $atoms{\cdot}mol^{-1}$

Another requirement for incorporation into a model was to account for the transformation of Ra-226 to Pb-210, and of Pb-210 to Po-210, linking the modules. Subscripts 1, 2 and 3 were assigned to Ra-226, Pb-210 and Po-210 respectively.

The sediment balance incorporating decay was from Equation A.1, representing nuclide *i* and parent nuclide *i-1*:

$$(D_{Di} + D_{TSi})\mathbb{A}_{Wi} + D_{\lambda Si-1}\mathbb{A}_{Si-1} - (D_{Ri} + D_{TWi} + D_{Bi} + D_{\lambda Si})\mathbb{A}_{Si} = 0 \quad (43)$$

Consistent with the definitions introduced earlier (Equation 19 and 20) to enable a separate sediment-water diffusion coefficient k_{TW}, a volumetric rate Q_{TS} and

transport parameter D_{TS} were made explicit for the water-sediment diffusion coefficient k_{TS}:

$$Q_{TS} = k_{TS} A_{SE} \tag{44}$$

$$D_{TS} = Q_{TS} \mathbb{Z}_W \tag{45}$$

The new terms accounted for transformation in the sediment: ingrowth from the parent nuclide, *i-1*, and decay *i*:

$$D_{\lambda Si-1} \mathbb{A}_{Si-1} \tag{46}$$

$$D_{\lambda Si} \mathbb{A}_{Si} \tag{47}$$

The water balance incorporating decay was from Equation A.2:

$$E_{wi} + (D_{Xi} + D_{Ii})\mathbb{A}_{WIi} + \left(D_{Mi} + D_{Ci} + D_{Qi} + D_{Vi}\right)\mathbb{A}_{Ai} + (D_{TWi} + D_{Ri})\mathbb{A}_{Si} + D_{\lambda Wi-1}\mathbb{A}_{Wi-1} - \left(D_{Ji} + D_{Yi} + D_{Di} + D_{TSi} + D_{Vi} + D_{\lambda Wi}\right)\mathbb{A}_{Wi} = 0 \tag{48}$$

The new terms accounted for transformation in the water: ingrowth from the parent nuclide, *i-1*, and decay *i*:

$$D_{\lambda Wi-1} \mathbb{A}_{Wi-1} \tag{49}$$

$$D_{\lambda Wi} \mathbb{A}_{Wi} \tag{50}$$

The sediment balance incorporating decay from Equation 43 was:

$$\mathbb{A}_{Si} = \frac{(D_{Di} + D_{TSi})\mathbb{A}_{Wi} + D_{\lambda Si-1}\mathbb{A}_{Si-1}}{D_{Ri} + D_{TWi} + D_{Bi} + D_{\lambda Si}} \tag{51}$$

The water aquivalence from Equation 48 and 51 was:

$$\mathbb{A}_{Wi} = \frac{E_{wi} + (D_{Xi} + D_{Ii})\mathbb{A}_{WIi} + \left(D_{Mi} + D_{Ci} + D_{Qi} + D_{Vi}\right)\mathbb{A}_{Ai} + D_{\lambda Wi-1}\mathbb{A}_{Wi-1} + \frac{(D_{TWi} + D_{Ri})(D_{\lambda Si-1}\mathbb{A}_{Si-1})}{D_{Ri} + D_{TWi} + D_{Bi} + D_{\lambda Si}}}{D_{Ji} + D_{Yi} + D_{Di} + D_{TSi} + D_{Vi} + D_{\lambda Wi} - \frac{(D_{TWi} + D_{Ri})(D_{Di} + D_{TSi})}{D_{Ri} + D_{TWi} + D_{Bi} + D_{\lambda Si}}} \tag{52}$$

The last two terms in the numerator applied only to Pb-210 and Po-210, since Ra-226 has no precursor in the Ra-226 model.

The water column mean removal residence time to sediment, τ_{TW} **(TALBOT, 1984)**, was a product of the volumetric concentration $\mathbb{Z}_{WT}\mathbb{A}_W$ (Equations A.5, A.9) and volume $A_{LA} \cdot d_{LA}$ divided by the settling and net diffusion flux process rates from Table A-2 :

$$\tau_{TW} = \frac{\mathbb{Z}_{WT}\mathbb{A}_W A_{LA} d_{LA}}{q_{TS} - q_{TW} + q_D} \tag{53}$$

The water column mean removal residence time by all processes, τ_T, was from the removal process rates from Table A-2 :

$$\tau_T = \frac{\mathbb{Z}_{WT}\mathbb{A}_W A_{LA} d_{LA}}{q_J + q_Y + q_{VA} + (q_{TS} - q_{TW} + q_D) + q_{\lambda W}} \quad (54)$$

3.3.2 Optimization

In each study modelled, the sediment concentrations were unmeasured, so the Ra-226, Pb-210 and Po-210 input sediment concentration C_{OS} model parameters were adjusted during optimization. The Bickford Pond study Ra-226 water concentration is also unmeasured, so the Ra-226 observed water concentration C_{OW} in that scenario was adjusted. These concentrations were input to the sediment distribution coefficients K_d, which along with the other input parameters, were used in the Ra-226 model to calculate the output concentrations.

The general optimization method was to find values for adjusted parameters that result in consistent input and model concentrations for water, SPM and sediment: $C_{OW}/C_W = C_{OP}/C_{OP} = C_{OS}/C_S = 1$. The concentrations were adjusted with the other unfixed parameters (alone or together as required). The adjusted parameters were generally settling flux F_S, and as necessary diffusion k_{TW} or k_{TS}, and emission E_w. C_{OW} and C_{OP} were summarized from measurement data and fixed for each scenario, except for the Ra-226 water concentration C_{OW3} (and corresponding C_{OP3} by the set K_{p3}) in the Crystal Lake scenario. Sediment concentrations of each nuclide C_{OS} were adjusted in each scenario. The unfixed parameter adjustments were made for each of the nuclides in decay sequence: Ra-226, Pb-210 and Po-210. The sequence enabled Equations 51 and 52 to be solved for each of the nuclides without iteration.

The Ra-226 model was constructed with scaling factors to enable initial parameter estimates to be adjusted in steps during optimization **(Southwood, 1989)(Mackay, 2001)**.

3.3.3 Crystal Lake

Pb-210 and Po-210 are measured in aerosol and rain at a site near Crystal Lake to estimate wet and dry deposition **(Talbot, 1983)**. Talbot analyzes the lake with a two-layer model to explore the reduced conditions that are thought to develop near the sediment during stratification, where removal is by particle deposition only **(Talbot, 1984)**.

A scenario was optimized for Crystal Lake according to the parameters detailed in Appendix F by adjusting:

- Flux of settling particles F_S
- Pb-210 diffusion coefficient water-sediment k_{TS}
- Pb-210 emission to water E_W
- Po-210 diffusion coefficient sediment-water k_{TW}

3.3.4 BICKFORD POND

Benoit studies the 1982/83 data with a two-layer, first order model having an epilimnion accepting atmospheric and stream input, and a hypolimnion. Scavenging is the balance of in-growth, decay, and time-step concentration change, and additionally in the epilimnion inflow, precipitation, and outflow. Sedimentation is the balance of in-growth, scavenging, decay, and time-step concentration change, and additionally in the epilimnion inflow and outflow. Sedimentation in the hypolimnion also includes a term for input from epilimnion sedimentation. **(BENOIT, 1987)**

Studies during intervening years reveal that anoxic conditions were typical, and comprehensive data in 1985/86 shows an increase in Pb-210 and Po-210 concentrations. Benoit analyzes these data with more detailed models **(BENOIT, 1990)**.

A scenario was optimized for Bickford Pond according to the parameters detailed in Appendix G by adjusting:

- Flux of settling particles F_S
- Ra-226 diffusion coefficient water-sediment k_{TS}
- Pb-210 diffusion coefficient sediment-water k_{TW}
- Pb-210 emission to water E_W
- Po-210 diffusion coefficient sediment-water k_{TW}

3.3.5 CLINTON RIVER

A scenario was optimized for Clinton River according to the parameters detailed in Appendix H by adjusting the Ra-226, Pb-210 and Po-210 emissions to water E_W.

3.4 RESULTS

Table 18 shows the sediment distribution coefficient K_d values determined by the optimization process and those from the literature that were used as reference guides during the optimization process. The Pb-210 and Po-210 values cover a relatively narrow range, representing field measurements at Perch Lake, Ontario and nearby Maskinonge Lake, and laboratory conditions simulating Perch Lake and the local stretch of the Ottawa River **(WANG, 1993)**. The Ra-226 model optimization set Pb-210 and Po-210 sediment distribution coefficients K_d for Crystal Lake and Bickford Pond about an order of magnitude above the reference values. The Pb-210 and Po-210 sediment distribution coefficients K_d set for Clinton River were marginally below the reference values. Among the Ra-226 sediment distribution coefficients K_d, only the Bickford Pond value was set outside the reference range, higher by an order of magnitude. Table 19 shows that the Clinton

River Pb-210 and Po-210 SPM distribution coefficients K_p were out of the reference range, being lower by an order of magnitude.

Table 18. Sediment distribution coefficients – model and literature

Sediment K_d ($L \cdot kg^{-1}$)	Ra-226	Pb-210	Po-210
Crystal Lake (section 3.4.1, Appendix F)	6.6E+03	1.8E+06	2.6E+06
Bickford Pond (section 3.4.2, Appendix G)	7.5E+04	1.5E+06	1.6E+06
Clinton River (section 3.4.3, Appendix H)	7.9E+03	4.4E+04	5.8E+04
literature - lower	3.0E+02[10]	6.7E+04[11]	1.3E+05[11]
literature - upper	7.9E+03[12]	1.3E+05[11]	3.8E+05[11]

Table 19. SPM distribution coefficients –model and literature

SPM K_p ($L \cdot kg^{-1}$)	Ra-226	Pb-210	Po-210
Crystal Lake (section 3.4.1, Appendix F)	7.9E+03[13]	3.1E+06	3.9E+06
Bickford Pond (section 3.4.2, Appendix G)		2.8E+06	1.5E+06
Clinton River (section 3.4.3, Appendix H)		5.4E+04	7.5E+04
literature – lower		5.4E+05[11]	6.8E+05[11]
literature - upper		5.6E+06[11]	6.1E+06[11]

3.4.1 CRYSTAL LAKE

Figure 4 shows the process diagram for Crystal Lake from the optimization detailed in Appendix F. The settling flux F_S was adjusted to set the contribution by Ra-226 decay to Pb-210 water column inputs at 3% as estimated in the original study **(TALBOT, 1984)**. Then the Pb-210 water-sediment diffusion coefficient k_{TS2} and emission to water E_{W2} were adjusted to set the net water-sediment flux (accounting for the Table A-2 settling and diffusion process rates, $q_D+q_{TS}-q_{TW}$) to the sedimentation rate estimated in the original study, 1.73E-11 $mol \cdot h^{-1}$ **(TALBOT, 1984)**. Finally, the sediment-water diffusion coefficient k_{TW3} was adjusted to make the input and output dissolved water concentration of Po-210 consistent.

[10] From *p.S343* **(MLJAČ, 1996)**
[11] From *Table 4* range of central values over Perch Lake & Maskinonge Lake **(WANG, 1993)**
[12] From *Table 3* & *Table 5* calculated geometric mean **(SANCHEZ, 1999)**
[13] From *Table 6* mode $Log_{10}(K_d)=3.9$ **(CIFFROY, 2009)**; scenario constraint

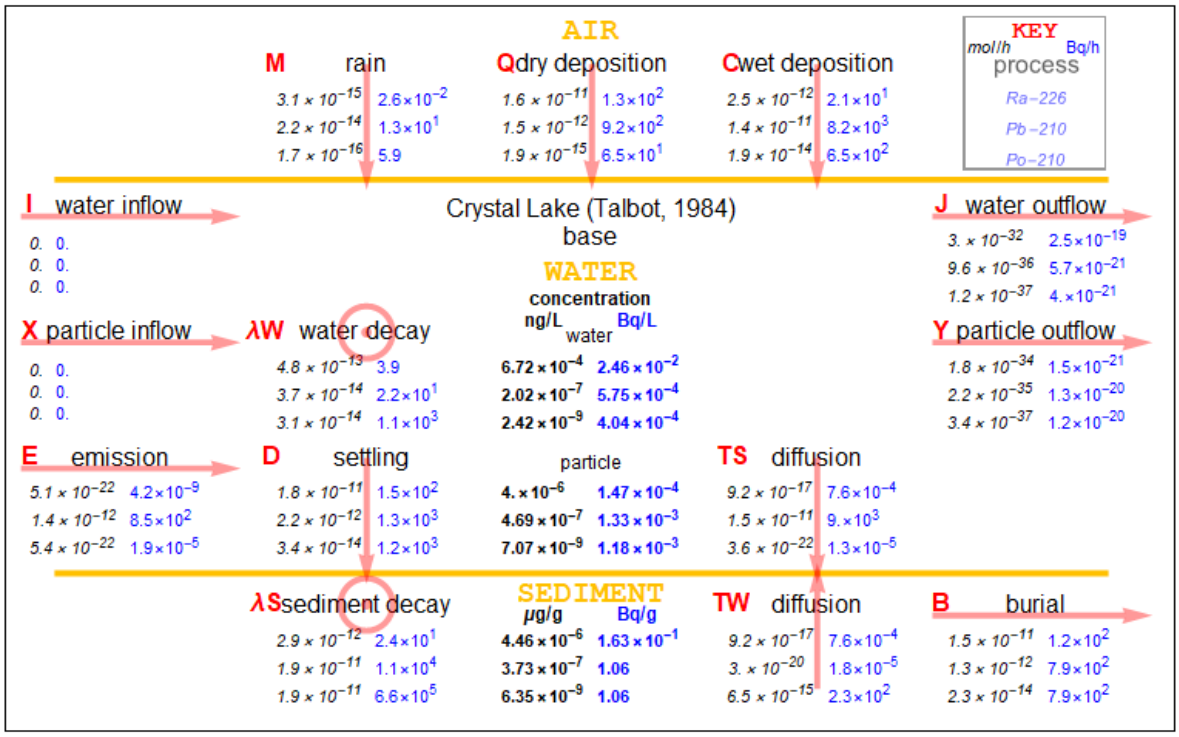

Figure 4. Crystal Lake process diagram

Table 20 shows the overall water process rates for each of the nuclides and contributions to input and output

Table 20. Crystal Lake water process rates and contributions

process	Ra-226		Pb-210		Po-210	
	mol·h^{-1}	%	mol·h^{-1}	%	mol·h^{-1}	%
Inflow	0	0	0	0	0	0
Atm. deposition	1.81E-11	100	1.54E-11	89	2.07E-14	36
Decay in	NA	NA	4.77E-13	3	3.67E-14	64
Emission	0	0	1.42E-12	8	0	0
Total in	1.81E-11	100	1.73E-11	100	5.75E-14	100
Outflow	0	0	0	0	0	0
Sedimentation	1.76E-11	97	1.73E-11	100	2.70E-14	47
Decay out	4.77E-13	3	3.67E-14	0	3.05E-14	53
Total out	1.81E-11	100	1.73E-11	100	5.75E-14	100

Table 20 demonstrates the ingrowth contribution to Pb-210 input (3%) and Pb-210 sedimentation rate (1.73E-11 mol·h^{-1}) constraints. The imposed 8% emission contribution to total Pb-210 input to water was a small contribution relative to the atmospheric input. Ingrowth contributes 64% of the Po-210 inputs, yielding a net

radioactive balance (ingrowth minus decay) of +11% of the rate of input or output. The balance was lost to sediment. Sedimentation accounts for 47% of the water column sink, representing 1.3 times the atmospheric deposition.

Table 21 shows the water column removal residence times to sediment reported in the Crystal Lake study **(TALBOT, 1984)(TANAKA, 1983)**, and the times calculated from the Ra-226 model for the Appendix F Crystal Lake scenario by Equation 53, τ_{TW}, and to all sinks by Equation 57, τ_T (including decay).

Table 21. Crystal Lake water residence times

removal residence time	Ra-226	Pb-210	Po-210
	y	d	d
study sedimentation **(TALBOT, 1984)**	NA	35	95
Ra-226 model by Eq. 53,τ_{TW}: sedimentation	62	25	225
Ra-226 model by Eq. 57,τ_T: all sinks	61	25	106

The Ra-226 model sedimentation residence time versus the study for Pb-210 was 71%, and for Po-210 was 240%.

3.4.2 BICKFORD POND

Figure 5 shows the process diagram for Bickford Pond from the optimization detailed in Appendix G. The flux of settling particles F_S and Pb-210 emission to water E_{W2} were adjusted to set the Pb-210 settling flux (accounting for the Table A-2 settling process rate, q_D) to the settling rate estimated in the original study, 7.69E-11 mol·h^{-1} (from the *Table III* average at 11.2 m, 1.65 dpm·cm^{-2}·a^{-1}) **(BENOIT, 1990)** and to make the input and output dissolved water concentration of Pb-210 consistent. The Ra-226 water-sediment diffusion coefficient k_{TS1} and Po-210 sediment-water diffusion coefficient k_{TW3} were adjusted to make the input and output dissolved water concentrations of Ra-226 and Pb-210 consistent.

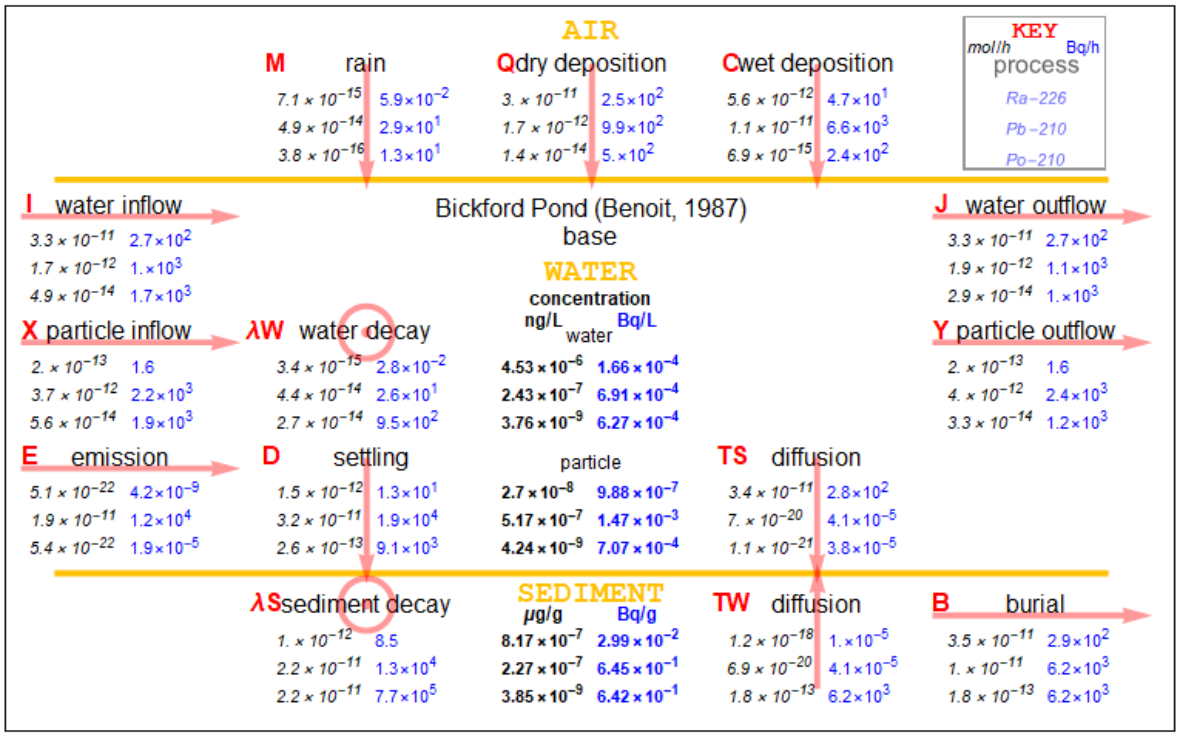

Figure 5. Bickford Pond process diagram

Table 22 shows the overall water process rates for each of the nuclides and contributions to input and output.

Table 22. Bickford Pond water process rates and contributions

process	Ra-226		Pb-210		Po-210	
	mol·h^{-1}	%	mol·h^{-1}	%	mol·h^{-1}	%
Inflow	3.31E-11	48	5.47E-12	15	1.05E-13	61
Atm. deposition	3.59E-11	52	1.28E-11	34	2.16E-14	13
Decay in	NA	NA	3.41E-15	0	4.41E-14	26
Emission	0	0	1.93E-11	51	0	0
Total in	6.90E-11	100	3.76E-11	100	1.70E-13	100
Outflow	3.31E-11	48	5.95E-12	16	6.25E-14	37
Sedimentation	3.58E-11	52	3.16E-11	84	8.07E-14	47
Decay out	3.41E-15	0	4.41E-14	0	2.73E-14	16
Total out	6.90E-11	100	3.76E-11	100	1.70E-13	100

The flux of settling particles F_S was adjusted for Pb-210, in contrast to the Crystal Lake scenario for which F_S was adjusted for Ra-226. Table 22 shows that substantial emission to water E_{W2} was required to supply Pb-210 to meet the Pb-210 settling process rate constraint, comprising 51% of the Pb-210 water

column inputs. The resulting Pb-210 sedimentation contribution was predominant at 84%. Only 15% of the scenario inputs were due to the water inflow concentration, and 34% due to atmospheric deposition. Benoit concludes that streams supply (from groundwater) half of the Pb-210 inputs to Bickford Pond **(BENOIT, 1987)**. Discounting emission, only one-third of the scenario input was due to inflow.

Table 22 shows that scenario Po-210 sources were very similar to those determined in the original study, for which epilimnion contributions are 63% by stream, 5% by atmosphere, and 32% by in-growth from Pb-210 **(BENOIT, 1987)**. Scenario Po-210 losses were marginally different from the study, for outflow at 37% versus 53%, and for sedimentation at 47% versus 32%. The scenario Pb-210 ingrowth by decay contribution to Po-210 was similar to the original study at 13% versus 15% **(BENOIT, 1987)**.

Table 23 shows the water column removal times reported in the Bickford Pond study for scavenging (partition to settling particles) and sedimentation, and the time calculated from the Ra-226 model for the Appendix G Bickford Pond scenario by Equation 53, τ_{TW}, and to all sinks by Equation 57, τ_T (including decay).

Table 23. Bickford Pond water residence times

removal residence time	Ra-226	Pb-210	Po-210
	d	d	d
study scavenging **(BENOIT, 1987)**	NA	39	85
study sedimentation **(BENOIT, 1987)**	NA	41	50
Ra-226 model by Eq. 53, τ_{TW}: sedimentation	80	16	68
Ra-226 model by Eq. 57, τ_T: all sinks	42	14	32

The scavenging process was not a feature of the Ra-226 model; phase partitioning was implicit, determined by the SPM distribution coefficient K_p. The scenario Pb-210/Po-210 activity ratios for dissolved and SPM water concentrations were 1.1 and 2.1, versus near 1 and 1.7 found in the 1982/83 study **(BENOIT, 1987)**. The scenario Pb-210/Po-210 activity ratio of sedimentary flux was 2.1, versus 2.4 determined from the 1985/86 study data **(BENOIT, 1990)**.

3.4.3 CLINTON RIVER

Figure 6 shows the process diagram for Clinton River from the optimization detailed in Appendix H. Emissions E_W for each of the nuclides were set and sediment concentrations adjusted to make the input and output water concentrations consistent.

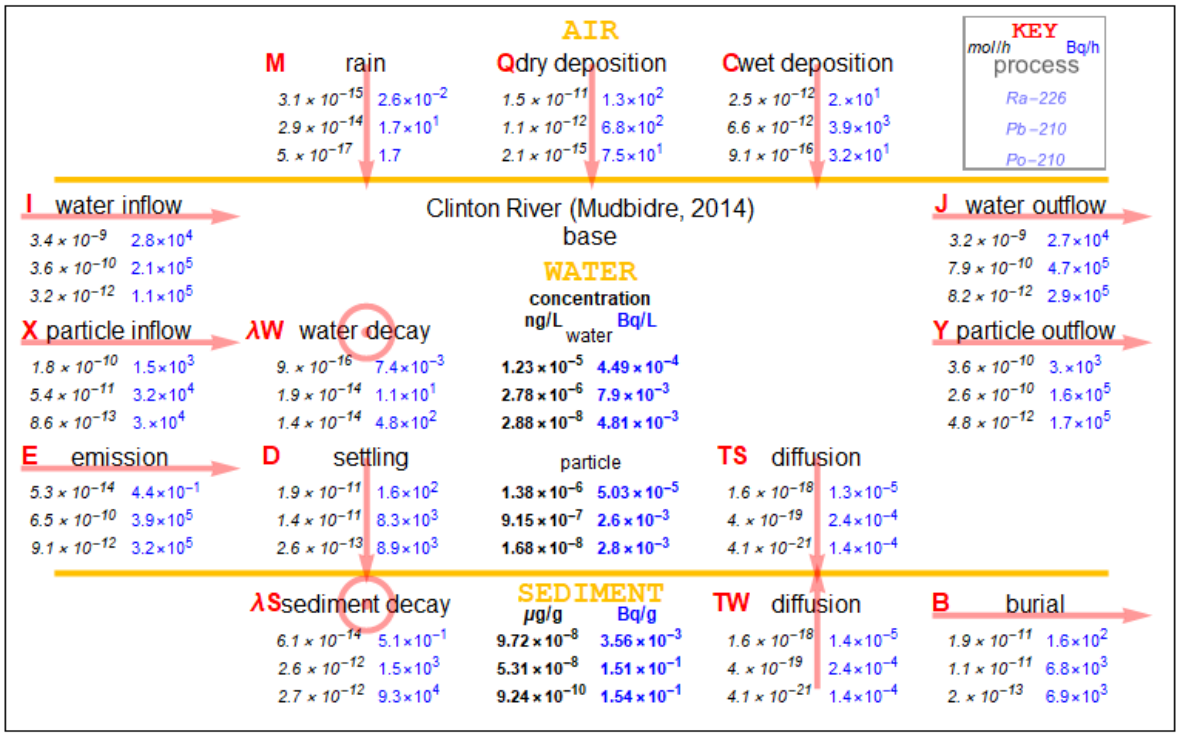

Figure 6. Clinton River process diagram

The SPM distribution coefficients K_p were fixed by the assumed dissolved and SPM water concentrations. The sediment distribution coefficients K_d were determined by the adjusted (set) emission values to water and resulting sediment concentrations. Table 24 shows the overall water process rates for each of the nuclides and contributions to input and output.

Ra-226 was not a subject of the original study **(MUDBIDRE, 2014)**, but the Ra-226 model was nearly satisfied with the assumed inflow concentration, requiring only a small emission value. Significant emissions were required for Pb-210 and Po-210, amounting to 61% and 69% of the inputs respectively. The balance of inputs was made up almost entirely of inflow. Notably the ingrowth to Po-210 by Pb-210 decay was not significant. Despite a large assumed settling flux of 3.6 $g \cdot m^{-2} \cdot d^{-1}$ (Table H-1), the settling rate represents about 1% and 2% of the water column output for Pb-210 and Po-210. The losses for each nuclide were almost entirely by outflow.

Table 25 shows the water column removal times from the Ra-226 model for the Appendix H Clinton River scenario by Equation 53, τ_{TW}, and to all sinks by Equation 57, τ_T (including decay).

Table 24. Clinton River water process rates and contributions

process	Ra-226		Pb-210		Po-210	
	$mol \cdot h^{-1}$	%	$mol \cdot h^{-1}$	%	$mol \cdot h^{-1}$	%
Inflow	3.61E-09	100	4.11E-10	39	4.09E-12	31
Atm. deposition	1.76E-11	0	7.77E-12	1	3.10E-15	0
Decay in	NA	NA	8.96E-16	0	1.88E-14	0
Emission	5.30E-14	0	6.47E-10	61	9.13E-12	69
Total in	3.63E-09	100	1.07E-09	100	1.32E-11	100
Outflow	3.61E-09	99	1.05E-09	99	1.30E-11	98
Sedimentation	1.94E-11	1	1.39E-11	1	2.55E-13	2
Decay out	8.96E-16	0	1.88E-14	0	1.36E-14	0
Total out	3.63E-09	100	1.07E-09	100	1.32E-11	100

Table 25. Clinton River water residence times

removal residence time	Ra-226	Pb-210	Po-210
	d	d	d
Ra-226 model by Eq. 53, τ_{TW}: sedimentation	39	16	11
Ra-226 model by Eq. 57, τ_T: all sinks	0.21	0.21	0.21

The residence times of each of the nuclides was about 5 h along the assumed 10 km stretch of Clinton River, driven by flow throughput. The sedimentation residence times were on the order of days. The Ra-226 and Po-210 residence times by sedimentation were shorter than those determined for Bickford Pond (Table 23), but the Pb-210 time was similar.

3.5 DISCUSSION

Both Crystal Lake and Bickford Pond are dimictic, completing two cycles of thermal layering and mixing annually **(TALBOT, 1984)(BENOIT, 1987)**. These cycles create variation in lake processes and may introduce bias in a steady-state model.

Single settling particle rate and SPM concentration values apply to all the Ra-226 model nuclides. Differentiation in the nuclide settling rates was controlled by the SPM distribution coefficients. Optimization sets the particle settling rates in decay sequence order: Ra-226, Pb-210, and Po-210 (section 3.3.2). This was convenient since the Ra-226 model was optimized manually, and the sequence avoids iteration to reset Pb-210 or Po-210 parameters due to decay ingrowth. This ideal procedure was possible for the Crystal Lake scenario since the constraint for net Pb-210 sediment flux included both settling and diffusion, and the Pb-210 diffusion coefficient could be adjusted after particle settling flux had been set by considering only Ra-226. However, since the Bickford Pond scenario was constrained by only the Pb-210 settling rate, the particle settling rate was set by considering it, and

some iteration was necessary to establish the Ra-226 diffusion coefficient. But this was not difficult since the long half-life of Ra-226 makes ingrowth a minor contribution to Pb-210 input. The particle settling flux was a fixed input in the Clinton River scenario.

Atmospheric deposition accounted for 85% of the Pb-210 supplied to the water column of Lake 239 of the Experimental Lakes Area, ON **(BRUNSKILL, 1987)**, which is a 57 ha headwater lake with a 418 ha catchment and an outflow **(NATURAL RESOURCES CANADA, 2000)**. The contributions to Pb-210 from atmospheric deposition was for the Crystal Lake scenario 89%, which may have been up to 97% if seasonal deposition had been considered, and for the Bickford Pond scenario 15%. The contribution from atmospheric deposition to Lake 239 inputs of Pb-210 was closer to Crystal Lake than to Bickford Pond.

The Crystal Lake scenario concentration of Pb-210 in the water column gave a decay rate of 22 $Bq \cdot h^{-1}$ (3.67E-14 $mol \cdot h^{-1}$), or 64% of the total when combined, consistent with the original study estimate that the primary source of Po-210 in the lake was decay **(TALBOT, 1984)**. The author of the Bickford Pond study found that 32% of the water column Po-210 was by ingrowth from Pb-210 decay **(BENOIT, 1987)**. The Bickford Pond scenario found that this contribution was 26%.

Water phase partitioning was implicit in the Ra-226 model, determined by the nuclide-specific SPM distribution coefficients K_p. In contrast the detailed study time-series models wrote explicit terms for transfer between the phases **(TALBOT, 1984)(BENOIT, 1987)(BENOIT, 1990)**, and estimated the process using detailed study data.

3.5.1 CRYSTAL LAKE

Talbot attributes the discrepancy between the study assumptions for atmospheric deposition of Pb-210 and sedimentation to measurement bias, due to either annual variation in atmospheric deposition or winter deposition escaping measurement **(TALBOT, 1984)**. An emission rate was set during optimization for the difference.

Talbot assigns atmospheric deposition of Pb-210 to the dissolved phase, giving consideration to solubility and pH **(TALBOT, 1984)**. The Ra-226 model represented phase partitioning through the SPM distribution coefficient, established by the effective concentrations assumed. For this to be a source of error in the Ra-226 model, SPM adsorption sites would have to be limiting, but this is less likely in a freshwater than in a marine system. In coastal waters, Pb-210 is scavenged faster than in the open ocean due to higher SPM concentration **(THENG, 2005)**.

Table 21 reports removal residence times for Crystal Lake. The time-averaged residence times calculated in the original study model were 35 d for Pb-210 and 95 d for Po-210. Talbot suggests that the rate is affected by biologically-mediated removal **(TALBOT, 1984)**. The removal residence times to sediment found by the Ra-226 model using Equation 53 were 25 d and 106 d, respectively. The Ra-226

model was optimized using the sedimentation rate reported from sediment core measurements at 1.73E-11 $mol \cdot h^{-1}$ (0.79 $pCi \cdot cm^{-2} \cdot a^{-1}$), which was found to be close to the value calculated from the model in the original study, 1.80E-11 $mol \cdot h^{-1}$ (0.82 $pCi \cdot cm^{-2} \cdot a^{-1}$) **(TALBOT, 1984)**. Since the Ra-226 model was constrained to the study sedimentation rate, the ratio of residence times, 25 d / 35 d, suggests that the Ra-226 model water activity concentration was 70% of the effective concentration of the original study model.

The Ra-226 model Po-210 removal residence time to sediment was found from Equation 53 at 225 d, and the removal residence time to all sinks was found from Equation 57 at 106 d, the difference between which was due to the radioactive decay term. The detailed study model showed removal intervals coinciding with spring and summer plankton blooms having a removal flux of 0.26 $Bq \cdot m^{-2} \cdot d^{-1}$ (0.26 $pCi \cdot cm^{-2} \cdot a^{-1}$). These episodes are interspersed by intervals of release flux of 0.070 $Bq \cdot m^{-2} \cdot d^{-1}$ (0.069 $pCi \cdot cm^{-2} \cdot a^{-1}$) enabled by seasonal redox cycling through Fe and Mn release from sediments, resulting in a mean removal flux of 0.13 $Bq \cdot m^{-2} \cdot d^{-1}$ (0.13 $pCi \cdot cm^{-2} \cdot a^{-1}$), representing one-sixth or 17% of the Pb-210 sedimentation flux **(TALBOT, 1984)**. The mean flux is low relative to that suggested by other studies in Table 14. It represents a sedimentation rate of 1700 $Bq \cdot h^{-1}$, relative to the Ra-226 model rate of 945 $Bq \cdot h^{-1}$. Accounting for this discrepancy in sedimentation rate, the Ra-226 model water activity concentration was (225 d / 95 d) x (945 $Bq \cdot h^{-1}$ / 1700 $Bq \cdot h^{-1}$) = 130% of the effective concentration implied by the original study model. The relative sedimentation rates do not fully account for the discrepancy in removal times to sediment. The Ra-226 model implies an overestimate in Po-210 concentration that contrasts with the underestimate in Pb-210 concentration. These discrepancies may be due in part to the time-average method of time constant calculation in the original model **(TALBOT, 1984)**. However, it likely also suggests limitation of the single-compartment, steady-state model relative to the two-layer, time step model applied to the detailed data in the original study. Talbot suggests that sediment accumulation flux is uncertain by up to 20% error due to sediment anisotropy, driven by bioturbation and sediment focusing, and that the focusing would be enhanced in the deepest part of the lake by higher organic matter content driving Pb-210 uptake **(TALBOT, 1984)**.

3.5.2 BICKFORD POND

Benoit notices little variation in Pb-210 and Po-210 in phase concentration, including lake depth, and in inflow concentration **(BENOIT, 1987)**. The finding may be due to greater mixing bytributary and drainage flow and diminish the utility of a layered model. The discrepancies apparent between the Ra-226 model and study sedimentation rates in the Crystal Lake scenario may not affect the Bickford Pond scenario to the same extent. Detailed study data indicates the SPM-adsorbed Pb-210/Po-210 ratio was 1.7 and the settling ratio was 3.9, arguing against simple gravitational settling **(BENOIT, 1987)**. These ratios were both 2.1 in the Bickford Pond scenario, demonstrating that a single particle settling rate does not represent

such detail. Considering diffusion of Po-210 from sediment to water, the Ra-226 model rate of Pb-210 settling was 6.7 times the rate of Po-210 settling.

The Ra-226 model showed that the emission rate to water assigned for Pb-210 was 1.1 times the total of atmospheric deposition and inflow initially assumed. Benoit finds that Pb-210 inputs were split evenly between atmospheric deposition and inflow, and the output were split evenly between sedimentation and outflow. The Ra-226 model found that the assigned emission rate of Pb-210 to water amounted to 51% of total input and 66% when combined with inflow; 84% of the sinks were to sediment.

Benoit calculates Pb-210 removal residence times for scavenging (dissolved to SPM phase) of 39 d and for sedimentation of 41 d, and Po-210 removal residence times for scavenging of 85 d and for sedimentation of 50 d **(BENOIT, 1987)**. Scavenging appears to be limiting for Po-210, but not for Pb-210. Despite this, the study Pb-210 removal time to sediment is 2.6 times the 16 days that was found by the Ra-226 model. The sediment trap measurements that provide the sedimentation rate for the scenario may not reflect the actual rate to the sediment due to recycling and/or diffusion. Benoit concludes from sediment trap data that there was no significant Pb-210 diffusion to sediment, but found it likely that Pb-210 (and Po-210) is released from sediment, associated with low dissolved oxygen and elevated Fe concentrations **(BENOIT, 1987)**. There is likely diffusion of Pb-210 out of the sediment accounting for at least some of discrepancy between the Ra-226 model and the original study removal times to sediment. Despite a relatively high hydrologic flushing rate of 4.2 a^{-1}, the proportion of Pb-210 to sediment is 84%.

Balistrieri studies the larger, deeper Lake Sammamish, Washington, having more sulfidic anoxic periods compared to Bickford Pond. That study shows stronger evidence of both Pb-210 and Po-210 diffusion into and out of the sediment, accompanied by lower concentrations of SPM and the nuclides **(BALISTRIERI, 1995)**. Sediment recycling could account for the emissions that were added in the Ra-226 model to satisfy the imposed sedimentation rate constraint. Account for seasonal variation of Po-210 in a study of the 81-ha, 12-m deep Pond B, South Carolina suggests that the input accounts for only about 5% of the mobile sediment inventory, but similar variation is not observed for Pb-210 **(KIM, 2005)**. Pb-210 and Fe show strong mobility correlation; release differentiation between the nuclides may be enhanced by apparent similarity in Po-210 and Mn redox potential **(BENOIT, 1990)**. Hypolimnion association of Po-210 and Mn is also evident in the Lake Sammamish study, creating a steep concentration gradient during stratification **(BALISTRIERI, 1995)**. Sediment exchange may explain some of the apparent deficit of Pb-210 in the Bickford Pond scenario, but the explanation is not as well supported as it would be for Po-210.

Benoit concludes that stream surface area could not supply the measured tributary activity concentrations, since rainfall runoff should result in pulsed concentrations and biota regulation result in seasonal differences. The Bickford Pond tributary

watershed and rainfall imply that the maximum average runoff rate is 62% of the average tributary flow rate, and the average rainfall concentration is 35 times the average total tributary concentration **(BENOIT, 1987)**. A significant portion of the Pb-210 concentration in the tributaries may be delivered from a stock of Pb-210 partitioned in watershed soil. The following paragraphs detail analysis of the model results to sources in the watershed.

The watershed "input-output" equation is **(DOMINIK, 1987)**:

$$q_{WA} - I_W \cdot \left(\lambda + \frac{1}{\tau_W}\right) = 0 \tag{55}$$

where

q_{WA} = atmospheric deposition to the watershed [N·T^{-1}]

I_W = watershed inventory [N]

λ = decay constant [T^{-1}]

τ_W = watershed mean erosional residence time

The watershed erosional runoff q_{WR} [N·T^{-1}] is **(DOMINIK, 1987)**:

$$q_{WR} = \frac{I_W}{\tau_W} \tag{56}$$

The watershed mean erosional residence time is from Equation 55 and 56 **(DOMINIK, 1987)**:

$$\tau_W = \frac{q_{WA} - q_{WR}}{\lambda \cdot q_{WR}} \tag{57}$$

The fraction of watershed input to the water body f_C is from Equation I.3:

$$f_C = \frac{q_{WR}}{q_{WA}} \tag{58}$$

The watershed mean erosional residence time considering the Ra-226 model Pb-210 atmospheric deposition rate to the 760 ha and 770 ha tributary watersheds, accounting only for the inflow determined from the original study data **(BENOIT, 1987)** was from Equation 57 τ_W = 1870 y, and accounting for the inflow and Ra-226 model emission term was τ_W = 390 y. These represented from Equation 58 watershed fractions to lake f_C = 1.7% and f_C = 7.6% respectively. Some of the emission assigned in the Ra-226 model fitting may represent runoff. The steep local topography may enhance watershed input: the terrain rises almost 300 m vertically over 2900 m eastwards to Mount Wachusett.

3.5.3 CLINTON RIVER

SPM concentration and Pb-210 and Po-210 activities approximately double along the measured length of the Clinton River **(MUDBIDRE, 2014)**. The Clinton River drains a watershed area of 1980 km^2 containing suburban areas **(MUDBIDRE, 2014)**. About 1200 km^2 falls between inflow sampling location (labelled *CR6*) and Lake St Clair, of which about 500 km^2 is suburban area having a high proportion of hard surfaces.

The Ra-226 and Pb-210 inventories I_W represent potential ingrowth sources within the watershed for Pb-210 and Po-210, respectively. Ra-226 was disregarded on the basis that the physical form would be derived from atmospherically entrained particles that would mostly keep decay products locked in a mineral matrix once deposited in the watershed. In contrast, Pb-210 originates from Rn-222 decay and would be adsorbed to microparticles and relatively mobile in the watershed.

Equation 55 was modified to represent Po-210 ingrowth from the watershed inventory of Pb-210:

$$q_{WA.Po} + I_{W.Pb} \cdot \lambda_{Pb} - I_{W.Po} \cdot \left(\lambda_{Po} + \frac{1}{\tau_{W.Po}}\right) = 0 \qquad (59)$$

where

$q_{WA.Po}$ = Po-210 atmospheric deposition to the watershed [N·T^{-1}]

$I_{W.Pb}$ = Pb-210 watershed inventory [N]

$I_{W.Po}$ = Po-210 watershed inventory [N]

λ_{Pb} = Pb-210 decay constant [T^{-1}]

λ_{Po} = Po-210 decay constant [T^{-1}]

$\tau_{W.Po}$ = Po-210 watershed mean erosional residence time

Equation 58 was modified to represent the fraction of watershed Po-210 input to the river $f_{C.Po}$ from both atmospheric deposition and ingrowth from the watershed inventory of Pb-210:

$$f_{C.Po} = \frac{q_{WR.Po}}{q_{WA.Po} + I_{W.Pb} \cdot \lambda_{Pb}} \qquad (60)$$

Table 26 shows the result of watershed source calculations by applying Equation 55 to Ra-226 and Pb-210, and Equation 59 to Po-210 to account for ingrowth. Ra-226 model emissions E_W, and atmospheric deposition (rain q_M, wet q_Q, and dry q_C) applied to the watershed area as q_{WA} were used to calculate the fraction of watershed inputs to the river f_C from Equation 58 (Equation 60 for Po-210 to account for ingrowth). The watershed mean erosion residence time τ_W was

calculated from Equation 57, and the watershed inventory I_W was calculated from Equation 56.

Table 26. Clinton River Ra-226 model inputs and watershed residence times

nuclide	river		watershed			
	emission E_W (mol·h^{-1})	deposition $q_M+q_Q+q_C$ (mol·h^{-1})	deposition q_{WA} (mol·h^{-1})	fraction f_c (%)	res. time τ_W (y)	inventory I_W (mol)
Ra-226	5.3E-14	1.8E-11	7.0E-08	8E-5	3E+9	1.4E+00
Pb-210	6.5E-10	7.8E-12	3.1E-08	2.1	1510	8.5E-03
Po-210	9.1E-12	3.1E-15	1.2E-11	0.03	1820	1.5E-04

Most atmospherically supplied Pb-210 is trapped in organic rich soils **(TUREKIAN, 1977)**. Pb-210 is measured to have a watershed residence time of 6200 y in the Ottawa River watershed soil **(JOSHI, 1990)** and 1400 y in the Rhone watershed Switzerland **(DOMINIK, 1987)**. Precipitation runoff from the hard surface suburban areas does not appear to have a major influence on the Pb-210 erosional residence time. Table 26 shows that the mean erosional residence times of Po-210 and Pb-210 were similar. The Pb-210 and Po-210 inventories reflected radioactive equilibrium in the watershed. The watershed inventory of Po-210 was almost completely from Pb-210 ingrowth. The Ra-226 model Po-210/Pb-210 emission activity ratio was 71% (Table 24). The fraction of watershed Pb-210 to the river was almost 100 times that of Po-210. The results suggest that partitioning in the watershed of Po-210 is greater than of Pb-210.

3.6 CONCLUSION

The Crystal Lake scenario removal times to sediment underestimate by 30% for Pb-210 and overestimate by 30% for Po-210 the times estimated in the original study **(TALBOT, 1984)**. A two-layer lake model may reduce some of this error.

The Bickford Pond scenario constrained by sediment trap measurements **(BENOIT, 1987)** suggests significant diffusion recycling of Pb-210 from the sediment to water, runoff input from the watershed, or both.

The source of Pb-210 emission to Clinton River found by the Ra-226 model fitting procedure may be due runoff of atmospheric deposition to the watershed, but the large proportion of suburban area in the watershed does not appear to strongly influence the runoff transport. The source of Po-210 could be explained by Pb-210 ingrowth of the inventory partitioned in the watershed from atmospheric deposition.

3.7 FUTURE WORK

Crystal scenario could be studied further by adapting the Hamilton Harbour model applied to lead (Appendix B and Appendix C) for water stratification into epilimnion and hypolimnion. The model could better represent chemical properties, atmospheric deposition, settling and redox recycling.

4 Radium series in freshwater

4.1 INTRODUCTION

Chapter 3 documented the development and application of a partitioning aquivalence (fugacity) model to the Ra-226 decay series including Pb-210 and Po-210. Volatility of the species was demonstrated to be insignificant relative to other system processes and was neglected. The Ra-226 model was formulated to calculate process rates and concentrations, as are the QWASI models. Availability of some water concentration and sedimentation data required the Ra-226 model fitting procedure to predict particle settling, atmospheric deposition, diffusion or emission instead. Information was triaged during setup, from available measurements, to parameters easily inferred, to those less certain that were assumed from literature and subsequently adjusted. Each lake featured a unique set of information detailed in the appendices.

The Ra-226 model was applied to a set of lakes in the Ottawa River watershed that were the subject of a previous study **(CORNETT, 1984)**, and to a northern lake in Nunavut **(GUERIN, 2012)**. Sediment data were available for both studies. During July 2016 a set of water samples was collected from streams in the Ottawa River watershed and measured for Pb-210 and Po-210, which informed the water concentration assumptions for the application to the Ottawa River watershed lakes.

The Ra-226 model developed in Chapter 3 was applied to investigate two hypotheses:

1. The proportions of Pb-210 input lost to the sediment of the Laurentian study lakes are as determined in the original study **(CORNETT, 1984)**.

2. The watershed contributes to Pb-210 and Po-120 in the water and sediment of Judge Sissons Lake **(GUERIN, 2012)**.

4.1.1 LAKE STUDIES

4.1.1.1 *LAURENTIAN LAKES*

The study area is in the Ottawa River valley near Chalk River Laboratories, Ontario, having seven lakes located between 45°40′N and 46°00′N and between 77°10′W and 77°30′W. The lakes were chosen to represent a diversity of physical, chemical and hydrologic characteristics. The catchments rest on Precambrian granite having deposits of glacial till, aeolian or fluvial sands and peat wetlands. Surficial litter and humus overlay fine to medium sand. Pb-210 is measured from lake sediment cores. Sediment concentrations are not correlated with lake depth, which is attributed to lack of redistribution focusing caused by relatively shallow depth and littoral vegetation **(CORNETT, 1984)**.

In the original study, areal distribution of Pb-210 measured in the lake sediment is relatively uniform. Pb-210 is measured in the top 12 cm of sediment. Sediment

flux is determined by equating it to radioactive decay losses determined by the difference between the concentration at the top of the core and the concentration of Ra-226 measured at the bottom of the core, assumed to be in equilibrium with Pb-210 at background **(CORNETT, 1984)**. Table I-6 lists these sediment fluxes that were used as initial values in the optimizations for each lake.

Measurements from soil cores at two nearby locations were used to estimate atmospheric deposition. All lakes except Otterson Lake are headwaters **(CORNETT, 1984)**. Study limnological properties listed in Table I-2 are drainage area, lake area, average depth, dissolved organic carbon, and particulate organic carbon.

4.1.1.2 *JUDGE SISSONS LAKE*

Kiggavik was a proposed uranium mine in the Kivalliq region of Nunavut, Canada, about 80 km west of Baker Lake. Monitoring of waterways is conducted over several years to make measurements including water and sediment concentrations of Ra-226, Pb-210 and Po-210. Judge Sissons Lake is the largest lake adjacent to the project site, receiving water from headwater lakes at the proposed mines. Most tributary streams in the watershed are less than 1 m deep and frozen to the bottom during the winter. These streams become active in the spring and reach peak level and volumetric flow in mid-June. The regional terrain is flat or gently sloping with frequent bedrock outcrops. Surficial deposits consist of thin organic soil underlain by glacial till. Vegetation is typical of the tundra: short shrubs, sedges and grasses, herbs, mosses and lichens. **(GUERIN, 2012)**.

Judge Sissons Lake is centred about 64°20′N, 97°30′W. It is 9550 ha in area, has a mean depth of 4.6 m, and is 20 m at the deepest. The lake drains a 705 km^2 watershed. Lake ice is measured at 1.8 m in May, which typically thaws by the end of June. Judge Sissons Lake sediment has nearly equal proportions of fine sand, very fine sand, silt and clay. A 1991 core sample shows sticky glacial clay with no soft organic sediment and suggested sporadic deposition. Dissolved oxygen near the sediment is measured to be 0.3 $mg \cdot L^{-1}$. Discharge peaks sharply at about 35 $m^3 \cdot s^{-1}$ at the end of June **(AREVA, 2011B)**.

4.1.2 STREAM SAMPLES

Sediment from seven (Laurentian study) lakes in the Ottawa River watershed are sampled and measured to determine sedimentation flux and estimate the input contribution from atmospheric deposition **(CORNETT, 1984)**.

Water from streams surrounding the Laurentian study lakes were sampled for measurement of Pb-210 and Po-210. The locations were selected to balance proximity and range of watershed geology. Samples were collected in three sets in 2016 July, September and November from the Ottawa River and Gull River watersheds in eastern Ontario.

4.2 METHOD

4.2.1 OPTIMIZATION

The Ra-226 model described in section 3.3.1 was applied to a study of Laurentian Shield lakes described in section 4.1.1.1 and to Judge Sissons Lake described in section 4.1.1.2. The optimization procedure detailed in section 3.3.2 was followed to identify and adjust parameter values including the input concentrations at each step to be consistent with the Ra-226 model output concentrations according to Equation 32.

In the Laurentian lakes scenarios, the input sediment concentrations C_{OS} were assigned initial estimates and adjusted, and other concentrations determined according to Table I-5. In the Kiggavik Judge Sissons Lake scenario, the sediment concentrations were assumed from measurements, and other input concentrations were determined according to Table J-9.

4.2.1.1 *LAURENTIAN LAKES*

For each of the Laurentian lakes, base scenarios 1 through 7 were optimized with total input water concentrations of Pb-210 and Po-210 assigned from the average of measurements at Grant Creek (section 4.3.3), the sample location closest to McSourley Lake, and five of the other lakes around Chalk River Laboratories. Although other sample locations are closer to Petznick Lake, the same total input water concentrations were chosen for a consistent analysis. Alternate scenarios 1B through 7B were optimized with total input water concentrations of Pb-210 and Po-210 assumed as twice the average of the Grant Creek measurements.

All Laurentian lakes scenarios were optimized according to the parameters detailed in Appendix I by adjusting:

- Ra-226, Pb-210 and Po-210 concentrations on sediment solids C_{OS}
- Pb-210 and Po-210 concentrations dissolved in water C_{OW2} and C_{OW3}
- Ra-226 and Pb-210 concentrations on aerosol C_{OA1} and C_{OA2}
- Pb-210 concentration in water inflow C_{OI}
- Flux of settling particles F_S
- Po-210 diffusion coefficient sediment-water k_{TW}

Initial values for the concentration of Pb-210 on aerosol and the flux of settling particles for each lake were estimated from the study soil and lake sediment core sample measurements, respectively. Initial Pb-210 concentration in water inflow was assumed from the study estimates of the watershed contributions. Taken together these assumptions resulted in excess Pb-210 within the water column for each lake: the Ra-226 model predicted higher water concentrations C_W relative to the input water concentration C_{OW} ($C_W/C_{OW} > 1$) within the assumed Table I-7

sediment distribution coefficient K_d range constraints. No input total water concentrations of Pb-210 C_{OWP2} could be assigned for any of the lakes near the range of expected concentrations (section 3.1.3.2) to satisfy the Ra-226 model constraint $C_W/C_{OW} = 1$. Instead, the scenarios were optimized by reducing Pb-210 inputs to the water column by decreasing:

- inflow concentration C_{OI}, and if reduced to 0:
- concentration on aerosol C_{OA}.

The rationale for this ordering was that there should be minimal variation in atmospheric deposition by lake area within the study region. In contrast, the contribution of Pb-210 from the watershed was considered less certain. For example, the residence time of Pb-210 in the Ottawa River watershed was estimated at 6200 a **(JOSHI, 1990)** and in the Rhone watershed Switzerland at 1400 a **(DOMINIK, 1987)**. Such watershed retention is long relative to the half-life of Pb-210, 22.2 a. Although the study watersheds are much smaller, the possibility of no significant watershed contribution from Pb-210 was assumed. This was really a matter of convenience and simplification of analysis, since the magnitude of net input rather than assignment to source term was relevant to the rest of the Ra-226 model. The assignment of inputs to source was considered in section 4.4.1.

4.2.1.2 *JUDGE SISSONS LAKE*

Since all 18 Judge Sisson Lake water measurements were below detection limit, the water activity concentrations were assumed from all 130 Kiggavik site water measurements, except the 8 representing locations of inflow to the lake. From the balance of 122 measurements, most were below detection limits. The estimates of the distribution means using the *elnormCensored* function from the *EnvStats* package for *R,* as lognormally distributed Type I censored data having values below a detection limit **(MILLARD, 2013)**, gave a Po-210/Pb-210 activity ratio of 0.27. More of the Pb-210 measurements were below detection (118) than Po-210 measurements (80), suggesting that the activity ratio may be higher, since the assumed lognormal distributions have an unbound lower limit. Similary, all the Pb-210 measurements and 3 out of 8 Po-210 measurements of samples from locations inflow to Judge Sissons Lake were below detection limit. (The *elnormCensored* function requires two measurements; two of the Pb-210 measurements were assigned to the detection limit.) The resulting Po-210/Pb-210 activity ratio was 0.38, which may be an underestimate by the same reasoning. However, all sediment measurements were of Judge Sissons Lake samples. Only 15 of the 30 Pb-210 measurements were below detection limit, and none of the Po-210 were below the detection limit. The estimated Po-210/Pb-210 ratio was 1.79, which may be another underestimate that would represent a greater excess of Po-210. A marginal excess of Po-210 is measured in the top 2 cm of sediment at two of three sampling stations in Quirke Lake, Ontario **(MCKEE, 1987)**.

One scenario was optimized for Judge Sissons Lake according to the parameters detailed in Appendix J by adjusting:

- Ra-226, Pb-210 and Po-210 water concentrations C_{OW}
- Ra-226 concentration on aerosols C_{OA1}
- Flux of settling particles F_S
- Po-210 emission to water E_{W3}
- Ra-226 and Pb-210 diffusion coefficients sediment-water k_{TW1} and k_{TW2}
- Po-210 diffusion coefficient water-sediment k_{TS3}

4.2.2 STREAM SAMPLES

4.2.2.1 *SAMPLING*

Water samples were collected in 3 sets in 2016. Set 1 samples were collected in July in duplicate from 11 streams in the western (Ontario) watershed of the Ottawa River from locations shown in Table 27. Situation of the sample location watersheds are indicated in Figure 7. Set 2 samples were collected from 5 of the set 1 locations in duplicate in September. Set 3 samples were collected from 9 locations along the Burnt River, Drag River, and Irondale River in the Gull River watershed near Minden, Ontario, and from 3 of the set 2 Ottawa River locations in duplicate in November. Set 2 and 3 measurements, indicated in Figure K-2 and Table K-12, were judged unreliable as explained in section 4.4.3.

Table 27. Ottawa River waterway set 1 sampling locations

sample	waterway	sampling location	
		latitude	longitude
1,2	Grant's Creek[1,2]	46°12′41″	77°55′34″
3,4	Pleasant Valley Creek[1,2]	45°46′08″	76°47′39″
5,6	Hurd's Creek[1]	45°32′24″	77°07′18″
7,8	Gull Creek	44°52′23″	76°51′57″
9,10	Egan Creek	45°04′01″	77°43′55″
11,12	Little Mississippi River[1]	45°14′21″	77°34′24″
13,14	Aylen River	45°35′12″	77°52′28″
15,16	Sherwood River	45°38′04″	77°34′18″
17,18	Carp River[1,2]	45°28′55″	76°13′19″
19,20	Constance Creek	45°27′07″	76°01′51″
20,21	McCrearys Creek	45°06′47″	76°12′34″

[1] resampled in duplicate 2016 September (set 2)

[2] resampled in duplicate 2016 November (set 3)

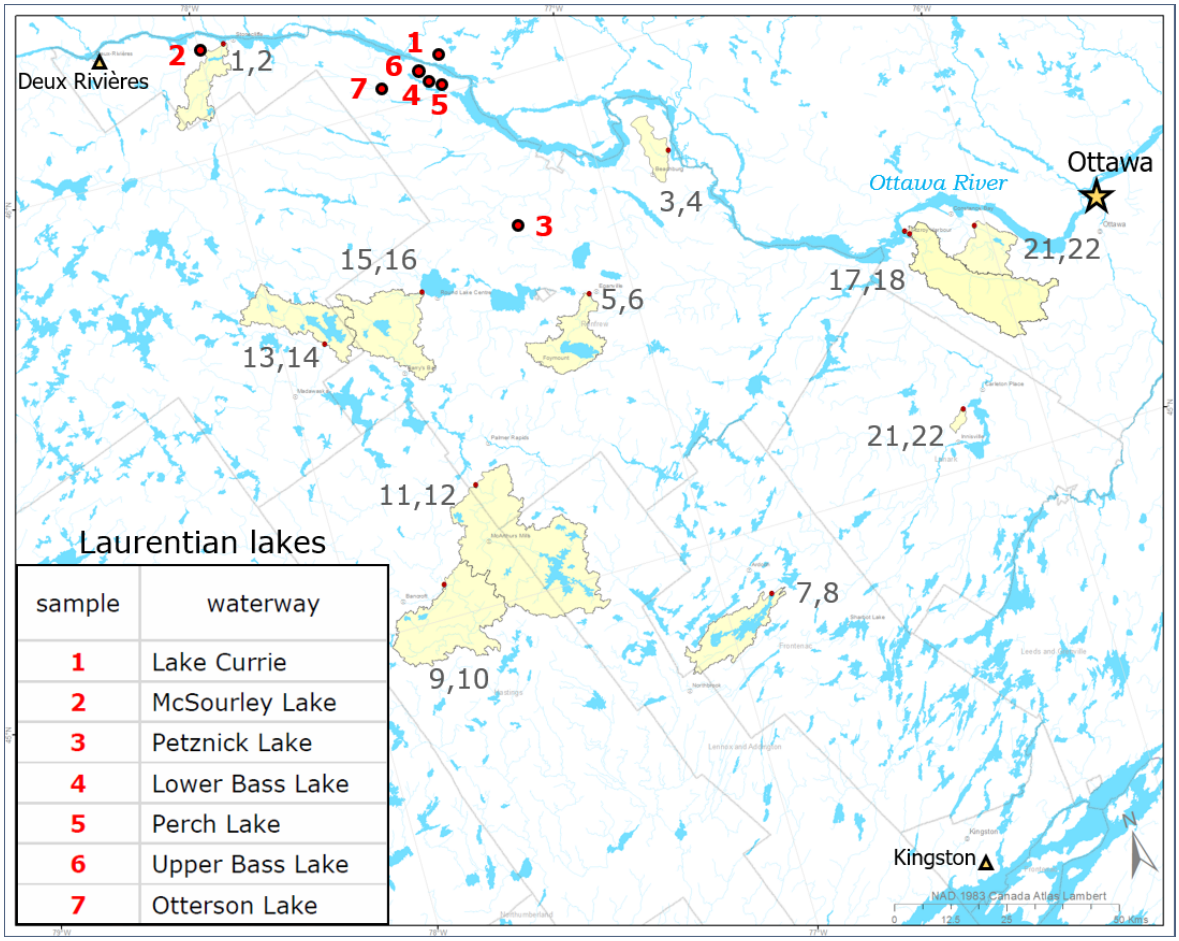

Figure 7. Ottawa River sample and Laurentian lakes **(CORNETT, 1984)** locations

Duplicate samples were collected in 20 L collapsible water containers and stabilized by adding 10-20 mL of 16 M HNO_3 to bring the pH in the range 2-3. The samples were weighed and filtered through coarse fiberglass cloth. The containers were sub-sampled and diluted 2:1 with 2% HNO_3 for ICP-MS.

The samples were pumped through columns packed with TrisKem MnO_2-PAN (polyacrylnitrile) Resin-B at about 1 $mL \cdot s^{-1}$. The resin was collected, dried, and analyzed separately for Cs-137 by gamma spectrometry as part of separate work. The post-column samples were sub-sampled, diluted 2:1 with 2% HNO_3, and together with the previous sub-samples, run on a Bruker Aurora M90 **(WANG, 2011)** ICP-MS by Lalonde laboratory personnel.

4.2.2.2 *PO-210 MEASUREMENT*

Samples were spiked with 100 µL of 1.86 $Bq \cdot L^{-1}$ Po-209 tracer for the determination of measurement efficiency (wet chemistry and alpha spectrometry), and 100 µL of 1 $g \cdot L^{-1}$ stable Pb to confirm precipitation yield. To each sample was added 2 mL of 44.73 $g \cdot L^{-1}$ Fe as $FeCl_3$ in 2% HNO_3. Sub-samples were extracted for ICP-MS. Between 20-50 mL 14.5 M NH_4OH was added to bring the pH of samples near 10 to

precipitate $Fe(OH)_2$. N_2 was bubbled through the sample containers for 10 minutes. The supernatant was pumped off and sub-sampled and run together with the previous sub-samples on the M90 ICP-MS by Lalonde laboratory personnel.

The preparations for Po-210 electrodeposition followed previous experience and principles **(SETHY, 2015)**. The precipitate was collected in 50 mL centrifuge tubes, to which was added 10 mL DI water and 1 mL 12 M HCl. The precipitate was dissolved and transferred to 60 mL glass vials, to which was added 16 M HNO_3 (making aqua regia). The vials were transferred to a hotplate at 120°C for 1 h. To the vials were added 10 mL of 12 M HCl, and 0.5 h allowed to pass before transfer to the hotplate at 120°C covered overnight. The covers were removed, and the vials left on the hotplate until the contents evaporated to 20 mL. The removed vials cooled and were transferred to 50 mL centrifuge tubes. The tubes were centrifuged at 3500 rpm for 20 minutes. The supernatant was transferred to 20 mL vials, which were placed on the hotplate at 120°C overnight to dryness. To the vials were added 2 mL of 12 M HCl, which were left on the hotplate to dryness. Another 2 mL of 12 M HCl were added to the vials, which were left on the hotplate to dryness. The vials were removed, to which 2 mL of 12 M HCl were added and caps applied pending electrodeposition preparation.

4.2.2.3 *ELECTRODEPOSITION*

The 20-mL vials were uncapped and placed on the hotplate at 80°C. A solution of 250 $g \cdot L^{-1}$ ascorbic acid was prepared in warm DI water, with which 0.8 mL was added to each vial. About 18 mL (to near full) of warm DI water was added to each vial. A silver planchet was placed in each vial, which were capped and placed on the hotplate at 95°C for 4 h. The planchets were removed, rinsed with acetone, mounted on paper, and transferred to a Canberra R7400 alpha spectrometer for counting by Lalonde laboratory personnel. The 20-mL vials were capped and stored. Separate counts of Pb-210 and Po-209 (to determine overall wet chemistry and detection apparatus efficiency) were made over intervals of 24-48 h.

4.2.2.4 *PB-210 MEASUREMENT*

After 18 weeks, allowing ingrowth of Po-210 to about one-half the equilibrium activity, 150 μL of 1.86 $Bq \cdot L^{-1}$ Po-209 tracer was added the 20-mL vials. The 20-mL vials were placed on the hotplate at 120°C and 2 mL of 16 M HNO_3 was added to each. The vials were covered Black precipitate (ascorbic polymer) lingered in the sample 1 vial, to which was added 0.7 mL of H_2O_2 solution. A further 2 mL of 16 M HNO_3 was added to each 20-mL vial, which were covered on the hotplate for 10 minutes. The 20-mL vial contents were transferred to 60 mL glass vials, and the 20-mL vials rinsed with 4 mL of 16 M HNO_3 to remove all black precipitate. The 60 mL glass vial contents and 2 mL of DI water rinse were transferred to the 20-mL vials, which were placed on the hotplate at 120°C for 5 h to dryness. To each vial was added 2 mL of 12 M HCl, and the electrodeposition procedure detailed in section 4.2.2.3 was followed to count Po-210 resulting from Pb-210 ingrowth.

4.3 RESULTS

4.3.1 LAURENTIAN LAKES

Following the sequence described in section 4.2.1.1, the inflow concentrations of Pb-210 for all scenarios (except Otterson Lake) were fully reduced to 0, and the atmospheric concentrations reduced to further lower the net input to water. For both Otterson Lake scenarios, the inflow concentrations were only partially reduced, and the atmospheric concentration was not changed.

Figure 8 shows the Ra-226 model Pb-210 water input process rates. Atmospheric deposition accounts for the inputs to all lakes except Otterson, showing nearly equal inflow rates for the base and alternate 'B' scenarios. There was little discrepancy in atmospheric deposition rates between the base and alternate scenarios for all lakes except Upper Bass Lake, for which the alternate scenario was higher by a factor of 1.3. Input discrepancy for Otterson Lake appears as inflow, according to section 4.2.1.1, amounting to a factor of 2.4, greater than the concentration ratio of 2 defining the base and alternate scenarios.

Figure 9 shows the Ra-226 model Pb-210 water output process rates. Each of the lakes' base and alternate 'B' scenarios were constrained by the same sedimentation rate. The outflow and decay rates for the alternate scenario of each lake were double the base scenario rates. Sedimentation was the predominant removal mechanism by a wide margin in all but Otterson Lake, and to a lesser extent Upper Bass Lake. Discrepancies in total Pb-210 rate in the water for the latter two lakes (either as input or output) between the base and alternate scenarios can be seen more clearly in the Figure 10 Ra-226 model plot against catchment area and the Figure 11 Ra-226 model plot against lake area. These plots also suggest that lake area was more highly correlated than catchment area with the total rate. Although linear regressions indicated coefficients of determination $R^2 < 0.55$ for all four (base, alternate) total inputs and (lake, catchment) area permutations, when Otterson Lake was removed as an outlier, base and alternate total inputs versus lake area yielded $R^2 = 0.90$ and 0.92.

Figure 12 shows the Ra-226 model Po-210 water input process rates. Atmospheric deposition was not a significant input to any of the lakes. There was a diffusion of Po-210 from sediment in all scenarios. The rates for inflow, in-growth decay from Pb-210 and diffusion from sediment vary between the base and alternate scenarios.

Between the base and alternate scenarios for all lakes, both the inflow and decay ingrowth from Pb-210 differ by a factor of 2. Diffusion from sediment varies between the base and alternate scenario, ranging from 2.1 to 2.6 among the lakes. Figure 13 shows the Ra-226 model Po-210 water output process rates. Both outflow and decay differ by a factor of 2 between the base and alternate scenarios among the lakes. The proportion of losses by radioactive decay varies among the lakes.

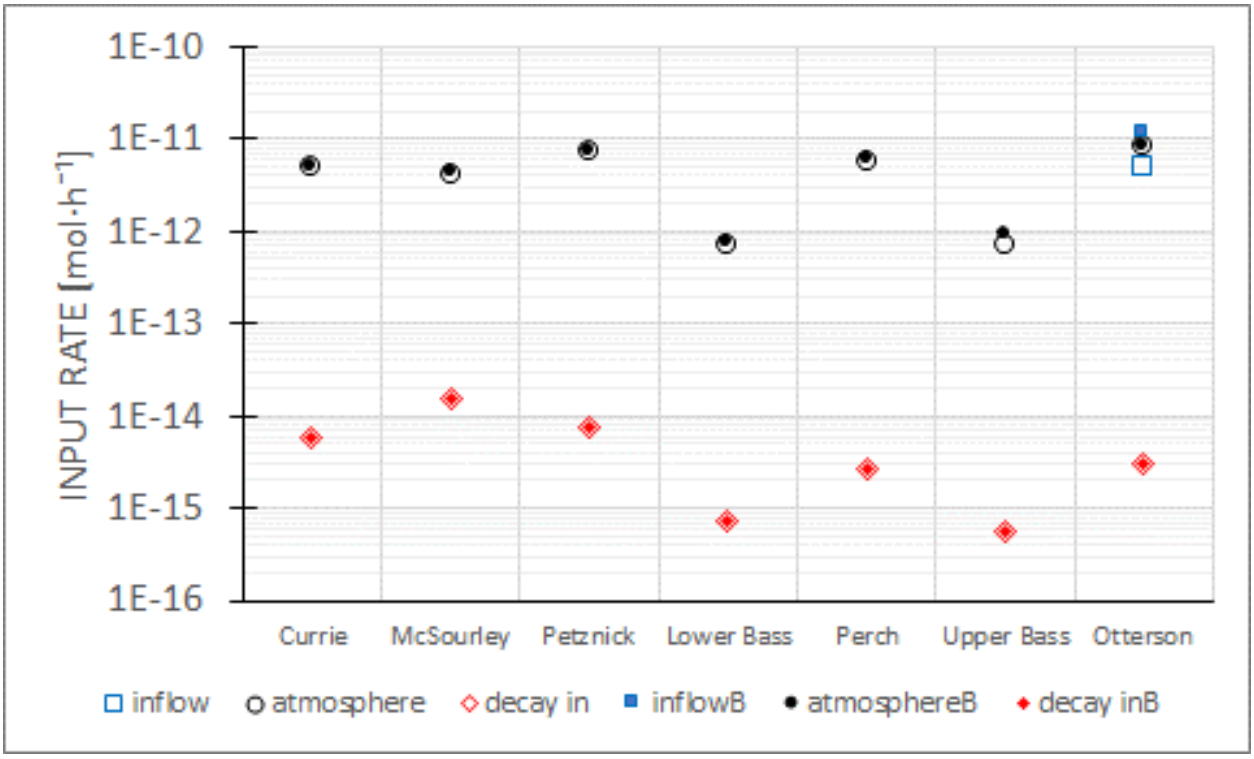

Figure 8. Laurentian lakes Ra-226 model Pb-210 input processes

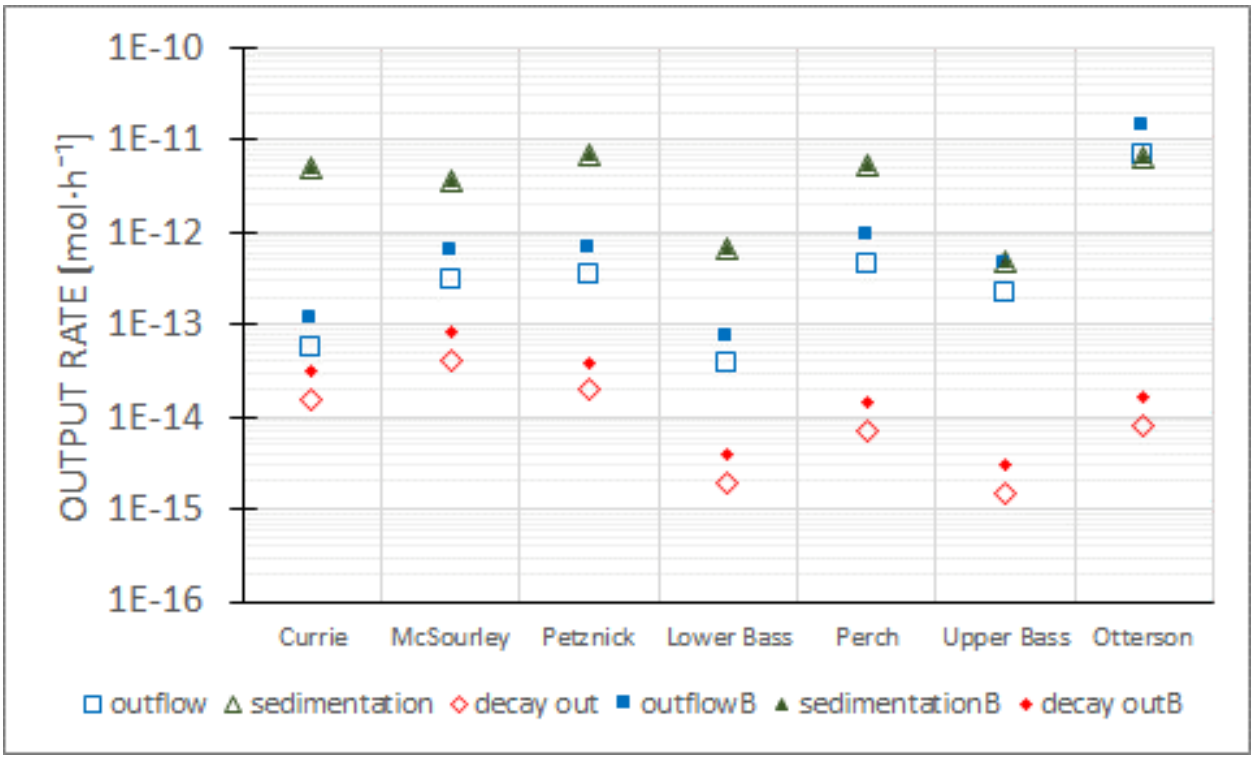

Figure 9. Laurentian lakes Ra-226 model Pb-210 output processes

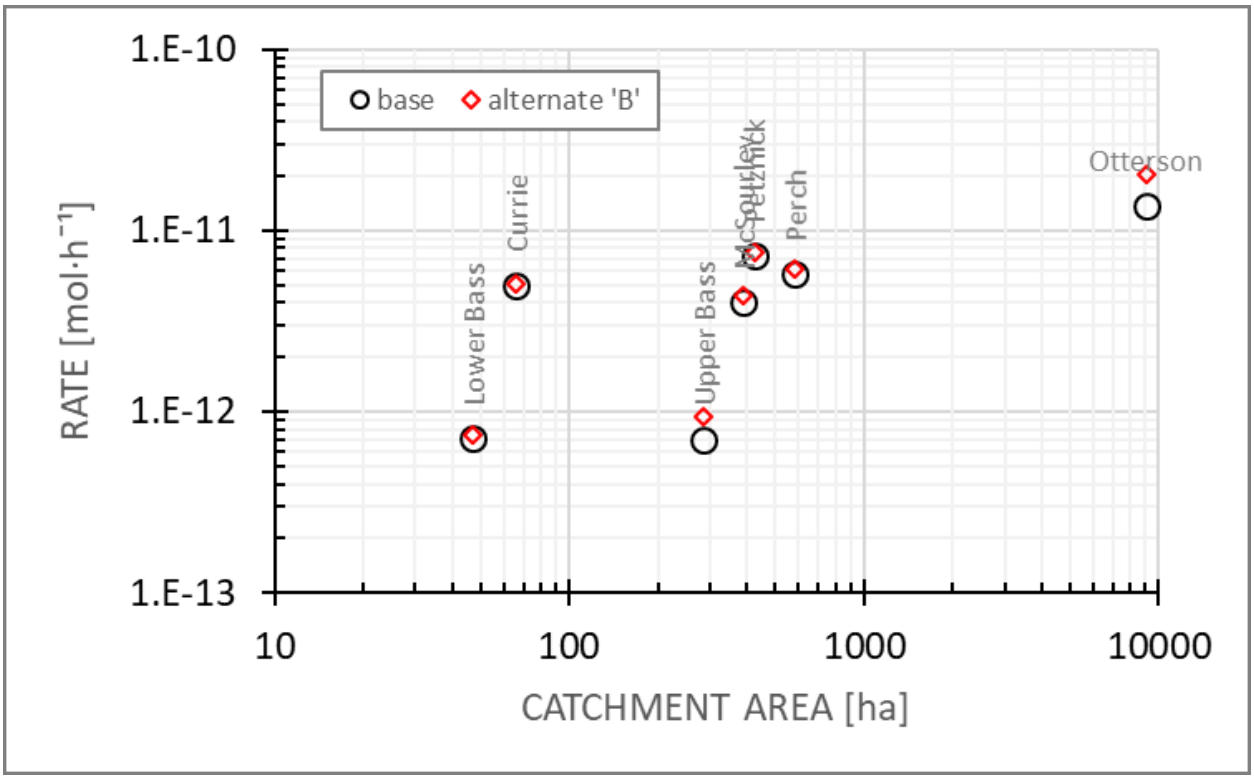

Figure 10. Laurentian lakes Ra-226 model Pb-210 rate versus catchment area

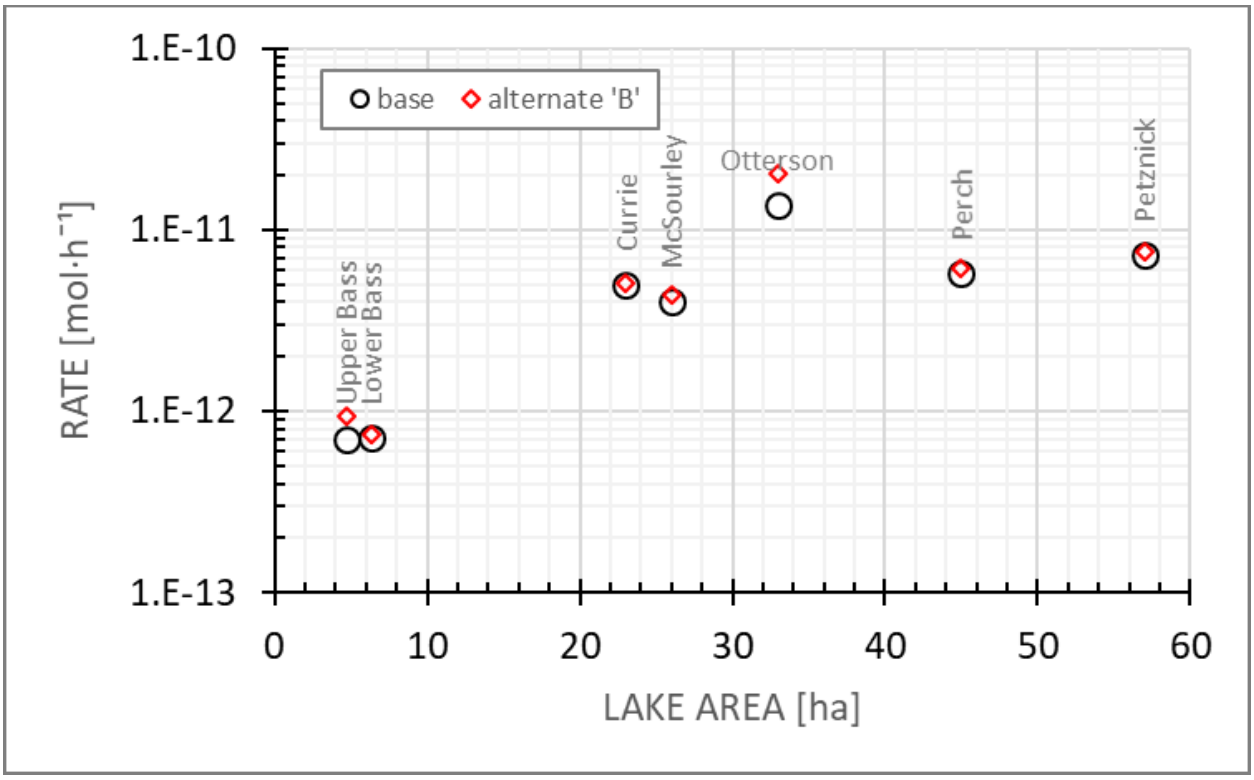

Figure 11. Laurentian lakes Ra-226 model Pb-210 rate versus lake area

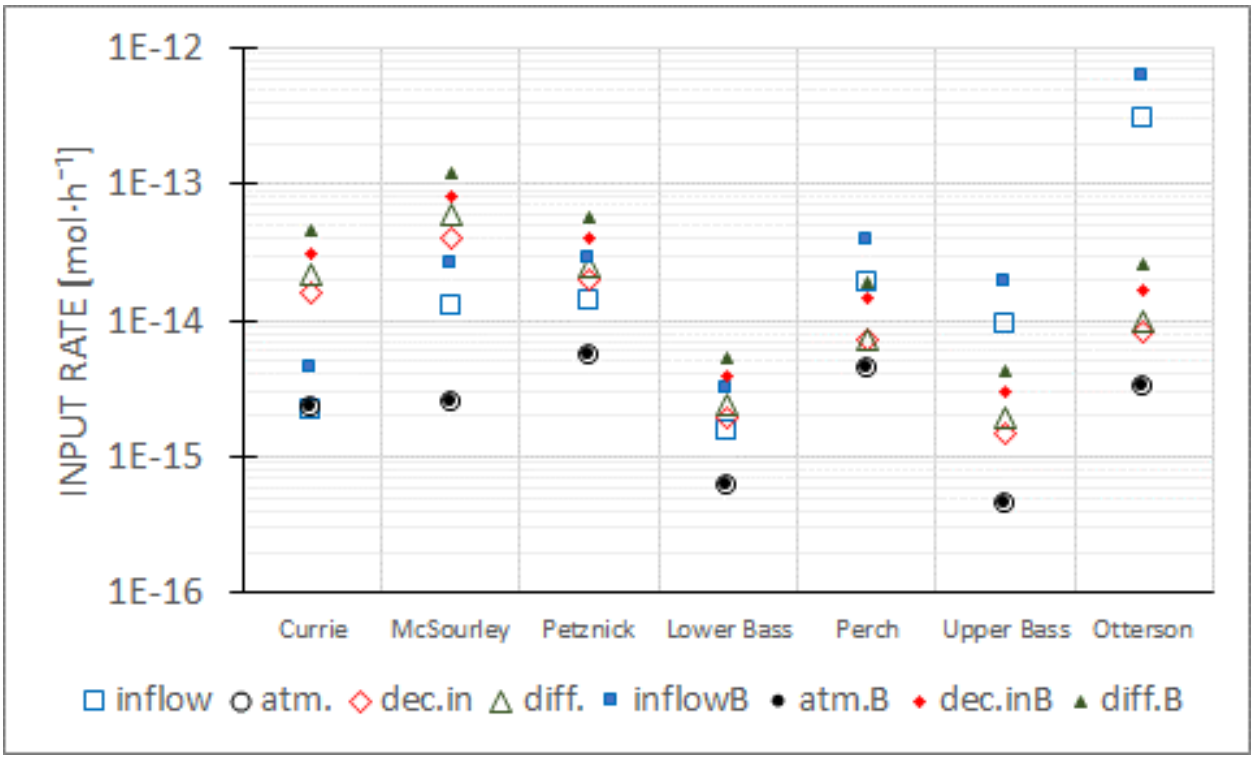

Figure 12. Laurentian lakes Ra-226 model Po-210 input processes

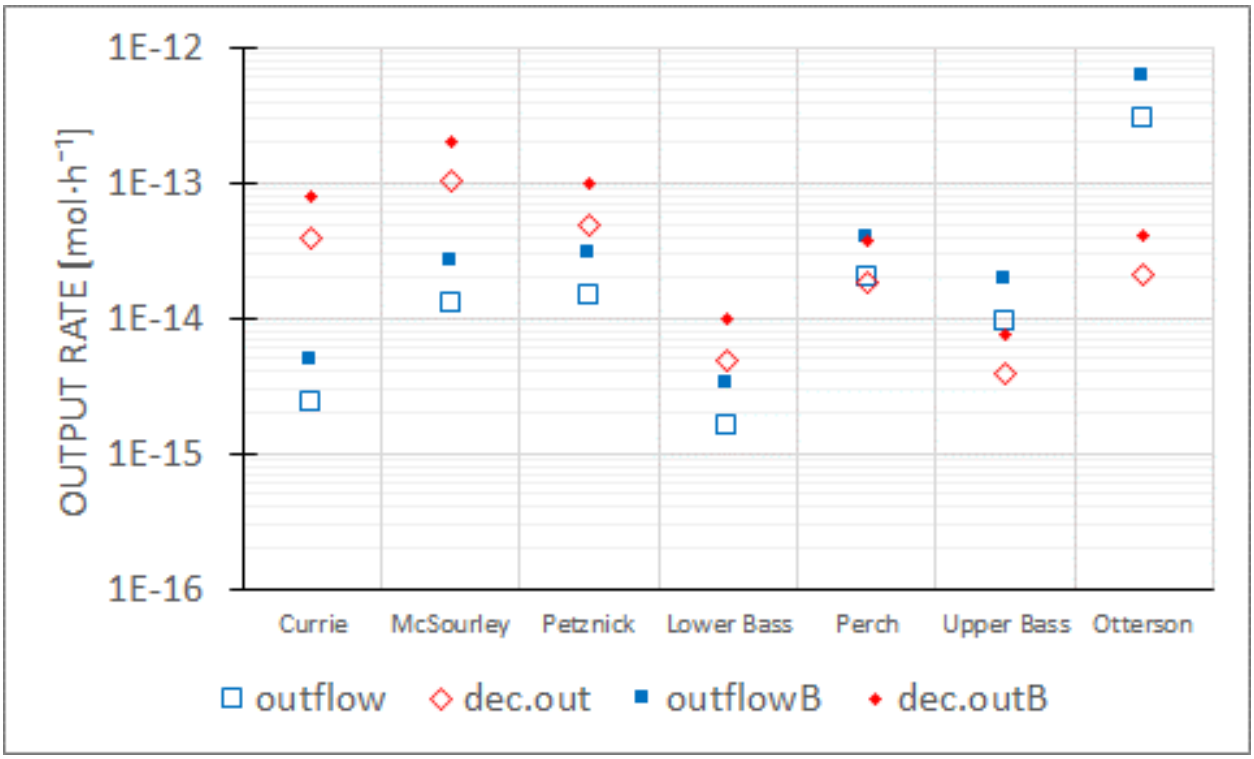

Figure 13. Laurentian lakes Ra-226 model Po-210 output processes

Residence times calculated from the Ra-226 model for the Appendix I Laurentian lakes scenarios to sediment by Equation 53, τ_{TW}, and to all sinks by Equation 57, τ_T (including decay), are shown in Figure 14 for Ra-226, Figure 15 for Pb-210 and Figure 16 for Po-210. The range of residence time to sediment among the lakes was similar for Ra-226 and Pb-210, about an order of magnitude. The alternate scenarios result in Ra-226 residence times to sediment that range 3 to 4 times the base scenarios, but little to no difference results between scenarios considering all sinks (Figure 14). The difference in Pb-210 residence times to sediment between base and alternate scenarios were a factor of 2 for all lakes, and nearly a factor of 2 considering all sinks for all lakes except Lower Bass Lake and Otterson Lake, for which the scenarios differ by a factor of 1.5 and 1.3 respectively (Figure 15). There were no residence times to sediment for Po-210 since each scenario resulted in net diffusion from sediment to water (Figure 16), and no discrepancy in residence times to all sinks between the base and alternate scenarios.

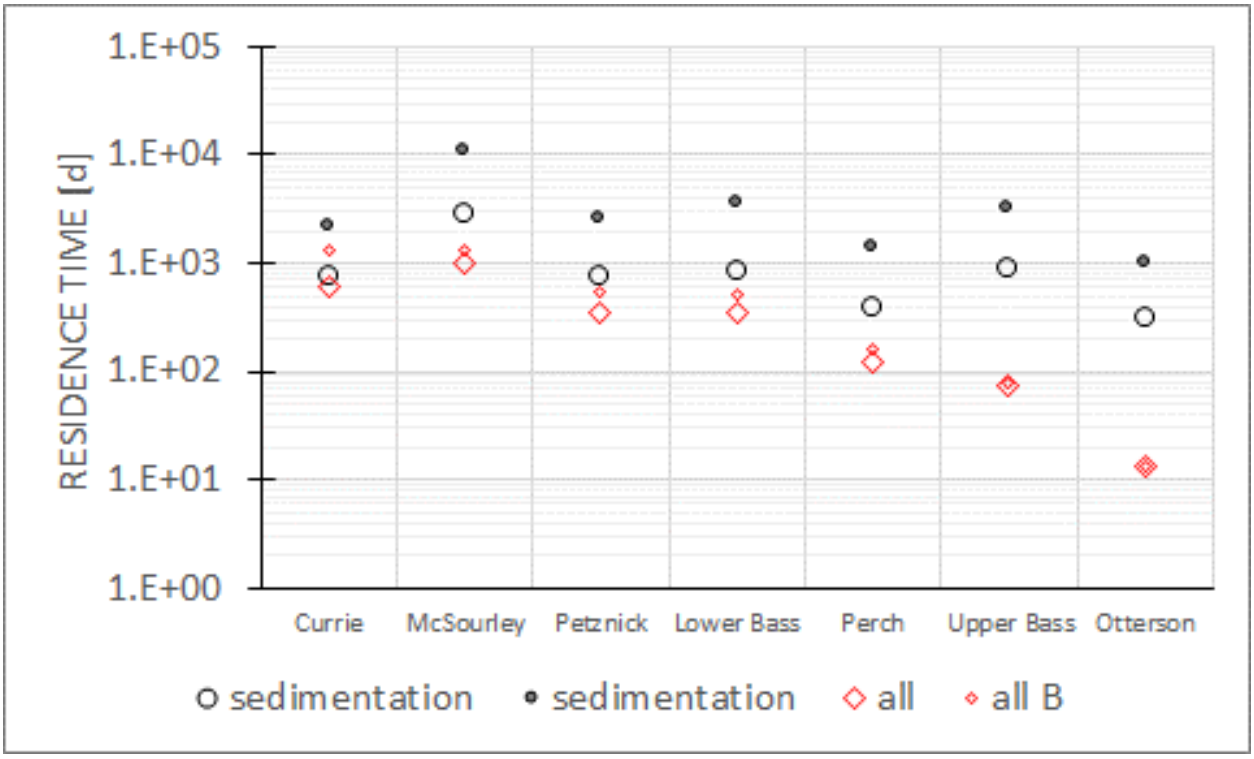

Figure 14. Laurentian lakes Ra-226 model Ra-226 residence times

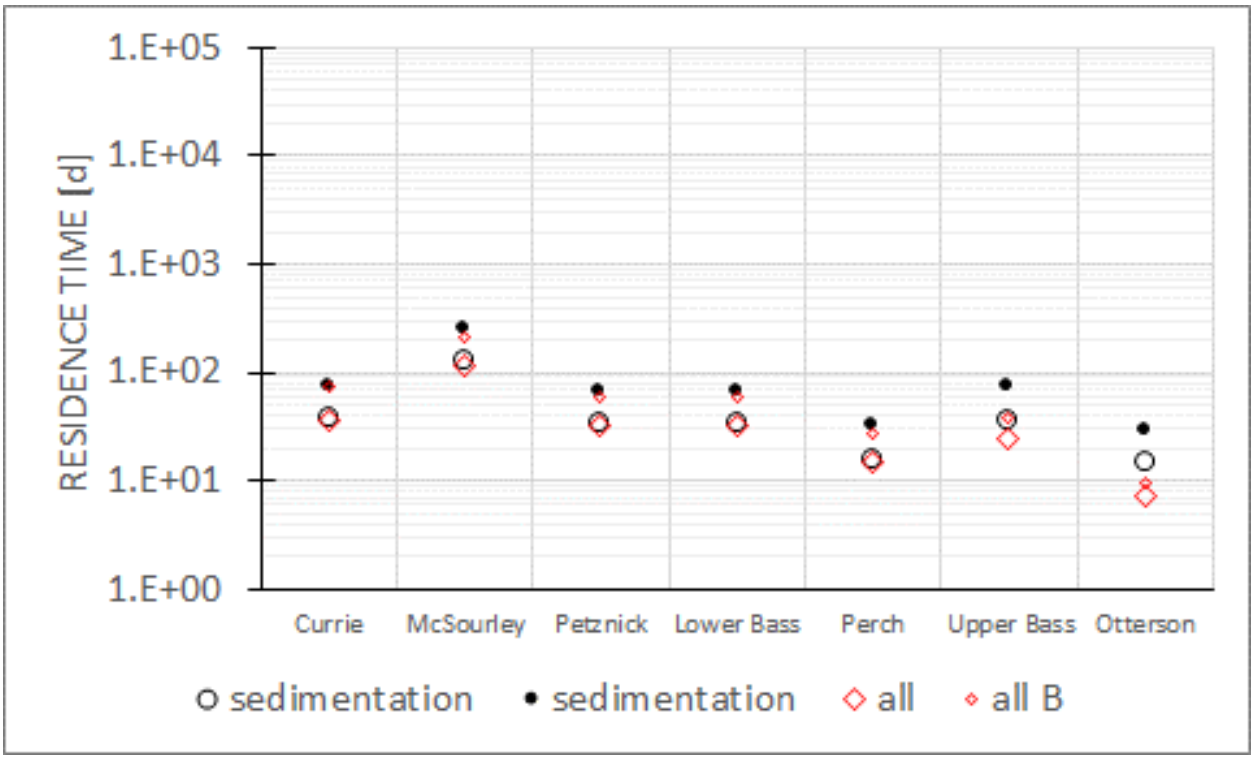

Figure 15. Laurentian lakes Ra-226 model Pb-210 residence times

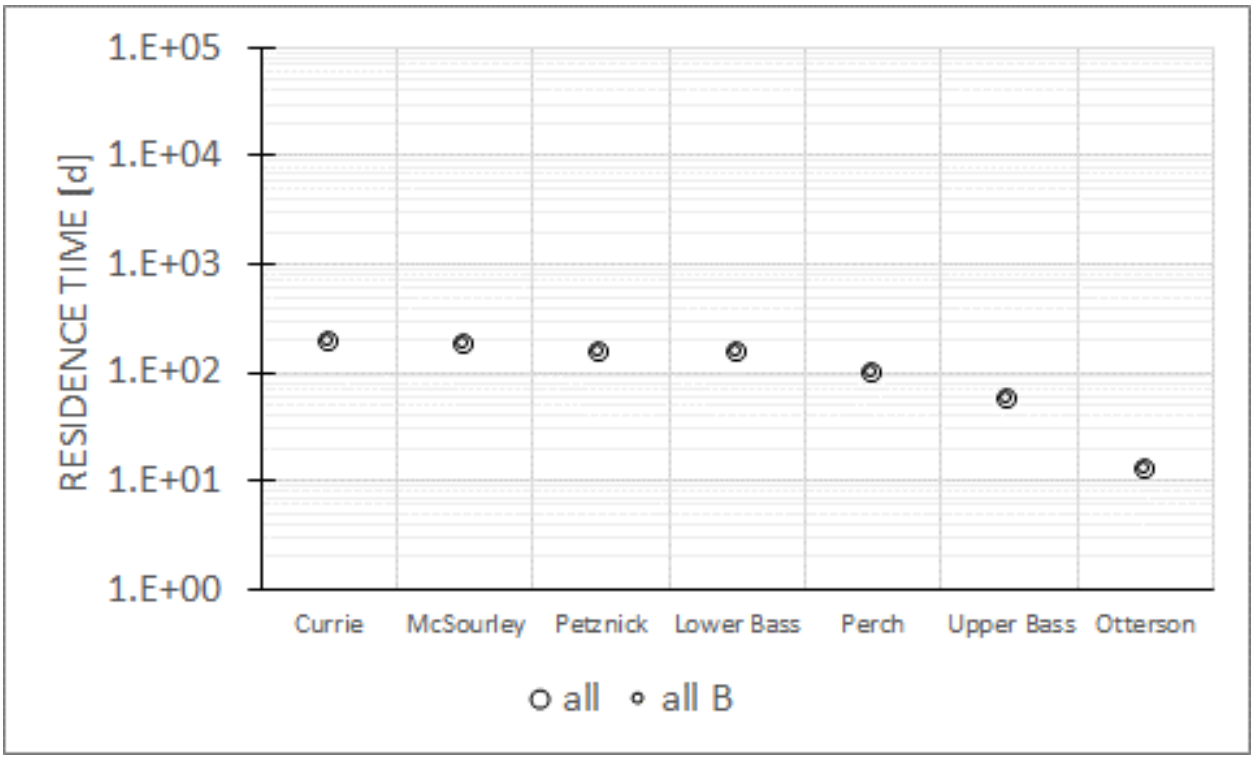

Figure 16. Laurentian lakes Ra-226 model Po-210 residence times

4.3.2 JUDGE SISSONS LAKE

Figure 17 shows the process diagram for Judge Sissons Lake from the optimization detailed in Appendix J. The settling flux F_S was adjusted upward from the measured value to set the dissolved water concentration of Pb-210, and both sediment-water diffusion coefficients k_{w1} and k_{w2} were set to balance the sediment and dissolved water concentrations for Ra-226 and Pb-210. Emissions to water E_{w3} and the diffusion coefficient k_{TS3} were set to balance the sediment and dissolved water concentrations for Po-210.

As with the other scenarios studied, the set of settling flux and diffusion coefficients cannot be considered uniquely valid, since other settings were possible, and the nuclides in the lake are expected to have specific particle associations by size and composition. Table 28 shows the overall water process rates for each of the nuclides and contributions to input and output. Sedimentation represents the net of flux and diffusion, $q_D+q_{TS}-q_{TW}$.

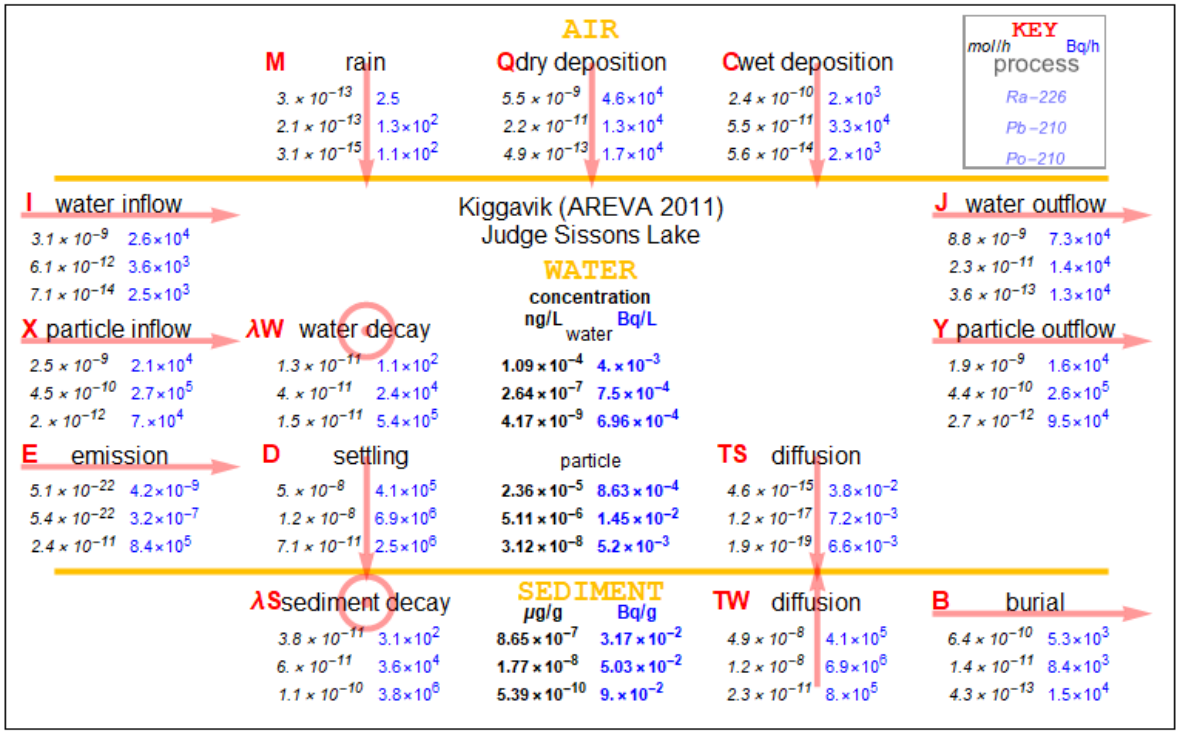

Figure 17. Judge Sissons Lake process diagram

Table 28. Judge Sissons Lake water process rates

process	Ra-226		Pb-210		Po-210	
	$mol \cdot h^{-1}$	%	$mol \cdot h^{-1}$	%	$mol \cdot h^{-1}$	%
Inflow	5.61E-09	49	4.52E-10	83	2.07E-12	3
Atm. deposition	5.79E-09	51	7.74E-11	14	5.50E-13	1
Decay in	NA	NA	1.28E-11	2	4.00E-11	60
Emission	0	0	0	0	2.39E-11	36
Total in	1.14E-08	100	5.42E-10	100	6.65E-11	100
Outflow	1.07E-08	94	4.65E-10	86	3.06E-12	5
Sedimentation	6.78E-10	6	3.64E-11	7	4.80E-11	72
Decay out	1.28E-11	0	4.00E-11	7	1.55E-11	23
Total out	1.14E-08	100	5.42E-10	100	6.65E-11	100

Outflow dominated the Ra-226 and Pb-210 sinks, despite a hydrologic flushing rate of only 0.3 a^{-1}. The Ra-226 outflow proportion of all sinks was equivalent only to Otterson Lake among the Laurentian study lakes (which has a hydrologic flushing rate of 27 a^{-1}). The Pb-210 outflow proportion of all sinks was greater than all Laurentian study lakes. However, the Po-210 outflow proportion of all sinks was small; all sinks instead comprised sedimentation at 72%. The decay proportion of Pb-210 losses was much larger than any Laurentian study lake at 7%, yielding a proportion of Po-210 input by radioactive decay ingrowth at 60%, nearly that found for Crystal Lake, which is without tributaries. The decay proportion of Po-210 losses was 23%, like Upper Bass Lake, which has a higher hydrologic flushing rate, 4.6 a^{-1}.

The Po-210/Pb-210 settling flux activity ratio was approximately the water activity concentration ratio. However, the values for the sediment-water diffusion coefficients set during optimization process resulted in sediment to water diffusion rates, as a proportion of settling flux, of 99.7% for Pb-210 and 31% for Po-210. The resulting net sedimentation rate of Po-210 to sediment was 80 times that of Pb-210, corresponding to sedimentation proportions of all sinks for Po-210 of 72% and for Pb-210 of 7%. A Po-210 input emission term of almost half the amount lost to sediment was required in the Ra-226 model, amounting to a total input proportion of 36%.

Table 29 shows the water column residence times calculated for the Appendix J Judge Sissons Lake scenario to sediment by Equation 53, τ_{TW}, and to all sinks by Equation 57, τ_T (including decay).

Table 29. Judge Sissons Lake water residence times

residence time	Ra-226	Pb-210	Po-210
	d	d	d
Ra-226 model by Eq. 53, τ_{TW}: sedimentation	15900	12900	64
Ra-226 model by Eq. 57, τ_T: all sinks	945	864	46

The residence times of Pb-210 were very long for both sedimentation and all sinks, nearly the same as Ra-226. In contrast the Po-210 residence time to all sinks was comparable to Upper Bass Lake.

4.3.3 STREAM SAMPLES

Table 30 shows radionuclide concentrations measured in the Ottawa River watershed stream sample set 1. Appendix K contains the laboratory results and calculations. The sampling and first Po-210 plating details for sample sets 2 and 3 are shown in Table K-13.

Table 30. Ottawa River stream radionuclide concentrations

Sample	Location	Concentration (mBq·L^{-1})		
		U-238	Pb-210	Po-210
1	Grant's Cr	2.35±0.02	1.49±0.11	2.96±0.12
2	Grant's Cr	2.38±0.12	1.19±0.08	2.74±0.10
3	Pleasant Valley Cr	10.48±0.08	1.15±0.07	0.75±0.03
4	Pleasant Valley Cr	10.12±0.11	1.18±0.08	0.78±0.04
5	Hurd's Cr	3.75±0.11	0.30±0.04	0.99±0.06
6	Hurd's Cr	3.78±0.12	0.82±0.06	1.13±0.05
7	Gull Ck	2.33±0.14	1.22±0.08	1.85±0.06
8	Gull Ck	2.35±0.05	0.67±0.05	2.09±0.13
9	Egan Cr	4.08±0.16	1.18±0.06	2.19±0.11
10	Egan Cr	4.05±0.13	1.37±0.07	2.07±0.11
11	Little Mississippi R	4.95±0.14	0.64±0.05	1.23±0.10
12	Little Mississippi R	4.99±0.07	0.51±0.05	1.50±0.11
13	Aylen R	2.2±0.3	1.28±0.07	2.42±0.12
14	Aylen R	2.18±0.18	1.21±0.07	2.16±0.11
15	Sherwood R	2.34±0.15	NA	NA
16	Sherwood R	2.32±0.06	NA	NA
17	Carp R	7.75±0.07	0.53±0.05	0.83±0.06
18	Carp R	7.97±0.04	0.21±0.03	0.67±0.06
19	Constance Cr	2.5±0.2	0.69±0.06	1.80±0.12
20	Constance Cr	2.66±0.06	0.30±0.04	1.21±0.12
21	McCrearys Ck	15.93±0.17	2.90±0.13	2.35±0.12
22	McCrearys Ck	16.2±0.5	2.43±0.10	1.93±0.09

Table 31 shows major cation concentrations measured in the stream samples by ICP-MS. The concentrations of Mg-24 and Fe-56 were not distinguished from background and the calibration curve of Th-232 was poorly resolved. The concentrations of Cs-133 in all samples were below the limit of quantification, 3.8 ppb (Appendix K.1.1).

Table 31. Ottawa River stream major cation concentrations

Sample	Location	Concentration (ppb)			
		Mn-55	Sr-88	Ba-137	Pb-208
1	Grant's Cr	24.08±0.19	24.6±0.5	6.94±0.13	0.261±0.005
2	Grant's Cr	20.5±0.5	24.2±0.2	6.62±0.13	0.243±0.007
3	Pleasant Valley Cr	36.9±0.5	249.6±1.1	29.7±0.07	0.422±0.003
4	Pleasant Valley Cr	32.03±0.19	243±6	27.05±0.08	0.372±0.007
5	Hurd's Cr	42.3±0.5	123±2	101.4±0.6	0.180±0.005
6	Hurd's Cr	42.6±0.7	124.1±1.9	102.1±1.0	0.265±0.005
7	Gull Ck	20.5±0.4	31.2±0.4	14.0±0.3	0.194±0.007
8	Gull Ck	20.8±0.4	30.8±0.7	13.2±0.2	0.176±0.003
9	Egan Cr	80±3	74.5±1.0	40.8±1.5	0.230±0.003
10	Egan Cr	56.9±0.8	72.1±0.9	38.6±0.9	0.238±0.004
11	Little Mississippi R	24.57±0.07	53.6±0.4	27.4±0.4	0.251±0.009
12	Little Mississippi R	24.8±0.2	53.3±1.3	26.8±0.5	0.196±0.007
13	Aylen R	8.50±0.05	25.4±0.4	11.0±0.2	0.218±0.008
14	Aylen R	9.02±0.19	25.6±0.9	11.1±0.3	0.2131±0.0008
15	Sherwood R	36.20±0.18	38.4±0.7	12.0±0.3	0.311±0.005
16	Sherwood R	34.6±0.5	37.2±0.5	11.30±0.13	0.306±0.005
17	Carp R	21.59±0.13	870±16	42.9±0.3	0.2015±0.0015
18	Carp R	10.01±0.08	890±9	42.7±0.6	0.160±0.004
19	Constance Cr	115±2	433±6	44.9±0.9	0.445±0.003
20	Constance Cr	82±2	420±4	41.2±0.3	0.246±0.005
21	McCrearys Ck	497±4	298±3	130±2	0.526±0.005
22	McCrearys Ck	479±5	285±5	125±2	0.440±0.006

The measured concentrations of Pb-210 and Po-210 are plotted in Figure 18 labelled with the Table 30 sample numbers.

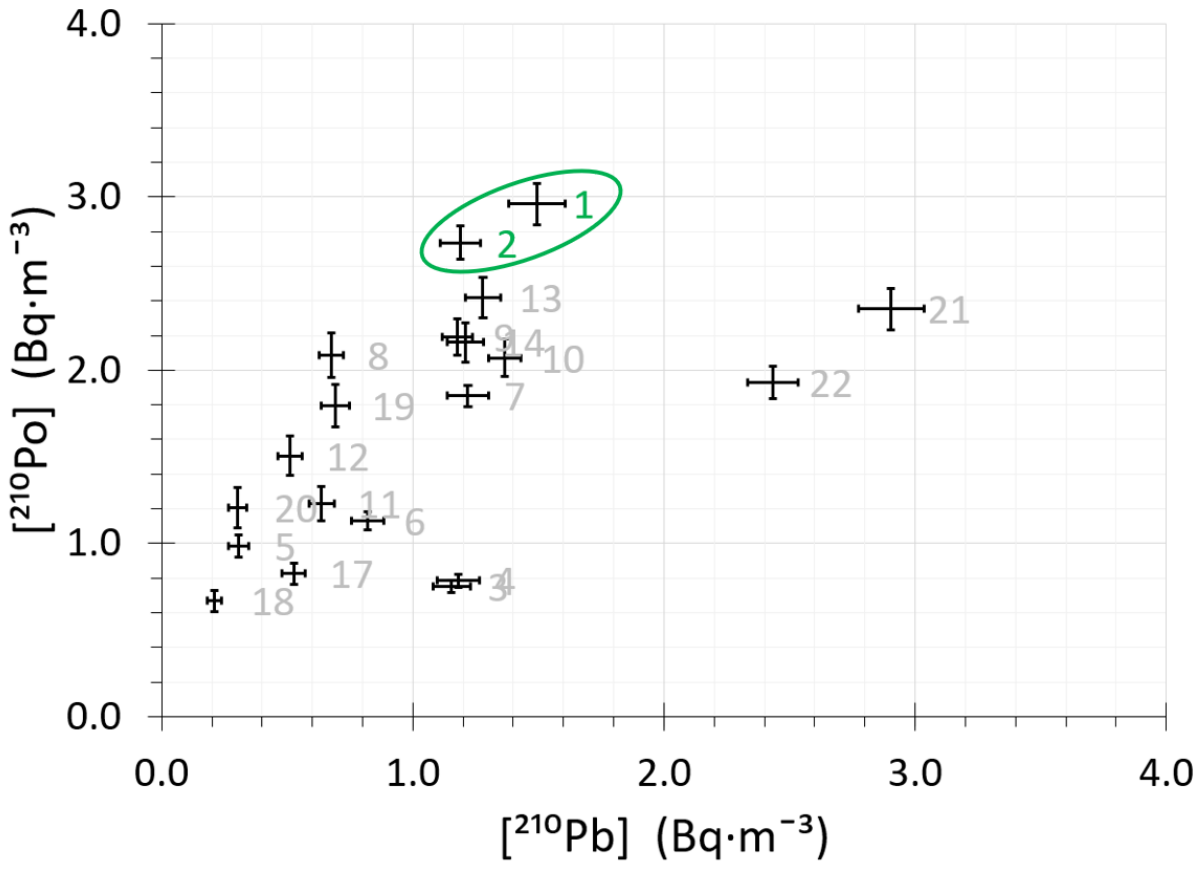

Figure 18. Po-210 versus Pb-210 (Grant Creek samples indicated)

4.4 DISCUSSION

4.4.1 LAURENTIAN LAKES

In the original study, the Pb-210 sedimentation rate constants are concluded to be lower than expected, as found in previous studies, including Crystal Lake **(TALBOT, 1984)(CORNETT, 1984)**. As explanations, the effects of anomalously low SPM settling flux, inert chemical form of atmospheric deposition, and overestimate of the catchment contribution are dismissed in favour of seasonal deposition and flushing associated with winter ice and break-up **(CORNETT, 1984)**. Neither effect is within the scope of the Ra-226 model, and they are a potential source of error in the estimate of atmospheric deposition that would otherwise represent an annual average.

The optimization process eliminated (reduced for Otterson Lake) the estimated watershed contribution to Pb-210 that is calculated **(CORNETT, 1984)** and was assumed for each lake's initial model input as inflow concentrations. These estimated watershed contributions are determined in the original study as a fraction of watershed deposition based on the results of previous studies **(LEWIS,**

1977)(BENNINGER, 1978)(CORNETT, 1984). The remaining reductions in Pb-210 input were to the concentration on aerosol (lowering each of the wet, dry and rain deposition rates proportionally). The prioritization of reduction in watershed inflow over atmospheric deposition was convenient for the optimization process, but the apportioning of the resulting total input required further consideration.

As indicated in section 4.3.1, the Ra-226 model lake input of Pb-210 found through optimization was highly correlated with lake area, excluding Otterson Lake ($R^2 > 0.90$). This result suggested that direct atmospheric deposition was the predominant input to those lakes, but that there was an additional significant source contributing to Otterson Lake input. This result would be consistent with the conclusion of an Experimental Lakes Area study, which finds that atmospheric deposition accounts for at least 85% of the Pb-210 supplied to the water column of Lake 239 **(BRUNSKILL, 1987)**. No significant difference was expected in the atmospheric concentration and deposition parameters of Pb-210 among the Laurentian lakes. Regional uniformity in atmospheric Pb-210 deposition is concluded from the consistency between measurements of direct deposition and excess of decay support in soil profiles **(TUREKIAN, 1977)(BENNINGER, 1978)**. The finding is expected to apply to the Laurentian study lakes: five are within a 7-km radius centred along the western boundary of the Chalk River Laboratories site, and McSourley Lake and Petznick Lake are located 45 km to the northwest and 40 km to the southeast respectively.

Watershed soil partitioning is found to result in mean residence times for Pb-210 of 2000 a in the Susquehanna River basin **(LEWIS, 1977)**, 6200 a in the Ottawa River basin **(JOSHI, 1990)**, and 1400 a in the in the Rhone watershed Switzerland **(DOMINIK, 1987)**.

From Equation 58, the foregoing mean residence times corresponded to the fraction of watershed atmospheric deposition to lake f_c = 1.6%, 0.52%, and 2.2%. As detailed in Appendix I, the Susquehanna River study **(LEWIS, 1977)** and a Connecticut River study **(BENNINGER, 1978)** are used to estimate f_c = 1.3% in the Laurentian lakes study **(CORNETT, 1984)**. The Ottawa River f_c = 0.52% **(JOSHI, 1990)** was better supported by the Ra-226 model results.

Figure 19 shows the sedimentation rate that is calculated in the original study from measurements of sediment samples **(CORNETT, 1984)**, to which the Ra-226 model scenarios were constrained. Figure 20 shows the Ra-226 model input per unit area of lake resulting from the optimization for the base and alternate scenarios plotted against hydrologic flushing rate. The hydrologic flushing rate is calculated in the original study from Perch Lake watershed inflow measurements **(BARRY, 1975)** and extrapolated to the other study lakes **(CORNETT, 1984)**. Both the atmospheric component and total including watershed (inflow) were plotted for Otterson Lake. The plot suggests a baseline total areal atmospheric deposition rate could be represented by Lower Bass Lake, at 1.13 $mol \cdot h^{-1} \cdot m^{-2}$ (optimized as 43% of the initial model input rate, 2.6 $mol \cdot h^{-1} \cdot m^{-2}$). Table 32 represents the Ra-226 model

Pb-210 inputs above the Lower Bass Lake baseline to each Laurentian study lake as a fraction of the atmospheric deposition on the watershed (Equation 58); and the watershed mean Pb-210 erosional residence time from for each lake and scenario (Equation 57). Besides Currie Lake (and Lower Bass Lake), the fraction of water atmospheric deposition to the lakes were within a factor of 2 of the value calculated from the Ottawa River study **(JOSHI, 1990)**, f_c = 0.52%.

Table 32. Ra-226 model Pb-210 watershed fractions above baseline

Lake	Fraction of Pb-210 watershed atmospheric deposition to lake inputs above baseline f_c (%)		watershed mean Pb-210 erosional residence time τ_W (y)	
	Base	Alternate 'B'	Base	Alternate 'B'
Currie	13.9	13.5	199	205
McSourley	1.11	1.29	2860	2460
Petznick	0.68	0.68	4700	4660
Lower Bass[1]	0	0	NA	NA
Perch	0.42	0.54	7670	5940
Upper Bass	0.24	0.50	13600	6380
Otterson	0.42	0.71	7640	4500

[1] baseline having the lowest total areal inputs, which was assigned as the regional areal atmospheric deposition

The hydrologic flushing rate may affect the efficiency of Pb-210 sedimentation as an explanation for the high proportion of lake input from watershed indicated for Currie Lake and McSourley Lake indicated in Table 32. Lower hydrologic flushing rates may correspond to conditions that better enable partitioning and settling **(BINFORD, 1993)**. Currie Lake has a low watershed to lake area ratio of 2.9, which may result in a higher efficiency of watershed transport. Figure 20 and Table 32 show that the Ra-226 model requires higher inputs in the alternate 'B' scenarios (having double water concentration) for Perch Lake, Upper Bass Lake and Otterson Lake, the lakes with the greatest hydrologic flushing rates. Conversely, the concentration of Pb-210 in these lakes may be considered sensitive to the input rate.

Otterson Lake among the Laurentian study lakes is uniquely not a headwater **(CORNETT, 1984)**, receiving tributary inflow from Chalk River and a network of marshy tributaries situated in the watershed several kilometers to the northwest. This watershed is 9075 ha, 30 times larger than the others in the study. Despite these features, the fraction of watershed deposition to lake and mean erosional residence time shown in Table 32 are close to the other high hydrologic flushing rate lakes (Upper Bass Lake and Perch Lake).

The range of total Po-210 rates was greater than the range of total Pb-210 rates by a factor of 4 (base scenarios) or 3 (alternate scenarios). This higher sensitivity of Po-210 rates resulted because the inflow concentrations were not reduced during

optimization and there was no net sedimentation. These features and radioactive decay explain the identical Po-210 residence times between base and alternate 'B' scenarios, having the total rate double with the concentration. The large difference (factors of 3 or 4) between base and alternate 'B' scenario Ra-226 residence times was an artifact of the corresponding reductions in particle settling flux required for the doubled Pb-210 concentrations in the alternate 'B' scenarios. The Pb-210 residence times for the alternate 'B' scenarios are double the base scenarios because they are dominated by the sedimentation rates assumed from the original study **(CORNETT, 1984)**, except for the higher hydrologic flushing rate Upper Bass Lake and Otterson Lake having residence time factors slightly less than 2.

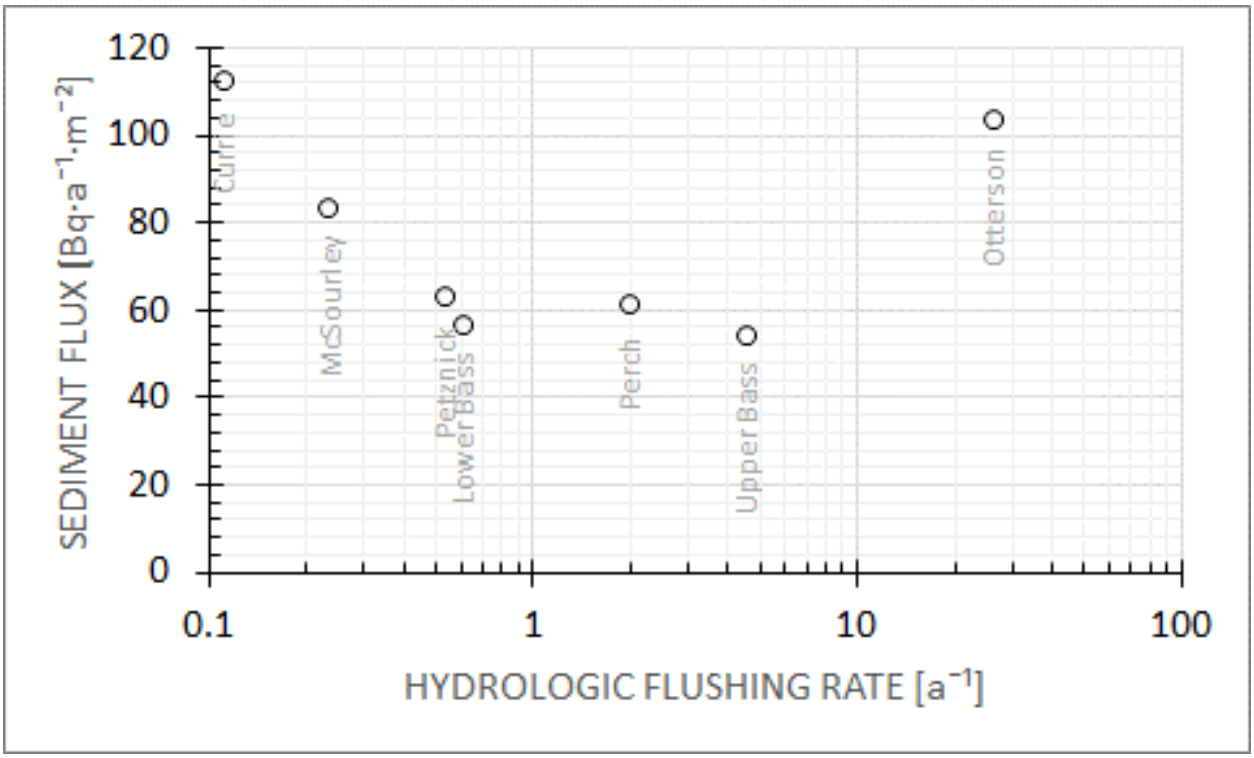

Figure 19. Laurentian lakes study sediment flux **(CORNETT, 1984)**

Table 33 shows the sedimentation proportion of Pb-210 sinks reported in the original study **(CORNETT, 1984)**, and as determined by the Ra-226 model in the base and alternate 'B' scenarios. The Pb-210 proportion of sedimentation to total losses determined by the Ra-226 model for all but the highest hydrologic flushing rate Upper Bass Lake (4.6 a^{-1}) and Otterson Lake (26 a^{-1}) were >90% in the base scenarios and >85% in the alternate 'B' scenarios. The discrepancy in the results stems from the Ra-226 model accounting for processes in detail whereas the original study assumed watershed inputs as a constant fraction of the watershed area and assigned excess flux to outflow. The original study and Ra-226 model results are plotted in Figure 21 as a function of the hydrologic flushing rate.

There appears to be a transition in sensitivity of sedimentation to hydrologic flushing rate between Perch Lake and Upper Bass Lake, in the range 2-4 a^{-1}. This

range of flushing rates would be several times greater than might correspond generally to the 2-a residence time that is suggested for Pb-210 between near complete and adsorption site-limited sedimentation efficiency **(BINFORD, 1993)**. The effect may result from seasonal processes contributing to sedimentation. The sedimentation proportion for the lakes above this hydrologic flushing rate was more sensitive to concentration and by extension the total input rate to the water. Deposition onto lake ice and subsequent rapid flushing in the spring is identified as potential causes of low sedimentation rates **(CORNETT, 1984)**. The greatest model overestimate of lake concentration and sedimentation proportion is expected for lakes with the highest hydrologic flushing rate.

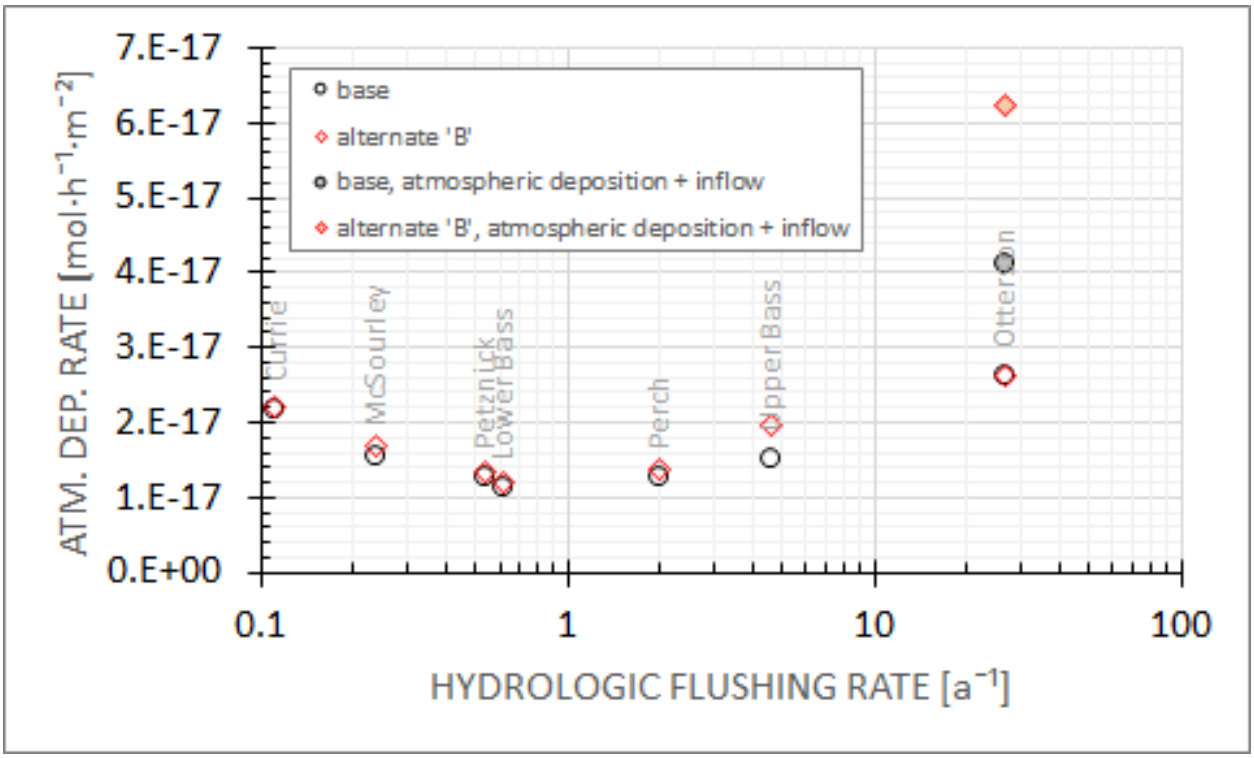

Figure 20. Laurentian lakes model Pb-210 atmospheric deposition

Table 33. Laurentian lakes Pb-210 proportion to sediment

Lake	Study (%) **(CORNETT, 1984)**	Ra-226 model (%)	
		Base	Alternate 'B'
Currie	80	99	97
McSourley	52	91	84
Petznick	42	95	90
Lower Bass	39	94	89
Perch	39	92	85
Upper Bass	21	69	52
Otterson	17	48	32

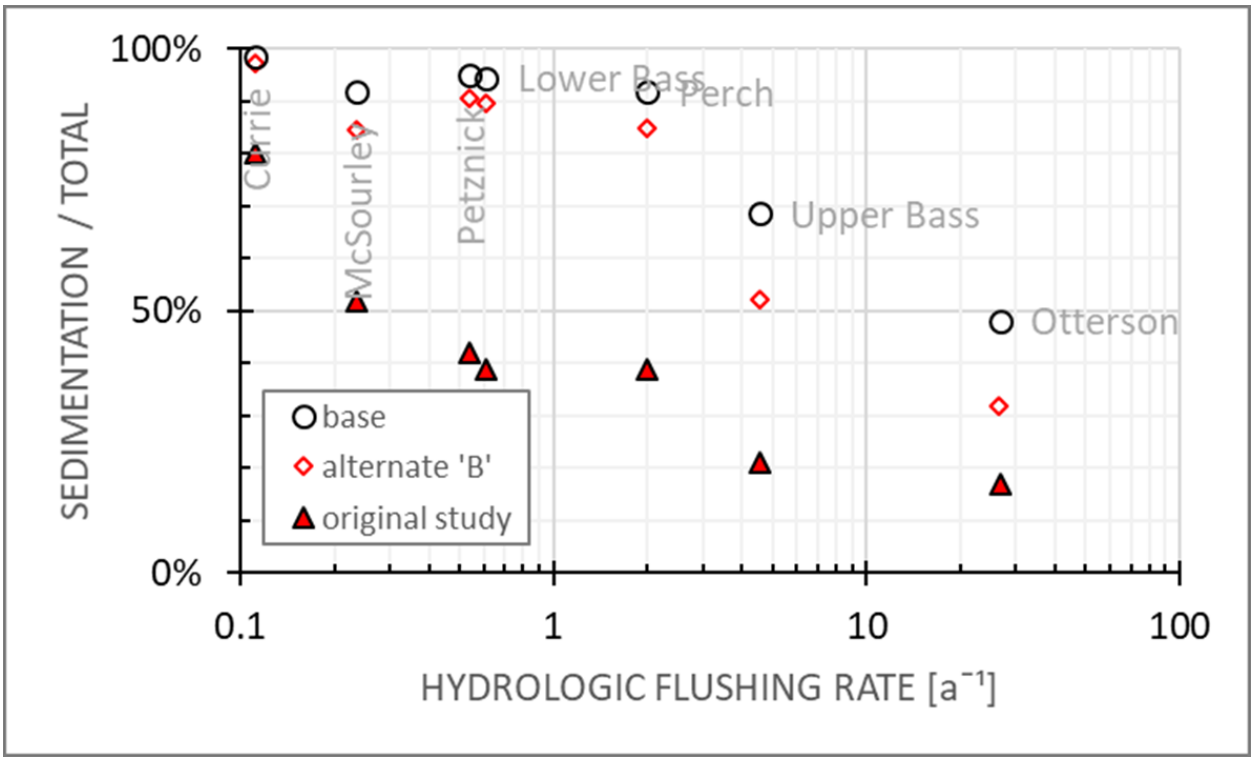

Figure 21. Laurentian lakes model sedimentation proportion

4.4.2 JUDGE SISSONS LAKE

As outlined in the method section 4.2.1.2, the assumed inflow and water concentrations and particularly Po-210/Pb-210 activity ratios may have been underestimated by detection limit-censored measurements. However, the 0.5 Po-210/Pb-210 sediment activity ratio is well supported by the measurements. Excess Po-210 in sediment is observed and attributed to biological uptake **(CHAI, 2004)** and faster sedimentation rates of Po-210 **(NELSON, 2017)**. Sediment in Quirke Lake, Ontario, including Ra-226, Pb-210 and Po-210 may be enhanced by local uranium ore processing, where sedimentation loading in the postmining period (Table 14) is estimated to be 1-3 times greater than in uncontaminated arctic lakes **(MCKEE, 1987)**, suggesting a higher natural loading rate in northern relative to temperate lakes. The net annual hydrologic flushing rate of Judge Sissons Lake is comparable to Upper Bass Lake and Otterson Lake. As suggested by Figure 20, from the perspective of lake processes affecting water concentrations, these lakes are less sensitive than lower hydrologic flushing rate lakes. Further, at the assumed sediment depth (3 cm), total activities in the sediment were greater than in the water, by a factor of 1.5 for Pb-210 and by a factor of 7 for Po-210. The assumed sediment concentrations drove most of the net flux from water to sediment within the Ra-226 model at a Po-210/Pb-210 activity ratio of 77. As indicated in Table 28, these activities represented a molar ratio of 1.32. The sedimentation processes, whether by settling particle adsorption, biological

interaction or diffusion, may favour Po-210 over Pb-210 in Judge Sissons Lake. The adsorption sites or other factors important to settling in the lake would appear to be more limiting for Pb-210 than for Po-210.

The proportion of Po-210 input by atmospheric deposition was 1% and by inflow was 3%. The relatively high contributions of Pb-210 decay to total losses, 7%, and Po-210 ingrowth to total inputs, 60%, was due to relatively low overall Pb-210 process rates in the water and the high total water concentration assumed from measurements, 15 $mBq \cdot L^{-1}$. The proportion of Ra-226 input through atmospheric deposition was much larger at 51%. Although site measurements indicate a concentration of Ra-226 on aerosol 3.5 times greater **(AREVA, 2011c)** than typical for the lower troposphere **(Moore, 1976)**, the concentration was reduced during model optimization to 33% of that initially assumed to nearly the typical troposphere value. The activity of Pb-210 on aerosol assumed from the site measurements was similarly reduced to 25% of the initial value. The resulting concentration was an order of magnitude lower than the reference value **(UNSCEAR, 2000)** and measured at other sites **(Talbot, 1983)(RPB, 2017)**. The discrepancy could indicate a bias in the sampling for or measurement of activity on aerosol. The concentration of Po-210 on aerosol measured at the site is close to the reference value **(UNSCEAR, 2000)**.

The emission rate set for Po-210 within the Ra-226 model was 9.1 times the combined inflow and atmospheric deposition rates. Accounting for the reduced Pb-210 atmospheric deposition rate to the lake surface within the Ra-226 model, to 25% of the value initially assumed, the activity proportion of atmospheric deposition of Po-210 relative to Pb-210 was 86%, representing a mean residence time of 1227 d **(Gavini, 1974)(Lehmann, 1959)**. Although the Po-210/Pb-210 activity ratio approaches 1 in the stratosphere **(Jacobi, 1963)** and the stratosphere may contribute air mass to the troposphere periodically **(Gavini, 1974)**, these phenomena likely do not explain such a high activity ratio. Neither would the lake water, inflow and sediment measurements, all of which have more samples with Pb-210 than Po-210 measurements below detection limit (section 4.2.1.2). The Po-210/Pb-210 aerosol activity ratio is measured to range 8-35% at ground level in England **(Peirson, 1966)**. Snow and ice cover at remote northern sites may reduce **(Persson, 2011)** or greatly reduce **(El-Daoushy, 1988)** aerosol Pb-210 concentration by impairing Rn-222 release. This appears to be the most likely explanation for a high Po-210/Pb-210 activity ratio. On the other hand, the highest concentrations of Rn-222 in air are found in central Canada **(Grasty, 1994)**, which may add significant quantities of Pb-210 to the central and eastern arctic **(Macdonald, 1996)**.

Instead the watershed was considered the source of added input, which was added as emission to water during the Ra-226 model optimization. The large Po-210 emission added during optimization accounted for 36% of the total input to water, while ingrowth from Pb-210 accounted for 60%. However, the watershed

atmospheric deposition cannot account for all the added Po-210, which was 6 times the atmospheric deposition to the watershed.

Table 34 shows the result of watershed source calculations (as for Clinton River, section 3.5.3) by applying Equation 55 for Ra-226 and Pb-210, and Equation 59 for Po-210 to account for ingrowth. Ra-226 model emission for Pb-210 E_W, and unadjusted atmospheric deposition (rain q_M, wet q_Q, and dry q_C) applied to the watershed area as $\mathcal{J}_A$ were used to calculate the fraction of watershed inputs to the lake f_C from Equation 58 (Equation 60 for Po-210 to account for ingrowth). The watershed mean erosion residence time τ_W was calculated from Equation 57, and the watershed inventory I_W was calculated from Equation 56. The unadjusted atmospheric deposition rates representing the site measurements (Table J-9 and section J.3) were used so that the atmospheric contribution was not underestimated.

Table 34. Judge Sissons Lake watershed residence times

nuclide	lake		watershed			
	emission E_W (mol·h^{-1})	deposition $n_M+n_Q+n_C$ (mol·h^{-1})	deposition q_{WA} (mol·h^{-1})	fraction f_c (%)	res. time τ_W (a)	inventory I_W (mol)
Ra-226	0	5.8E-09	1.3E-07	4.3	51000	2.9E-04
Pb-210	0	7.7E-11	2.3E-09	20	129	5.1E-04
Po-210	2.4E-11	5.5E-13	4.1E-12	1.4	38	8.5E-06

The mean Pb-210 erosional residence time for is 129 a, less than the reported 6200 a for the Ottawa River watershed **(JOSHI, 1990)** and 1400 a for the Rhone River watershed **(DOMINIK, 1987)**, and that was determined for Bickford Pond (390 a, section 3.5.2) and Clinton River (1510 a, section 3.5.3). Judge Sissons Lake is ice covered for 8 months of the year between October and June **(AREVA, 2011B)**. Ice-bound accumulation of atmospheric deposition and spring flushing is greater there than at the more temperate Laurentian study lakes **(CORNETT, 1984)**. The ratio of winter to summer average atmospheric Pb-210 concentrations is determined to be about 4 at the 65°N Kiggavik location **(ZHANG, 2015)**, so much of the annual atmospheric deposition would be trapped in snow and ice and released with spring melt. These factors may contribute to a large fraction of the watershed inputs to the lake, f_C = 20%, and to the low mean Pb-210 erosional residence time. The effective inventories determined by the watershed calculation are at a slight Po-210/Pb-210 activity deficit, 98.8%. The Table 34 mean erosional residence times and inventories were constrained to watershed inputs from atmospheric deposition. Components of lake input from watershed rock and soil (in addition to atmospheric deposition) would correspond to a higher mean erosional residence time.

Equation 55 was modified to account for additional watershed input from the ground:

$$q_{WA} + q_{WG} - I_W \cdot \left(\lambda + \frac{1}{\tau_W}\right) = 0 \qquad (61)$$

where

q_{WG} = input from geological source in watershed [N·T^{-1}]

The additional ground source would contribute to the effective watershed inventory I_W. Equation 59 represents the Po-210 watershed balance as before. The proportion of Pb-210 watershed input supporting the inventory from the ground source is q_{WG} / (q_{WG} + q_{WA}), which is plotted in Figure 22 versus the mean Pb-210 and Po-210 erosional residence times $\tau_{W.Pb}$ and $\tau_{W.Po}$. At $\tau_{W.Pb}$ = 390 a, corresponding to the value estimated for Bickford Pond (section 3.5.2), about 2/3 of the Pb-210 would come from the ground in the watershed. The proportion of the Po-210 watershed inputs from atmospheric deposition is 0.5% in the no ground source case shown in Table 34, and the proportion decreases as the proportion of Pb-210 from the ground increases.

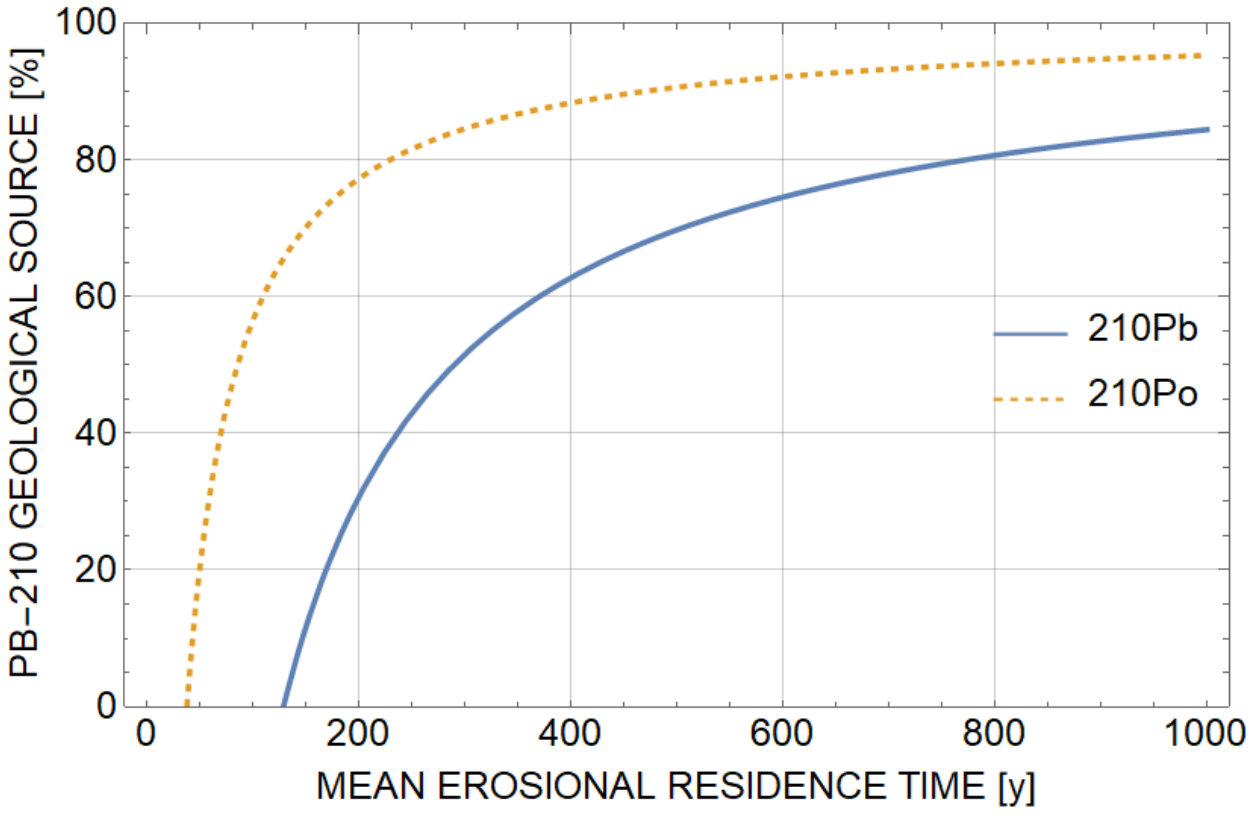

Figure 22. Judge Sissons Lake Pb-210 geological source contribution

4.4.3 STREAM SAMPLES

The measurement of stream samples showed that excess of Po-210 above equilibrium concentration with Pb-210 was observed in all stream samples except Pleasant Valley Creek and McCrearys Creek. The measurements represent total concentrations of dissolved and SPM activity, since sample acidification to pH 2 should have released the adsorbed portions. The results of ICP-MS revealed that pumping through the resin column for Cs-137 removal did not affect the concentration of Pb-208, and presumably neither did it of Pb-210. Greater inconsistency between Pb-210 measurements suggests that the observation was at least partly analytical. Regeneration of Po-210 from biological particles results in excess in the ocean, and is attributed further to release from sediment in the Black Sea **(WEI, 1994)**. Observed excess is attributed to earlier release of Po-210 versus Pb-210 from sediment during developing anoxic conditions in Bickford Pond **(BENOIT, 1990)**. The lack of such excess in Lake Sammammish is attributed to the presence of sulfide **(BALISTRIERI, 1995)**. Excess is observed in some samples of stream inflow to Experimental Lakes Area Lake 239 **(BRUNSKILL, 1987)**. Excess of Po-210 is measured generally in samples from the Euphrates River collected during the summer, but not the winter **(AL-MASRI, 2004)**. Excess Po-210 may be an indication of groundwater rather than meteoric Pb-210 **(BENOIT, 1987)**.

The measurement of Po-210 hinged on subsequent determination of the original Pb-210 content by ingrowth through the second plating step to correct for the ingrowth in the interval leading to the first plating. Although the first plating alpha spectrometry of the second and third set of samples collected in 2016 September and 2016 November were successful, no counts above background were recorded in the second plating alpha spectrometry. As such the ingrowth contribution to the concentration of Po-210 could not be determined. Having affected all the samples from the second and third sets, the error was evidently procedural or involved a common reagent. Contamination by Fe used in the precipitation step, known to interfere with subsequent Po deposition, has been argued in favour of MnO_2 for coprecipitation **(IAEA, 2009A)**. However, this stage of wet chemistry preparation was common to both Po-210 platings.

4.5 CONCLUSION

The fraction of atmospheric deposition of Pb-210 falling on the watershed that was transported to the Laurentian study lakes was <1%, except for Currie Lake and McSourley Lake which have the lowest hydrologic flushing rates. The Currie Lake fraction was about 14%, which may reflect a low watershed to lake area ratio of 2.9. The fraction of Laurentian study lake total Pb-210 input from transport of atmospheric deposition falling on the watershed appears to indicate a minimum for Lower Bass Lake, which had an intermediate hydrologic flushing rate of 0.61 a^{-1}. There may be a combination of causes leading to this effect including low watershed to lake area ratio (Currie Lake); higher efficiency of watershed transport and/or sedimentation at low hydrologic flushing rate (Currie Lake and McSourley

Lake); efficient transport atmospheric meltwater in lakes with high hydrologic flushing rate (Upper Bass Lake and Otterson Lake); and a tributary effect in lakes that are not headwaters (Otterson Lake).

The sedimentation fraction of Pb-210 was >85% for all Laurentian study lakes except Upper Bass Lake and Otterson Lake, which have the highest hydrologic flushing rates. A bias in the Ra-226 model to indicate a higher proportion of sedimentation was expected to be greatest in lakes with higher hydrological flushing rate because of seasonal SPM partitioning and meltwater flushing. The effect would have been compensated in the Ra-226 model applications to the Laurentian study lakes by the biased sedimentation rates to which they were constrained.

The proportion of atmospheric deposition of Pb-210 directly to Judge Sissons Lake to total lake input is 17%, which is the same proportion as the lake area to the watershed area. The balance of 85% is from the watershed. If atmospheric deposition is the only watershed source, mean erosional residence times of Pb-210 and Po-210 are 129 y and 38 y. A higher watershed mean erosional residence time of Pb-210 would imply that there is a significant ground source in the watershed.

About 98% of Po-210 in Judge Sissons Lake water comes from the watershed, of which at least 99.5% is ingrowth from Pb-210 decay, which would increase in relation to the ground source proportion of Pb-210.

The Po-210/Pb-210 activity ratio of the rates of net sedimentation is about 75. The proportion of Pb-210 lost to outflow is about 85%, and the proportion of Po-210 lost to sediment is about 70%.

4.6 FUTURE WORK

Further analysis of the Laurentian lakes **(CORNETT, 1984)** would benefit by water measurements, particularly of separate dissolved and SPM activities and SPM concentrations. The study of Judge Sissons Lake would benefit from more sensitive measurements of water and sediment samples to reduce or eliminate the number of results below the limit of detection.

5 Conclusion

The proportion inputs to Laurentian study lake Pb-210 lost to sediment was >85%, except for the lakes with the highest hydrologic flushing rates. and greater than estimated in the original study **(CORNETT, 1984)**. The Ra-226 model applied the upper bound of local lake water sample measurements, which were expected to bias low the calculated sedimentation proportion. The result indicates that sedimentation rates in the lakes are a better measure of atmospheric deposition than previously estimated.

The Judge Sissons Lake watershed is the source of up to 85% of the Pb-210 and 98% of the Po-210 input to the water. The watershed mean erosional residence times were 129 y and 38 y considering only atmospheric deposition to the watershed. Longer residence times would be associated with additional Pb-210 input from the watershed ground. Relative to other study sites, shorter residence times are expected due to rapid spring flushing of atmospheric deposition which is weighted to the winter season. However, there is likely a significant watershed ground contribution to the Pb-210 and Po-210 in the water and sediment of Judge Sissons Lake since a contribution of 50% is implied by a Pb-210 residence time as low as 250 y.

The steady-state partitioning Ra-226 model is subject to epistemic error, several examples of which were identified in the applications. The model was developed by reformulating and testing QWASI aquivalence lead applications, and then by linking modules for Ra-226, Pb-210 and Po-210 with decay terms and testing on two lakes and a river. This work provided insights into parameter selection and constraint. A comprehensive understanding of the epistemic error is complicated by the combinations of parameters to which the Ra-226 model may be applied. However, this versatility enabled the testing of both hypotheses posed in Chapter 1.

Future work is recommended to develop a radiological series partitioning model by using a layered water compartment and Monte Carlo techniques. Applications could be made of a layered model to the Crystal Lake study, and of a Markov Chain Monte Carlo method to parameter adjustment. Study of the Laurentian lakes could be enhanced by direct measurements of lake water, most effectively involving separate dissolved and SPM-adsorbed fractions. The study of Judge Sissons Lake could be improved by the application of more sensitive techniques to reduce the number of measurements below the limit of detection.

A QWASI Aquivalence Formulation

A.1 MODEL

A.1.1 BALANCE

Figure A-1 shows the QWASI aquivalence box model box model components **(MACKAY, 1989)** in terms of aquivalence $\mathcal{A}$, transport parameters D and emission E_W. The system boundaries are drawn to differentiate the bulk media where the aquivalences $\mathcal{A}$ are defined. An arbitrary boundary is drawn within the water column to differentiate the water medium and aquivalence $\mathcal{A}_W$ from the inflow water medium and aquivalence $\mathcal{A}_{WI}$. The compartments are assumed to be well-mixed internally.

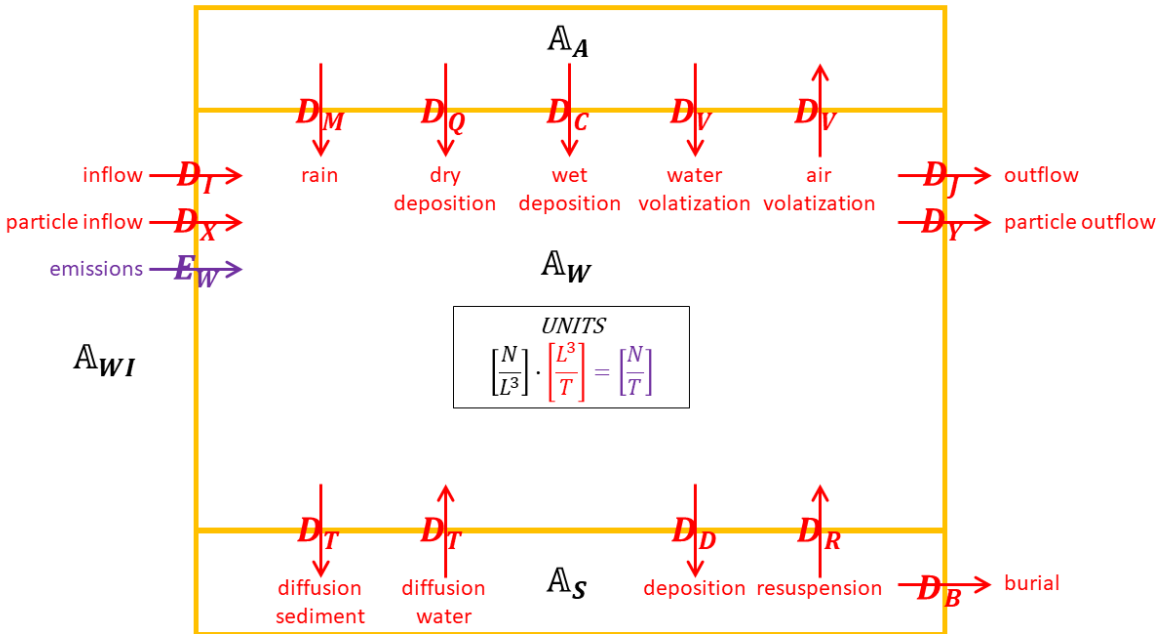

Figure A-1. QWASI aquivalence model aquivalence, transport and emission

Molar rate expressions for the water and the sediment boxes are **(MACKAY, 1989)**:

$$(D_D + D_T)\mathbb{A}_W - (D_R + D_T + D_B)\mathbb{A}_S = 0 \tag{A.1}$$

$$E_w + (D_X + D_I)\mathbb{A}_{WI} + (D_V + D_M + D_C + D_Q)\mathbb{A}_A + (D_T + D_R)\mathbb{A}_S - (D_V + D_D + D_T + D_J + D_Y)\mathbb{A}_W = 0 \tag{A.2}$$

where

E_W emissions to water [N·L^{-3}]

Bulk (media) aquivalence capacities are defined on a volume basis from **(MACKAY, 1989)**:

Air $$\mathbb{Z}_{AT} = (1 - f_{AV})\mathbb{Z}_A + f_{AV}\mathbb{Z}_Q \quad \text{(A.3)}$$

Water inflow $$\mathbb{Z}_{IT} = \frac{Q_I\mathbb{Z}_W + Q_X\mathbb{Z}_P}{Q_I + Q_X} \quad \text{(A.4)}$$

Water $$\mathbb{Z}_{WT} = (1 - f_{WV})\mathbb{Z}_W + f_{WV}\mathbb{Z}_P \quad \text{(A.5)}$$

Sediment $$\mathbb{Z}_{ST} = (1 - f_{SV})\mathbb{Z}_W + f_{SV}\mathbb{Z}_S \quad \text{(A.6)}$$

where

f_{AV} volume fraction of aerosol [-]

f_{SV} volume fraction of sediment particles [-]

f_{WV} volume fraction of SPM [-]

Aquivalences are defined by extension from **(MACKAY, 1989)**:

Air $$\mathbb{A}_A = \frac{C_A}{\mathbb{Z}_{AT}} \quad \text{(A.7)}$$

Water inflow $$\mathbb{A}_{WI} = \frac{C_I}{\mathbb{Z}_{IT}} \quad \text{(A.8)}$$

Water $$\mathbb{A}_W = \frac{E_w + (D_I + D_X)\mathbb{A}_{WI} + \left(D_V + D_M + D_C + D_Q\right)\mathbb{A}_A}{D_T + D_D + D_V + D_J + D_Y - (D_T + D_R)\frac{D_T + D_D}{D_B + D_T + D_R}} \quad \text{(A.9)}$$

Sediment $$\mathbb{A}_S = \frac{D_T + D_D}{D_B + D_T + D_R}\mathbb{A}_W \quad \text{(A.10)}$$

where

C_A = concentration of lead in air [M·L^{-3}]

C_I = concentration of nuclide in inflow water (total) [M·L^{-3}]

A.1.2 CONCENTRATIONS

Table A-1 defines the phase concentrations.

Table A-1. Phase concentration definitions

Phase	Concentration [N·L^{-3}]	
Air, gas	$C_G = (1 - f_{AV})\mathbb{A}_A\mathbb{Z}_A$	
Air, aerosol	$C_A = f_{AV}\mathbb{A}_A\mathbb{Z}_Q$	
Rain	$C_M = \mathbb{A}_A(\mathbb{Z}_W + f_{AV}W_g\mathbb{Z}_Q)$	(A.11)
Water, dissolved	$C_W = (1 - f_{WV})\mathbb{A}_W\mathbb{Z}_W$	(A.12)
Water, SPM	$C_P = f_{WV}\mathbb{A}_W\mathbb{Z}_P$	(A.13)
Sediment, pore water	$C_N = (1 - f_{SV})\mathbb{A}_S\mathbb{Z}_W$	
Sediment, solids	$C_S = f_{SV}\mathbb{A}_S\mathbb{Z}_S$	(A.14)
Bulk air	$C_{AB} = \mathbb{A}_A\mathbb{Z}_{AT}$	
Bulk water	$C_{WB} = \mathbb{A}_W\mathbb{Z}_{WT}$	
Bulk sediment	$C_{SB} = \mathbb{A}_S\mathbb{Z}_{ST}$	

where

W_g = rain scavenging ratio [-]

A.1.3 PROCESSES

Table A-2 defines the process rates *q* and transport parameters *D* for each process.

Table A-2. Process rates and transport parameters

Process	Rate [N·T^{-1}]		Transport [L^3·T^{-1}]	
Inflow, water	$q_I = D_I\mathbb{A}_{WI}$		$D_I = Q_I\mathbb{Z}_W$	
Inflow, SPM	$q_X = D_X\mathbb{A}_{WI}$		$D_X = Q_X\mathbb{Z}_P$	
Outflow, water	$q_J = D_J\mathbb{A}_W$		$D_J = Q_J\mathbb{Z}_W$	
Outflow, SPM	$q_Y = D_Y\mathbb{A}_W$		$D_Y = Q_Y\mathbb{Z}_P$	
Rain	$q_M = D_M\mathbb{A}_A$	(A.15)	$D_M = Q_M\mathbb{Z}_W$	(A.16)
Deposition, dry	$q_Q = D_Q\mathbb{A}_A$	(A.17)	$D_Q = Q_Q\mathbb{Z}_Q$	(A.18)
Deposition, wet	$q_C = D_C\mathbb{A}_A$	(A.19)	$D_C = Q_C\mathbb{Z}_Q$	(A.20)
Adsorption, air-water	$q_{VW} = D_V\mathbb{A}_A$		$D_V = Q_V\mathbb{Z}_W$	
Volatilization, water-air	$q_{VA} = D_V\mathbb{A}_W$			
Diffusion, water-sediment	$q_{TS} = D_T\mathbb{A}_W$		$D_T = Q_T\mathbb{Z}_W$	
Diffusion, sediment-water	$q_{TW} = D_T\mathbb{A}_S$	(A.21)		
SPM deposition	$q_D = D_D\mathbb{A}_W$	(A.22)	$D_D = Q_D\mathbb{Z}_P$	(A.23)
Sediment resuspension	$q_R = D_R\mathbb{A}_S$		$D_R = Q_R\mathbb{Z}_S$	
Sediment burial	$q_B = D_B\mathbb{A}_S$		$D_B = Q_B\mathbb{Z}_S$	

Table A-3 defines the volumetric rates *Q*.

Table A-3. Volumetric rates

Process	Volumetric rate [$L^3 \cdot T^{-1}$]	
Inflow, water	Q_I	
Inflow, SPM	$Q_X = \frac{Q_I C_{PI}}{\rho_W}$	
Outflow, water	Q_J	
Outflow, SPM	$Q_Y = f_{WV} Q_J$	
Rain	$Q_M = v_{RA} A_{LA}$	(A.24)
Deposition, dry	$Q_Q = f_{AV} v_{AD} A_{LA}$	(A.25)
Deposition, wet	$Q_C = f_{AV} W_g Q_M$	(A.26)
Diffusion, air	$Q_V = k_V A_{LA}$	
Diffusion, sediment	$Q_T = k_T A_{SE}$	
Particle deposition	$Q_D = \frac{F_S A_{LA}}{\rho_W}$	
Sediment resuspension	$Q_R = \frac{F_R A_{LA}}{\rho_S}$	
Sediment burial	$Q_B = \frac{F_B A_{LA}}{\rho_S}$	

where

A_{LA} = water body surface area [L^2]

A_{SE} = sediment surface area [L^2]

C_{PI} = concentration of inflow particulate [$M \cdot L^{-3}$]

v_{RA} = rate of rain [$L \cdot T^{-1}$]

v_{AD} = rate of aerosol deposition [$L \cdot T^{-1}$]

F_S = flux adsorbed on SPM, settling [$M \cdot L^{-2} \cdot T^{-1}$]

F_R = flux adsorbed on SPM, resuspension [$M \cdot L^{-2} \cdot T^{-1}$]

F_B = flux of sediment particles, burial [$M \cdot L^{-2} \cdot T^{-1}$]

k_T = mass transfer coefficient: water/sediment [$L \cdot T^{-1}$]

k_V = mass transfer coefficient: net air/water [$L \cdot T^{-1}$]

The particle flux terms should be constrained by mass balance, if burial accounts for sediment accumulation:

$$F_S = F_R + F_B \tag{A.27}$$

Process rates across the system boundary express the molar rate balance:

$$\dot{n}_{IN} = E_w + q_I + q_X + q_M + q_Q + q_C + q_{VW} \quad \text{(A.28)}$$

$$\dot{n}_{OUT} = q_J + q_Y + q_{VA} + q_B \quad \text{(A.29)}$$

A.1.4 SYSTEM PROPERTIES

The fraction of aerosols f_{AV} is:

$$f_{AV} = \frac{C_{PA}}{\rho_A} \quad \text{(A.30)}$$

where

C_{PA} = concentration of aerosol [M·L^{-3}]

ρ_A = density of air particles [M·L^{-3}]

The fraction of SPM is:

$$f_{WV} = \frac{C_{PL}}{\rho_W} \quad \text{(A.31)}$$

where

C_{PL} = concentration of suspended particulate matter [M·L^{-3}]

The overall mass transfer coefficient k_V is **(MACKAY, 2001)**:

$$k_V = \frac{1}{\frac{1}{k_{VW}} + \frac{RT_W}{k_{VA}H}} \quad \text{(A.32)}$$

where

k_{VW} = mass transfer coefficient water-side [L·T^{-1}]

k_{VA} = mass transfer coefficient air-side [L·T^{-1}]

The distribution coefficients for sediment K_d and suspended particulate K_p may be set from the literature, or from the system observations of water concentration C_{OW}, sediment concentration C_{OS} and particle concentration C_{OP}:

$$K_d = \frac{C_{OS}}{C_{OW}} \quad \text{(A.33)}$$

$$K_p = \frac{C_{OP}}{C_{OW}C_{PL}} \quad \text{(A.34)}$$

The total water concentration C_{OWP} may be available instead, and by the fraction of SPM in water f_{PW}, the particle and water concentrations C_{OP} and C_{OW} found:

$$C_{\mathrm{OP}} = f_{\mathrm{PW}} C_{\mathrm{OWP}} \quad \text{(A.35)}$$

$$C_{\mathrm{OW}} = (1 - f_{\mathrm{PW}}) C_{\mathrm{OWP}} \quad \text{(A.36)}$$

where

f_{PW} = SPM adsorption fraction [-]

A.2 INPUTS

A.2.1 PHYSICAL PROPERTIES

Table A-4 shows physical properties required for the model **(MACKAY, 1989)**.

Table A-4. Physical properties

Property	Symbol	Value	Units
Ideal gas constant	R	8.314	$m^3 \cdot Pa \cdot K^{-1} \cdot mol^{-1}$
Mass transfer coefficient: water-air	k_{VA}	1[14]	$m \cdot h^{-1}$
Mass transfer coefficient: air-water	k_{VW}	0.01[14]	$m \cdot h^{-1}$

A.2.2 CHEMICAL PROPERTIES

The vapour phase does not factor significantly into the transport and concentrations of stable lead. The available data was input to the reproduced QWASI aquivalence model to make a general assessment of magnitude for the volatilization process.

This polynomial expression for solid lead cited over the temperature range 298 K to melting point gives a vapour pressure of 4E-24 Pa at 25°C **(ALCOCK, 1984)**:

$$\log P\,[atm] = 5.643 - \frac{10143}{T[K]} \quad \text{(A.37)}$$

This temperature and pressure are upper bounds for natural waters. No volatile lead compounds have been identified that would result biogeochemically.

Over the range of natural water assumed approximately as pH 6.7-10, the solubility of Pb was determined to be 3 mg/L with $PbCl_2$ and $PbSO_4$, and 0.2 mg/L with $PbCO_3$; over the intermediate range pH 8-9 these were measured to be 0.5 mg/L and 0.1 mg/L respectively **(PEIRRARD, 2002)**.

The concentration of anions in Lake Ontario were reported to be 42.2 mg/L HCO_3^-, 13 mg/L Cl^-, and 8 mg/L SO_4^{2-}, and at the surface pH is about 8 **(ALLEN, 1977)**.

[14] Mackay assigns $k_V = 0$ for the involatility of lead, although values of k_{VA} and k_{VW} are tabled **(ALCOCK, 1984)**; k_V is calculated with Equation A.32 but assigned $k_V = 0$ for verification.

The solubility in Lake Ontario was taken to be limited by HCO_3^- at 0.1 mg/L for application in the QWASI aquivalence model.

Table A-5 summarizes the chemical properties of lead.

Table A-5. Properties of lead

Property	Symbol	Value	Units
Vapour pressure	P_V	4E-24[15]	Pa
Chemical solubility	S	0.1[16]	$mg \cdot L^{-1}$
Molar mass	M	207	$g \cdot mol^{-1}$

A.2.3 LAKE PROPERTIES

A temperature T_W = 12°C was adopted from the value applied to Lake Ontario for PCB. Table A-6 lists lake inputs to the model **(MACKAY, 1989)**.

The observed concentrations shown in Table A-8 were used to calculate the distribution coefficient by Equations (A.33) and (A.34):

K_d = 3.33E+05 $L \cdot kg^{-1}$

K_p = 6.67E+05 $L \cdot kg^{-1}$

[15] From **(PEIRRARD, 2002)**
[16] From **(MACKAY, 1989)**

Table A-6. QWASI Lake Ontario properties

Property			Value
Area of lake	A_{LA}	m^2	1.95E+10
Area of sediment	A_{SE}	m^2	1.95E+10
Density of SPM	ρ_w	$g \cdot cm^{-3}$	2.4
Density of aerosol	ρ_A	$g \cdot cm^{-3}$	1.5
Density of sediment	ρ_S	$g \cdot cm^{-3}$	2.4
Concentration of water particulate	C_{PL}	$mg \cdot L^{-1}$	0.5
Concentration of inflow particulate	C_{PI}	$mg \cdot L^{-1}$	24[17]
Concentration of aerosol	C_{PA}	$\mu g \cdot m^{-3}$	30
Rate of rain	v_{RA}	$m \cdot a^{-1}$	0.84
Rate of dry aerosol deposition	v_{AD}	$m \cdot h^{-1}$	7.2[18]
Rain scavenging ratio	W_g	-	133,000[19]
Mass transfer coefficient: sediment/water	k_T	$m \cdot h^{-1}$	4E-04
Volumetric rate of water inflow	Q_I	$m^3 \cdot h^{-1}$	2.40E+07
Volumetric rate of water outflow	Q_J	$m^3 \cdot h^{-1}$	2.44E+07
Volume fraction of sediment particles	f_{SV}	-	0.15
Flux of particles, settling	F_S	$g \cdot m^{-2} \cdot d^{-1}$	fit[20]
Flux of particles, resuspension	F_R	$g \cdot m^{-2} \cdot d^{-1}$	fit[20]
Flux of particles, burial	F_B	$g \cdot m^{-2} \cdot d^{-1}$	fit[20]
Emissions to water	E_W	$kg \cdot a^{-1}$	1752
Concentration in air, aerosol	C_{OA}	$\mu g \cdot m^{-3}$	0.075
Concentration in water inflow	C_{OI}	$ng \cdot L^{-1}$	1000

A.3 OUTPUT

Particle flux values were adjusted by trial and error to optimize the Pb model. No set of flux values could be found that achieve correspondence between each of the water, SPM and sediment concentration observations and model outputs. Table A-7 shows the initial and adjusted particle flux values that result in correspondence between the reported and recalculated model concentrations.

[17] Inferred from the reported inflow particle transport parameter D_X **(MACKAY, 1989)**.
[18] As 0.2 $cm \cdot s^{-1}$ **(HOFF, 1996) (STRACHAN, 1988)**
[19] Found from the rain/aerosol concentration ratio **(MACKAY, 1989)** 10000/0.075 $ng \cdot L^{-1}$ reported in *Table 6* of **(STRACHAN, 1988)**.
[20] Optimized parameter; see section A.3

Table A-7. QWASI aquivalence formulation particle fluxes

Process		Particle flux ($g \cdot m^{-2} \cdot h^{-1}$)	
		Initial[21]	Final
Settling	F_S	0.1	1.41
Resuspension	F_R	0.0875	1.16
Burial	F_B	0.125	0.59

Table A-8 shows the reported observed and model estimated concentrations **(MACKAY, 1989)** and the recalculated model concentrations using the final flux values.

Table A-8. QWASI formulation concentrations

Phase			Reported		Model Estimated
			(Observed)	Estimated	
Air, gas	(C_{OG}) C_G	$\mu g/m^3$	0	0	3.8E-24
Air, aerosol	(C_{OA}) C_A	$\mu g/m^3$	0.075[22]	0.075	0.075
Rain	(C_{OM}) C_M	$\mu g/m^3$	10,000[23]	10,037	10,013
Water	(C_{OW}) C_W	ng/L	300[22]	186	185
Water particles	(C_{OP}) C_P	ng/L	100[22]	62	62
Total water	(C_{OWP}) C_{WP}	ng/L	400	247	247
Sediment solids	(C_{OS}) C_S	µg/g	100[22]	99	99

Output aquivalence capacities, contributions to bulk media, transport parameters and process rates correspond to the reported values **(MACKAY, 1989)**, except for discrepancies between the SPM lead outflow transport parameter and process rate:

- D_Y = 8.13 $m^3 \cdot h^{-1}$ versus 9.53 $m^3 \cdot h^{-1}$ reported
- q_Y = 13,203 $m^3 \cdot h^{-1}$ versus 15,473 $m^3 \cdot h^{-1}$ reported

The reported model values for these parameters were 0.853 of the recalculated values. The difference was attributed to the original calculation for particle outflow volumetric rate Q_Y.

[21] From **(ETHIER, 2008)** citing O'Driscoll NJ, Rencz AN, Lean DR (2005) Mercury cycling in a wetland-dominated ecosystem: a multidisciplinary study. Society of Environmental Toxicology and Chemistry (SETAC).
[22] From **(MACKAY, 1989)(STRACHAN, 1988)**
[23] From **(STRACHAN, 1987)(STRACHAN, 1988)**

Model process diagrams show process rates (kg·a^{-1}), contributions as percentages to inflow, outflow and internal processes, and concentrations, according to the separate adjustments detailed in Table 2:

- Figure A-2 base: adjusted particle flux to fit original study **(MACKAY, 1989)**
- Figure A-3 case 1: adjusted particle flux to Equation A.27 particle balance by resuspension flux F_R decrease
- Figure A-4 case 2: K_d alignment by resuspension flux F_R increase
- Figure A-5 case 3: K_d alignment by burial flux F_R increase
- Figure A-6 case 4: K_d alignment by upward sediment diffusion coefficient k_{TW} increase

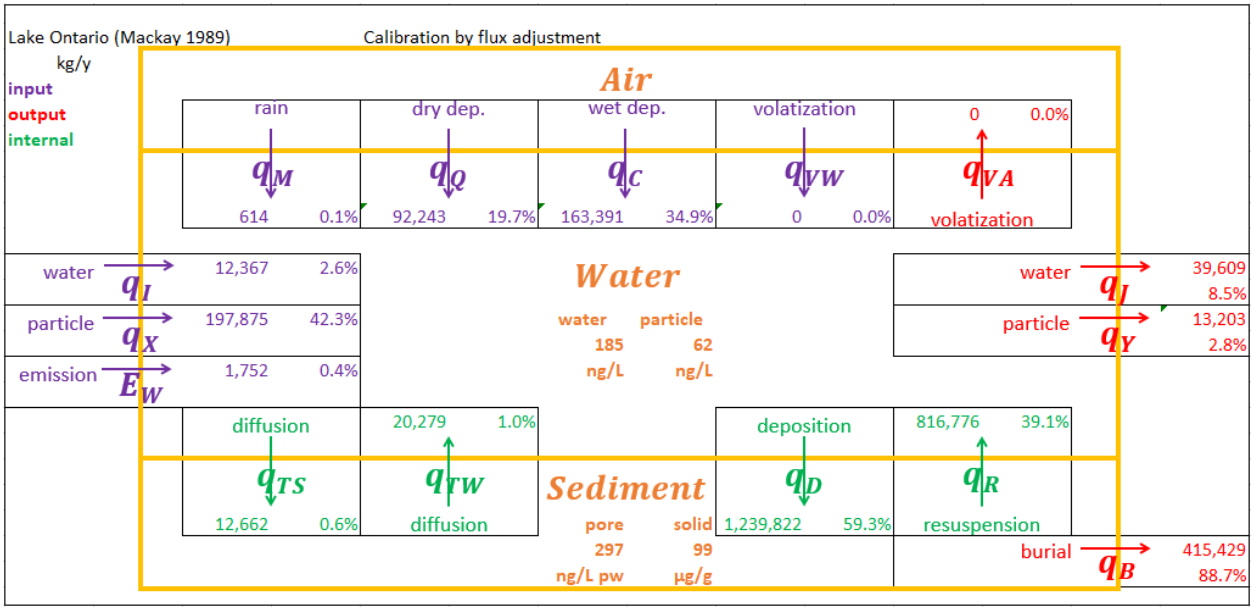

Figure A-2. QWASI base scenario

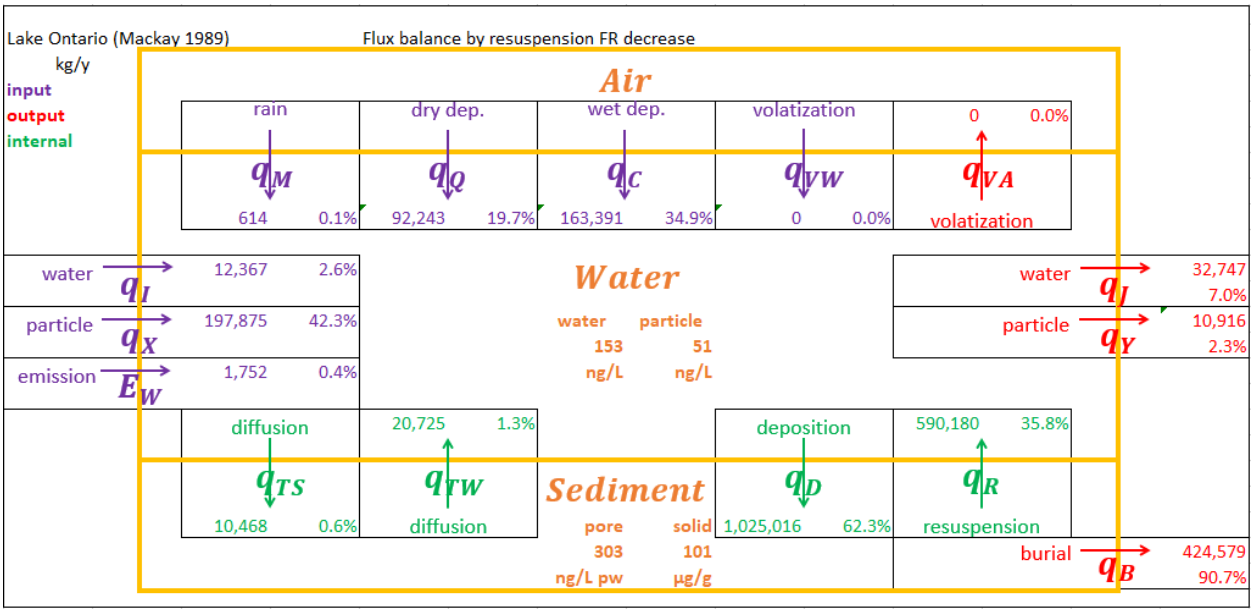

Figure A-3. QWASI case 1: F_R decrease

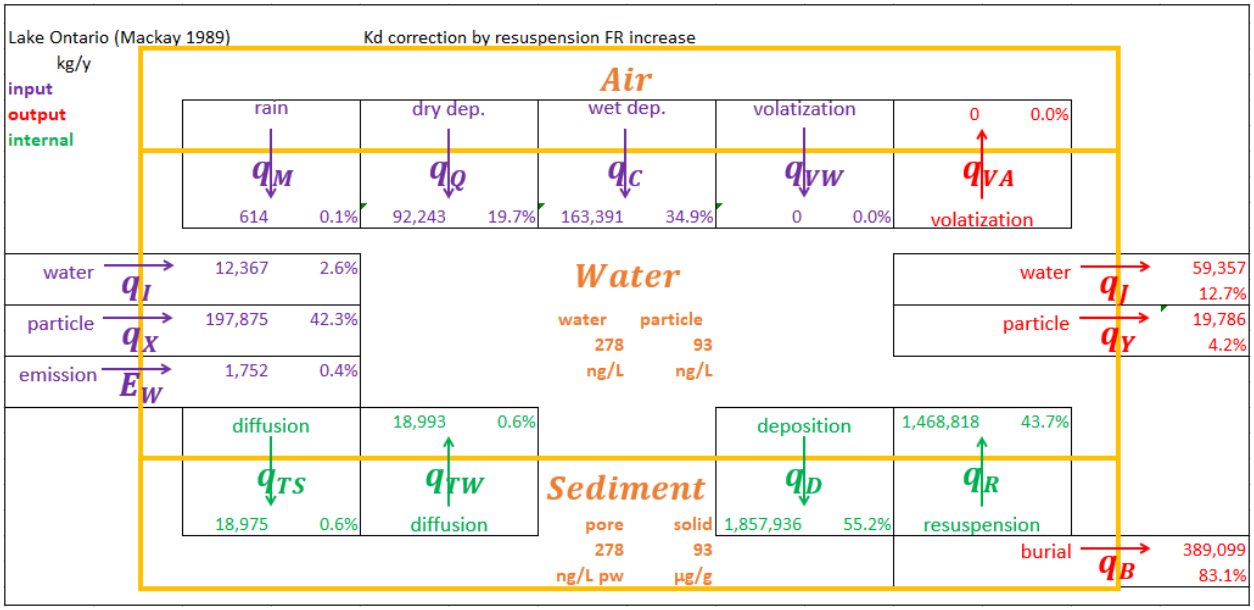

Figure A-4. QWASI case 2: F_R increase

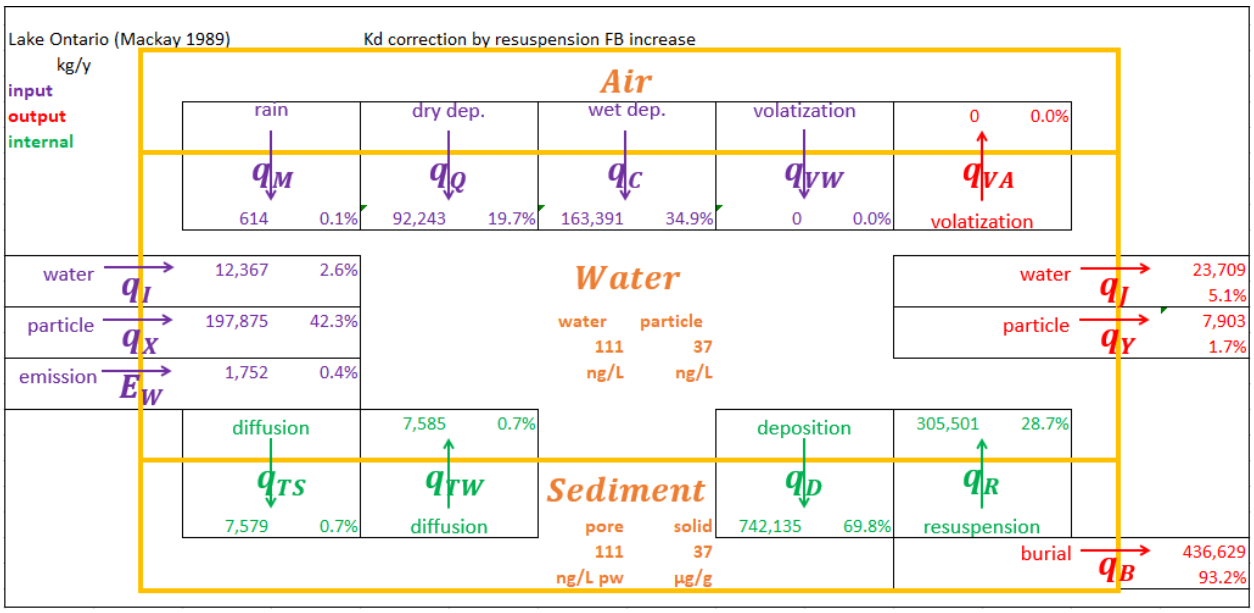

Figure A-5. QWASI case 3: F_B increase

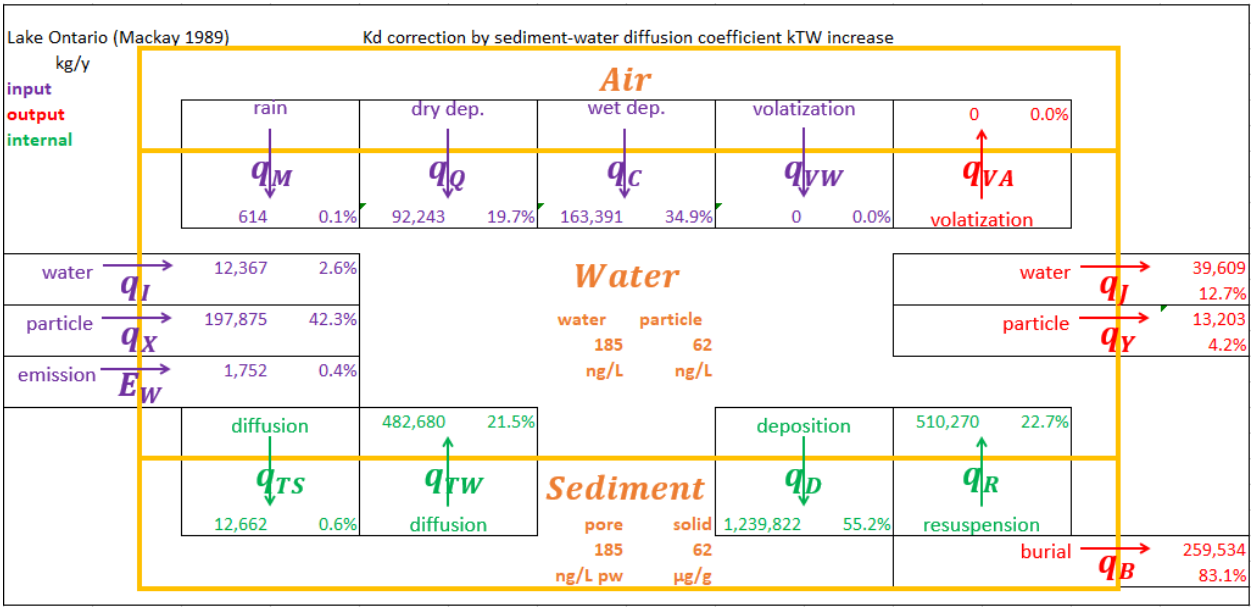

Figure A-6. QWASI case 4: k_{TW} increase

B Hamilton Harbour

B.1 MODEL

This section presents a reproduction of the two-layer epilimnion / hypolimnion QWASI aquivalence steady-state model shown in Table B-1 **(LING, 1993)**.

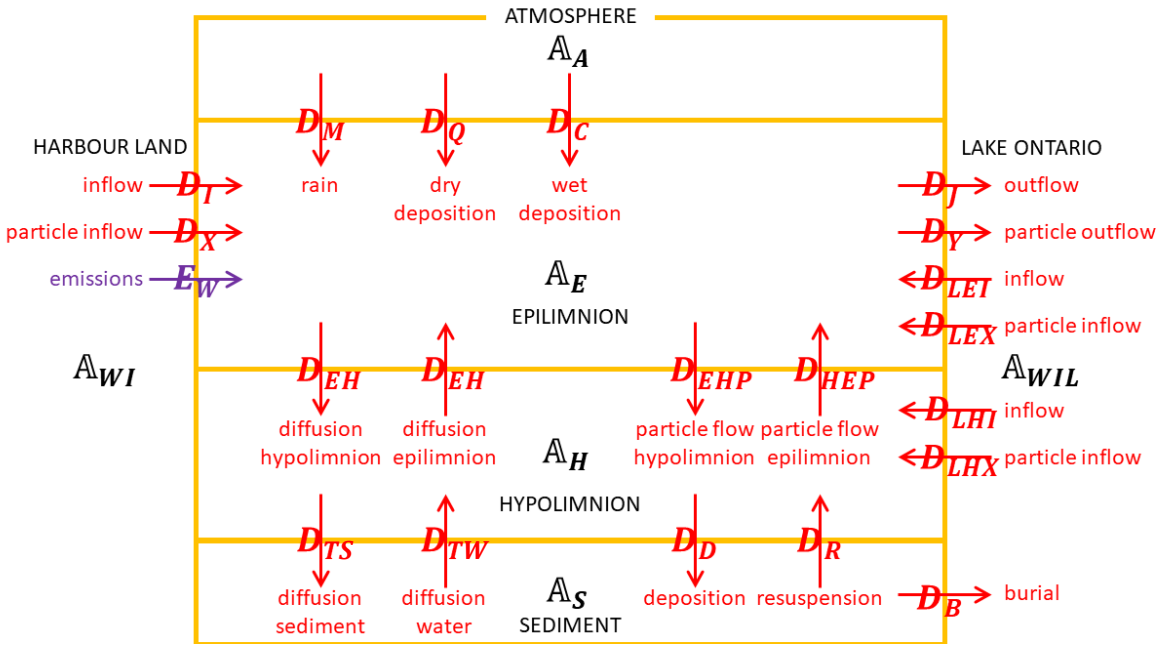

Figure B-1. Hamilton Harbour layer model media and processes

B.1.1 AQUIVALENCE

Lake Ontario SPM aquivalence capacity:

$$\mathbb{Z}_{PL} = K_p \rho_{WL} \tag{B.1}$$

where

ρ_{WL} = SPM density in Lake Ontario [M·L^{-3}]

Lake Ontario bulk water inflow aquivalence capacity:

$$\mathbb{Z}_{ITL} = (1 - f_{WVL})\mathbb{Z}_W + f_{WVL}\mathbb{Z}_{PL} \tag{B.2}$$

where

f_{WVL} = volume fraction of SPM in Lake Ontario [-]

Aquivalences are as defined for the general model. Water inflow bulk aquivalence $\mathbb{A}_{WI}$ represents industrial, municipal and sewer inflows to the harbour. Lake Ontario inflow bulk aquivalence $\mathbb{A}_{WIL}$:

$$\mathbb{A}_{WIL} = \frac{C_{OI}}{\mathbb{Z}_{ITL}} \tag{B.3}$$

B.1.2 BALANCE

The mass balance for sediment overlain by the hypolimnion is:

$$(D_D + D_{TS})\mathbb{A}_H - (D_R + D_{TW} + D_B)\mathbb{A}_S = 0 \tag{B.4}$$

The mass balance for hypolimnion is:

$$(D_{LHX} + D_{LHI})\mathbb{A}_{WIL} + (D_{EH} + D_{EHP})\mathbb{A}_E + (D_{TW} + D_R)\mathbb{A}_S - (D_{EH} + D_{HEP} + D_D + D_{TS})\mathbb{A}_H = 0 \tag{B.5}$$

The mass balance for epilimnion is:

$$E_E + (D_X + D_I)\mathbb{A}_{WI} + \left(D_M + D_C + D_Q\right)\mathbb{A}_A + (D_{LEX} + D_{LEI})\mathbb{A}_{WIL} + (D_{EH} + D_{HEP})\mathbb{A}_H - \left(D_{EH} + D_{EHP} + D_J + D_Y\right)\mathbb{A}_E = 0 \tag{B.6}$$

Solving by {solve [(solve (B.4) for $\mathbb{A}_S$) sub into (B.5)] for $\mathbb{A}_E$} and {solve (B.6) for $\mathbb{A}_E$} for $\mathbb{A}_H$, $\mathbb{A}_E$ and $\mathbb{A}_S$:

$$\mathbb{A}_H = \frac{\begin{matrix}\left[(D_{EH} + D_{EHP})(D_{LEX} + D_{LEI}) + \left(D_{EH} + D_{EHP} + D_J + D_Y\right)(D_{LHX} + D_{LHI})\right]\mathbb{A}_{WIL} \\ +(D_{EH} + D_{EHP})\left[E_E + (D_X + D_I)\mathbb{A}_{WI} + \left(D_M + D_C + D_Q\right)\mathbb{A}_A\right]\end{matrix}}{\left(D_{EH} + D_{EHP} + D_J + D_Y\right)\left(D_{EH} + D_{HEP} + D_D + D_{TS} - \frac{(D_{TW} + D_R)(D_D + D_{TS})}{D_R + D_{TW} + D_B}\right) - (D_{EH} + D_{EHP})(D_{EH} + D_{HEP})} \tag{B.7}$$

$$\mathbb{A}_E = \frac{(D_{EH} + D_{HEP})\mathbb{A}_H + (D_X + D_I)\mathbb{A}_{WI} + \left(D_M + D_C + D_Q\right)\mathbb{A}_A + (D_{LEX} + D_{LEI})\mathbb{A}_{WIL}}{D_{EH} + D_{EHP} + D_J + D_Y} \tag{B.8}$$

$$\mathbb{A}_S = \frac{(D_D + D_{TS})\mathbb{A}_H}{(D_R + D_{TW} + D_B)} \tag{B.9}$$

The original study solves the bulk media molar balances by grouping terms **(LING, 1993)**. With the following corrections, the method results in the same values for the aquivalences calculated with the foregoing as shown in Table B-6, simplified by neglecting transport parameters for volatilization D_V and decay (molecular chemical transformation) D_{WE}, D_{WH}, D_S. Reformulations of the original expressions for $\mathbb{A}_H$, $\mathbb{A}_E$ give results consistent with (B.7) and (B.8):

$$D_2 = D_{EH} + D_{HEP} + D_D + D_T \tag{B.10}$$

$$\mathbb{A}_H = \frac{D_1 D_{LH} A_L + (D_{EH} + D_{EHP})(I + D_4 A_A + D_{LE} A_L)}{D_1 D_2 - D_1 D_5 - (D_{EH} + D_{EHP})(D_{EH} + D_{HEP})} \tag{B.11}$$

$$\mathbb{A}_E = \frac{I + D_4 A_A + (D_{EH} + D_{HEP})A_H + D_{LE} A_L}{D_1} \tag{B.12}$$

where

$$A_L = A_{WIL}$$

$$D_{LH} = D_{LHI} + D_{LHX}$$

B.1.3 CONCENTRATIONS

Concentrations are as defined in Table A-1 except that the water and SPM are separate for the epilimnion and hypolimnion:

$$C_{HW} = (1 - f_{WV})\mathbb{A}_H\mathbb{Z}_W \quad \text{(B.13)}$$

$$C_{EW} = (1 - f_{WV})\mathbb{A}_E\mathbb{Z}_W \quad \text{(B.14)}$$

$$C_{HP} = f_{WV}\mathbb{A}_H\mathbb{Z}_P \quad \text{(B.15)}$$

$$C_{EP} = f_{WV}\mathbb{A}_E\mathbb{Z}_P \quad \text{(B.16)}$$

B.1.4 PROCESSES

Process rates and transport parameters are as defined in Table A-2, neglecting volatilization and adsorption, and/or as defined in Table B-1. Volumetric rates are as defined in Table A-3, and/or as defined in Table B-2.

The fraction of SPM is:

$$f_{WVL} = \frac{C_{PLL}}{\rho_{WL}} \quad \text{(B.17)}$$

Parameters $\dot{m}_{LEX}$, $\dot{m}_{LHX}$, $\dot{m}_{HX}$, $\dot{m}_{HLY}$, k_{EH} and C_{PLL} are defined in Table B-4.

Table B-1. Hamilton Harbour process rates and transport parameters

Process	Process [N·T^{-1}]	Transport [L^3·T^{-1}]
Inflow, water lake–epilimnion	$q_{LEI} = D_{LEI}\mathbb{A}_{WIL}$	$D_{LEI} = Q_{LEI}\mathbb{Z}_W$
Inflow, water lake–hypolimnion	$q_{LHI} = D_{LHI}\mathbb{A}_{WIL}$	$D_{LHI} = Q_{LHI}\mathbb{Z}_W$
Inflow, particle lake–epilimnion	$q_{LEI} = D_{LEX}\mathbb{A}_{WIL}$	$D_{LEX} = Q_{LEX}\mathbb{Z}_{PL}$
Inflow, particle lake–hypolimnion	$q_{LHI} = D_{LHX}\mathbb{A}_{WIL}$	$D_{LHX} = Q_{LHX}\mathbb{Z}_{PL}$
Particle, hypolimnion-epilimnion	$q_{HEP} = D_{HEP}\mathbb{A}_H$	$D_{HEP} = Q_{HEP}\mathbb{Z}_P$
Particle, epilimnion-hypolimnion	$q_{EHP} = D_{EHP}\mathbb{A}_E$	$D_{EHP} = Q_D\mathbb{Z}_P$
Outflow, water epilimnion-lake	$q_J = D_J\mathbb{A}_E$	$D_J = Q_J\mathbb{Z}_W$
Outflow, particle epilimnion-lake	$q_Y = D_Y\mathbb{A}_E$	$D_Y = Q_Y\mathbb{Z}_P$
Diffusion, epilimnion-hypolimnion	$q_{EH} = D_{EH}\mathbb{A}_H$	$D_{EH} = Q_{EH}\mathbb{Z}_W$
Diffusion, epilimnion-hypolimnion	$q_{HE} = D_{EH}\mathbb{A}_E$	
Diffusion, water-sediment	$q_W = D_T\mathbb{A}_H$	$D_T = Q_T\mathbb{Z}_W$
Particle deposition	$q_D = D_D\mathbb{A}_H$	$D_D = Q_D\mathbb{Z}_P$

Table B-2. Hamilton Harbour volumetric rates

Process	Volumetric rate [L^3·T^{-1}]
Inflow, water lake-epilimnion	Q_{LEI}
Inflow, water lake-hypolimnion	Q_{LHI}
Inflow, particle lake-epilimnion	$Q_{LEX} = \frac{\dot{m}_{LEX}}{\rho_{WL}}$
Inflow, particle lake-hypolimnion	$Q_{LHX} = \frac{\dot{m}_{LHX}}{\rho_{WL}}$
Inflow, particle from harbour land	$Q_X = \frac{\dot{m}_{HX}}{\rho_W}$
Outflow, particle epilimnion-lake	$Q_Y = \frac{\dot{m}_{HLY}}{\rho_W}$
Outflow, particle	$Q_Y = f_{WV}Q_J$
Diffusion across thermocline	$Q_{EH} = k_{EH}A_{LA}$
Flow, water hypolimnion-epilimnion	$Q_{HE} = Q_{LHI}$
Flow, particle hypolimnion-epilimnion	$Q_{HEP} = \frac{Q_{HE}C_{PL}}{\rho_W}$

B.2 INPUTS

Table B-3 lists inputs to the Hamilton Harbour model **(LING, 1993)** common to the original QWASI model described in Appendix A **(MACKAY, 1989)**. Table B-4 lists additional variables required to extend the original QWASI model for the two-layer

Hamilton Harbour model. Distribution coefficients K_d and K_p are the values calculated from the assumed concentrations in the original aquivalence model **(MACKAY, 1989)**.

B.2.1 LEAD CONCENTRATIONS

Hamilton Harbour sediments sampled 1983-1987 **(OME, 1992B)** from five stations measured for lead 200, 300, 330, 340, and 570 $\mu g \cdot g^{-1}$ **(OME, 1992C)**, having a geometric mean of 330 $\mu g \cdot g^{-1}$. A more extensive set of pooled data sampled 1975-1986 were reported as 260, 281, 310, 310, and 320 $\mu g \cdot g^{-1}$ **(OME, 1992A)**, having geometric mean of 295 $\mu g \cdot g^{-1}$. A contour map of the harbour show regions greater than 300 $\mu g \cdot g^{-1}$ covering at least half the surface area **(OME, 1992A)**, and which appears to corroborate the range 34-690 $\mu g \cdot g^{-1}$ cited by **(LING, 1993)**.

The average concentration of lead in water measured in the harbour in 1982 was 4.8 $\mu g \cdot L^{-1}$, and not detected for years 1984-1987 **(OME, 1992A)**. The observed concentration is tabled as <3 $\mu g \cdot L^{-1}$ **(LING, 1993)**, which corresponds to a reported detection limit **(OME, 1992C)**.

Recent sedimentation rates in the harbour, determined by the Pb-210 dating method, are about 410 $g \cdot m^{-2} \cdot a^{-1}$ in recent years and 1590 $g \cdot m^{-2} \cdot a^{-1}$ in the pre-dredging era **(NRIAGU, 1983)**.

Table B-3. Hamilton Harbour formulation properties

Property			Value
Area of lake	A_{LA}	m^2	2.15E+07[24]
Area of sediment	A_{SE}	m^2	2.15E+07[24]
Density of SPM	ρ_W	$g \cdot cm^{-3}$	2.0[25]
Density of aerosol	ρ_A	$g \cdot cm^{-3}$	1.5[26]
Density of sediment	ρ_S	$g \cdot cm^{-3}$	2.64[27]
Concentration of water particulate	C_{PL}	$mg \cdot L^{-1}$	10[24]
Concentration of inflow particulate	C_{PI}	$mg \cdot L^{-1}$	74.4[28]
Concentration of aerosol	C_{PA}	$\mu g \cdot m^{-3}$	30[26]
Rate of rain	v_{RA}	$m \cdot a^{-1}$	0.865[24]
Rate of dry aerosol deposition	v_{AD}	$m \cdot h^{-1}$	7.2[26]
Rain scavenging ratio	W_g	-	200,000[26]
Mass transfer coefficient: sediment	k_T	$m \cdot h^{-1}$	4E-04
Volumetric rate water inflow land-harbour	Q_I	$m^3 \cdot h^{-1}$	28,100[29]
Volumetric rate water outflow epilimnion	Q_J	$m^3 \cdot h^{-1}$	148,000[30]
Volume fraction of sediment particles	f_{SV}	-	0.085[31]
Flux of particles, settling	F_S	$g \cdot m^{-2} \cdot d^{-1}$	6.00[32]
Flux of particles, resuspension	F_R	$g \cdot m^{-2} \cdot d^{-1}$	1.63[32]
Flux of particles, burial	F_B	$g \cdot m^{-2} \cdot d^{-1}$	4.36[33]
Emissions to water	E_W	$kg \cdot a^{-1}$	7740[34]
Concentration in air, aerosol	C_{OA}	$\mu g \cdot m^{-3}$	0.063[35]
Concentration in water inflow	C_{OI}	$ng \cdot L^{-1}$	400[36]

[24] Coincides with **(OME, 1992A)**
[25] From OME, unpublished data **(LING, 1993)**.
[26] Assumed **(LING, 1993)**; except for W_g which corresponds to the PCB value, these are consistent with the lead values from **(MACKAY, 1989)**.
[27] Range 2.24-3.04 $g \cdot cm^{-3}$ (N. Rukavina, unpublished data) **(LING, 1993)**.
[28] Calculated as $\dot{m}_{HX}/Q_I$
[29] Consist of direct discharges to the harbour by municipal sewage treatment plants at 15,500 $m^3 \cdot h^{-1}$ and storm sewers and creeks at 12,600 $m^3 \cdot h^{-1}$ **(LING, 1993)** from 4.3 $m^3 \cdot s^{-1}$ and 3.5 $m^3 \cdot s^{-1}$
[30] From **(LING, 1993)**
[31] Sediment porosity n = 0.915 **(LING, 1993)** averaged over the top 3 cm from *Table 1* **(NRIAGU, 1983)**; f_{SV} = (1-n) = 0.085.
[32] Optimized from PCB model calibration **(LING, 1993)**.
[33] Represents pre-dredging era of harbour **(NRIAGU, 1983)**.
[34] *Figure 6* value representing industrial emissions, 0.883 $kg \cdot h^{-1}$ from *Table 3* **(LING, 1993)**.
[35] This value is applied instead of the 0.004 $\mu g \cdot m^{-3}$ indicated in *Table 7*, since it corresponds to the *Table 3* atmospheric loading value of 0.037 $kg \cdot h^{-1}$ and is consistent with the resulting

Table B-4. Hamilton Harbour thermocline properties

Property			Value
Depth of harbour	d_{LA}	m	13[24]
Depth of epilimnion	d_E	m	6[24]
Depth of hypolimnion	d_H	m	7[24]
Depth of sediment	d_{SE}	m	0.03[24]
Density of SPM, lake	ρ_w	$g \cdot cm^{-3}$	2.4
Concentration of inflow SPM, lake	C_{PLL}	$mg \cdot L^{-1}$	1.11[37]
Mass transfer coefficient: thermocline	k_{HE}	$m \cdot h^{-1}$	0.4[38]
Volumetric rate water inflow, epilimnion	Q_{LEI}	$m^3 \cdot h^{-1}$	44,100[39]
Volumetric rate water inflow, hypolimnion	Q_{LHI}	$m^3 \cdot h^{-1}$	73,500[39]
Mass rate inflow lake-epilimnion	$\dot{m}_{LEX}$	$g \cdot h^{-1}$	52,000[40]
Mass rate inflow lake-hypolimnion	$\dot{m}_{LHX}$	$g \cdot h^{-1}$	100,000[40]
Mass rate inflow land-harbour	$\dot{m}_{HX}$	$g \cdot h^{-1}$	2,090,000[41]
Mass rate outflow epilimnion-lake	$\dot{m}_{HLY}$	$g \cdot h^{-1}$	408,000[41]

B.2.2 PROCESSES

Table B-5 compares the Pb model transport parameters with those in the reported *Table 6* **(LING, 1993)**. Although the atmospheric deposition rain D_M, wet deposition D_C and dry deposition D_Q are not reported, the process rate formula and inputs are otherwise reported **(LING, 1993)**, and are consistent with inputs[35] and aquivalence reformulations.

atmospheric deposition mass rate 320 $kg \cdot a^{-1}$ shown in *Fig. 6* **(LING, 1993)** and confirmed in the recalculated model.

[36] As 1.93E-06 $mol \cdot m^{-3}$ from *Table 7* **(LING, 1993)**, *Table 6* **(MACKAY, 1989)**, *Table 6* **(STRACHAN, 1988)**, *Table 2* **(STRACHAN, 1987)**

[37] From *Table 2* **(BARICA, 1988)**

[38] From **(KLAPWIJK, 1985)**; the no-thermocline model variation is made by increasing k_{HE} by a factor of 1000 to simulate turnover conditions in a well-mixed water column **(LING, 1993)**.

[39] Estimated from a dissolved solid/temperature model representing peak spring flowrate **(KLAPWIJK, 1985)**.

[40] From **(OME, 1992A)**

[41] From (OME 1989, Remedial Action Plan for Hamilton Harbour, Environmental Conditions and Problem Definition, First Edition of Stage 1 Report) **(LING, 1993)**

Table B-5. Hamilton Harbour transport parameters

Property		Volumetric rate ($m^3 \cdot h^{-1}$)	
		Report	Model
Inflow water, land-harbour	D_I	2.81E+04	2.81E+04
Outflow water, harbour-lake	D_J	1.48E+05	1.48E+05
Inflow water, lake-epilimnion	D_{LEI}	4.41E+04	4.41E+04
Inflow water, lake-hypolimnion	D_{LHI}	7.35E+04	7.35E+04
Inflow water, total	D_{LI}	1.18E+05	1.18E+05
Diffusion, epilimnion/hypolimnion	D_{EH}	3.58E+05	3.58E+05
Inflow particle, land-harbour	D_X	1.40E+06	1.40E+06
Outflow particle, harbour-lake	D_Y	2.73E+05	2.73E+05
Flow particle, epilimnion-hypolimnion	D_{EHP}	3.59E+06	3.59E+06
Flow particle, hypolimnion-epilimnion	D_{HEP}	4.86E+05	4.91E+05
Inflow particle, lake-epilimnion	D_{LEX}	3.47E+04	3.47E+04
Inflow particle, lake-hypolimnion	D_{LHX}	6.68E+04	6.68E+04
Inflow particle, total lake-harbour	D_{LX}	1.02E+05	1.02E+05
Rain	D_M	NA	2.12E+03
Deposition, wet particle	D_C	NA	3.10E+05
Deposition, dry particle	D_Q	NA	8.49E-03
Settling particle-sediment	D_D	3.59E+06	3.59E+06
Resuspension sediment-particle	D_R	4.86E+05	4.86E+05
Burial	D_B	1.30E+06	1.30E+06
Volatilization	D_V	2.15E-05	9.07E-17
Diffusion, water/sediment	D_T	8.60E+03	8.60E+03
Degradation, epilimnion	D_{WE}	6.87E-12	NA
Degradation, hypolimnion	D_{WH}	8.01E-12	NA
Degradation, total harbour water	D_W	1.49E-11	NA
Degradation, sediment	D_S	3.34E-10	NA

B.3 OUTPUTS

Table B-6 compares the Pb model aquivalence values with those in the reported *Table 7* **(LING, 1993)**. Table B-7 compares the Pb model concentrations and amounts with those in the reported *Table 8* **(LING, 1993)**.

Table B-6. Hamilton Harbour aquivalences

Property	Aquivalence ($mol \cdot m^{-3}$)	
	Report	Model
Air concentration	1.93E-11	1.93E-11
Air aquivalence	9.65E-09	1.52E-07[42]
Lake Ontario concentration	1.93E-06	1.93E-06
Lake Ontario aquivalence	1.11E-06	1.11E-06
Thermocline, D_{EH} = 3.58E+05 $mol \cdot m^{-3}$		
Epilimnion	1.51E-06	1.36E-06
Hypolimnion	1.70E-06	1.60E-06
Sediment	3.41E-06	3.21E-06
No thermocline, DEH = 3.58E+08 $mol \cdot m^{-3}$, $A_H = A_E$		
Water column	1.67E-06	1.51E-06
Sediment	3.35E-06	3.03E-06

Table B-7. Hamilton Harbour concentrations and amounts

Property		Report	Model
Thermocline, D_{EH} = 3.58E+05 $mol \cdot m^{-3}$			
Concentration in epilimnion	$\mu g \cdot m^{-3}$	2,400	2,163
Concentration in hypolimnion	$\mu g \cdot m^{-3}$	2,700	2,543
Concentration in sediment	$\mu g \cdot g^{-1}$	235	221
Amount in epilimnion	kg	340	279
Amount in hypolimnion	kg	407	383
Amount in sediment	kg	34,000	31,990
Total	kg	34,747	32,652
No thermocline, DEH = 3.58E+08 $mol \cdot m^{-3}$, $A_H = A_E$			
Concentration in water	$\mu g \cdot m^{-3}$	2,660	2,489
Concentration in sediment	$\mu g \cdot g^{-1}$	231	216
Amount in water	kg	744	696
Amount in sediment	kg	33,500	31,333
Total	kg	34,244	32,029

Model process diagrams show process rates ($kg \cdot a^{-1}$), contributions as percentages to inflow, outflow and internal processes, and concentrations, according to the separate adjustments detailed in Table 3:

- Figure B-2 base: thermocline, $A_H > A_E$

[42] See footnote [35]. Aquivalence 9.66E-07 $mol \cdot m^{-3}$ is calculated from air concentration 0.004 $\mu g \cdot m^{-3}$. Formula corrections account for the other differences in the table, but not this value.

- Figure B-3 case 1: no thermocline, $A_H = A_E$
- Figure B-4 case 2: no thermocline, K_d alignment by particle resuspension flux F_R increase
- Figure B-5 case 3: no thermocline, K_d alignment by sediment burial flux F_B increase
- Figure B-6 case 4: no thermocline, K_d alignment by sediment-water diffusion coefficient k_{TW} increase

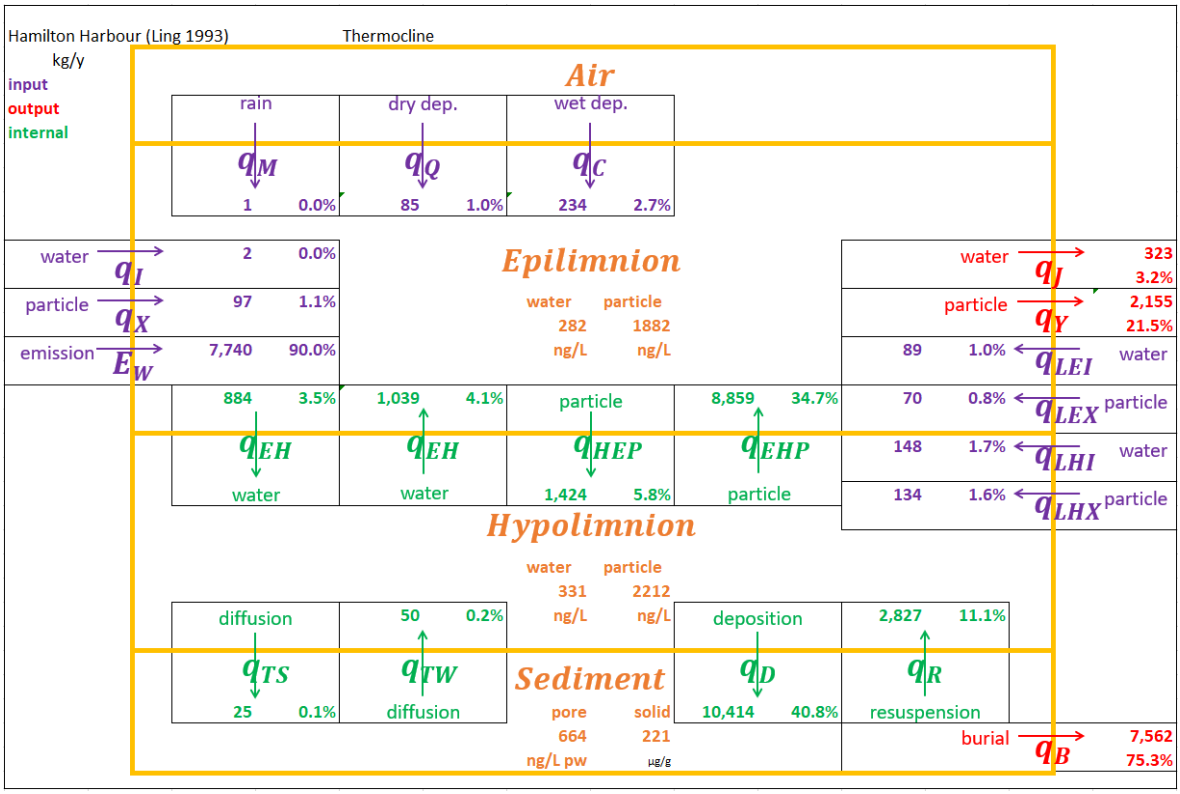

Figure B-2. Harbour base: with thermocline

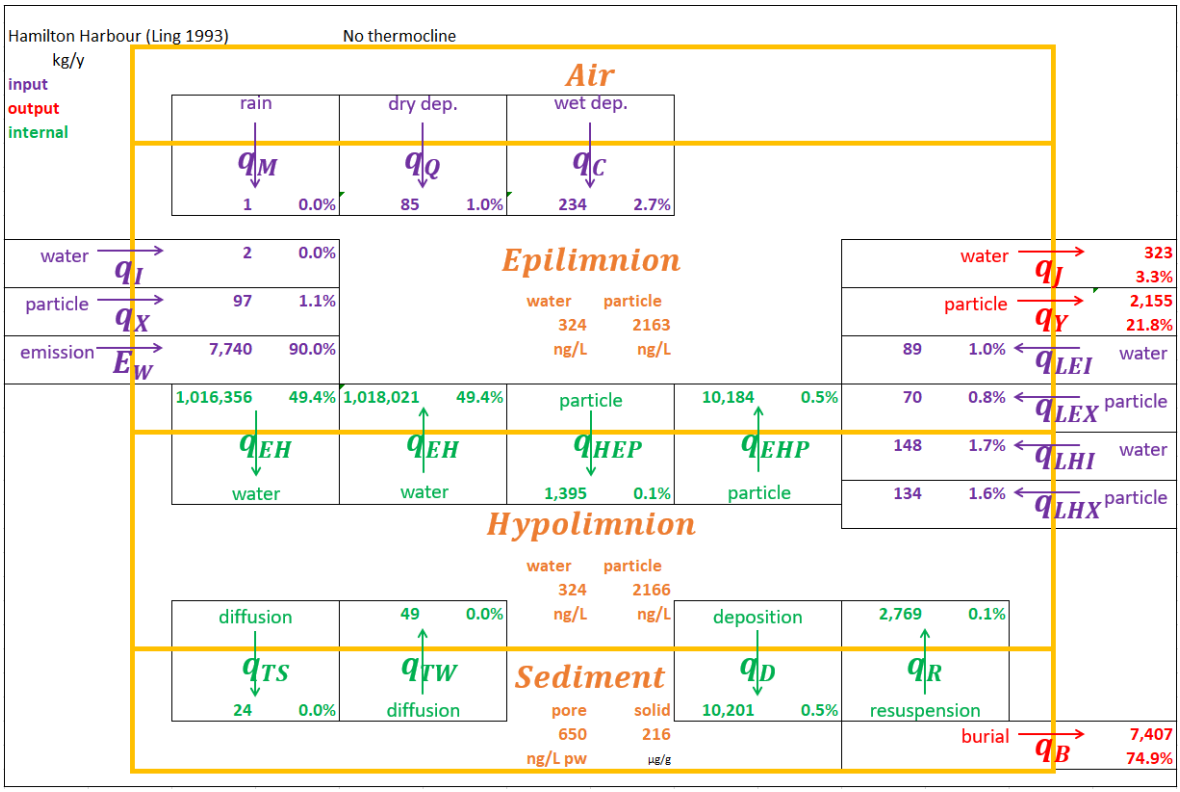

Figure B-3. Harbour case 1: no thermocline

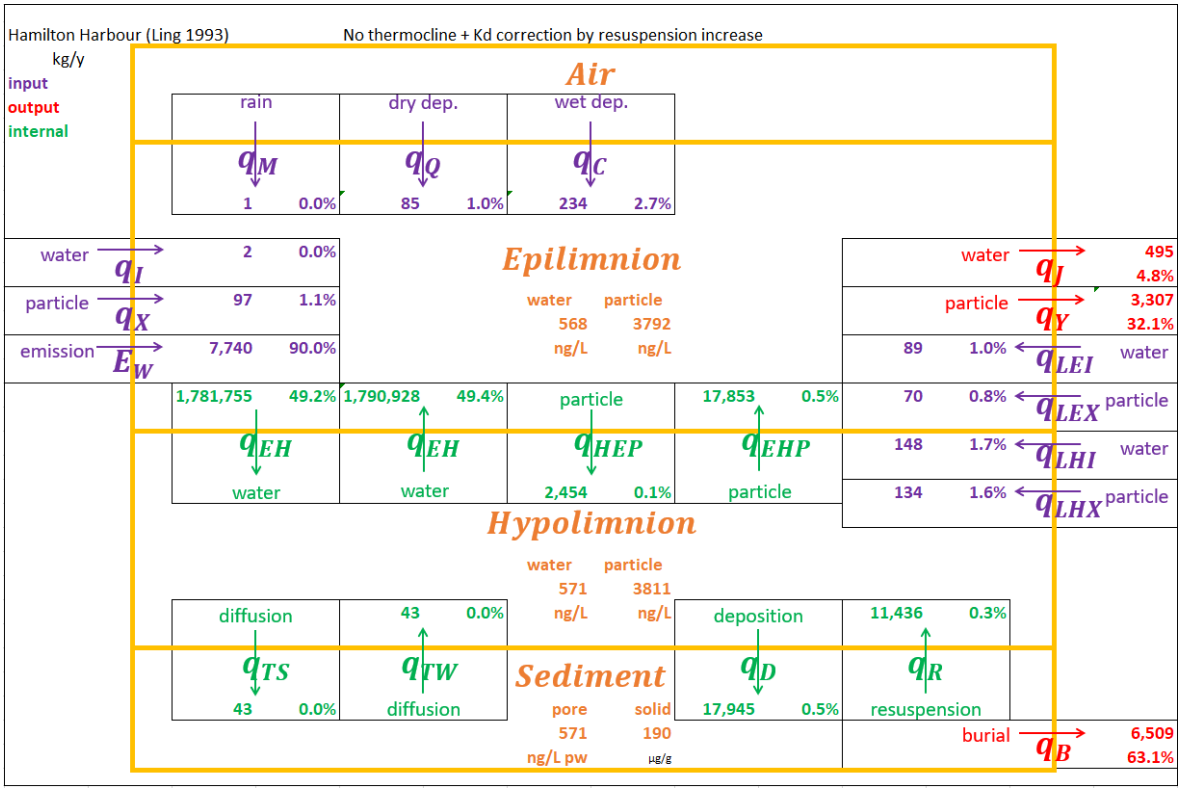

Figure B-4. Harbour case 2: no thermocline, F_R increase

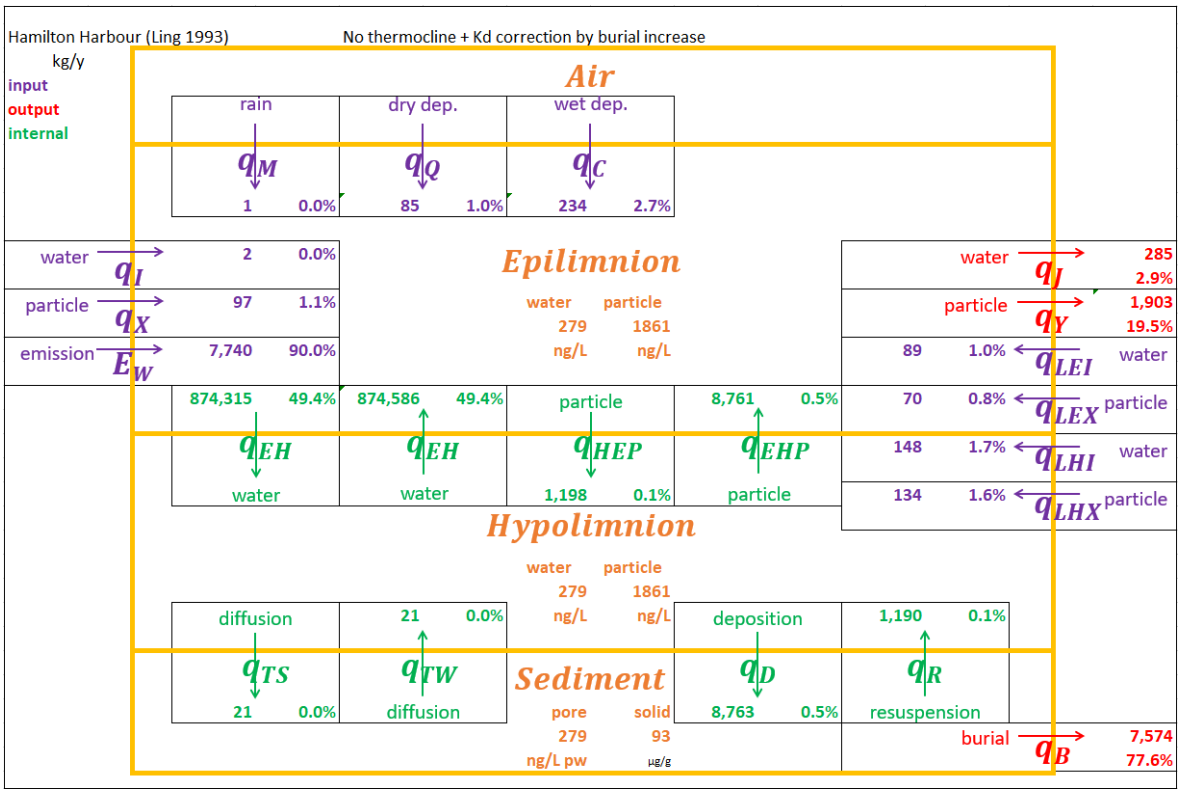

Figure B-5. Harbour case 3: no thermocline, F_B increase

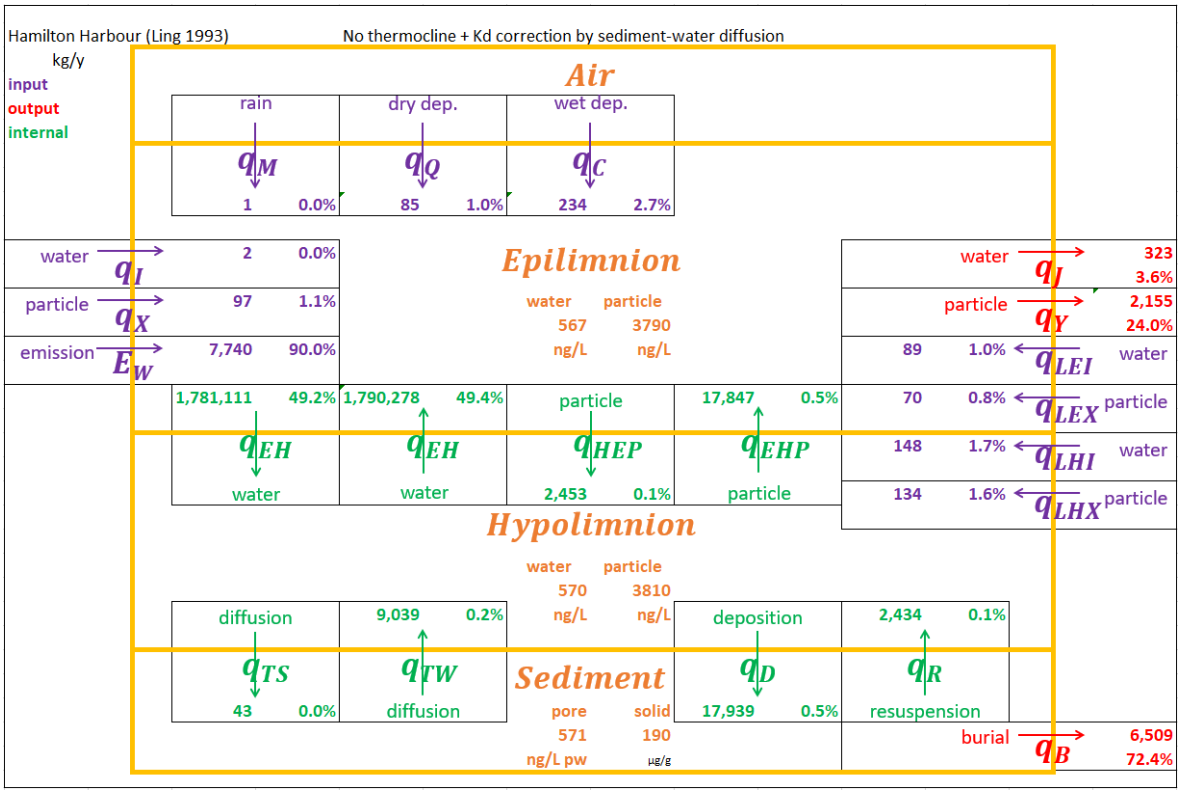

Figure B-6. Harbour case 4: no thermocline, k_{TW} increase

C Hamilton Harbour II

C.1 INPUTS

This was a reapplication of the two-layer QWASI aquivalence steady-state model described in Appendix B **(LING, 1993)** with updated inputs **(DIAMOND, 1996)**.

Table C-1 and Table C-2 are adapted from Table B-3 and Table B-4 **(LING, 1993)**, except as indicated. Distribution coefficients were calculated from measurements, for sediment K_d = 9.55E+04 L·kg^{-1} **(OME, 1992A)** and for SPM K_p = 1.10E+05 L·kg^{-1} (OME unpublished data)**(DIAMOND, 1996)**.

Table C-1. Hamilton Harbour II properties

Property			Value
Area of lake	A_{LA}	m^2	2.15E+07
Area of sediment	A_{SE}	m^2	2.15E+07
Density of SPM	ρ_w	g·cm^{-3}	2
Density of aerosol	ρ_A	g·cm^{-3}	1.5
Density of sediment	ρ_S	g·cm^{-3}	2.64
Concentration of water particulate	C_{PL}	mg·L^{-1}	5.69[43]
Concentration of inflow particulate	C_{PI}	mg·L^{-1}	63.2[43]
Concentration of aerosol	C_{PA}	µg·m^{-3}	30
Rate of rain	v_{RA}	m·a^{-1}	0.865
Rate of dry aerosol deposition	v_{AD}	m·h^{-1}	7.2
Rain scavenging ratio	W_g	-	200,000
Mass transfer coefficient: sediment	k_T	m·h^{-1}	4E-04
Volumetric rate of water inflow	Q_I	m^3·h^{-1}	2.81E+04
Volumetric rate of water outflow	Q_J	m^3·h^{-1}	1.48E+05
Volume fraction of sediment particles	f_{SV}	-	0.085
Flux of particles, settling	F_S	g·m^{-2}·d^{-1}	6.0
Flux of particles, resuspension	F_R	g·m^{-2}·d^{-1}	2.5
Flux of particles, burial	F_B	g·m^{-2}·d^{-1}	3.0[44]
Emissions to water	E_W	kg·a^{-1}	8395[45]
Concentration in air, aerosol	C_{OA}	µg·m^{-3}	0.004
Concentration in water inflow	C_{OI}	ng·L^{-1}	400

[43] From **(OME, 1992A)**
[44] From section *II.1.8* accumulation of 0.53 cm a^{-1} **(OME, 1992A)** gives 3.25 g·m^{-2}·d^{-1} from ρ_S and f_{SV}; represents 1100 g·m^{-2}·a^{-1} (range 410-1590 g·m^{-2}·a^{-1}) **(NRIAGU, 1983)**
[45] Includes both industrial and municipal emissions **(OME, 1992A)**

Table C-2. Hamilton Harbour II thermocline properties

Property			Value
Depth of harbour	d_{LA}	m	13
Depth of epilimnion	d_E	m	6
Depth of hypolimnion	d_H	m	7
Depth of sediment	d_{SE}	m	0.03
Density of SPM, lake	ρ_w	$g \cdot cm^{-3}$	2.4
Concentration of inflow particulate, lake	C_{PLL}	$mg \cdot L^{-1}$	2.26[46]
Mass transfer coefficient: thermocline	k_{HE}	$m \cdot h^{-1}$	0.4
Volumetric rate water inflow, epilimnion	Q_{LEI}	$m^3 \cdot h^{-1}$	44,100
Volumetric rate water inflow, hypolimnion	Q_{LHI}	$m^3 \cdot h^{-1}$	73,500
Mass rate inflow lake-epilimnion	$\dot{m}_{LEX}$	$g \cdot h^{-1}$	52,000
Mass rate inflow lake-hypolimnion	$\dot{m}_{LHX}$	$g \cdot h^{-1}$	100,000
Mass rate inflow land-harbour	$\dot{m}_{HX}$	$g \cdot h^{-1}$	1,775,000[46]
Mass rate outflow epilimnion-lake	$\dot{m}_{HLY}$	$g \cdot h^{-1}$	666,666[46]

C.2 OUTPUT

Table C-3 compares the lead concentrations reported from observations and the original study model in *Table 5* **(DIAMOND, 1996)** with those determined in the Pb model thermocline scenario.

Table C-3. Hamilton Harbour II concentrations in media

Medium		Observed[47]	Range[47]	Diamond	Model
epilimnion	$\mu g \cdot L^{-1}$	2.8	2.5-3.3	2.8	2.5
hypolimnion	$\mu g \cdot L^{-1}$	3.0	2.5-3.7	3.4	3.4
sediment	$\mu g \cdot g^{-1}$	241	34-690	247	249

[46] From **(OME, 1992A)**

[47] From OME data and **(MAYER, 1990)** in *Table 5* **(DIAMOND, 1996)**; suspended particulate lead at six stations averaged for April and September at 1 m are 329 $\mu g \cdot g^{-1}$ and at depth are 285 $\mu g \cdot g^{-1}$, which at C_{PL}=5.69 $mg \cdot L^{-1}$ are 1.87 $\mu g \cdot L^{-1}$ and 1.62 $\mu g \cdot L^{-1}$ **(MAYER, 1990)**.

Reformulated model process diagrams show process rates (kg·a^{-1}), contributions as percentages to inflow, outflow and internal processes, and concentrations, according to the separate adjustments detailed in Table 4:

- Figure C-1 base: thermocline, $A_H > A_E$
- Figure C-2 case 1: no thermocline, $A_H = A_E$
- Figure C-3 case 2: no thermocline, K_d alignment by particle resuspension flux F_R increase
- Figure C-4 case 3: no thermocline, K_d alignment by sediment burial flux F_R increase
- Figure C-5 case 4: no thermocline, K_d alignment by upward sediment diffusion coefficient k_{TW} increase

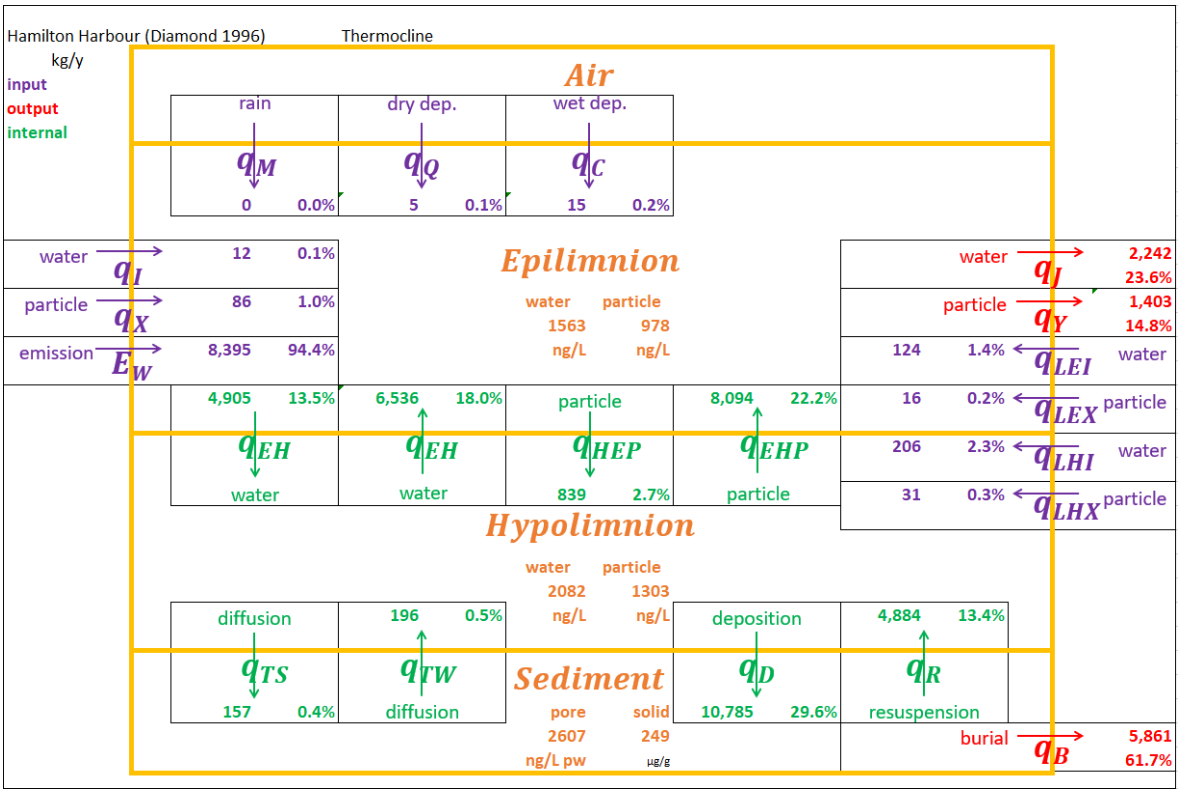

Figure C-1. Harbour II base: with thermocline

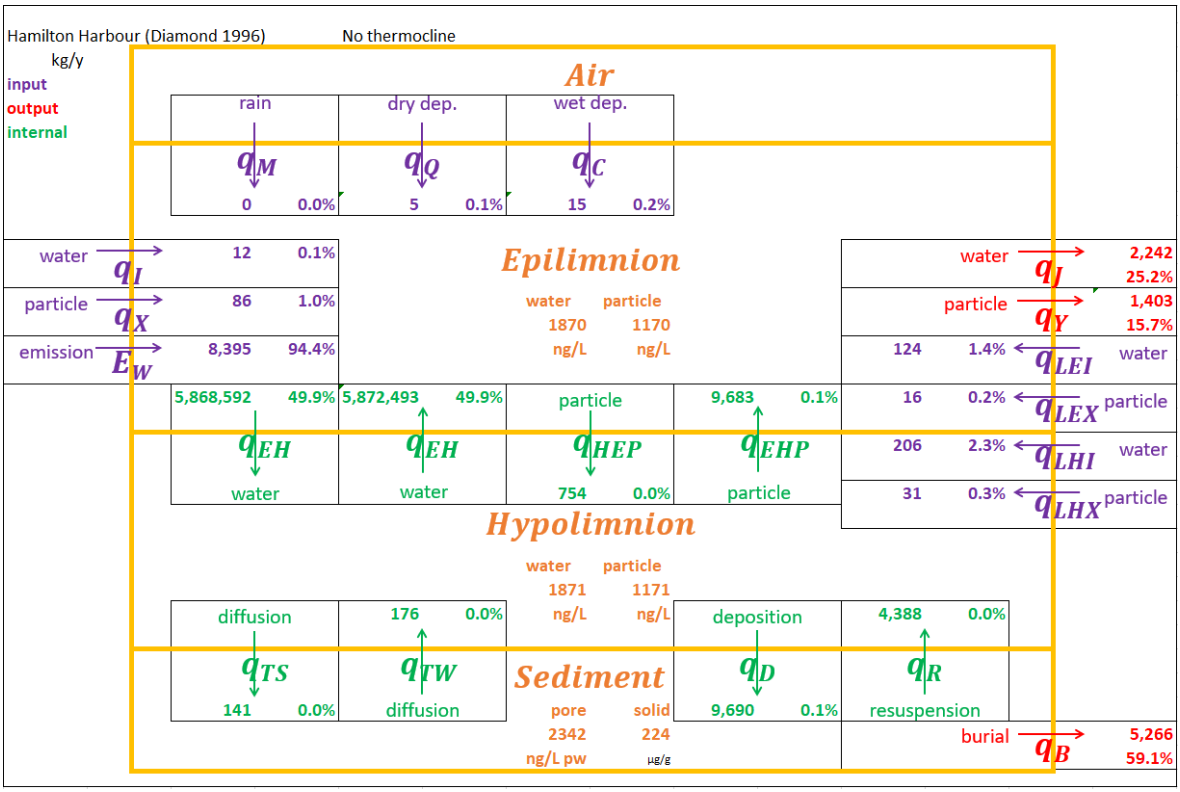

Figure C-2. Harbour II case 1: no thermocline

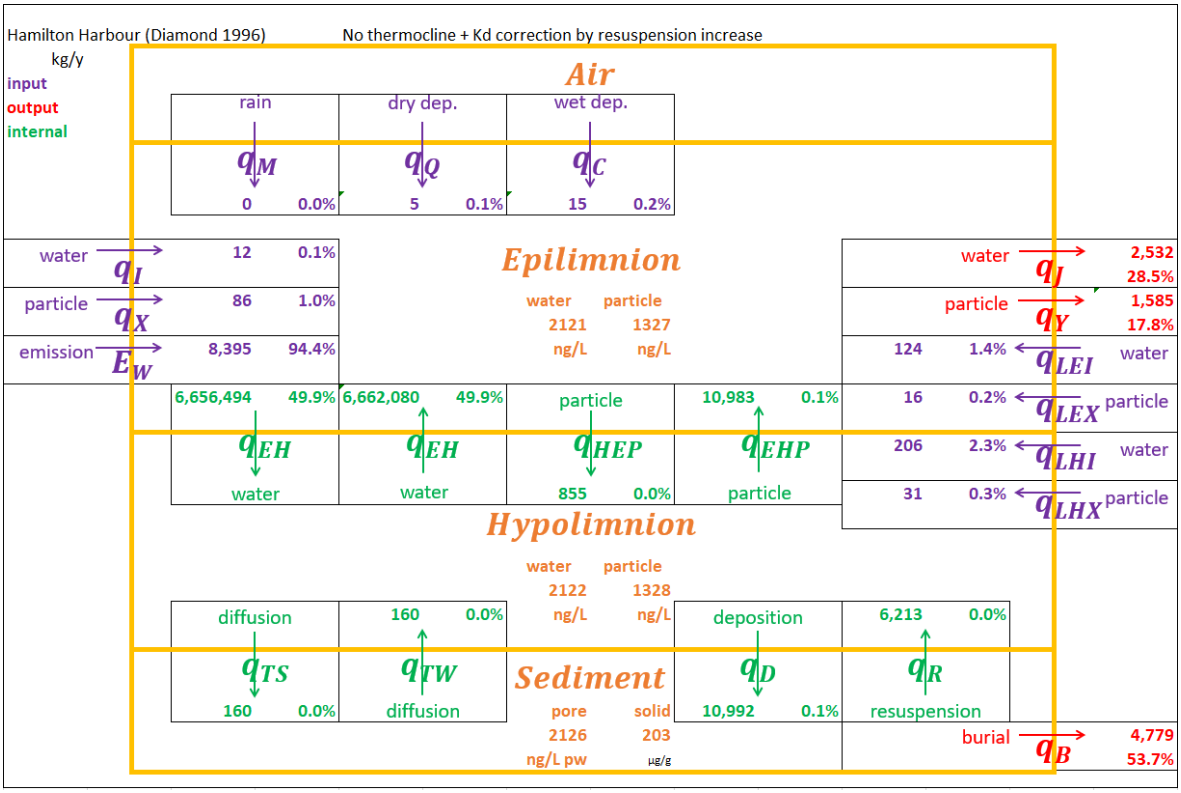

Figure C-3. Harbour II case 2: no thermocline, F_R increase

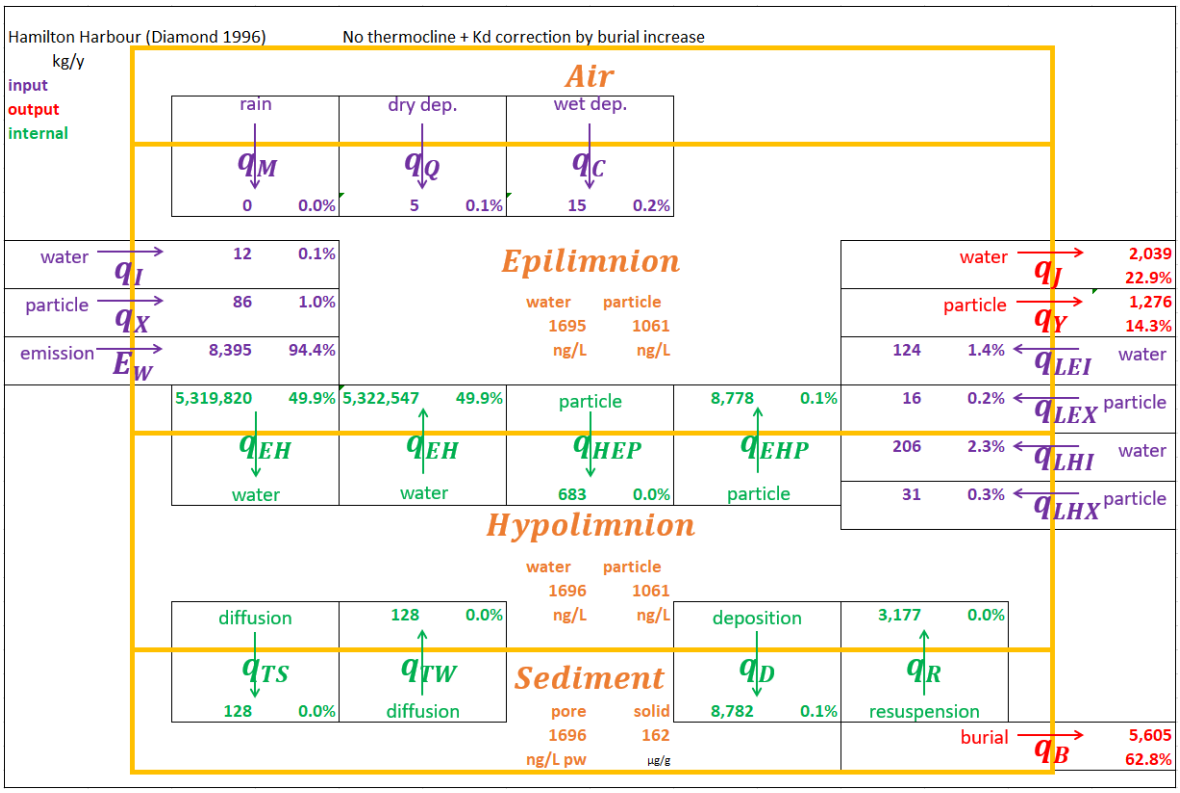

Figure C-4. Harbour II case 3: no thermocline, F_B increase

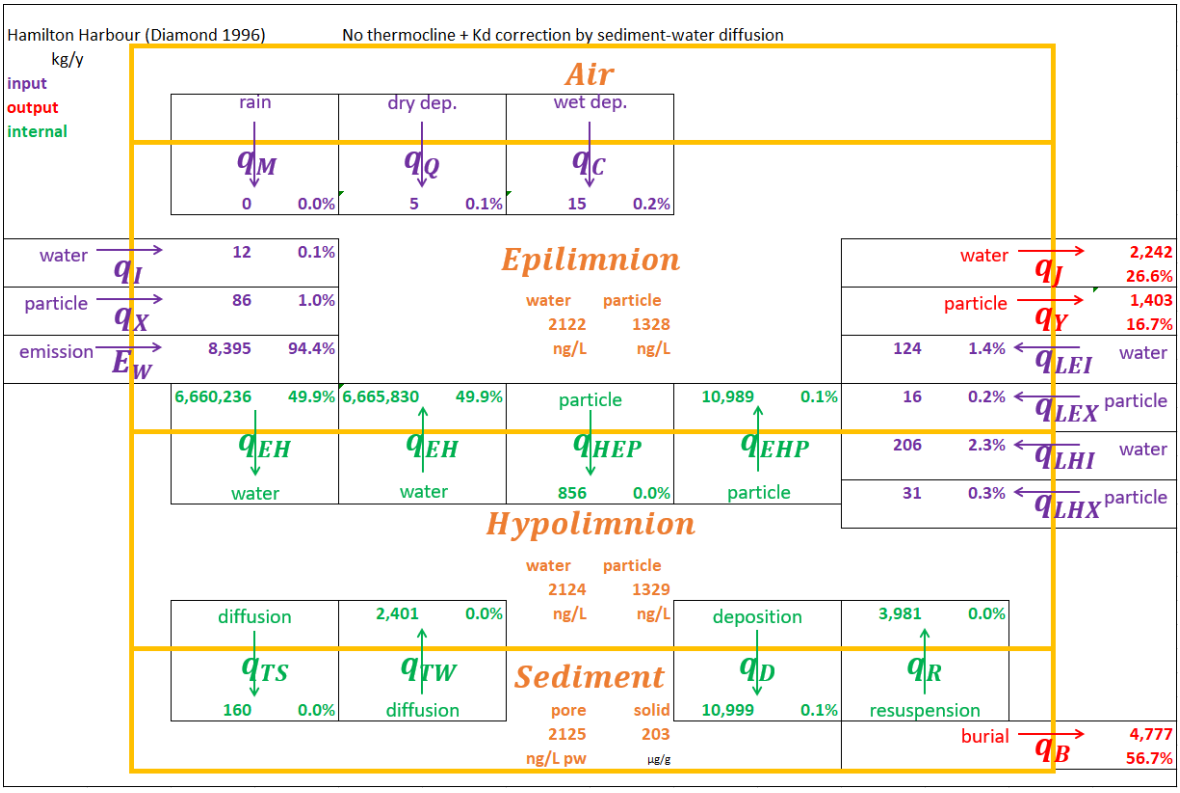

Figure C-5. Harbour II case 4: no thermocline, k_{TW} increase

D Lake Ontario Rate Constant Study

D.1 INPUTS

This was a case study of a rate constant model for assessment of Great Lakes toxic pollutants **(MACKAY, 1994)** applied to stable lead in Lake Ontario **(THOMPSON, 1999)** using the Appendix A aquivalent model. Table D-1 lists the lake inputs.

Table D-1. Lake Ontario Rate Constant Study properties

Property			Value
Area of lake	A_{LA}	m^2	1.95E+10[48]
Area of sediment	A_{SE}	m^2	1.17E+10[48]
Density of SPM	ρ_w	$g \cdot cm^{-3}$	2[49]
Density of aerosol	ρ_A	$g \cdot cm^{-3}$	1.5[50]
Density of sediment	ρ_S	$g \cdot cm^{-3}$	2[48]
Concentration of water particulate	C_{PL}	$mg \cdot L^{-1}$	4[48]
Concentration of inflow particulate	C_{PI}	$mg \cdot L^{-1}$	24[53]
Concentration of aerosol	C_{PA}	$\mu g \cdot m^{-3}$	30[50]
Rate of rain	v_{RA}	$m \cdot a^{-1}$	0.89[48]
Rate of dry aerosol deposition	v_{AD}	$m \cdot h^{-1}$	7.2[51]
Rain scavenging ratio	W_g	-	180,000[52]
Mass transfer coefficient: sediment	k_T	$m \cdot h^{-1}$	1E-04[52]
Volumetric rate of water inflow	Q_I	$m^3 \cdot h^{-1}$	2.93E+07[53]
Volumetric rate of water outflow	Q_J	$m^3 \cdot h^{-1}$	2.93E+07[53]
Volume fraction of sediment particles	f_{SV}	-	0.08[48]
Flux of particles, settling	F_S	$g \cdot m^{-2} \cdot d^{-1}$	1.27[54]
Flux of particles, resuspension	F_R	$g \cdot m^{-2} \cdot d^{-1}$	0.55[54]
Flux of particles, burial	F_B	$g \cdot m^{-2} \cdot d^{-1}$	0.72[54]
Emissions to water	E_W	$kg \cdot a^{-1}$	173,000[55]
Concentration in air, aerosol	C_{OA}	$\mu g \cdot m^{-3}$	0.0037[56]
Concentration in water inflow	C_{OI}	$ng \cdot L^{-1}$	888[57]

[48] From **(MACKAY, 1994)**
[49] From **(LING, 1993)**
[50] From Appendix A **(MACKAY, 1989)**
[51] From **(MACKAY, 1994)**; adjusted according to Footnote[60]
[52] From **(THOMPSON, 1999)**; adjusted according to Footnote[59]
[53] Inferred from Table D-2 V_{LA}/t_{LA}
[54] Optimized parameter – see discussion
[55] From **(THOMPSON, 1999)**; see Footnote[60]: 221,000-48,000
[56] From *Table 3* **(THOMPSON, 1999)** citing **(HOFF, 1996)**
[57] Niagara River concentration as (228,000 $kg \cdot a^{-1}$)/Q_I[60]

Inputs peculiar to the rate constant model are listed in Table D-2.

Table D-2. Lake Ontario Rate Constant Study supplemental properties

Property			Value[52]
Fraction on depositing particles in water	f_{WP}	-	0.8
Fraction dissolved in water	f_{WD}	-	0.2
Fraction dissolved in sediment (pore water)	f_N	-	0.00053
Water residence time	t_{LA}	y	6.5
Volume of lake	V_{LA}	m^3	1.67E+12
Depth of sediment	d_{SE}	m	0.01

Definitions of mass concentration as $C=m/V$, (mass) fraction on depositing particles f_{WP} and (mass) fraction dissolved in water f_{WD} determine the particle distribution coefficient K_p by Equation A.34:

$$C_{OP} = \frac{m_{WP.Pb}}{V_W}$$

$$C_{OW} = \frac{m_{WD.Pb}}{V_W}$$

$$f_{WP} = \frac{m_{WP.Pb}}{m_{W.Pb}}$$

$$f_{WD} = \frac{m_{WD.Pb}}{m_{W.Pb}}$$

$$K_p = \frac{C_{OP}}{C_{OW}C_{PL}} = \frac{m_{WP.Pb}}{m_{WD.Pb}C_{PL}} = \frac{f_{WP}}{f_{WD}C_{PL}} \quad \text{(D.1)}$$

The Table D-1 value for C_{PL} and the Table D-2 values for f_{PW} and f_{DW} give:

K_p = 1.00E+6 L·kg^{-1}

Definitions of volume fraction of sediment particles f_{SV}, (mass) fraction dissolved in sediment f_N, determine the sediment particle distribution coefficient K_d by Equation A.33:

$$f_{SV} = \frac{V_S}{V_N+V_S}$$

$$V_{SS} = f_{SV}(V_N + V_S) = \frac{f_{SV}V_N}{1-f_{SV}}$$

$$m_S = \frac{f_{SV}}{1-f_{SV}}\frac{\rho_S}{\rho_W}m_W$$

$$f_N = \frac{m_{W.Pb}}{m_{S.Pb}+m_{W.Pb}}$$

$$m_{S.Pb} = \frac{1-f_N}{f_N}m_{W.Pb}$$

$$K_d = \frac{C_S}{C_W} = \frac{m_{S.Pb}/m_S}{m_{W.Pb}/V_W} = \frac{(1-f_N)(1-f_{SV})}{f_{SV}f_N\rho_S} \quad \text{(D.2)}$$

The Table D-1 values for sediment particle density ρ_S and f_{SV} and Table D-2 value for f_{OS} give:

K_d = 1.08E+4 L·kg^{-1}

D.2 OPTIMIZATION

Description of the rate constant model **(THOMPSON, 1999)** did not include all input values listed for the aquivalence model case in Appendix A, specifically:

- ρ_w density of SPM
- ρ_A density of aerosol
- C_{PI} concentration of inflow particulate
- C_{PA} concentration of aerosol
- F_S flux of particles, settling
- F_R flux of particles, resuspension
- F_B flux of particles, burial

The density and concentration of aerosol ρ_A and C_{PA} are factors in only the process rate of rain q_M, but no account of rain is made in the report **(THOMPSON, 1999)**. By trial-and-error it was observed that the concentration of inflow particulate C_{PI} has little bearing on concentrations and process rates. Each of these values are assumed from the Appendix A original QWASI model **(MACKAY, 1989)**. Density of SPM was set ρ_w =2 g·cm^{-3} consistent with Appendix B Hamilton Harbour **(LING, 1993)**.

Scaling factors **(SOUTHWOOD, 1989)(MACKAY, 2001)** enabled optimization of the flux values to the reported concentrations and process rates **(THOMPSON, 1999)**. Initial values were assumed from Appendix C Hamilton Harbour II for settling, resuspension and deposition flux F_S = 6.0 g·m^{-2}·d^{-1}, F_R = 2.5 g·m^{-2}·d^{-1} and F_B = 3.0 g·m^{-2}·d^{-1} **(DIAMOND, 1996)**. These were adjusted by trial-and-error, while monitoring the differences between the reported and model parameter values for total water, deposition, resuspension and burial process rates, and total water and sediment concentrations. The flux values were selected to satisfy particle balance by Equation A.27. Final flux values are indicated in Table D-3.

D.3 OUTPUT

Table D-3 lists the reported model process rates from *Table 3* and *Figure 3* **(THOMPSON, 1999)** with reformulated target and model values. Loss terms from the water column and sediment were accounted for by a reduction in emissions and an increase in burial flux. Table D-4 summarizes the reported observed and model concentrations from *Table 6* **(THOMPSON, 1999)** with reformulated values. Table D-5 lists rate constants for the reported model which have been calculated for

processes based on either the water column or sediment **(THOMPSON, 1999)**, and for the Pb model base scenario from both medium and total system inventory.

Aquivalent model process diagrams show process rates, contributions as percentages to inflow, outflow and internal processes, and concentrations, according to the separate adjustments detailed in Table 5:

- Figure D-1 base: optimized by particle flux adjustment
- Figure D-2 case 1: K_d alignment by particle resuspension flux F_R increase
- Figure D-3 case 2: K_d alignment by sediment burial flux F_B increase
- Figure D-4 case 3: K_d alignment by sediment-water diffusion coefficient k_{TW} increase

Table D-3. Lake Ontario Rate Constant Study process rates

Process ($kg \cdot a^{-1}$)	Report	Model	
		Target	Base scenario
Wet deposition	41,000[56]	41,000	11,559[58]
Dry deposition	4,000[56]	4,000	4,551[59]
Land sources	449,000	401,000[60]	401,000
Outflow	148,000	148,000	146,667
Deposition	598,000	598,000	619,214
Resuspension	204,000	204,000	228,796
Burial	458,000	394,000[61]	299,514
Water column loss	48,000	0.[60]	0
Sediment loss	64,000	0.[61]	0

Table D-4. Lake Ontario Rate Constant Study concentrations

Medium		Report				Model - base
		Observed	Best	95% CI	Model	
Water[62]	$ng \cdot L^{-1}$	420-1250	500	230-1500	575	571
sediment[63]	$\mu g \cdot g^{-1}$	2-850	NA	41-310	113	97

[58] As calculated, depending on rain scavenging ratio W_g, rate of rain v_{RA}, lake area A_{LA} and aerosol concentration C_G; W_g was increased to 638,460 to adjust this value to 41,000 $kg \cdot a^{-1}$
[59] As calculated depending on deposition velocity v_{AD}, lake area A_{LA} and aerosol concentration C_G; v_{AD} was decreased to 6.33 $m \cdot h^{-1}$ to adjust this value to 4,000 $kg \cdot a^{-1}$
[60] 449,000-48,000 $kg \cdot a^{-1}$ accounting for water column loss by reduction in emissions; the total comprises 221,000 $kg \cdot a^{-1}$ from emissions and 228,000 $kg \cdot a^{-1}$ from the Niagara River.
[61] 458,000-64,000 $kg \cdot a^{-1}$ accounting for sediment loss by adjusting particle flux values so that burial is in excess according to Equation A.27, disregarding particle conservation.
[62] Data sources include **(ROSSMANN, 1988)**.
[63] Data sources include **(MUDROCH, 1992)**.

Table D-5. Lake Ontario Rate Constant Study rate constants

Process (a^{-1})	Report	Model - base	
		Medium	Total
Evaporation from water	2.04E-04	4.76E-26	2.96E-23
Outflow from lake	0.154	0.154	0.0528
Transformation in water	0	NA	NA
Water to sediment deposition	0.622	0.65	0.223
Water to sediment diffusion	0.00123	1.23E-03	4.21E-04
Water to sediment transport	0.623	0.651	0.223
Total rate constant from water	0.778	0.803	0.276
Transformation in sediment	0	NA	NA
Burial from sediment	0.217	0.164	0.108
Sediment resuspension to water	0.0502	0.125	0.0824
Sediment to water diffusion	0.0462	0.0505	0.0331
Sediment to water transport	0.0964	0.176	0.166
Total rate constant from sediment	0.313	0.34	0.223

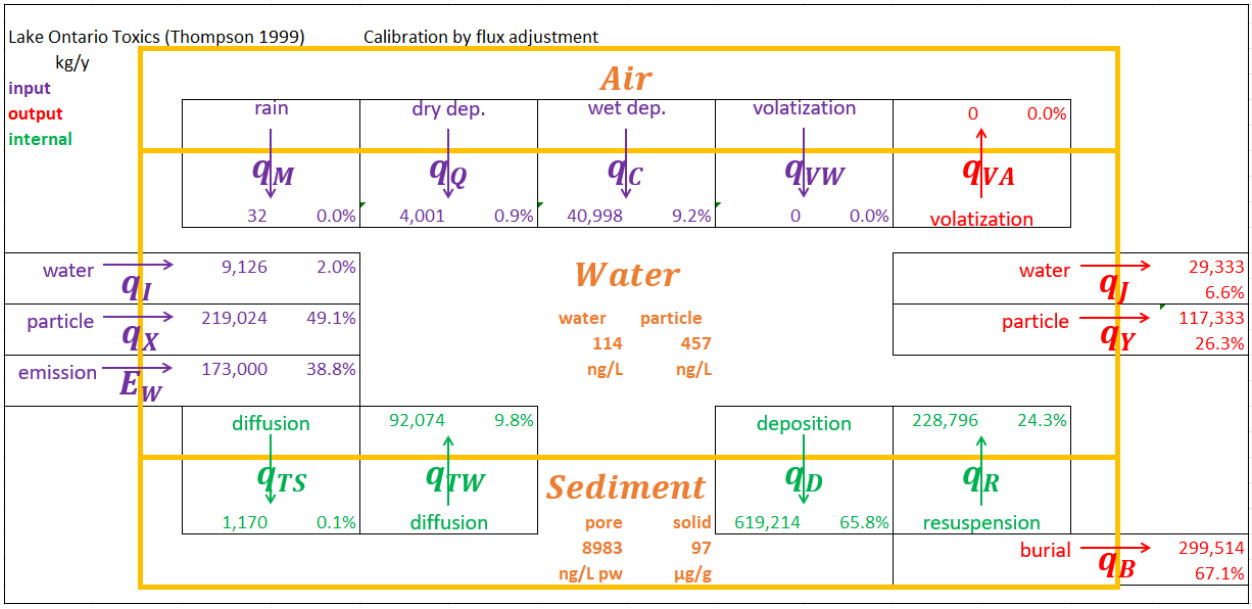

Figure D-1. Rate Constant Study base scenario

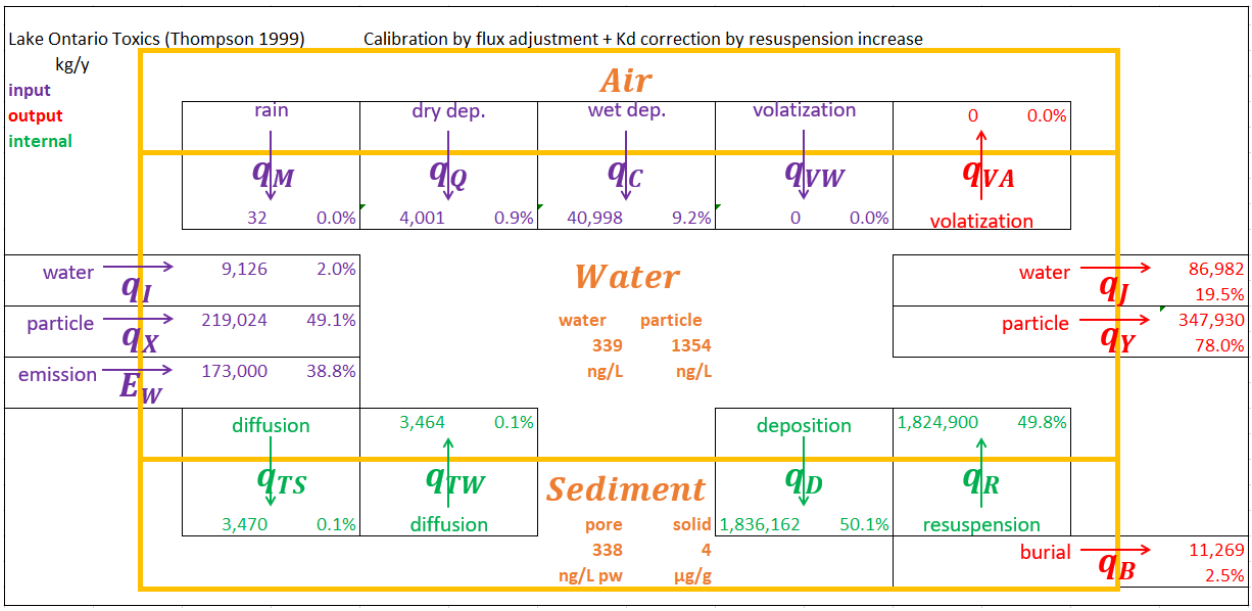

Figure D-2. Rate Constant Study case 1: F_R increase

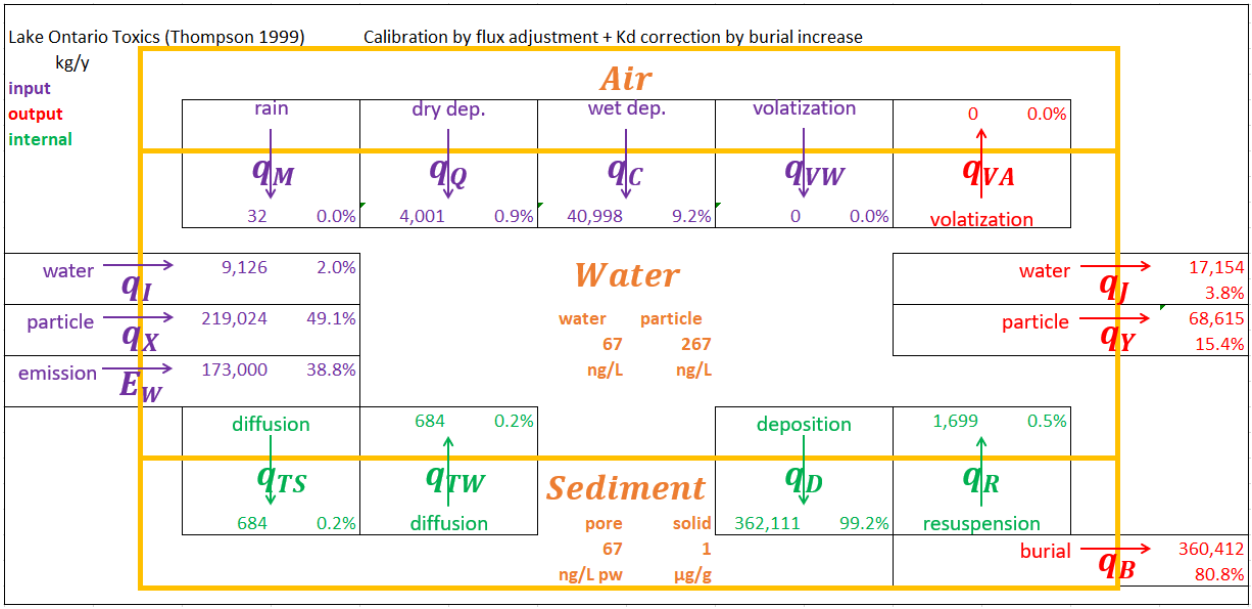

Figure D-3. Rate Constant Study case 2: F_B increase

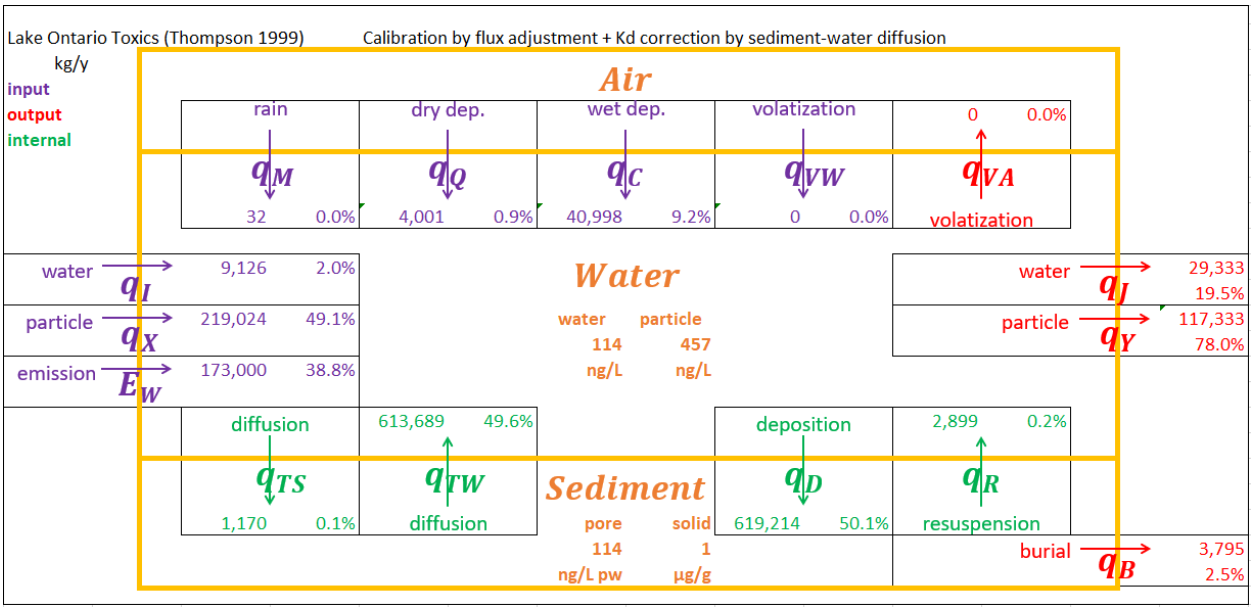

Figure D-4. Rate Constant Study case 3: k_{TW} increase

E Mississauga Basin

E.1 INPUTS

Table E-1 lists properties for the Mississauga Basin scenario; default values assumed from the Lake Ontario Rate Constant Study scenario **(THOMPSON, 1999)**.

Table E-1. Mississauga Basin properties

Property			Value
Area of lake	A_{LA}	m^2	1.95E+10
Area of sediment	A_{SE}	m^2	1.95E+10[64]
Density of SPM	ρ_w	$g \cdot cm^{-3}$	2
Density of aerosol	ρ_A	$g \cdot cm^{-3}$	1.5
Density of sediment	ρ_S	$g \cdot cm^{-3}$	2
Concentration of water particulate	C_{PL}	$mg \cdot L^{-1}$	1.55[65]
Concentration of inflow particulate	C_{PI}	$mg \cdot L^{-1}$	24
Concentration of aerosol	C_{PA}	$\mu g \cdot m^{-3}$	30
Rate of rain	v_{RA}	$m \cdot a^{-1}$	0.89
Rate of dry aerosol deposition	v_{AD}	$m \cdot h^{-1}$	7.2
Rain scavenging ratio	W_g	-	180,000
Mass transfer coefficient: sediment	k_T	$m \cdot h^{-1}$	0.146[66]
Volumetric rate of water inflow	Q_I	$m^3 \cdot h^{-1}$	2.93E+07
Volumetric rate of water outflow	Q_J	$m^3 \cdot h^{-1}$	2.93E+07
Volume fraction of sediment particles	f_{SV}	-	0.08
Flux of particles, settling	F_S	$g \cdot m^{-2} \cdot d^{-1}$	1.00[67]
Flux of particles, resuspension	F_R	$g \cdot m^{-2} \cdot d^{-1}$	0.70[67]
Flux of particles, burial	F_B	$g \cdot m^{-2} \cdot d^{-1}$	0.30[67]
Emissions to water	E_W	$kg \cdot a^{-1}$	0[68]
Concentration in air, aerosol	C_{OA}	$\mu g \cdot m^{-3}$	0.00125[69]
Concentration in water inflow	C_{OI}	$ng \cdot L^{-1}$	888

[64] From Appendix A **(MACKAY, 1989)**: 100% effective area in the Mississauga Basin
[65] From nepheloid layer average particulate metal concentration 384 $ng \cdot L^{-1}$ / particulate solid concentration 247 $\mu g \cdot g^{-1}$ in *Table 5* **(MUDROCH, 1992)(NRIAGU, 1981)**.
[66] Adjusted from initial 0.0004 $m \cdot h^{-1}$ (Appendix A)
[67] From Lake Ontario 403 (Mississauga Basin) average Apr-Nov of 2001, 2002 measurements: F_S at 174 m (0.97, 1.03), F_B at 60 m (0.24, 0.36) in *Table 1* **(MARVIN, 2007)**, assigning the difference to resuspension F_R
[68] Adjusted from initial 173,000 $kg \cdot a^{-1}$ (Appendix D)
[69] Fit to formulated wet and dry deposition over A_{LA} to result in 0.28 $mg \cdot m^{-2} \cdot a^{-1}$ measured for lead deposition at Plastic Lake, Dorset, ON using Equations A.15, A.17 and A.19 **(WATMOUGH, 2017)**

Dimensional and loading characteristics assume the full extent of Lake Ontario. The Pb model case was conceptually located at *Station 403* **(MARVIN, 2007)**, in the nepheloid zone several meters above 174 m depth during the summer. Unless indicated otherwise, values were assumed from Appendix D Table D-1.

Measurements of lead in rain at Point Petre, Ontario indicated 2400 $\mu g \cdot m^{-3}$ **(HOFF, 1996)**. A recent study estimated that the deposition of atmospheric lead has decreased by a factor of 15 since 1978, and estimated that deposition is presently 0.28 $mg \cdot m^{-2} \cdot a^{-1}$ measured for lead deposition at Plastic Lake, Dorset, Ontario **(WATMOUGH, 2017)**. Using Equations A.15, A.17 and A.19 and the parameters assumed in Table E-1, corresponding lead concentrations of 0.00125 $\mu g \cdot m^{-3}$ aerosol and of 226 $\mu g \cdot m^{-3}$ in rain were assumed.

E.2 OPTIMIZATION

Sediment trap measurements at the Mississauga Basin established the particle flux values **(MARVIN, 2007)**. In contrast, account of the lake-wide emission and inflow loading were uncertain in the middle of the lake at depth.

A study of five Lake Ontario sediment cores showed concentrations at depths estimated to be deposited pre-1850 to be less than 30 $\mu g \cdot g^{-1}$ **(KEMP, 1976)**, a result which was corroborated by another study in a literature survey citing a background range at 18-32 $\mu g \cdot g^{-1}$ **(MUDROCH, 1988)**. An alternate scenario representing historical conditions was fit to a sediment concentration of 25 $\mu g \cdot g^{-1}$.

Table E-2 shows the target water, SPM and sediment lead concentrations for the base and alternate scenarios. Both scenario variants were optimized by setting the emissions $E_W = 0$, assuming elimination occurs by deposition close to source or by outflow and does not reach the Mississauga Basin.

The other parameters adjusted to optimize the base scenario were:

- Q_I/Q_J inflow / outflow
- k_{TS} water-sediment diffusion coefficient

The alternate scenario assumes the inflow and outflow $Q_I = Q_J$ found in the base scenario since the effective flow through the basin was assumed to be unchanged over time. The other parameters adjusted to optimize the alternate scenario were:

- k_{TW} sediment-water diffusion coefficient
- C_{OI} inflow concentration

Table E-2. Mississauga Basin concentrations

Phase		Lead concentration		
		observed	base	alternate
Water, C_W	$ng \cdot L^{-1}$	15[70]	15	15
SPM, C_P	$ng \cdot L^{-1}$	90[71]	90	90
Sediment, C_S	$\mu g \cdot g^{-1}$	75[72]/25[73]	75	25

E.3 OUTPUT

Table E-3 shows the optimized parameters for the base and alternate scenarios.

Table E-3. Mississauga Basin optimization parameters

Parameter		Scenario		
		target	base	alternate
Emission, E_W	$kg \cdot a^{-1}$	173,000	0	0
Inflow / outflow, Q_I / Q_J	$m^3 \cdot h^{-1}$	2.93E+07	1.83E+07	1.83E+07
Water-sediment diff. coeff., k_{TS}	$m \cdot h^{-1}$	0.0004	0.0474	0.0004
Sediment-water diff. coeff., k_{TW}	$m \cdot h^{-1}$	0.0004	0.0004	0.0924
Inflow concentration, C_{OI}	$ng \cdot L^{-1}$	888	888	842

The Figure E-1 process diagram shows the base scenario process rates, contributions as percentages to inflow, outflow and internal processes, and concentrations are shown in Figure E-1 for the base scenario and in Figure E-2 for the alternate historical scenario.

[70] From *Table 3*, station LO-41 and LO-45 at depth: (14.7, 12.7 $ng \cdot L^{-1}$) **(NRIAGU, 1996)**
[71] From *Table II*, station Ont 403 May 2001 at 175 m **(MARVIN, 2007)**
[72] From *Table 1* for Mississauga Basin $\hat{C}_{OS}$ n=26 **(MARVIN, 2003)**
[73] From *Table II* at depth: 0.32 $\mu g \cdot g^{-1}$ **(KEMP, 1976)**, *Table 2* depositional basin background 18-32 $\mu g \cdot g^{-1}$ **(MUDROCH, 1988)**

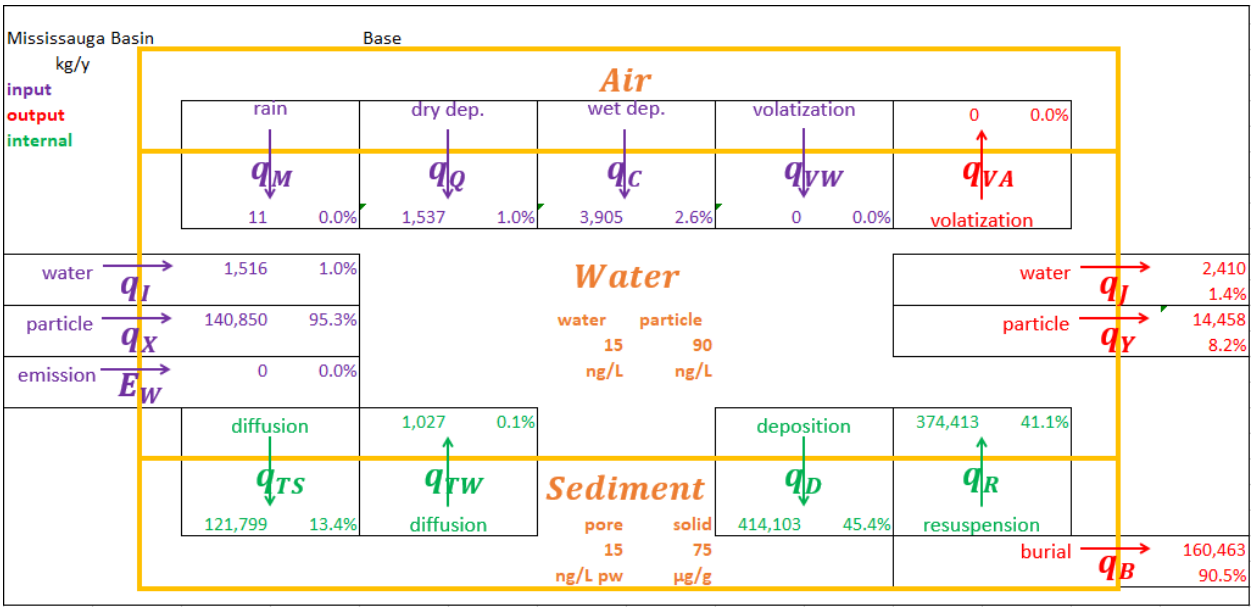

Figure E-1. Mississauga Basin base scenario

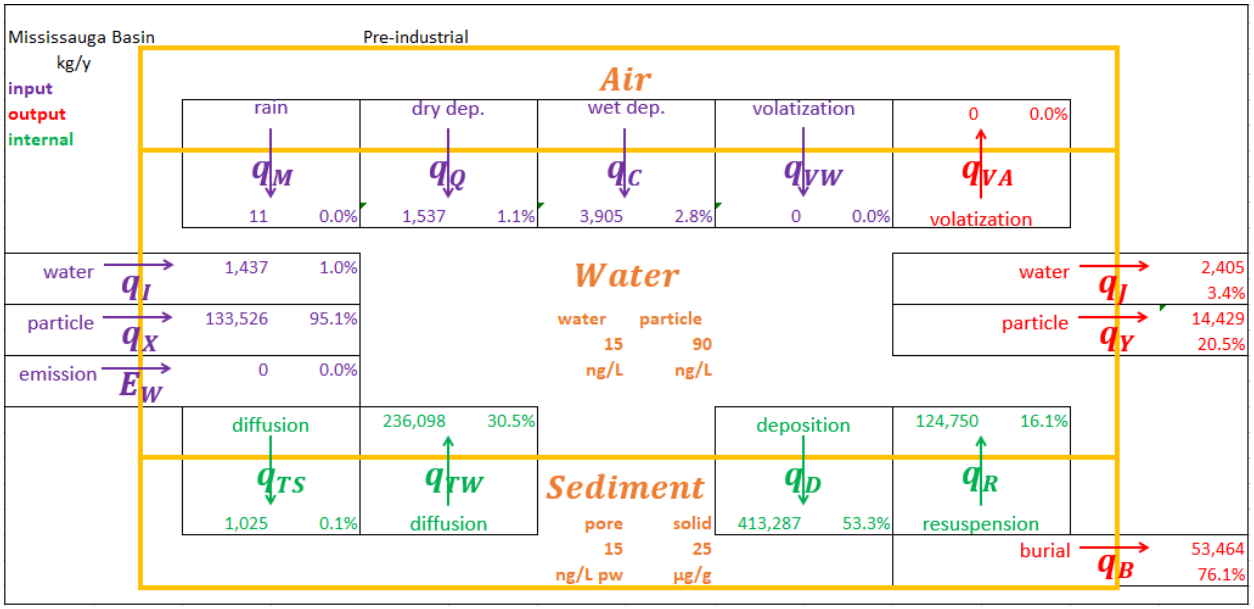

Figure E-2. Mississauga Basin alternate scenario: historical

F Crystal Lake

F.1 INPUT

Table F-1 lists properties for Crystal Lake, WI, Crystal Lake is at 46°3′N, 89°39′W **(TALBOT, 1983)**.

Table F-1. Crystal Lake properties

Property			Value
Depth of lake	d_{LA}	m	10.4[74]
Depth of sediment	d_{SE}	m	0.05[75]
Area of lake	A_{LA}	m^2	3.10E+05[74]
Area of sediment	A_{SE}	m^2	3.10E+05[75]
Density of SPM	ρ_w	$g \cdot cm^{-3}$	2.4[76]
Density of aerosol	ρ_A	$g \cdot cm^{-3}$	1.5[76]
Density of sediment	ρ_S	$g \cdot cm^{-3}$	2.4[76]
Concentration of water particulate	C_{PL}	$mg \cdot L^{-1}$	0.75[77]
Concentration of inflow particulate	C_{PI}	$mg \cdot L^{-1}$	NA[74]
Concentration of aerosol	C_{PA}	$\mu g \cdot m^{-3}$	15[78]
Rate of rain	v_{RA}	$m \cdot a^{-1}$	1.00[79]
Volumetric rate of water inflow	Q_I	$m^3 \cdot h^{-1}$	1E-20[80]
Volumetric rate of water outflow	Q_J	$m^3 \cdot h^{-1}$	1E-20[80]
Volume fraction of sediment particles	f_{SV}	unitless	0.08[81]
Flux of particles, settling	F_S	$g \cdot m^{-2} \cdot d^{-1}$	fit
Flux of particles, resuspension	F_R	$g \cdot m^{-2} \cdot d^{-1}$	0[74]
Flux of particles, burial	F_B	$g \cdot m^{-2} \cdot d^{-1}$	F_S[82]

Table F-2 details the properties assumed for the Ra-226 model nuclides. Where indicated, "fit" refers to a parameter adjusted during the optimization.

[74] From **(TALBOT, 1984)**
[75] Estimated as lake area
[76] From *Table 2* **(MACKAY, 1989)**
[77] From annual average 0.5 $mg \cdot a^{-1}$ and summer peak 0.1 $mg \cdot a^{-1}$ **(TALBOT, 1983)**
[78] From *p.2055* **(TALBOT, 1984)**
[79] Estimated as 31 $in \cdot a^{-1}$ for central Wisconsin
[80] Nominally low value for 0 from **(THOMPSON, 1999)**
[81] From **(TALBOT, 1983)**
[82] From F_R and particle balance (A.27)

Table F-2. Crystal Lake nuclide properties

Property			Ra-226	Pb-210	Po-210
Molar mass[83]	M	g·mol^{-1}	226	210	210
Half-life[83]	t_H	y	1600	22.2	0.379
Vapour pressure[84]	P_V	NA	NA	NA	NA
Chemical solubility[84]	S	NA	NA	NA	NA
Rain scavenging ratio	W_g	-	7.94E+05[85]	6.36E+05[86]	1.11E+05[86]
Deposition velocity[87]	v_{AD}	m/h	568	8.07	1.27
MTC water-air[84]	k_{VA}	NA	NA	NA	NA
MTC air-water[84]	k_{VW}	NA	NA	NA	NA
MTC water-sediment	k_{TS}	m/h	fit	fit	fit
MTC sediment-water	k_{TW}	m/h	fit	fit	fit

F.2 OPTIMIZATION

Table F-3 lists concentrations and Table F-4 lists processes for Crystal Lake.

Table F-3. Crystal Lake phase concentrations

Phase			Ra-226	Pb-210	Po-210
Air, aerosol	C_{OA}	μg·m^{-3}	2.00E-11[88]	1.29E-10[89]	9.98E-13[90]
Rain	C_{OM}	μg/m^{-3}	1.59E-05[91]	1.02E-04[92]	1.31E-07[93]
Water[94]	C_{OW}	ng·L^{-1}	fit	2.02E-07	2.42E-09
Water particles[95]	C_{OP}	ng·L^{-1}	0.00596·C_W[96]	4.67E-07	7.07E-09
Sediment solids	C_{OS}	μg·g^{-1}	fit	fit	fit

[83] From *Chart of the Nuclides* **(NNDC, 2018)**
[84] Volatilization processes are neglected (section3.1.2)
[85] From section F.2.1.1
[86] From section F.2.1.2
[87] From section F.2.2
[88] From *Table 2* 4.4 dpm·1E+5m^{-3} **(MOORE, 1976)**
[89] Weighted mean 9.9 fCi·m^{-3} from Pb-210 (range 6-17 fCi·m^{-3}) **(TALBOT, 1983)**
[90] Weighted mean 4.5 fCi·m^{-3} from Po-210 (range <1-13 fCi·m^{-3}) **(TALBOT, 1983)**
[91] From *Table 2* 0.035 dpm·L^{-1} **(THOMAS, 2000)**
[92] From 7.8 pCi·m^{-3}, ranging 6-11 pCi·m^{-3} **(TALBOT, 1983)**
[93] From 0.59 pCi·m^{-3} for spring and fall; summer below detection limit, <0.01 pCi·m^{-3} **(TALBOT, 1984)**
[94] From *Table 1* average 1.55 pCi·100 L^{-1} Pb-210, 1.09 pCi·100 L^{-1} Po-210 **(TALBOT, 1984)**
[95] From *Table 1* average 3.59 pCi·100 L^{-1} Pb-210, 3.19 pCi·100 L^{-1} Po-210 **(TALBOT, 1984)**
[96] From *Table 6* $Log_{10}K_p$=3.9 **(CIFFROY, 2009)**, C_{PL}=0.75 mg·L^{-1} (A.34)

Table F-4. Crystal Lake process rates

Process			Ra-226	Pb-210	Po-210
Dry deposition	q_C'	mol·h^{-1}	1.56E-11[97]	1.54E-12[98]	1.87E-15[99]
Wet deposition	q_Q'	mol·h^{-1}	1.87E-11[100]	1.38E-11[101]	1.87E-14[101]
Sedimentation	q_D+q_{TS}	mol·h^{-1}	no data	1.73E-11[102]	no data

F.2.1 SCAVENGING RATIO

The scavenging ratio W_g from can be optimized from rain concentration C_{OM} (section F.2.1.1) or wet deposition rate q_M (section F.2.1.2), both of which rely on Table F-3 measurements of aerosol concentration C_{OA}.

F.2.1.1 *RAIN*

The scavenging ratio W_g was optimized for rain concentration from the expressions for air aquivalence $\mathbb{A}_A$ (A.7), air aquivalence capacity $\mathbb{Z}_{AT}$ (A.3), rain concentration C_{OM} (A.11) and aerosol fraction (A.30):

$$C_{OM} = C_{OA}\left(\frac{\rho_A \mathbb{Z}_W}{C_{PA}\mathbb{Z}_Q} + W_g\right) \tag{F.1}$$

Values for $\mathbb{Z}_W$ (10) and $\mathbb{Z}_Q$ (13), Table F-3 observed nuclide aerosol concentrations C_{OA} and rain concentrations C_{OM}, Table F-1 aerosol concentration C_{PA} and assumed aerosol density ρ_A constrain W_g:

$$W_g = \frac{C_{OM}}{C_{OA}} - \frac{\rho_A \mathbb{Z}_W}{C_{PA}\mathbb{Z}_Q} \tag{F.2}$$

The resulting scavenging ratios W_g were:

- Ra-226, 7.94E+05 (Table F-2)
- Pb-210, 7.87E+05
- Po-210, 1.30E+05

The values were dominated by the C_{OM}/C_{OA} term and were insensitive to the aerosol density ρ_A at the concentrations and assumed aerosol aquivalence capacity $\mathbb{Z}_Q$. Since the Po-210 measurement represents spring and fall measurements only,

---

[97] From *Figure 4* at 50 km from open-pit U mine: 0.01 Bq·m^{-2}·d^{-1} **(PETTERSSON, 1991)**
[98] From *p.6758* 0.07 pCi·cm^{-2}·a^{-1} (*Table 6* 0.7 pCi·cm^{-2}·a^{-1} is a typo, refer to *Table 5*) calculated with A_{LA}=3.1E+5 m^2 **(TALBOT, 1983)**
[99] From *Table 6* 0.005 pCi·cm^{-2}·a^{-1} calculated with A_{LA}=3.1E+5 m^2 **(TALBOT, 1983)**
[100] From *Table 4* 0.012 Bq·m^{-2}·d^{-1} **(THOMAS, 2000)**
[101] From *Table 6* Pb-210: 0.63 pCi·cm^{-2}·a^{-1}, Po-210: 0.05 pCi·cm^{-2}·a^{-1} calculated with A_{LA}=3.1E+5 m^3 **(TALBOT, 1983)**
[102] Calculated as 0.79 pCi·cm^{-2}·a^{-1} from sediment core data **(TALBOT, 1984)**

accounting for summer concentrations at the detection limit Table F-3[93], assuming 40% of the annual precipitation falling in summer would result in a W_g for Po-210 higher by at least a factor of 1.5 at 1.9E+05. This would be mitigated to some extent by the Po-210 aerosol measurements C_{OA}, some of which were below the detection limit.

F.2.1.2 *WET DEPOSITION*

As an alternative to the section F.2.1.1 determination from rain concentration, the scavenging ratio W_g can be optimized for wet deposition from the expressions for air aquivalence $\mathbb{A}_A$ (A.7), air aquivalence capacity $\mathbb{Z}_{AT}$ (A.3), Table A-2 process rate q_C (A.19) and transport parameter D_C (A.20), and aerosol fraction (A.30):

$$q_C = C_{OA} W_g v_{RA} A_{LA} \tag{F.3}$$

The Table F-3 values for observed nuclide aerosol concentrations C_{OA}, Table F-1 rate of rain v_{RA} and lake area A_{LA}, and Table F-4 wet deposition rate q_C' constrain W_g:

$$W_g = \frac{q_C{}'}{C_{OA} v_{RA} A_{LA}} \tag{F.4}$$

The resulting scavenging ratios W_g were[103]:

- Ra-226, 5.97E+06
- Pb-210, 6.36E+05 (Table F-2)
- Po-210, 1.11E+05 (Table F-2)

F.2.2 DEPOSITION VELOCITY

The dry deposition velocity v_{AD} was optimized from the expressions for air aquivalence $\mathbb{A}_A$ (A.7), air aquivalence capacity $\mathbb{Z}_{AT}$ (A.3), and Table A-2 process rate q_D (A.22) and transport parameter D_D (A.23):

$$q_Q = C_A v_{AD} A_{LA} \tag{F.5}$$

The Table F-3 values for observed nuclide aerosol concentrations C_{OA}, Table F-1 lake area A_{LA}, and Table F-4 dry deposition rate q_D' constrain v_{AD}:

$$v_{AD} = \frac{q_Q{}'}{C_{OA} A_{LA}} \tag{F.6}$$

Table F-2 shows the resulting values.

[103] The Ra-226 value is derived from wet deposition measured 5 km from a uranium mill[100] **(THOMAS, 2000)** and may overestimate background scavenging

F.3 PROCEDURE

The parameters adjusted to optimize the scenario were:

- F_S flux of settling particles (Table F-1)
- k_{TW} diffusion coefficients, sediment-water (Table F-2)
- k_{TS} diffusion coefficients, water-sediment (Table F-2)
- E_W emission
- C_{OW} Ra-226 concentration in water (Table F-3)
- C_{OS} concentrations of sediment solids (Table F-3)

The observed sediment concentrations C_{OS} of Ra-226, Pb-210 and Po-210 (C_{OS1}, C_{OS2} and C_{OS3}) were adjusted at each step of the optimization to set $C_S/C_{OS} = 1$.

Table F-5 details the optimization process:

- Step 1: setting the contribution of Ra-226 decay to Pb-210 water column inputs $q_{\lambda W1}/q_{IN2}$ = 3% **(TALBOT, 1984)** and Ra-226 $C_{W1}/C_{OW1} = 1$ by adjusting:
    - F_S flux of settling particles
- Step 2: setting the Pb-210 sedimentation ($q_{D1}+q_{TS1}$) = 1.73e-11 mol·h^{-1} (Table F-4) and Pb-210 $C_{W2}/C_{OW2} = 1$ by adjusting:
    - k_{TS2} Pb-210 diffusion coefficient, water-sediment
    - E_{W2} Pb-210 emission to water
- Step 3: setting Po-210 $C_{W3}/C_{OW3} = 1$ by adjusting:
    - k_{TW3} Po-210 diffusion coefficient, sediment-water

Table F-6 contains a key to the optimization table shading.

Table F-5. Crystal Lake optimization

parameter	nuclide	units	target	initial	step 1	step 2	step 3
F_S	all	$g \cdot m^{-2} \cdot d^{-1}$	NA	0	0.0578	0.0578	0.0578
k_{TS}	Pb-210	$m \cdot h^{-1}$	NA	1.00E-10	1.00E-10	5.03E-02	5.03E-02
k_{TW}	Po-210	$m \cdot h^{-1}$	NA	1.00E-10	1.00E-10	1.00E-10	1.83E-03
E_W	Pb-210	$kg \cdot a^{-1}$	NA	1.00E-18	1.00E-18	2.61E-09	2.61E-09
C_{OW}	Ra-226	$ng \cdot L^{-1}$	NA	1.00E-03	6.72E-04	6.72E-04	6.72E-04
C_{OS}	Ra-226	$\mu g \cdot g^{-1}$	NA	1.00E-09	4.46E-06	4.46E-06	4.46E-06
C_{OS}	Pb-210	$\mu g \cdot g^{-1}$	NA	1.00E-09	3.43E-07	3.71E-07	3.71E-07
C_{OS}	Po-210	$\mu g \cdot g^{-1}$	NA	1.00E-12	5.87E-09	6.35E-09	6.35E-09
$n_{\lambda W}1/n_{IN}2$	Ra-226	%	3%	54.03%	3.00%	3.00%	3.00%
C_W/C_{OW}	Ra-226	unitless	1.00E+00	2.55E+01	1.00E+00	1.00E+00	1.00E+00
C_S/C_{OS}	Ra-226	unitless	1.00E+00	3.86E+00	1.00E+00	1.00E+00	1.00E+00
C_W/C_{OW}	Pb-210	unitless	1.00E+00	9.14E+02	7.05E+00	1.00E+00	1.00E+00
C_S/C_{OS}	Pb-210	unitless	1.00E+00	9.81E-01	9.99E-01	1.00E+00	9.99E-01
C_W/C_{OW}	Po-210	unitless	1.00E+00	1.10E+03	4.35E+00	8.98E-01	1.00E+00
C_S/C_{OS}	Po-210	unitless	1.00E+00	1.67E+01	1.00E+00	1.00E+00	1.00E+00
q_D+q_{TS}	Pb-210	$mol \cdot h^{-1}$	1.73E-11	3.51E-14	1.56E-11	1.73E-11	1.73E-11

Table F-6. Optimization key

	adjusted at this step
	set to target at this step
	out of target range / different than target value

G Bickford Pond

G.1 INPUT

Table G-1 lists properties for Bickford Pond, MA. Bickford Pond is at 42°29′N, 71°56′W **(BENOIT, 1987)**.

Table G-1. Bickford Pond properties

Property			Value
Depth of lake	d_{LA}	m	5.7[104]
Depth of sediment	d_{SE}	m	0.05[105]
Area of lake	A_{LA}	m^2	6.0E+05[104]
Area of sediment	A_{SE}	m^2	6.0E+05[104]
Density of SPM	ρ_W	$g \cdot cm^{-3}$	2.4[106]
Density of aerosol	ρ_A	$g \cdot cm^{-3}$	1.5[106]
Density of sediment	ρ_S	$g \cdot cm^{-3}$	2.4[106]
Concentration of water particulate	C_{PL}	$mg \cdot L^{-1}$	0.75[107]
Concentration of inflow particulate	C_{PI}	$mg \cdot L^{-1}$	0.75[107]
Concentration of aerosol	C_{PA}	$\mu g \cdot m^{-3}$	15[108]
Rate of rain	v_{RA}	$m \cdot a^{-1}$	1.21[104]
Volumetric rate of water inflow	Q_I	$m^3 \cdot h^{-1}$	1563[109]
Volumetric rate of water outflow	Q_J	$m^3 \cdot h^{-1}$	1646[110]
Volume fraction of sediment particles	f_{SV}	unitless	0.08[111]
Flux of particles, settling	F_S	$g \cdot m^{-2} \cdot d^{-1}$	fit
Flux of particles, resuspension	F_R	$g \cdot m^{-2} \cdot d^{-1}$	0[104]
Flux of particles, burial	F_B	$g \cdot m^{-2} \cdot d^{-1}$	F_S[112]

Table G-2 lists the unique nuclide properties assumed for Bickford Pond. Other default values are listed in Table F-2. Where indicated, "fit" refers to a parameter adjusted during the optimization.

[104] From **(BENOIT, 1987)**
[105] Estimated as lake area
[106] From *Table 2* **(MACKAY, 1989)**
[107] Estimated from *Figure 10* isopleths **(BENOIT, 1990)**
[108] From *p.6755* **(TALBOT, 1983)**
[109] From 1.37E+07 m^3 a^{-1} runoff **(BENOIT, 1987)**
[110] From 1.37E+07 m^3 a^{-1} runoff and rainfall v_{RA} = 1.21 m a^{-1}, lake area A_{LA} = 6E+5 m^2 **(BENOIT, 1987)**
[111] From **(THOMPSON, 1999)**
[112] From F_R and particle balance (A.27)

Table G-2. Bickford Pond nuclide properties

Property			Ra-226	Pb-210	Po-210
Rain scavenging ratio	W_g	-	7.94E+05[113]	2.26E+05[114]	1.82E+04[113]
Deposition velocity[115]	v_{AD}	$m \cdot h^{-1}$	568	4.52	5.01
MTC water-sediment	k_{TS}	$m \cdot h^{-1}$	fit	fit	fit
MTC sediment-water	k_{TW}	$m \cdot h^{-1}$	fit	fit	fit

G.2 OPTIMIZATION

Table G-3 lists concentrations and Table G-4 lists processes for Bickford Pond.

Table G-3. Bickford Pond phase concentrations

Phase			Ra-226	Pb-210	Po-210
Air, aerosol[116]	C_{OA}	$\mu g \cdot m^{-3}$	2.00E-11	1.29E-10	9.98E-13
Water inflow	C_{OI}	$ng \cdot L^{-1}$	4.55E-06[117]	6.99E-07[118]	1.34E-08[118]
Rain	C_{OM}	$\mu g/m^{-3}$	1.59E-05[119]	2.82E-05[120]	1.92E-08[121]
Water	C_{OW}	$ng \cdot L^{-1}$	4.53E-06[122]	2.42E-07[123]	3.76E-09[124]
Water particles	C_{OP}	$ng \cdot L^{-1}$	2.70E-08[122]	5.15E-07[125]	4.24E-09[126]
Total water	C_{OWP}	$ng \cdot L^{-1}$	4.55E-06[117]	7.57E-07	7.99E-09
Sediment solids	C_{OS}	$\mu g \cdot g^{-1}$	fit	fit	fit

[113] From section G.2.1.1
[114] From section G.2.1.2
[115] From section G.2.2
[116] From Crystal Lake (Table F-3)
[117] From *p.1451* <1 dpm $100kg^{-1}$ **(BENOIT, 1987)**
[118] From dissolved + particulate, average of Provencial & W.Wachusett Brook: *Table 1* Pb-210: 11.9 dpm $100kg^{-1}$, *Table 2* Po-210: 13.4 dpm $100kg^{-1}$ **(BENOIT, 1987)**
[119] From *Table 2* 0.035 ± 0.020 dpm$\cdot L^{-1}$ (n=17) **(MOORE, 1976)**
[120] From *p.1446* measured 480 dpm $100kg^{-1}$ (range 180-890 dpm $100kg^{-1}$) **(BENOIT, 1987)**
[121] From *p.1446* as 4% of the Pb-210 concentration **(BENOIT, 1987)**
[122] From *Table 6* $Log_{10}K_p=3.9$ **(CIFFROY, 2009)**, $C_{PL}=0.75$ mg$\cdot L^{-1}$ & note [117] using (A.34)
[123] From *p.1225* 32% of average <10 m depth 12.9 ± 3.1 dpm $100kg^{-1}$ **(BENOIT, 1990)**
[124] From *p.1226* 47% of average <10 m depth 8.0 ± 2.2 dpm $100kg^{-1}$ **(BENOIT, 1990)**
[125] From *p.1225* 68% of average <10 m depth 12.9 ± 3.1 dpm $100kg^{-1}$ **(BENOIT, 1990)**
[126] From *p.1226* 53% of average <10 m depth 8.0 ± 2.2 dpm $100kg^{-1}$ **(BENOIT, 1990)**

Table G-4. Bickford Pond process rates

Process			Ra-226	Pb-210	Po-210
Dry deposition	q_C'	mol·h^{-1}	3.02E-11[127]	1.67E-12[128]	1.43E-14[127]
Wet deposition	q_Q'	mol·h^{-1}	no data	1.11E-11[129]	no data
Sedimentation	q_D'	mol·h^{-1}	no data	3.16E-11[130]	no data

G.2.1 SCAVENGING RATIO

G.2.1.1 *RAIN*

The scavenging ratio W_g was calculated following Appendix F (F.2) with the values for $\mathbb{Z}_W$ (10) and $\mathbb{Z}_Q$ (13), Table G-3 observed nuclide aerosol concentrations C_{OA} and rain concentrations C_{OM}, Table G-1 aerosol concentration C_{PA} and assumed aerosol density ρ_A:

- Ra-226, 7.94E+05 (Table G-2)
- Pb-210, 2.17E+05
- Po-210, 1.82E+04 (Table G-2)

G.2.1.2 *WET DEPOSITION*

The scavenging ratio W_g was calculated following Appendix F (F.4) with Table G-1 rate of rain v_{RA} and lake area A_{LA}, and Table G-4 wet deposition rate q_C':

- Pb-210, 2.26E+05 (Table G-2)

G.2.2 DEPOSITION VELOCITY

The deposition velocity v_{AD} was calculated following Appendix F (F.6) with the Table G-3 values for observed nuclide aerosol concentrations C_{OA}, Table G-1 lake area A_{LA}, and Table G-4 dry deposition rates q_D'. Table G-2 shows the resulting values.

G.3 PROCEDURE

The parameters adjusted to optimize the scenario were:

- F_S flux of settling particles (Table G-1)
- k_{TS} diffusion coefficients, water-sediment (Table G-2)

---

[127] From *Figure 4* at 50 km from open-pit U mine, Ra-226: 0.02 Bq·m^{-2}·d^{-1}, Po-210: 0.01 Bq·m^{-2}·d^{-1} **(PETTERSSON, 1991)** with Table G-1 A_{LA}=6E+5 m^3
[128] From *p.1446* 15% (10-20%) of wet deposition[129] **(BENOIT, 1987)**
[129] From *p.1446* 0.58 dpm·cm^{-2}·a^{-1} **(BENOIT, 1987)**
[130] From *Table III* 11.2 m average: 1.65 dpm·cm^{-2}·a^{-1} **(BENOIT, 1990)**

- k_{TW} diffusion coefficients, sediment-water (Table G-2)
- E_W emission to water
- C_{OS} observed concentrations of sediment solids (Table G-3)

The observed sediment concentrations C_{OS} of Ra-226, Pb-210 and Po-210 (C_{OS1}, C_{OS2}, and C_{OS3}) were adjusted at each step of the optimization to set C_S/C_{OS} = 1.

Table G-5 details the optimization process:

- Step 1: setting the Pb-210 settling flux q_{D1} = 7.69E-11 mol·h^{-1}, Ra-226 C_{W1}/C_{OW1} = 1, and Pb-210 C_{W2}/C_{OW2} = 1 by adjusting:
  - F_S flux of settling particles
  - k_{TS1} Ra-226 diffusion coefficient, water-sediment
  - E_{W2} Pb-210 diffusion coefficient, sediment-water
- Step 2: Po-210 C_{W3}/C_{OW3} = 1 by adjusting:
  - k_{TW3} Po-210 diffusion coefficient, sediment-water

Table F-6 contains a key to the optimization table shading.

Table G-5. Bickford Pond optimization

parameter	nuclide	units	target	initial	step 1	step 2
F_S	all	g·m^{-2}·d^{-1}	NA	1.00E-06	0.3850	0.3850
k_{TS}	Ra-226	m·h^{-1}	NA	1.00E-10	2.85E-03	2.85E-03
E_W	Pb-210	m·h^{-1}	NA	1.00E-18	3.55E-08	3.55E-08
k_{TW}	Po-210	m·h^{-1}	NA	1.00E-10	1.00E-10	1.66E-02
C_{OS}	Ra-226	µg·g^{-1}	NA	1.00E-13	8.15E-07	8.15E-07
C_{OS}	Pb-210	µg·g^{-1}	NA	1.00E-15	2.27E-07	2.27E-07
C_{OS}	Po-210	µg·g^{-1}	NA	1.00E-17	3.85E-09	2.85E-09
C_W/C_{OW}	Ra-226	unitless	1.00E+00	2.08E+00	1.00E+00	1.00E+00
C_S/C_{OS}	Ra-226	unitless	1.00E+00	3.76E-01	1.00E+00	1.00E+00
C_W/C_{OW}	Pb-210	unitless	1.00E+00	3.06E+00	1.00E+00	1.00E+00
C_S/C_{OS}	Pb-210	unitless	1.00E+00	2.30E+00	1.00E+00	1.00E+00
C_W/C_{OW}	Po-210	unitless	1.00E+00	2.91E+00	4.89E-01	1.00E+00
C_S/C_{OS}	Po-210	unitless	1.00E+00	2.54E+00	1.00E+00	1.00E+00
q_D	Pb-210	mol·h^{-1}	3.16E-11	2.50E-16	3.16E-11	3.16E-11

H Clinton River

H.1 INPUT

Table H-1 lists properties for the Clinton River, MI. The Clinton River empties into Lake St. Clair at 42°35′N, 82°48′W **(MUDBIDRE, 2014)**.

Table H-1. Clinton River properties

Property			Value
Depth of lake	m	d_{LA}	1.0[131]
Depth of sediment	m	d_{SE}	0.05[132]
Area of lake	m^2	A_{LA}	3.0E+05[133]
Area of sediment	m^2	A_{SE}	3.0E+05[133]
Density of SPM	$g \cdot cm^{-3}$	ρ_w	2.4[134]
Density of aerosol	$g \cdot cm^{-3}$	ρ_A	1.5[134]
Density of sediment	$g \cdot cm^{-3}$	ρ_S	2.4[134]
Concentration of water particulate	$mg \cdot L^{-1}$	C_{PL}	8.9[135]
Concentration of inflow particulate	$mg \cdot L^{-1}$	C_{PI}	9.0[136]
Concentration of aerosol	$\mu g \cdot m^{-3}$	C_{PA}	15[137]
Rate of rain	$m \cdot a^{-1}$	v_{RA}	1.0[138]
Volumetric rate of water inflow	$m^3 \cdot h^{-1}$	Q_I	5.97E+04[139]
Volumetric rate of water outflow	$m^3 \cdot h^{-1}$	Q_J	5.97E+04[139]
Volume fraction of sediment particles	unitless	f_{SV}	0.08[140]
Flux of particles, settling	$g \cdot m^{-2} \cdot d^{-1}$	F_S	3.6[141]
Flux of particles, resuspension	$g \cdot m^{-2} \cdot d^{-1}$	F_R	0
Flux of particles, burial	$g \cdot m^{-2} \cdot d^{-1}$	F_B	F_S[142]

Table H-2 lists the unique nuclide properties assumed for Clinton River. Other default values are listed in Table F-2.

---

[131] Estimated; from *p.376* the average depth of Lake St. Clair is 3.6 m **(MUDBIDRE, 2014)**
[132] Estimated from lake area
[133] Estimated from *Figure 1* 10 km between CR5 & CR3 **(MUDBIDRE, 2014)**, 30 m width
[134] From *Table 2* **(MACKAY, 1989)**
[135] From *p.378* geometric mean, range 4.2-15.2 $mg \cdot L^{-1}$, n=16 **(MUDBIDRE, 2014)**
[136] From *Table 2* average of upstream Stn. 5 (among Stns. 3, 4, 5) **(MUDBIDRE, 2014)**
[137] From *p.6755* **(TALBOT, 1983)**
[138] From 31 $in \cdot a^{-1}$ precipitation at Detroit, MI http://www.usclimatedata.com
[139] From *p.2* mean of discharge, Mt Clemens MI, 1934-2013 586 $ft^3 \cdot s^{-1}$ **(USGS, 2013)**
[140] From **(THOMPSON, 1999)**
[141] Estimated from 10% of the SPM increase from first to last station: $0.1 \cdot Q_I \cdot C'_{PL}/A_{LA}$, where C'_{PL} is *Table 2* average SPM (Stn.3 – Stn.6): (14.1-6.5) $mg \cdot L^{-1}$ **(MUDBIDRE, 2014)**
[142] From F_R and particle balance (A.27)

Table H-2. Clinton River nuclide properties

Property			Ra-226	Pb-210	Po-210
Rain scavenging ratio	W_g	-	7.94E+05[143]	2.26E+05[144]	1.82E+04[145]
Deposition velocity[146]	v_{AD}	$m \cdot h^{-1}$	568	4.52	5.01
MTC water-sediment	k_{TS}	$m \cdot h^{-1}$	fit	fit	fit
MTC sediment-water	k_{TW}	$m \cdot h^{-1}$	fit	fit	fit

H.2 OPTIMIZATION

Table H-3 lists concentrations assumed for Clinton River.

Table H-3. Clinton River phase concentrations

Phase			Ra-226	Pb-210	Po-210
Air, aerosol	C_{OA}	$\mu g \cdot m^{-3}$	2.00E-11[147]	1.76E-10[148]	3.00E-13[148]
Water inflow	C_{OI}	$ng \cdot L^{-1}$	1.37E-05[149]	1.44-06[150]	1.44E-08[150]
Rain	C_{OM}	$\mu g \cdot m^{-3}$	1.59E-05[151]	2.64E-05[152]	1.86E-07[152]
Water	C_{OW}	$ng \cdot L^{-1}$	1.30E-05[153]	2.78E-06[154]	2.88E-08[154]
Water particles	C_{OP}	$ng \cdot L^{-1}$	6.71E-07[153]	9.16E-07[155]	1.68E-08[155]
Total water	C_{OWP}	$ng \cdot L^{-1}$	1.37E-05[149]	3.70E-06	4.56E-08
Sediment solids	C_{OS}	$\mu g \cdot g^{-1}$	fit	fit	fit

[143] From section F.2.1.1 as Crystal Lake (Table F-2) and section G.2.1.1 as Bickford Pond (Table G-2)
[144] From section G.2.1.1 as Bickford Pond (Table G-2)
[145] From section G.2.1.2 as Bickford Pond (Table G-2)
[146] From section G.2.2 as Bickford Pond (Table G-2)
[147] From *Table 2* 4.4 $dpm \cdot 1E+5m^{-3}$ **(MOORE, 1976)**
[148] Initial from *Table 14* Pb-210: 500 $\mu g \cdot m^{-3}$, Po-210: 50 $\mu g \cdot m^{-3}$ **(UNSCEAR, 2000)**
[149] From *App. B Table 15* drinking water reference value 0.5 $mBq \cdot kg^{-1}$ **(UNSCEAR, 2000)**
[150] From *Table 2* average (bulk-dissolved)+(dissolved) at Stn. 6; Pb-210:0.41 $Bq \cdot 100L^{-1}$ Po-210:0.24 $Bq \cdot 100L^{-1}$ **(MUDBIDRE, 2014)**
[151] From *Table 2* 0.035 ± 0.020 $dpm \cdot L^{-1}$ (n=17) **(MOORE, 1976)**
[152] From *Table 1* Pb-210: 0.075 $Bq \cdot L^{-1}$, Po-210: 0.031 $Bq \cdot L^{-1}$ **(THOMAS, 2000)**
[153] From *Table 6* $Log_{10}K_p=3.9$ **(CIFFROY, 2009)**, $C_{PL}=14.1$ $mg \cdot L^{-1}$ (A.34), Note [149]
[154] From *Table 2* average (dissolved) at Stn. 3; Pb-210:0.79 $Bq \cdot 100L^{-1}$ Po-210:0.48 $Bq \cdot 100L^{-1}$ **(MUDBIDRE, 2014)**
[155] From *Table 2* average (particulate) at Stn. 3; Pb-210:0.26 $Bq \cdot 100L^{-1}$ Po-210:0.28 $Bq \cdot 100L^{-1}$ **(MUDBIDRE, 2014)**

H.3 PROCEDURE

The parameters adjusted to optimize the scenario were:

- E_W emission to water
- C_{OS} observed concentrations of sediment solids Table H-3

The observed sediment concentrations C_{OS} of Ra-226, Pb-210 and Po-210 (C_{OS1}, C_{OS2} and C_{OS3}) were adjusted at each step of the optimization to set C_S/C_{OS} = 1.

Table H-4 details the optimization process:

- Step 1: setting the Ra-226 C_{W1}/C_{OW1} = 1 by adjusting:
  - E_{W1} Ra-226 emission to water
- Step 2: setting the Pb-210 C_{W2}/C_{OW2} = 1 by adjusting:
  - E_{W2} Pb-210 emission to water
- Step 3: setting the Po-210 C_{W3}/C_{OW3} = 1 by adjusting:
  - E_{W3} Po-210 emission to water

Table F-6 contains a key to the optimization table shading.

Table H-4. Clinton River optimization

par.	nuclide	units	target	initial	step 1	step 2	step 3
E_W	Ra-226	$kg \cdot a^{-1}$	NA	1.00E-18	1.05E-10	1.05E-10	1.05E-10
E_W	Pb-210	$kg \cdot a^{-1}$	NA	1.00E-18	1.00E-18	1.19E-06	1.19E-06
E_W	Po-210	$kg \cdot a^{-1}$	NA	1.00E-18	1.00E-18	1.00E-18	1.68E-08
C_{OS}	Ra-226	$\mu g \cdot g^{-1}$	NA	1.00E-08	9.68E-08	9.68E-08	9.68E-08
C_{OS}	Pb-210	$\mu g \cdot g^{-1}$	NA	1.00E-09	2.09E-08	5.29E-08	5.29E-08
C_{OS}	Po-210	$\mu g \cdot g^{-1}$	NA	1.00E-10	3.57E-10	8.63E-10	9.20E-10
K_d low	Ra-226	$L \cdot kg^{-1}$	NA	8.14E+02	7.88E+03	7.88E+03	7.88E+03
K_d low	Pb-210	$L \cdot kg^{-1}$	NA	3.59E+02	7.51E+03	1.90E+04	1.90E+04
K_d low	Po-210	$L \cdot kg^{-1}$	NA	3.48E+03	1.24E+04	3.00E+04	3.20E+04
C_W/C_{OW}	Ra-226	unitless	1.00E+00	9.99E-01	1.00E+00	1.00E+00	1.00E+00
C_S/C_{OS}	Ra-226	unitless	1.00E+00	9.72E+00	1.00E+00	1.00E+00	1.00E+00
C_W/C_{OW}	Pb-210	unitless	1.00E+00	3.93E-01	3.93E-01	1.00E+00	1.00E+00
C_S/C_{OS}	Pb-210	unitless	1.00E+00	2.09E+01	1.00E+00	1.00E+00	1.00E+00
C_W/C_{OW}	Po-210	unitless	1.00E+00	3.10E-01	3.10E-01	3.11E-01	1.00E+00
C_S/C_{OS}	Po-210	unitless	1.00E+00	3.61E+00	1.00E+00	1.00E+00	1.00E+00

I Laurentian Lakes

I.1 INPUT

Table I-1 lists common properties for the Laurentian lakes. Table I-2 lists individual lake properties (from *Table 1*) **(CORNETT, 1984)**.

Table I-1. Laurentian lake properties

Property			Value
Depth of lake	d_{LA}	m	Table I-2
Depth of sediment	d_{SE}	m	0.03[156]
Area of lake	A_{LA}	m^2	Table I-2
Area of sediment	A_{SE}	m^2	Table I-2
Density of SPM	ρ_w	$g \cdot cm^{-3}$	2.4[157]
Density of aerosol	ρ_A	$g \cdot cm^{-3}$	1.5[157]
Density of sediment	ρ_S	$g \cdot cm^{-3}$	2.4[157]
Concentration of water particulate	C_{PL}	$mg \cdot L^{-1}$	Table I-2[158]
Concentration of inflow particulate	C_{PI}	$mg \cdot L^{-1}$	Table I-2[158]
Concentration of aerosol	C_{PA}	$\mu g \cdot m^{-3}$	15[159]
Rate of rain	v_{RA}	$m \cdot a^{-1}$	0.86[160]
Volumetric rate of water inflow	Q_I	$m^3 \cdot h^{-1}$	Table I-3
Volumetric rate of water outflow	Q_J	$m^3 \cdot h^{-1}$	Table I-3
Volume fraction of sediment particles	f_{SV}	unitless	0.08[161]
Flux of particles, settling	F_S	$g \cdot m^{-2} \cdot d^{-1}$	Table I-3
Flux of particles, resuspension	F_R	$g \cdot m^{-2} \cdot d^{-1}$	0
Flux of particles, burial	F_B	$g \cdot m^{-2} \cdot d^{-1}$	F_S[162]

[156] From *p.99* sediment cores were up to 30 cm in length **(CORNETT, 1984)**
[157] From *Table 2* **(MACKAY, 1989)**
[158] From *Table 1* **(CORNETT, 1984)** as particulate organic carbon (Table I-2)
[159] From *p.6755* **(TALBOT, 1983)**
[160] From *Chalk River Stn* 1981-2010 http://climate.weather.gc.ca/climate_normals/
[161] From **(THOMPSON, 1999)**
[162] From F_R and particle balance (A.27)

Table I-2. Laurentian lake limnological properties

Lake	Drainage area	Lake, sediment area	Average depth	Dissolved organic carbon	Particulate organic carbon
	A_d	$A_{LA} = A_{SE}$	d_{LA}		$C_{PL} = C_{PI}$
	ha	ha	m	$mg \cdot L^{-1}$	$mg \cdot L^{-1}$
Currie	66	23	8.5	3.4	0.47
McSourley	389	26[163]	19.4	4.4	0.36
Petznick	424	57	4.3	13.7	0.98
Lower Bass	47	6.3	3.8	5.6	0.72
Perch	584	45	2.0	11.5	0.77
Upper Bass	285	4.7	4.0	11.6	0.94
Otterson	9075	33	3.1	8.6	0.30

Table I-3 lists the outflow rate Q_J, which was estimated **(CORNETT, 1984)**:

$$Q_J = v_R A_d + v_N A_{LA} \tag{I.1}$$

from Perch Lake measurements[164] consistent with previously reported results **(BARRY, 1975)**:

- v_R 0.30 $m \cdot a^{-1}$ catchment runoff
- v_N 0.09 $m \cdot a^{-1}$ net precipitation (minus evaporation)

Table I-3 lists the inflow rate Q_I, which is the catchment portion of Equation I.1:

$$Q_I = v_R A_d \tag{I.2}$$

Table I-3 lists the hydrological properties calculated from Table I-2, using Equation I.1 for the flowrate Q_I.

In the original study, watershed Pb-210 flux to each lake, I_C, was assumed (*Table 4*) as a fraction of watershed deposition on the basis of studies of the Susquehanna River **(LEWIS, 1977)** and the Connecticut River **(BENNINGER, 1978) (CORNETT, 1984)**, which was shown to have been calculated by assuming the fraction f_C = 1.27% for:

$$I_C = \frac{A_d}{A_{LA}} f_C \cdot \mathcal{J}_A \tag{I.3}$$

where $\mathcal{J}_A$ is the average of atmospheric deposition fluxes, 132 $Bq \cdot m^{-2} \cdot a^{-1}$ and 139 $Bq \cdot m^{-2} \cdot a^{-1}$, measured from the two study sites of soil samples **(CORNETT,**

[163] From *p.100* for McSourley Lake, $A_{SE}=0.9A_{LA}=23.4$ ha **(CORNETT, 1984)**
[164] Robertson, E., & Barry, P. J. (1984). *A summary of the water and energy balances at Perch Lake over an eleven-year period* (Rep. No. AECL-8189). Chalk River, ON: Atomic Energy of Canada Ltd.

1984). The total Pb-210 flux to each lake was assumed (*Table 4*) as **(CORNETT, 1984)**:

$$I_T = \mathcal{J}_A + I_C \tag{I.4}$$

The fraction of total annual Pb-210 input retained in the sediments, $\mathcal{R}$, is defined as:

$$\mathcal{R} = \frac{\mathcal{k}}{\mathcal{k} + \mathcal{r}} \tag{I.5}$$

Where $\mathcal{k}$ is the rate constant for Pb-210 sedimentation and $\mathcal{r}$ is the hydraulic rate constant given in Table I-3 (*Table 1*) **(CORNETT, 1984)**. It was demonstrated that the lake values of $\mathcal{R}$ correspond as:

$$\mathcal{R} = \frac{\mathcal{J}_S}{I_T} \tag{I.6}$$

where $\mathcal{J}_S$ are the fluxes to sediment calculated from sediment samples of the study lakes (*Table 3*, *Table 4*) **(CORNETT, 1984)**. The apparent settling velocity, v_S (*Table 4*) **(CORNETT, 1984)**, was shown to follow from a definition as:

$$v_S = \frac{V_{LA} \cdot \mathcal{k}}{A_{LA}} \tag{I.7}$$

using $V_{LA} = A_{LA} \cdot d_{LA}$, $\mathcal{r} = Q/V$ and Equation I.5:

$$v_S = \frac{\mathcal{R} \cdot Q}{(1 - \mathcal{R}) A_{LA}} \tag{I.8}$$

Table I-3 lists the settling flux F_S determined from Equation I.8 and Table I-2 C_{PL} as:

$$F_S = v_S C_{PL} \tag{I.9}$$

Table I-4 lists the nuclide properties assumed for Laurentian lakes. Other default values are listed in Table F-2.

Table I-3. Laurentian lake hydrological properties

Lake	Inflow rate[165]	Outflow rate	Volume[166]	Hydrologic rate[167]	Settling flux[168]
	Q_I	Q_J	V_{LA}	r	F_S
	$m^3 \cdot a^{-1}$	$m^3 \cdot a^{-1}$	m^3	a^{-1}	$g \cdot m^{-2} \cdot d^{-1}$
Currie	2.19E+05	1.98E+05	1.96E+06	0.112	0.00482
McSourley	1.19E+06	1.17E+06	5.04E+06	0.236	0.00482
Petznick	1.32E+06	1.27E+06	2.45E+06	0.540	0.00458
Lower Bass	1.47E+05	1.41E+05	2.39E+05	0.613	0.00279
Perch	1.79E+06	1.75E+06	9.00E+05	1.99	0.00530
Upper Bass	8.59E+05	8.55E+05	1.88E+05	4.57	0.01369
Otterson	2.73E+07	2.72E+07	1.02E+06	26.6	0.01394

Table I-4. Laurentian lake nuclide properties

Property			Ra-226	Pb-210	Po-210
Rain scavenging ratio	W_g	-	7.94E+05[169]	3.06E+05[170]	1.82E+04[171]
Deposition velocity	v_{AD}	$m \cdot h^{-1}$	568[172]	4.49[170]	5.01[172]
MTC water-sediment	k_{TS}	$m \cdot h^{-1}$	fit[173]	fit	fit
MTC sediment-water	k_{TW}	$m \cdot h^{-1}$	fit[173]	fit	fit

I.2 OPTIMIZATION

The net average flux of Pb-210 from the atmosphere to soils was measured in samples from two locations central to the Laurentian lakes at $\mathcal{J}_A$ = 136±16 $Bq \cdot m^{-2} \cdot a^{-1}$ **(CORNETT, 1984)**. Measurements of airborne Pb-210 at Ottawa reported weekly from 2009-2016 indicated a concentration of C_{OA} = 0.45±0.19 $mBq \cdot m^{-3}$ **(RPB, 2017)**.

The atmospheric deposition flux consists of the lake unit surface area process rates for rain q_M, dry deposition q_Q and wet deposition q_C, which are expressed in the input variables from the definitions in Table A-2 for the process rates (A.15)(A.17)(A.19) and transport parameters D (A.16)(A.18)(A.20), in Table A-3 for

[165] From Equation I.1
[166] From Table I-2 $A_{LA} \cdot d_{LA}$
[167] From *Table 1* **(CORNETT, 1984)** as Q_J / V
[168] Initial values, then 'fit' or adjusted upwards during optimization
[169] From section F.2.1.1 as Crystal Lake (Table F-2) and section G.2.1.1 as Bickford Pond (Table G-2)
[170] From section I.2
[171] From section G.2.1.2 as Bickford Pond (Table G-2)
[172] From section G.2.2 as Bickford Pond (Table G-2)
[173] Values for neither Ra-226 diffusion coefficient k_{TS1} or k_{TW1} were required for optimization

the volumetric rates Q (A.15)(A.17)(A.19), and from the air aquivalence $\mathcal{A}_A$ (A.7) and bulk air aquivalence capacity $\mathcal{Z}_{AT}$ (A.3):

$$\mathcal{J}_A A_{LA} = q_Q + q_C + q_M \tag{I.10}$$

$$\mathcal{J}_A = C_{OA}\left[v_{AD} + v_{RA}\left(W_g + \frac{\mathbb{Z}_W}{f_{AV}\mathbb{Z}_Q}\right)\right] \tag{I.11}$$

The contribution of dry deposition relative to wet deposition are known from the studies of Crystal Lake (Table F-4) to be 11%[98,101] **(TALBOT, 1983)** and of Bickford Pond (Table G-4) to be 15%[128] **(BENOIT, 1987)**. Ignoring the small contribution of rain due to the last term in (I.11) relative to the wet and dry deposition, and assuming a 13% contribution of dry to total deposition $q_Q = 0.13\cdot(q_Q + q_C)$, the scavenging ratio W_g was:

$$W_g = \frac{0.87\mathcal{J}_A}{C_{OA}v_{RA}} \tag{I.12}$$

W_g = 3.06E+05

Dry deposition velocity v_{AD} follows:

$$v_{AD} = \frac{0.13\mathcal{J}_A}{C_{OA}} \tag{I.13}$$

v_{AD} = 4.49 m·h^{-1}

These were assumed for Pb-210 and listed with corresponding values for Ra-226 and Po-210 in Table I-4.

Table I-5 lists aerosol, rain, and total water concentrations applied to all lakes, and values fit to each scenario. Table I-6 lists concentration calculated for Ra-226 in the water and SPM phases, and the sediment flux.

Table I-7 lists distribution coefficient limits assumed for Laurentian lakes.

Table I-5. Laurentian lakes aerosol, rain and fit concentrations

Phase			Ra-226	Pb-210	Po-210
Air, aerosol[174]	C_{OA}	$\mu g \cdot m^{-3}$	2.00E-11[175]	1.58E-10[176]	3.00E-13[177]
Water inflow[174]	C_{OI}	$ng \cdot L^{-1}$	C_{OWP}	C_{OWP}	C_{OWP}
Rain	C_{OM}	$\mu g \cdot m^{-3}$	1.59E-05[178]	2.64E-05[179]	1.86E-07[179]
Water	C_{OW}	$ng \cdot L^{-1}$	Table I-6	fit	fit
SPM	C_{OP}	$ng \cdot L^{-1}$	Table I-6	$C_{OWP} - C_{OW}$	$C_{OWP} - C_{OW}$
Total water	C_{OWP}	$ng \cdot L^{-1}$	1.37E-05[180]	4.72E-07[181]	2.04E-08[181]
Total water B[182]	C_{OWP}	$ng \cdot L^{-1}$	C_{OWP}	$2 \cdot C_{OWP}$	$2 \cdot C_{OWP}$
Sediment solids	C_{OS}	$\mu g \cdot g^{-1}$	fit	fit	fit

Table I-6. Laurentian lakes water and SPM concentrations

Lake	Water[183]	SPM[183]	Sediment flux[184]
	Ra-226	Ra-226	Pb-210
	C_{OW}	C_{OP}	$(q_D+q_{TS}-q_{TW})'$
	$ng \cdot L^{-1}$	$ng \cdot L^{-1}$	$mol \cdot h^{-1}$
Currie	1.36E-05	5.08E-08	4.93E-12
McSourley	1.36E-05	3.89E-08	3.73E-12
Petznick	1.36E-05	1.06E-07	6.85E-12
Lower Bass	1.36E-05	7.77E-08	6.75E-13
Perch	1.36E-05	8.30E-08	5.26E-12
Upper Bass	1.36E-05	1.01E-07	4.86E-13
Otterson	1.36E-05	3.25E-08	6.54E-12

[174] Initial values
[175] From *Table 2* 4.4 $dpm \cdot 1E+5m^{-3}$ **(MOORE, 1976)**; initial value, fit
[176] From Ottawa weekly average 2009-2016: 0.45 $mBq \cdot m^{-3}$ **(RPB, 2017)**; initial value, fit
[177] From *Table 14* 50 $\mu g \cdot m^{-3}$ **(UNSCEAR, 2000)**
[178] From *Table 2* 0.035 ± 0.020 $dpm \cdot L^{-1}$ (n=17) **(MOORE, 1976)**
[179] From *Table 1* Pb-210: 0.075 $Bq \cdot L^{-1}$, Po-210: 0.031 $Bq \cdot L^{-1}$ **(THOMAS, 2000)**
[180] From *App. B Table 15* drinking water reference value 0.5 $mBq \cdot kg^{-1}$ **(UNSCEAR, 2000)**
[181] Average of Grant's Creek measurements (section 4.3.3) + 20% for Po-210; alternate 'B' scenarios optimized with double these concentrations
[182] Applied to scenarios 1B through 7B
[183] From *Table 6* $Log_{10}K_p=3.9$ **(CIFFROY, 2009)**, Table I-2 C_{PL}, (A.34), Note [180]
[184] From *Table 3* weighted average of composite & individual sample fluxes **(CORNETT, 1984)**

Table I-7. Laurentian lakes distribution coefficients

$L \cdot kg^{-1}$	sediment		SPM	
	lower	upper	lower	upper
Ra-226	3.0E+02[185]	7.9E+03[186]	7.9E+03[187]	
Pb-210[188]	6.7E+04	1.3E+05	5.4E+05	5.6E+06
Po-210[188]	1.3E+05	3.8E+05	6.8E+05	6.1E+06

I.3 PROCEDURE

The parameters adjusted to optimize the scenarios were:

- F_S settling flux Table I-3
- C_{OS} observed concentrations on sediment solids Table I-5
- C_{OW} observed concentrations in water, dissolved Table I-5
- C_{OWP} observed water + particle concentration Table I-5
- C_{OA} observed concentrations on aerosols Table I-5
- C_{OI} observed inflow water concentration Table I-5
- k_{TW} diffusion coefficient for sediment-water Table I-4

The observed solid sediment concentrations C_{OS} of Ra-226, Pb-210 and Po-210 (C_{OS1}, C_{OS2} and C_{OS3}) were adjusted at each step of the optimization to maintain sediment distribution coefficients K_d within the Table I-7 limits and to set each $C_S/C_{OS} = 1$.

Pb-210 and Po-210 total water concentrations were assigned the Table I-6 values for base scenarios 1 through 7:

- C_{OWP2} = 4.72E-07 $ng \cdot L^{-1}$
- C_{OWP3} = 2.04E-08 $ng \cdot L^{-1}$

Pb-210 and Po-210 total water concentrations were assigned twice the Table I-6 values for alternate scenarios 1B through 7B:

- C_{OWP2} = 9.44E-07 $ng \cdot L^{-1}$
- C_{OWP3} = 4.08E-08 $ng \cdot L^{-1}$

The optimization sequence for each scenario was:

[185] From *p.S343* **(MLJAČ, 1996)**
[186] From *Table 3* & *Table 5* calculated geometric mean **(SANCHEZ, 1999)**
[187] From *Table 6* mode $Log_{10}(K_d)$=3.9 **(CIFFROY, 2009)**
[188] From *Table 4* range of central values over Perch Lake & Maskinonge Lake **(WANG, 1993)**

- Step 1: setting Ra-226 C_{W1}/C_{OW1} = 1, Pb-210 sediment flux $q_{D2}+q_{TS2}-q_{TW2}$ to the Table I-6 value, and Pb-210 C_{W2}/C_{OW2} = 1 by adjusting:
    - C_{OI} observed inflow water concentration (reducing from initial value)
    - F_S flux of settling particles (increasing from initial Table I-3 value)
    - C_{OA1} Ra-226 observed concentration on aerosols
    - C_{OA2} Pb-210 observed concentration on aerosols
- Step 2: setting Po-210 C_{W3}/C_{OW3} = 1 by adjusting:
    - k_{TW3} Po-210 diffusion coefficient for sediment-water

The optimization steps for Laurentian lakes are detailed:

- cases 1, 1B (Table I-8, Table I-9): Currie Lake
- cases 2, 2B (Table I-10, Table I-11): McSourley Lake
- cases 3, 3B (Table I-12, Table I-13): Petznick Lake
- cases 4, 4B (Table I-14, Table I-15): Lower Bass Lake
- cases 5, 5B (Table I-16, Table I-17): Perch Lake
- cases 6, 6B (Table I-18, Table I-19): Upper Bass Lake
- cases 7, 7B (Table I-20, Table I-21): Otterson Lake

The process charts are shown:

- cases 1, 1B (Figure I-1, Figure I-2): Currie Lake
- cases 2, 2B (Figure I-3, Figure I-4): McSourley Lake
- cases 3, 3B (Figure I-5, Figure I-6): Petznick Lake
- cases 4, 4B (Figure I-7, Figure I-8): Lower Bass Lake
- cases 5, 5B (Figure I-9, Figure I-10): Perch Lake
- cases 6, 6B (Figure I-11, Figure I-12): Upper Bass Lake
- cases 7, 7B (Figure I-13, Figure I-14): Otterson Lake

Table I-8. Laurentian case 1 Currie Lake optimization

par.	nuclide	units	target	initial	step 1	step 2
F_S	all	$g \cdot m^{-2} \cdot d^{-1}$	0.004824	0.004824	1.41	1.41
C_{OA}	Ra-226	$\mu g \cdot m^{-3}$	2.00E-11	2.00E-11	1.01E-11	1.01E-11
C_{OA}	Pb-210	$\mu g \cdot m^{-3}$	1.58E-10	1.58E-10	1.32E-10	1.32E-10
k_{TW}	Po-210	$m \cdot h^{-1}$	NA	1.00E-10	1.00E-10	2.43E-01
C_{OI}	Pb-210	$kg \cdot a^{-1}$	NA	2.02E-06	0.00E+00	0.00E+00
C_{OW}	Pb-210	$ng \cdot L^{-1}$	NA	1.00E-07	4.36E-07	4.36E-07
C_{OW}	Po-210	$ng \cdot L^{-1}$	NA	1.00E-08	7.19E-09	7.00E-09
C_{OWP}	Pb-210	$ng \cdot L^{-1}$	4.72E-07	4.72E-07	4.72E-07	4.72E-07
C_{OWP}	Po-210	$ng \cdot L^{-1}$	2.04E-08	2.04E-08	2.04E-08	2.04E-08
C_{OS}	Ra-226	$\mu g \cdot g^{-1}$	NA	1.00E-08	1.08E-07	1.08E-07
C_{OS}	Pb-210	$\mu g \cdot g^{-1}$	NA	1.00E-08	5.69E-08	5.69E-08
C_{OS}	Po-210	$\mu g \cdot g^{-1}$	NA	1.00E-10	9.38E-10	9.09E-10
$n_D+n_{TS}-n_{TW}$	Pb-210	$mol \cdot h^{-1}$	4.93E-12	4.45E-12	4.94E-12	4.94E-12
K_d low	Ra-226	$L \cdot kg^{-1}$	3.00E+02	7.35E+02	-	-
K_d high	Ra-226	$L \cdot kg^{-1}$	7.90E+03	-	7.94E+03	7.94E+03
K_d low	Pb-210	$L \cdot kg^{-1}$	6.70E+04	-	-	-
K_d high	Pb-210	$L \cdot kg^{-1}$	1.30E+05	1.00E+05	1.30E+05	1.30E+05
K_d low	Po-210	$L \cdot kg^{-1}$	1.30E+05	1.00E+04	1.30E+05	1.30E+05
K_d high	Po-210	$L \cdot kg^{-1}$	3.80E+05	-	-	-
K_p low	Pb-210	$L \cdot kg^{-1}$	5.40E+05	-	1.75E+05	1.75E+05
K_p high	Pb-210	$L \cdot kg^{-1}$	5.60E+06	7.92E+06	-	-
K_p low	Po-210	$L \cdot kg^{-1}$	6.80E+05	-	-	-
K_p high	Po-210	$L \cdot kg^{-1}$	6.10E+06	2.22E+06	3.92E+06	4.08E+06
C_W/C_{OW}	Ra-226	unitless	1.00E+00	9.46E+00	1.00E+00	1.00E+00
C_S/C_{OS}	Ra-226	unitless	1.00E+00	4.21E+01	1.00E+00	1.00E+00
C_W/C_{OW}	Pb-210	unitless	1.00E+00	2.55E+01	1.00E+00	1.00E+00
C_S/C_{OS}	Pb-210	unitless	1.00E+00	2.01E+01	1.00E+00	1.00E+00
C_W/C_{OW}	Po-210	unitless	1.00E+00	8.58E+00	1.08E-02	1.00E+00
C_S/C_{OS}	Po-210	unitless	1.00E+00	3.45E+01	1.00E+00	1.00E+00

Table I-9. Laurentian case 1B Currie Lake optimization

par.	nuclide	units	target	initial	step 1	step 2
F_S	all	$g \cdot m^{-2} \cdot d^{-1}$	0.004824	0.004824	0.502	0.502
C_{OA}	Ra-226	$\mu g \cdot m^{-3}$	2.00E-11	2.00E-11	3.73E-12	3.73E-12
C_{OA}	Pb-210	$\mu g \cdot m^{-3}$	1.58E-10	1.58E-10	1.34E-10	1.34E-10
k_{TW}	Po-210	$m \cdot h^{-1}$	NA	1.00E-10	1.00E-10	9.01E-02
C_{OI}	Pb-210	$kg \cdot a^{-1}$	NA	2.02E-06	0.00E+00	0.00E+00
C_{OW}	Pb-210	$ng \cdot L^{-1}$	NA	1.00E-07	8.43E-07	8.43E-07
C_{OW}	Po-210	$ng \cdot L^{-1}$	NA	1.00E-08	1.43E-08	1.38E-08
C_{OWP}	Pb-210	$ng \cdot L^{-1}$	9.44E-07	9.44E-07	9.44E-07	9.44E-07
C_{OWP}	Po-210	$ng \cdot L^{-1}$	4.08E-08	4.08E-08	4.08E-08	4.08E-08
C_{OS}	Ra-226	$\mu g \cdot g^{-1}$	NA	1.00E-08	1.07E-07	1.07E-07
C_{OS}	Pb-210	$\mu g \cdot g^{-1}$	NA	1.00E-08	1.09E-07	1.09E-07
C_{OS}	Po-210	$\mu g \cdot g^{-1}$	NA	1.00E-10	1.85E-09	1.79E-09
$n_D+n_{TS}-n_{TW}$	Pb-210	$mol \cdot h^{-1}$	4.93E-12	4.61E-12	4.93E-12	4.93E-12
K_d low	Ra-226	$L \cdot kg^{-1}$	3.00E+02	7.35E+02	-	-
K_d high	Ra-226	$L \cdot kg^{-1}$	7.90E+03	-	7.83E+03	7.83E+03
K_d low	Pb-210	$L \cdot kg^{-1}$	6.70E+04	-	-	-
K_d high	Pb-210	$L \cdot kg^{-1}$	1.30E+05	1.00E+05	1.30E+05	1.30E+05
K_d low	Po-210	$L \cdot kg^{-1}$	1.30E+05	1.00E+04	1.30E+05	1.30E+05
K_d high	Po-210	$L \cdot kg^{-1}$	3.80E+05	-	-	-
K_p low	Pb-210	$L \cdot kg^{-1}$	5.40E+05	-	2.55E+05	2.55E+05
K_p high	Pb-210	$L \cdot kg^{-1}$	5.60E+06	1.80E+07	-	-
K_p low	Po-210	$L \cdot kg^{-1}$	6.80E+05	-	-	-
K_p high	Po-210	$L \cdot kg^{-1}$	6.10E+06	6.56E+06	3.96E+06	4.17E+06
C_W/C_{OW}	Ra-226	unitless	1.00E+00	9.46E+00	1.00E+00	1.00E+00
C_S/C_{OS}	Ra-226	unitless	1.00E+00	4.21E+01	1.00E+00	1.00E+00
C_W/C_{OW}	Pb-210	unitless	1.00E+00	1.16E+01	1.00E+00	1.00E+00
C_S/C_{OS}	Pb-210	unitless	1.00E+00	2.08E+01	1.00E+00	1.00E+00
C_W/C_{OW}	Po-210	unitless	1.00E+00	3.76E+00	2.76E-02	1.00E+00
C_S/C_{OS}	Po-210	unitless	1.00E+00	3.58E+01	1.00E+00	1.00E+00

Table I-10. Laurentian case 2 McSourley Lake optimization

par.	nuclide	units	target	initial	step 1	step 2
F_S	all	$g \cdot m^{-2} \cdot d^{-1}$	0.004824	0.004824	0.924	0.924
C_{OA}	Ra-226	$\mu g \cdot m^{-3}$	2.00E-11	2.00E-11	6.03E-12	6.03E-12
C_{OA}	Pb-210	$\mu g \cdot m^{-3}$	1.58E-10	1.58E-10	9.49E-11	9.49E-11
k_{TW}	Po-210	$m \cdot h^{-1}$	NA	1.00E-10	1.00E-10	2.15E-01
C_{OI}	Pb-210	$kg \cdot a^{-1}$	NA	2.02E-06	0.00E+00	0.00E+00
C_{OW}	Pb-210	$ng \cdot L^{-1}$	NA	1.00E-07	4.41E-07	4.41E-07
C_{OW}	Po-210	$ng \cdot L^{-1}$	NA	1.00E-08	7.52E-09	6.95E-09
C_{OWP}	Pb-210	$ng \cdot L^{-1}$	4.72E-07	4.72E-07	4.72E-07	4.72E-07
C_{OWP}	Po-210	$ng \cdot L^{-1}$	2.04E-08	2.04E-08	2.04E-08	2.04E-08
C_{OS}	Ra-226	$\mu g \cdot g^{-1}$	NA	1.00E-08	1.07E-07	1.07E-07
C_{OS}	Pb-210	$\mu g \cdot g^{-1}$	NA	1.00E-08	5.71E-08	5.71E-08
C_{OS}	Po-210	$\mu g \cdot g^{-1}$	NA	1.00E-10	9.77E-10	9.01E-10
$n_D+n_{TS}-n_{TW}$	Pb-210	$mol \cdot h^{-1}$	3.73E-12	3.25E-12	3.73E-12	3.73E-12
K_d low	Ra-226	$L \cdot kg^{-1}$	3.00E+02	7.34E+02	-	-
K_d high	Ra-226	$L \cdot kg^{-1}$	7.90E+03	-	7.89E+03	7.89E+03
K_d low	Pb-210	$L \cdot kg^{-1}$	6.70E+04	-	-	-
K_d high	Pb-210	$L \cdot kg^{-1}$	1.30E+05	1.00E+05	1.30E+05	1.30E+05
K_d low	Po-210	$L \cdot kg^{-1}$	1.30E+05	1.00E+04	1.30E+05	1.30E+05
K_d high	Po-210	$L \cdot kg^{-1}$	3.80E+05	-	-	-
K_p low	Pb-210	$L \cdot kg^{-1}$	5.40E+05	-	1.96E+05	1.96E+05
K_p high	Pb-210	$L \cdot kg^{-1}$	5.60E+06	1.03E+07	-	-
K_p low	Po-210	$L \cdot kg^{-1}$	6.80E+05	-	-	-
K_p high	Po-210	$L \cdot kg^{-1}$	6.10E+06	2.89E+06	4.77E+06	5.38E+06
C_W/C_{OW}	Ra-226	unitless	1.00E+00	2.78E+00	1.00E+00	1.00E+00
C_S/C_{OS}	Ra-226	unitless	1.00E+00	1.24E+01	1.00E+00	1.00E+00
C_W/C_{OW}	Pb-210	unitless	1.00E+00	1.40E+01	1.00E+00	1.00E+00
C_S/C_{OS}	Pb-210	unitless	1.00E+00	1.42E+01	1.00E+00	1.00E+00
C_W/C_{OW}	Po-210	unitless	1.00E+00	4.76E+00	3.40E-02	1.00E+00
C_S/C_{OS}	Po-210	unitless	1.00E+00	2.44E+01	1.00E+00	1.00E+00

Table I-11. Laurentian case 2B McSourley Lake optimization

par.	nuclide	units	target	initial	step 1	step 2
F_S	all	$g \cdot m^{-2} \cdot d^{-1}$	0.004824	0.004824	0.258	0.258
C_{OA}	Ra-226	$\mu g \cdot m^{-3}$	2.00E-11	2.00E-11	1.92E-12	1.92E-12
C_{OA}	Pb-210	$\mu g \cdot m^{-3}$	1.58E-10	1.58E-10	1.03E-10	1.03E-10
k_{TW}	Po-210	$m \cdot h^{-1}$	NA	1.00E-10	1.00E-10	7.00E-02
C_{OI}	Pb-210	$kg \cdot a^{-1}$	NA	2.02E-06	0.00E+00	0.00E+00
C_{OW}	Pb-210	$ng \cdot L^{-1}$	NA	1.00E-07	8.32E-07	8.32E-07
C_{OW}	Po-210	$ng \cdot L^{-1}$	NA	1.00E-08	1.45E-08	1.33E-08
C_{OWP}	Pb-210	$ng \cdot L^{-1}$	9.44E-07	9.44E-07	9.44E-07	9.44E-07
C_{OWP}	Po-210	$ng \cdot L^{-1}$	4.08E-08	4.08E-08	4.08E-08	4.08E-08
C_{OS}	Ra-226	$\mu g \cdot g^{-1}$	NA	1.00E-08	1.06E-07	1.06E-07
C_{OS}	Pb-210	$\mu g \cdot g^{-1}$	NA	1.00E-08	1.08E-07	1.08E-07
C_{OS}	Po-210	$\mu g \cdot g^{-1}$	NA	1.00E-10	1.88E-09	1.73E-09
$n_D+n_{TS}-n_{TW}$	Pb-210	$mol \cdot h^{-1}$	3.73E-12	3.50E-12	3.73E-12	3.73E-12
K_d low	Ra-226	$L \cdot kg^{-1}$	3.00E+02	7.34E+02	-	-
K_d high	Ra-226	$L \cdot kg^{-1}$	7.90E+03	-	7.77E+03	7.77E+03
K_d low	Pb-210	$L \cdot kg^{-1}$	6.70E+04	-	-	-
K_d high	Pb-210	$L \cdot kg^{-1}$	1.30E+05	1.00E+05	1.30E+05	1.30E+05
K_d low	Po-210	$L \cdot kg^{-1}$	1.30E+05	1.00E+04	1.30E+05	1.30E+05
K_d high	Po-210	$L \cdot kg^{-1}$	3.80E+05	-	-	-
K_p low	Pb-210	$L \cdot kg^{-1}$	5.40E+05	-	3.74E+05	3.74E+05
K_p high	Pb-210	$L \cdot kg^{-1}$	5.60E+06	2.35E+07	-	-
K_p low	Po-210	$L \cdot kg^{-1}$	6.80E+05	-	-	-
K_p high	Po-210	$L \cdot kg^{-1}$	6.10E+06	8.57E+06	5.05E+06	5.75E+06
C_W/C_{OW}	Ra-226	unitless	1.00E+00	2.78E+00	1.00E+00	1.00E+00
C_S/C_{OS}	Ra-226	unitless	1.00E+00	1.24E+01	1.00E+00	1.00E+00
C_W/C_{OW}	Pb-210	unitless	1.00E+00	6.66E+00	1.00E+00	1.00E+00
C_S/C_{OS}	Pb-210	unitless	1.00E+00	1.53E+01	1.00E+00	1.00E+00
C_W/C_{OW}	Po-210	unitless	1.00E+00	2.26E+00	9.90E-02	1.00E+00
C_S/C_{OS}	Po-210	unitless	1.00E+00	2.64E+01	1.00E+00	1.00E+00

Table I-12. Laurentian case 3 Petznick Lake optimization

par.	nuclide	units	target	initial	step 1	step 2
F_S	all	$g \cdot m^{-2} \cdot d^{-1}$	0.00458	0.00458	0.719	0.719
C_{OA}	Ra-226	$\mu g \cdot m^{-3}$	2.00E-11	2.00E-11	5.25E-12	5.25E-12
C_{OA}	Pb-210	$\mu g \cdot m^{-3}$	1.58E-10	1.58E-10	7.67E-11	7.67E-11
k_{TW}	Po-210	$m \cdot h^{-1}$	NA	1.00E-10	1.00E-10	6.85E-02
C_{OI}	Pb-210	$kg \cdot a^{-1}$	NA	2.02E-06	0.00E+00	0.00E+00
C_{OW}	Pb-210	$ng \cdot L^{-1}$	NA	1.00E-07	3.90E-07	3.90E-07
C_{OW}	Po-210	$ng \cdot L^{-1}$	NA	1.00E-08	6.55E-09	6.40E-09
C_{OWP}	Pb-210	$ng \cdot L^{-1}$	4.72E-07	4.72E-07	4.72E-07	4.72E-07
C_{OWP}	Po-210	$ng \cdot L^{-1}$	2.04E-08	2.04E-08	2.04E-08	2.04E-08
C_{OS}	Ra-226	$\mu g \cdot g^{-1}$	NA	1.00E-08	1.07E-07	1.07E-07
C_{OS}	Pb-210	$\mu g \cdot g^{-1}$	NA	1.00E-08	5.05E-08	5.05E-08
C_{OS}	Po-210	$\mu g \cdot g^{-1}$	NA	1.00E-10	8.51E-10	8.32E-10
$n_D+n_{TS}-n_{TW}$	Pb-210	$mol \cdot h^{-1}$	6.85E-12	5.77E-12	6.85E-12	6.85E-12
K_d low	Ra-226	$L \cdot kg^{-1}$	3.00E+02	7.38E+02	-	-
K_d high	Ra-226	$L \cdot kg^{-1}$	7.90E+03	-	7.90E+03	7.90E+03
K_d low	Pb-210	$L \cdot kg^{-1}$	6.70E+04	-	-	-
K_d high	Pb-210	$L \cdot kg^{-1}$	1.30E+05	1.00E+05	1.30E+05	1.30E+05
K_d low	Po-210	$L \cdot kg^{-1}$	1.30E+05	1.00E+04	1.30E+05	1.30E+05
K_d high	Po-210	$L \cdot kg^{-1}$	3.80E+05	-	-	-
K_p low	Pb-210	$L \cdot kg^{-1}$	5.40E+05	-	2.15E+05	2.15E+05
K_p high	Pb-210	$L \cdot kg^{-1}$	5.60E+06	3.80E+06	-	-
K_p low	Po-210	$L \cdot kg^{-1}$	6.80E+05	-	-	-
K_p high	Po-210	$L \cdot kg^{-1}$	6.10E+06	1.06E+06	2.16E+06	2.24E+06
C_W/C_{OW}	Ra-226	unitless	1.00E+00	4.51E+00	1.00E+00	1.00E+00
C_S/C_{OS}	Ra-226	unitless	1.00E+00	1.94E+01	1.00E+00	1.00E+00
C_W/C_{OW}	Pb-210	unitless	1.00E+00	2.93E+01	1.00E+00	1.00E+00
C_S/C_{OS}	Pb-210	unitless	1.00E+00	1.05E+01	1.00E+00	1.00E+00
C_W/C_{OW}	Po-210	unitless	1.00E+00	8.50E+00	3.25E-02	1.00E+00
C_S/C_{OS}	Po-210	unitless	1.00E+00	1.80E+01	1.00E+00	1.00E+00

Table I-13. Laurentian case 3B Petznick Lake optimization

par.	nuclide	units	target	initial	step 1	step 2
F_S	all	$g \cdot m^{-2} \cdot d^{-1}$	0.00458	0.00458	0.214	0.214
C_{OA}	Ra-226	$\mu g \cdot m^{-3}$	2.00E-11	2.00E-11	1.74E-12	1.74E-12
C_{OA}	Pb-210	$\mu g \cdot m^{-3}$	1.58E-10	1.58E-10	8.06E-11	8.06E-11
k_{TW}	Po-210	$m \cdot h^{-1}$	NA	1.00E-10	1.00E-10	2.61E-02
C_{OI}	Pb-210	$kg \cdot a^{-1}$	NA	2.02E-06	0.00E+00	0.00E+00
C_{OW}	Pb-210	$ng \cdot L^{-1}$	NA	1.00E-07	6.67E-07	6.67E-07
C_{OW}	Po-210	$ng \cdot L^{-1}$	NA	1.00E-08	1.14E-08	1.12E-08
C_{OWP}	Pb-210	$ng \cdot L^{-1}$	9.44E-07	9.44E-07	9.44E-07	9.44E-07
C_{OWP}	Po-210	$ng \cdot L^{-1}$	4.08E-08	4.08E-08	4.08E-08	4.08E-08
C_{OS}	Ra-226	$\mu g \cdot g^{-1}$	NA	1.00E-08	1.05E-07	1.05E-07
C_{OS}	Pb-210	$\mu g \cdot g^{-1}$	NA	1.00E-08	8.64E-08	8.64E-08
C_{OS}	Po-210	$\mu g \cdot g^{-1}$	NA	1.00E-10	1.48E-09	1.45E-09
$n_D+n_{TS}-n_{TW}$	Pb-210	$mol \cdot h^{-1}$	6.85E-12	6.25E-12	6.85E-12	6.85E-12
K_d low	Ra-226	$L \cdot kg^{-1}$	3.00E+02	7.38E+02	-	-
K_d high	Ra-226	$L \cdot kg^{-1}$	7.90E+03	-	7.72E+03	7.72E+03
K_d low	Pb-210	$L \cdot kg^{-1}$	6.70E+04	-	-	-
K_d high	Pb-210	$L \cdot kg^{-1}$	1.30E+05	1.00E+05	1.30E+05	1.30E+05
K_d low	Po-210	$L \cdot kg^{-1}$	1.30E+05	1.00E+04	1.30E+05	1.30E+05
K_d high	Po-210	$L \cdot kg^{-1}$	3.80E+05	-	-	-
K_p low	Pb-210	$L \cdot kg^{-1}$	5.40E+05	-	4.23E+05	4.23E+05
K_p high	Pb-210	$L \cdot kg^{-1}$	5.60E+06	8.62E+06	-	-
K_p low	Po-210	$L \cdot kg^{-1}$	6.80E+05	-	-	-
K_p high	Po-210	$L \cdot kg^{-1}$	6.10E+06	3.15E+06	2.63E+06	2.72E+06
C_W/C_{OW}	Ra-226	unitless	1.00E+00	4.51E+00	1.00E+00	1.00E+00
C_S/C_{OS}	Ra-226	unitless	1.00E+00	1.94E+01	1.00E+00	1.00E+00
C_W/C_{OW}	Pb-210	unitless	1.00E+00	1.40E+01	1.00E+00	1.00E+00
C_S/C_{OS}	Pb-210	unitless	1.00E+00	1.14E+01	1.00E+00	1.00E+00
C_W/C_{OW}	Po-210	unitless	1.00E+00	4.01E+00	8.54E-02	1.00E+00
C_S/C_{OS}	Po-210	unitless	1.00E+00	1.95E+01	1.00E+00	1.00E+00

Table I-14. Laurentian case 4 Lower Bass Lake optimization

par.	nuclide	units	target	initial	step 1	step 2
F_S	all	$g \cdot m^{-2} \cdot d^{-1}$	0.00279	0.00279	0.552	0.552
C_{OA}	Ra-226	$\mu g \cdot m^{-3}$	2.00E-11	2.00E-11	4.09E-12	4.09E-12
C_{OA}	Pb-210	$\mu g \cdot m^{-3}$	1.58E-10	1.58E-10	6.88E-11	6.88E-11
k_{TW}	Po-210	$m \cdot h^{-1}$	NA	1.00E-10	1.00E-10	6.66E-02
C_{OI}	Pb-210	$kg \cdot a^{-1}$	NA	2.02E-06	0.00E+00	0.00E+00
C_{OW}	Pb-210	$ng \cdot L^{-1}$	NA	1.00E-07	4.02E-07	4.02E-07
C_{OW}	Po-210	$ng \cdot L^{-1}$	NA	1.00E-08	6.80E-09	6.70E-09
C_{OWP}	Pb-210	$ng \cdot L^{-1}$	4.72E-07	4.72E-07	4.72E-07	4.72E-07
C_{OWP}	Po-210	$ng \cdot L^{-1}$	2.04E-08	2.04E-08	2.04E-08	2.04E-08
C_{OS}	Ra-226	$\mu g \cdot g^{-1}$	NA	1.00E-08	1.07E-07	1.07E-07
C_{OS}	Pb-210	$\mu g \cdot g^{-1}$	NA	1.00E-08	5.24E-08	5.24E-08
C_{OS}	Po-210	$\mu g \cdot g^{-1}$	NA	1.00E-10	8.84E-10	8.68E-10
$n_D+n_{TS}-n_{TW}$	Pb-210	$mol \cdot h^{-1}$	6.75E-13	5.64E-13	6.75E-13	6.75E-13
K_d low	Ra-226	$L \cdot kg^{-1}$	3.00E+02	7.36E+02	-	-
K_d high	Ra-226	$L \cdot kg^{-1}$	7.90E+03	-	7.87E+03	7.87E+03
K_d low	Pb-210	$L \cdot kg^{-1}$	6.70E+04	-	-	-
K_d high	Pb-210	$L \cdot kg^{-1}$	1.30E+05	1.00E+05	1.30E+05	1.30E+05
K_d low	Po-210	$L \cdot kg^{-1}$	1.30E+05	1.00E+04	1.30E+05	1.30E+05
K_d high	Po-210	$L \cdot kg^{-1}$	3.80E+05	-	-	-
K_p low	Pb-210	$L \cdot kg^{-1}$	5.40E+05	-	2.42E+05	2.42E+05
K_p high	Pb-210	$L \cdot kg^{-1}$	5.60E+06	5.17E+06	-	-
K_p low	Po-210	$L \cdot kg^{-1}$	6.80E+05	-	-	-
K_p high	Po-210	$L \cdot kg^{-1}$	6.10E+06	1.45E+06	2.78E+06	2.84E+06
C_W/C_{OW}	Ra-226	unitless	1.00E+00	4.51E+00	1.00E+00	1.00E+00
C_S/C_{OS}	Ra-226	unitless	1.00E+00	1.40E+01	1.00E+00	1.00E+00
C_W/C_{OW}	Pb-210	unitless	1.00E+00	3.13E+01	1.00E+00	1.00E+00
C_S/C_{OS}	Pb-210	unitless	1.00E+00	9.28E+00	1.00E+00	1.00E+00
C_W/C_{OW}	Po-210	unitless	1.00E+00	8.89E+00	3.00E-02	1.00E+00
C_S/C_{OS}	Po-210	unitless	1.00E+00	1.59E+01	1.00E+00	1.00E+00

Table I-15. Laurentian case 4B Lower Bass Lake optimization

par.	nuclide	units	target	initial	step 1	step 2
F_S	all	$g \cdot m^{-2} \cdot d^{-1}$	0.00279	0.00279	0.138	0.138
C_{OA}	Ra-226	$\mu g \cdot m^{-3}$	2.00E-11	2.00E-11	1.18E-12	1.18E-12
C_{OA}	Pb-210	$\mu g \cdot m^{-3}$	1.58E-10	1.58E-10	7.26E-11	7.26E-11
k_{TW}	Po-210	$m \cdot h^{-1}$	NA	1.00E-10	1.00E-10	1.00E-10
C_{OI}	Pb-210	$kg \cdot a^{-1}$	NA	2.02E-06	0.00E+00	0.00E+00
C_{OW}	Pb-210	$ng \cdot L^{-1}$	NA	1.00E-07	6.63E-07	6.63E-07
C_{OW}	Po-210	$ng \cdot L^{-1}$	NA	1.00E-08	1.14E-08	1.12E-08
C_{OWP}	Pb-210	$ng \cdot L^{-1}$	9.44E-07	9.44E-07	9.44E-07	9.44E-07
C_{OWP}	Po-210	$ng \cdot L^{-1}$	4.08E-08	4.08E-08	4.08E-08	4.08E-08
C_{OS}	Ra-226	$\mu g \cdot g^{-1}$	NA	1.00E-08	1.03E-07	1.03E-07
C_{OS}	Pb-210	$\mu g \cdot g^{-1}$	NA	1.00E-08	8.65E-08	8.65E-08
C_{OS}	Po-210	$\mu g \cdot g^{-1}$	NA	1.00E-10	1.49E-09	1.45E-09
$n_D+n_{TS}-n_{TW}$	Pb-210	$mol \cdot h^{-1}$	6.75E-13	6.14E-13	6.75E-13	6.75E-13
K_d low	Ra-226	$L \cdot kg^{-1}$	3.00E+02	7.36E+02	-	-
K_d high	Ra-226	$L \cdot kg^{-1}$	7.90E+03	-	7.57E+03	7.57E+03
K_d low	Pb-210	$L \cdot kg^{-1}$	6.70E+04	-	-	-
K_d high	Pb-210	$L \cdot kg^{-1}$	1.30E+05	1.00E+05	1.30E+05	1.30E+05
K_d low	Po-210	$L \cdot kg^{-1}$	1.30E+05	1.00E+04	1.30E+05	1.30E+05
K_d high	Po-210	$L \cdot kg^{-1}$	3.80E+05	-	-	-
K_p low	Pb-210	$L \cdot kg^{-1}$	5.40E+05	-	5.89E+05	5.89E+05
K_p high	Pb-210	$L \cdot kg^{-1}$	5.60E+06	1.17E+07	-	-
K_p low	Po-210	$L \cdot kg^{-1}$	6.80E+05	-	-	-
K_p high	Po-210	$L \cdot kg^{-1}$	6.10E+06	4.28E+06	3.59E+06	3.70E+06
C_W/C_{OW}	Ra-226	unitless	1.00E+00	4.51E+00	1.00E+00	1.00E+00
C_S/C_{OS}	Ra-226	unitless	1.00E+00	1.40E+01	1.00E+00	1.00E+00
C_W/C_{OW}	Pb-210	unitless	1.00E+00	1.50E+01	1.00E+00	1.00E+00
C_S/C_{OS}	Pb-210	unitless	1.00E+00	1.01E+01	1.00E+00	1.00E+00
C_W/C_{OW}	Po-210	unitless	1.00E+00	4.24E+00	9.12E-02	1.00E+00
C_S/C_{OS}	Po-210	unitless	1.00E+00	1.73E+01	1.00E+00	1.00E+00

Table I-16. Laurentian case 5 Perch Lake optimization

par.	nuclide	units	target	initial	step 1	step 2
F_S	all	$g \cdot m^{-2} \cdot d^{-1}$	0.0053	0.0053	0.641	0.641
C_{OA}	Ra-226	$\mu g \cdot m^{-3}$	2.00E-11	2.00E-11	4.75E-12	4.75E-12
C_{OA}	Pb-210	$\mu g \cdot m^{-3}$	1.58E-10	1.58E-10	7.73E-11	7.73E-11
k_{TW}	Po-210	$m \cdot h^{-1}$	NA	1.00E-10	1.00E-10	7.16E-02
C_{OI}	Pb-210	$kg \cdot a^{-1}$	NA	2.02E-06	0.00E+00	0.00E+00
C_{OW}	Pb-210	$ng \cdot L^{-1}$	NA	1.00E-07	4.01E-07	4.01E-07
C_{OW}	Po-210	$ng \cdot L^{-1}$	NA	1.00E-08	6.80E-09	6.70E-09
C_{OWP}	Pb-210	$ng \cdot L^{-1}$	4.72E-07	4.72E-07	4.72E-07	4.72E-07
C_{OWP}	Po-210	$ng \cdot L^{-1}$	2.04E-08	2.04E-08	2.04E-08	2.04E-08
C_{OS}	Ra-226	$\mu g \cdot g^{-1}$	NA	1.00E-08	1.07E-07	1.07E-07
C_{OS}	Pb-210	$\mu g \cdot g^{-1}$	NA	1.00E-08	5.23E-08	5.23E-08
C_{OS}	Po-210	$\mu g \cdot g^{-1}$	NA	1.00E-10	8.87E-10	8.73E-10
$n_D+n_{TS}-n_{TW}$	Pb-210	$mol \cdot h^{-1}$	5.26E-12	4.49E-12	5.26E-12	5.26E-12
K_d low	Ra-226	$L \cdot kg^{-1}$	3.00E+02	7.37E+02	-	-
K_d high	Ra-226	$L \cdot kg^{-1}$	7.90E+03	-	7.87E+03	7.87E+03
K_d low	Pb-210	$L \cdot kg^{-1}$	6.70E+04	-	-	-
K_d high	Pb-210	$L \cdot kg^{-1}$	1.30E+05	1.00E+05	1.30E+05	1.30E+05
K_d low	Po-210	$L \cdot kg^{-1}$	1.30E+05	1.00E+04	1.30E+05	1.30E+05
K_d high	Po-210	$L \cdot kg^{-1}$	3.80E+05	-	-	-
K_p low	Pb-210	$L \cdot kg^{-1}$	5.40E+05	-	2.29E+05	2.29E+05
K_p high	Pb-210	$L \cdot kg^{-1}$	5.60E+06	4.83E+06	-	-
K_p low	Po-210	$L \cdot kg^{-1}$	6.80E+05	-	-	-
K_p high	Po-210	$L \cdot kg^{-1}$	6.10E+06	1.35E+06	2.60E+06	2.66E+06
C_W/C_{OW}	Ra-226	unitless	1.00E+00	3.05E+00	1.00E+00	1.00E+00
C_S/C_{OS}	Ra-226	unitless	1.00E+00	1.43E+01	1.00E+00	1.00E+00
C_W/C_{OW}	Pb-210	unitless	1.00E+00	1.97E+01	1.00E+00	1.00E+00
C_S/C_{OS}	Pb-210	unitless	1.00E+00	1.03E+01	1.00E+00	1.00E+00
C_W/C_{OW}	Po-210	unitless	1.00E+00	3.71E+00	2.96E-02	1.00E+00
C_S/C_{OS}	Po-210	unitless	1.00E+00	1.76E+01	1.00E+00	1.00E+00

Table I-17. Laurentian case 5B Perch Lake optimization

par.	nuclide	units	target	initial	step 1	step 2
F_S	all	$g \cdot m^{-2} \cdot d^{-1}$	0.0053	0.0053	0.176	0.176
C_{OA}	Ra-226	$\mu g \cdot m^{-3}$	2.00E-11	2.00E-11	1.48E-12	1.48E-12
C_{OA}	Pb-210	$\mu g \cdot m^{-3}$	1.58E-10	1.58E-10	8.35E-11	8.35E-11
k_{TW}	Po-210	$m \cdot h^{-1}$	NA	1.00E-10	1.00E-10	2.52E-02
C_{OI}	Pb-210	$kg \cdot a^{-1}$	NA	2.02E-06	0.00E+00	0.00E+00
C_{OW}	Pb-210	$ng \cdot L^{-1}$	NA	1.00E-07	6.88E-07	6.88E-07
C_{OW}	Po-210	$ng \cdot L^{-1}$	NA	1.00E-08	1.17E-08	1.15E-08
C_{OWP}	Pb-210	$ng \cdot L^{-1}$	9.44E-07	9.44E-07	9.44E-07	9.44E-07
C_{OWP}	Po-210	$ng \cdot L^{-1}$	4.08E-08	4.08E-08	4.08E-08	4.08E-08
C_{OS}	Ra-226	$\mu g \cdot g^{-1}$	NA	1.00E-08	1.04E-07	1.04E-07
C_{OS}	Pb-210	$\mu g \cdot g^{-1}$	NA	1.00E-08	8.90E-08	8.90E-08
C_{OS}	Po-210	$\mu g \cdot g^{-1}$	NA	1.00E-10	1.53E-09	1.50E-09
$n_D+n_{TS}-n_{TW}$	Pb-210	$mol \cdot h^{-1}$	5.26E-12	4.88E-12	5.26E-12	5.26E-12
K_d low	Ra-226	$L \cdot kg^{-1}$	3.00E+02	7.37E+02	-	-
K_d high	Ra-226	$L \cdot kg^{-1}$	7.90E+03	-	7.67E+03	7.67E+03
K_d low	Pb-210	$L \cdot kg^{-1}$	6.70E+04	-	-	-
K_d high	Pb-210	$L \cdot kg^{-1}$	1.30E+05	1.00E+05	1.30E+05	1.30E+05
K_d low	Po-210	$L \cdot kg^{-1}$	1.30E+05	1.00E+04	1.30E+05	1.30E+05
K_d high	Po-210	$L \cdot kg^{-1}$	3.80E+05	-	-	-
K_p low	Pb-210	$L \cdot kg^{-1}$	5.40E+05	-	4.85E+05	4.85E+05
K_p high	Pb-210	$L \cdot kg^{-1}$	5.60E+06	1.10E+07	-	-
K_p low	Po-210	$L \cdot kg^{-1}$	6.80E+05	-	-	-
K_p high	Po-210	$L \cdot kg^{-1}$	6.10E+06	4.01E+06	3.23E+06	3.31E+06
C_W/C_{OW}	Ra-226	unitless	1.00E+00	3.05E+00	1.00E+00	1.00E+00
C_S/C_{OS}	Ra-226	unitless	1.00E+00	1.43E+01	1.00E+00	1.00E+00
C_W/C_{OW}	Pb-210	unitless	1.00E+00	9.41E+00	1.00E+00	1.00E+00
C_S/C_{OS}	Pb-210	unitless	1.00E+00	1.12E+01	1.00E+00	1.00E+00
C_W/C_{OW}	Po-210	unitless	1.00E+00	1.88E+00	8.59E-02	1.00E+00
C_S/C_{OS}	Po-210	unitless	1.00E+00	1.91E+01	1.00E+00	1.00E+00

Table I-18. Laurentian case 6 Upper Bass Lake optimization

par.	nuclide	units	target	initial	step 1	step 2
F_S	all	$g \cdot m^{-2} \cdot d^{-1}$	0.0137	0.0137	0.559	0.559
C_{OA}	Ra-226	$\mu g \cdot m^{-3}$	2.00E-11	2.00E-11	4.31E-12	4.31E-12
C_{OA}	Pb-210	$\mu g \cdot m^{-3}$	1.58E-10	1.58E-10	9.13E-11	9.13E-11
k_{TW}	Po-210	$m \cdot h^{-1}$	NA	1.00E-10	1.00E-10	5.58E-02
C_{OI}	Pb-210	$kg \cdot a^{-1}$	NA	2.02E-06	0.00E+00	0.00E+00
C_{OW}	Pb-210	$ng \cdot L^{-1}$	NA	1.00E-07	3.85E-07	3.85E-07
C_{OW}	Po-210	$ng \cdot L^{-1}$	NA	1.00E-08	6.74E-09	6.40E-09
C_{OWP}	Pb-210	$ng \cdot L^{-1}$	4.72E-07	4.72E-07	4.72E-07	4.72E-07
C_{OWP}	Po-210	$ng \cdot L^{-1}$	2.04E-08	2.04E-08	2.04E-08	2.04E-08
C_{OS}	Ra-226	$\mu g \cdot g^{-1}$	NA	1.00E-08	1.07E-07	1.07E-07
C_{OS}	Pb-210	$\mu g \cdot g^{-1}$	NA	1.00E-08	5.02E-08	5.02E-08
C_{OS}	Po-210	$\mu g \cdot g^{-1}$	NA	1.00E-10	8.73E-10	8.30E-10
$n_D+n_{TS}-n_{TW}$	Pb-210	$mol \cdot h^{-1}$	4.86E-13	4.02E-13	4.86E-13	4.86E-13
K_d low	Ra-226	$L \cdot kg^{-1}$	3.00E+02	7.38E+02	-	-
K_d high	Ra-226	$L \cdot kg^{-1}$	7.90E+03	-	7.88E+03	7.88E+03
K_d low	Pb-210	$L \cdot kg^{-1}$	6.70E+04	-	-	-
K_d high	Pb-210	$L \cdot kg^{-1}$	1.30E+05	1.00E+05	1.30E+05	1.30E+05
K_d low	Po-210	$L \cdot kg^{-1}$	1.30E+05	1.00E+04	1.30E+05	1.30E+05
K_d high	Po-210	$L \cdot kg^{-1}$	3.80E+05	-	-	-
K_p low	Pb-210	$L \cdot kg^{-1}$	5.40E+05	-	2.42E+05	2.42E+05
K_p high	Pb-210	$L \cdot kg^{-1}$	5.60E+06	3.96E+06	-	-
K_p low	Po-210	$L \cdot kg^{-1}$	6.80E+05	-	-	-
K_p high	Po-210	$L \cdot kg^{-1}$	6.10E+06	1.11E+06	2.16E+06	2.33E+06
C_W/C_{OW}	Ra-226	unitless	1.00E+00	1.45E+00	1.00E+00	1.00E+00
C_S/C_{OS}	Ra-226	unitless	1.00E+00	1.04E+01	1.00E+00	1.00E+00
C_W/C_{OW}	Pb-210	unitless	1.00E+00	7.94E+00	1.00E+00	1.00E+00
C_S/C_{OS}	Pb-210	unitless	1.00E+00	8.63E+00	1.00E+00	1.00E+00
C_W/C_{OW}	Po-210	unitless	1.00E+00	1.48E+00	1.28E-01	1.00E+00
C_S/C_{OS}	Po-210	unitless	1.00E+00	1.48E+01	1.00E+00	1.00E+00

Table I-19. Laurentian case 6B Upper Bass Lake optimization

par.	nuclide	units	target	initial	step 1	step 2
F_S	all	$g \cdot m^{-2} \cdot d^{-1}$	0.0137	0.0137	0.154	0.154
C_{OA}	Ra-226	$\mu g \cdot m^{-3}$	2.00E-11	2.00E-11	1.50E-12	1.50E-12
C_{OA}	Pb-210	$\mu g \cdot m^{-3}$	1.58E-10	1.58E-10	1.20E-10	1.20E-10
k_{TW}	Po-210	$m \cdot h^{-1}$	NA	1.00E-10	1.00E-10	0.00E+00
C_{OI}	Pb-210	$kg \cdot a^{-1}$	NA	2.02E-06	0.00E+00	0.00E+00
C_{OW}	Pb-210	$ng \cdot L^{-1}$	NA	1.00E-07	6.28E-07	6.28E-07
C_{OW}	Po-210	$ng \cdot L^{-1}$	NA	1.00E-08	1.10E-08	1.05E-08
C_{OWP}	Pb-210	$ng \cdot L^{-1}$	9.44E-07	9.44E-07	9.44E-07	9.44E-07
C_{OWP}	Po-210	$ng \cdot L^{-1}$	4.08E-08	4.08E-08	4.08E-08	4.08E-08
C_{OS}	Ra-226	$\mu g \cdot g^{-1}$	NA	1.00E-08	1.04E-07	1.04E-07
C_{OS}	Pb-210	$\mu g \cdot g^{-1}$	NA	1.00E-08	8.16E-08	8.16E-08
C_{OS}	Po-210	$\mu g \cdot g^{-1}$	NA	1.00E-10	1.43E-09	1.36E-09
$n_D+n_{TS}-n_{TW}$	Pb-210	$mol \cdot h^{-1}$	4.86E-13	4.45E-13	4.86E-13	4.86E-13
K_d low	Ra-226	$L \cdot kg^{-1}$	3.00E+02	7.38E+02	-	-
K_d high	Ra-226	$L \cdot kg^{-1}$	7.90E+03	-	7.64E+03	7.64E+03
K_d low	Pb-210	$L \cdot kg^{-1}$	6.70E+04	-	-	-
K_d high	Pb-210	$L \cdot kg^{-1}$	1.30E+05	1.00E+05	1.30E+05	1.30E+05
K_d low	Po-210	$L \cdot kg^{-1}$	1.30E+05	1.00E+04	1.30E+05	1.30E+05
K_d high	Po-210	$L \cdot kg^{-1}$	3.80E+05	-	-	-
K_p low	Pb-210	$L \cdot kg^{-1}$	5.40E+05	-	5.36E+05	5.36E+05
K_p high	Pb-210	$L \cdot kg^{-1}$	5.60E+06	8.98E+06	-	-
K_p low	Po-210	$L \cdot kg^{-1}$	6.80E+05	-	-	-
K_p high	Po-210	$L \cdot kg^{-1}$	6.10E+06	3.28E+06	2.89E+06	3.07E+06
C_W/C_{OW}	Ra-226	unitless	1.00E+00	1.45E+00	1.00E+00	1.00E+00
C_S/C_{OS}	Ra-226	unitless	1.00E+00	1.04E+01	1.00E+00	1.00E+00
C_W/C_{OW}	Pb-210	unitless	1.00E+00	3.88E+00	1.00E+00	1.00E+00
C_S/C_{OS}	Pb-210	unitless	1.00E+00	9.54E+00	1.00E+00	1.00E+00
C_W/C_{OW}	Po-210	unitless	1.00E+00	1.01E+00	3.11E-01	1.00E+00
C_S/C_{OS}	Po-210	unitless	1.00E+00	1.64E+01	1.00E+00	1.00E+00

Table I-20. Laurentian case 7 Otterson Lake optimization

par.	nuclide	units	target	initial	step 1	step 2
F_S	all	$g \cdot m^{-2} \cdot d^{-1}$	0.01394	0.01394	1.24	1.24
C_{OA}	Ra-226	$\mu g \cdot m^{-3}$	2.00E-11	2.00E-11	9.82E-12	9.82E-12
C_{OA}	Pb-210	$\mu g \cdot m^{-3}$	1.58E-10	1.58E-10	1.58E-10	1.58E-10
k_{TW}	Po-210	$m \cdot h^{-1}$	NA	1.00E-10	1.00E-10	3.13E-01
C_{OI}	Pb-210	$kg \cdot a^{-1}$	NA	2.02E-06	3.35E-07	3.35E-07
C_{OW}	Pb-210	$ng \cdot L^{-1}$	NA	1.00E-07	4.48E-07	4.48E-07
C_{OW}	Po-210	$ng \cdot L^{-1}$	NA	1.00E-08	8.41E-09	7.25E-09
C_{OWP}	Pb-210	$ng \cdot L^{-1}$	4.72E-07	4.72E-07	4.72E-07	4.72E-07
C_{OWP}	Po-210	$ng \cdot L^{-1}$	2.04E-08	2.04E-08	2.04E-08	2.04E-08
C_{OS}	Ra-226	$\mu g \cdot g^{-1}$	NA	1.00E-08	1.08E-07	1.08E-07
C_{OS}	Pb-210	$\mu g \cdot g^{-1}$	NA	1.00E-08	5.81E-08	5.81E-08
C_{OS}	Po-210	$\mu g \cdot g^{-1}$	NA	1.00E-10	1.09E-09	9.40E-10
$n_D+n_{TS}-n_{TW}$	Pb-210	$mol \cdot h^{-1}$	6.54E-12	5.35E-12	6.54E-12	6.54E-12
K_d low	Ra-226	$L \cdot kg^{-1}$	3.00E+02	7.34E+02	-	-
K_d high	Ra-226	$L \cdot kg^{-1}$	7.90E+03	-	7.93E+03	7.93E+03
K_d low	Pb-210	$L \cdot kg^{-1}$	6.70E+04	-	-	-
K_d high	Pb-210	$L \cdot kg^{-1}$	1.30E+05	1.00E+05	1.30E+05	1.30E+05
K_d low	Po-210	$L \cdot kg^{-1}$	1.30E+05	1.00E+04	1.30E+05	1.30E+05
K_d high	Po-210	$L \cdot kg^{-1}$	3.80E+05	-	-	-
K_p low	Pb-210	$L \cdot kg^{-1}$	5.40E+05	-	1.79E+05	1.79E+05
K_p high	Pb-210	$L \cdot kg^{-1}$	5.60E+06	1.24E+07	-	-
K_p low	Po-210	$L \cdot kg^{-1}$	6.80E+05	-	-	-
K_p high	Po-210	$L \cdot kg^{-1}$	6.10E+06	3.47E+06	4.76E+06	6.06E+06
C_W/C_{OW}	Ra-226	unitless	1.00E+00	1.10E+00	1.00E+00	1.00E+00
C_S/C_{OS}	Ra-226	unitless	1.00E+00	7.96E+00	1.00E+00	1.00E+00
C_W/C_{OW}	Pb-210	unitless	1.00E+00	4.73E+00	1.00E+00	1.00E+00
C_S/C_{OS}	Pb-210	unitless	1.00E+00	1.62E+01	1.00E+00	1.00E+00
C_W/C_{OW}	Po-210	unitless	1.00E+00	9.69E-01	8.78E-02	1.00E+00
C_S/C_{OS}	Po-210	unitless	1.00E+00	2.78E+01	1.00E+00	1.00E+00

Table I-21. Laurentian case 7B Otterson Lake optimization

par.	nuclide	units	target	initial	step 1	step 2
F_S	all	$g \cdot m^{-2} \cdot d^{-1}$	0.01394	0.01394	0.398	0.398
C_{OA}	Ra-226	$\mu g \cdot m^{-3}$	2.00E-11	2.00E-11	3.99E-12	3.99E-12
C_{OA}	Pb-210	$\mu g \cdot m^{-3}$	1.58E-10	1.58E-10	1.58E-10	1.58E-10
k_{TW}	Po-210	$m \cdot h^{-1}$	NA	1.00E-10	1.00E-10	1.02E-01
C_{OI}	Pb-210	$kg \cdot a^{-1}$	NA	2.02E-06	8.09E-07	8.09E-07
C_{OW}	Pb-210	$ng \cdot L^{-1}$	NA	1.00E-07	8.69E-07	8.69E-07
C_{OW}	Po-210	$ng \cdot L^{-1}$	NA	1.00E-08	1.65E-08	1.45E-08
C_{OWP}	Pb-210	$ng \cdot L^{-1}$	9.44E-07	9.44E-07	9.44E-07	9.44E-07
C_{OWP}	Po-210	$ng \cdot L^{-1}$	4.08E-08	4.08E-08	4.08E-08	4.08E-08
C_{OS}	Ra-226	$\mu g \cdot g^{-1}$	NA	1.00E-08	1.07E-07	1.07E-07
C_{OS}	Pb-210	$\mu g \cdot g^{-1}$	NA	1.00E-08	1.13E-07	1.13E-07
C_{OS}	Po-210	$\mu g \cdot g^{-1}$	NA	1.00E-10	2.14E-09	1.88E-09
$n_D+n_{TS}-n_{TW}$	Pb-210	$mol \cdot h^{-1}$	6.54E-12	5.96E-12	6.54E-12	6.54E-12
K_d low	Ra-226	$L \cdot kg^{-1}$	3.00E+02	7.34E+02	-	-
K_d high	Ra-226	$L \cdot kg^{-1}$	7.90E+03	-	7.84E+03	7.84E+03
K_d low	Pb-210	$L \cdot kg^{-1}$	6.70E+04	-	-	-
K_d high	Pb-210	$L \cdot kg^{-1}$	1.30E+05	1.00E+05	1.30E+05	1.30E+05
K_d low	Po-210	$L \cdot kg^{-1}$	1.30E+05	1.00E+04	1.30E+05	1.30E+05
K_d high	Po-210	$L \cdot kg^{-1}$	3.80E+05	-	-	-
K_p low	Pb-210	$L \cdot kg^{-1}$	5.40E+05	-	2.87E+05	2.87E+05
K_p high	Pb-210	$L \cdot kg^{-1}$	5.60E+06	2.81E+07	-	-
K_p low	Po-210	$L \cdot kg^{-1}$	6.80E+05	-	-	-
K_p high	Po-210	$L \cdot kg^{-1}$	6.10E+06	1.03E+07	4.94E+06	6.06E+06
C_W/C_{OW}	Ra-226	unitless	1.00E+00	1.10E+00	1.00E+00	1.00E+00
C_S/C_{OS}	Ra-226	unitless	1.00E+00	7.96E+00	1.00E+00	1.00E+00
C_W/C_{OW}	Pb-210	unitless	1.00E+00	2.32E+00	1.00E+00	1.00E+00
C_S/C_{OS}	Pb-210	unitless	1.00E+00	1.81E+01	1.00E+00	1.00E+00
C_W/C_{OW}	Po-210	unitless	1.00E+00	8.72E-01	2.26E-01	1.00E+00
C_S/C_{OS}	Po-210	unitless	1.00E+00	3.12E+01	1.00E+00	1.00E+00

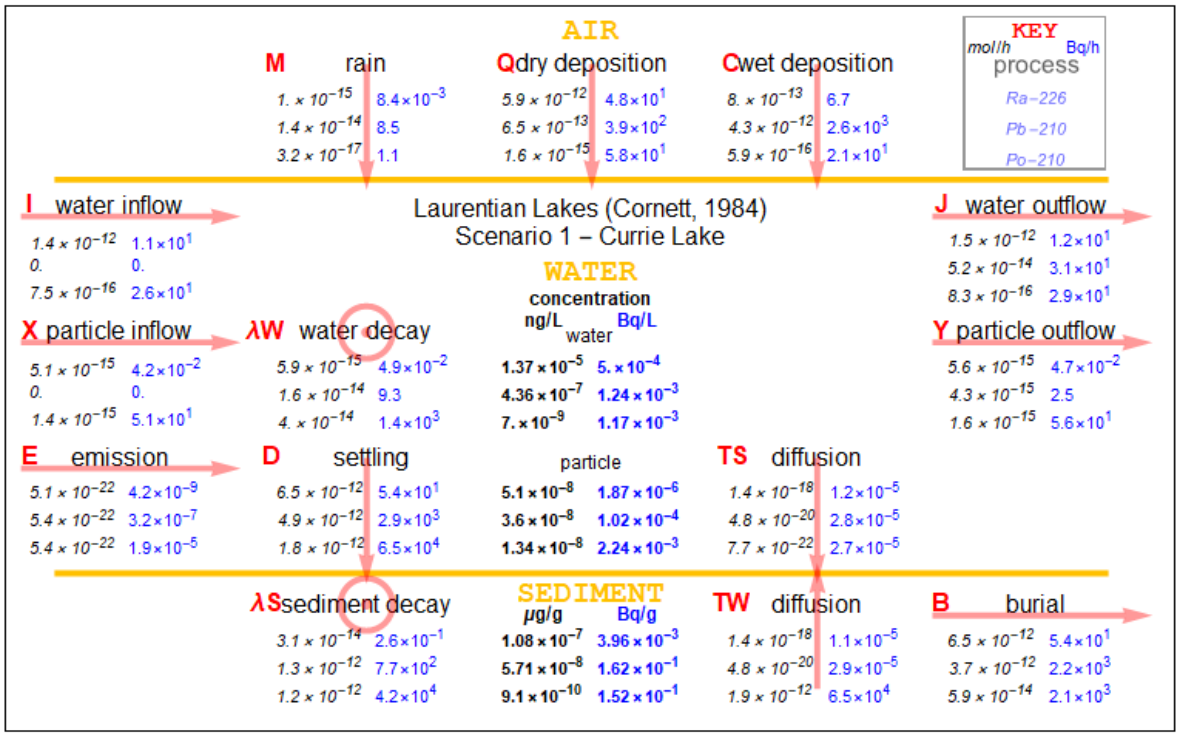

Figure I-1. Laurentian Currie Lake case 1

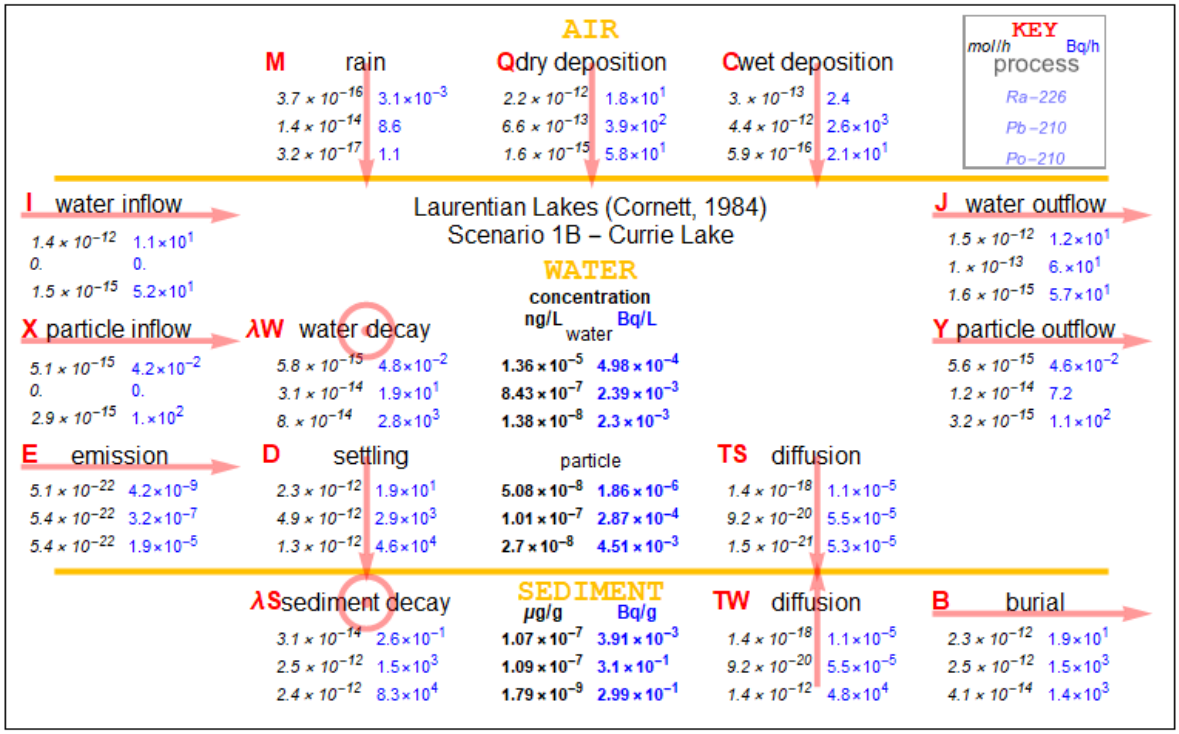

Figure I-2. Laurentian Currie Lake case 1B

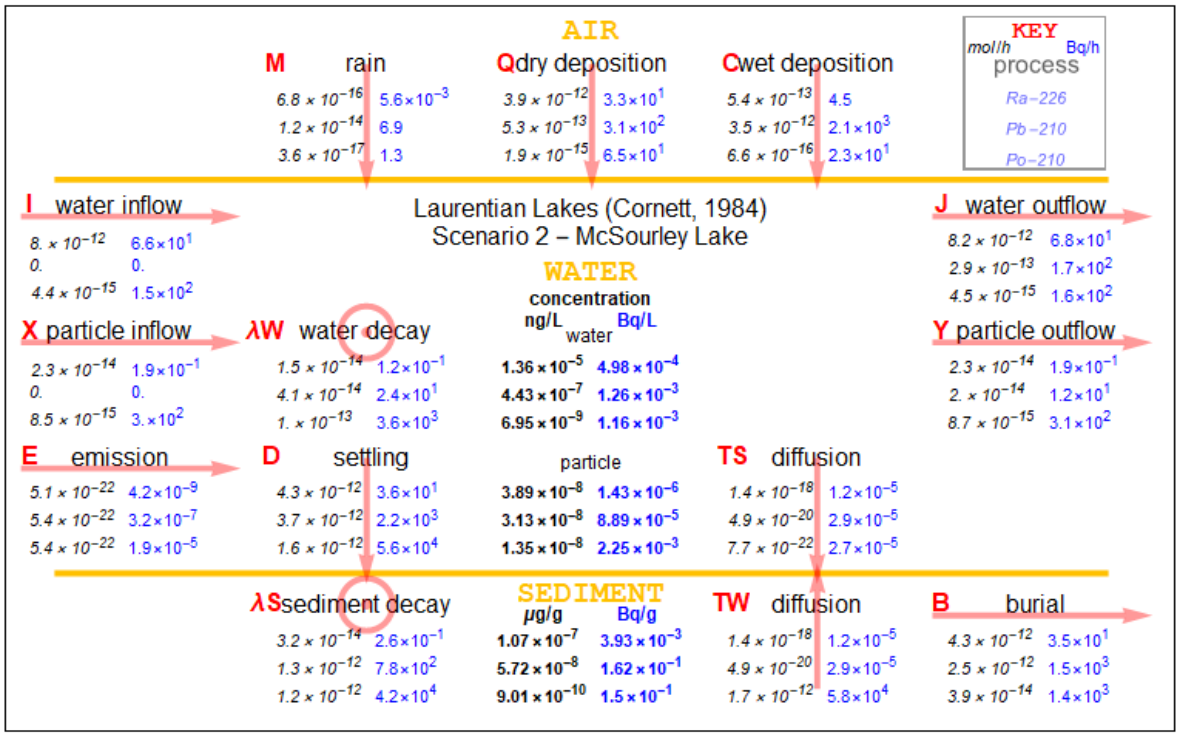

Figure I-3. Laurentian McSourley Lake case 2

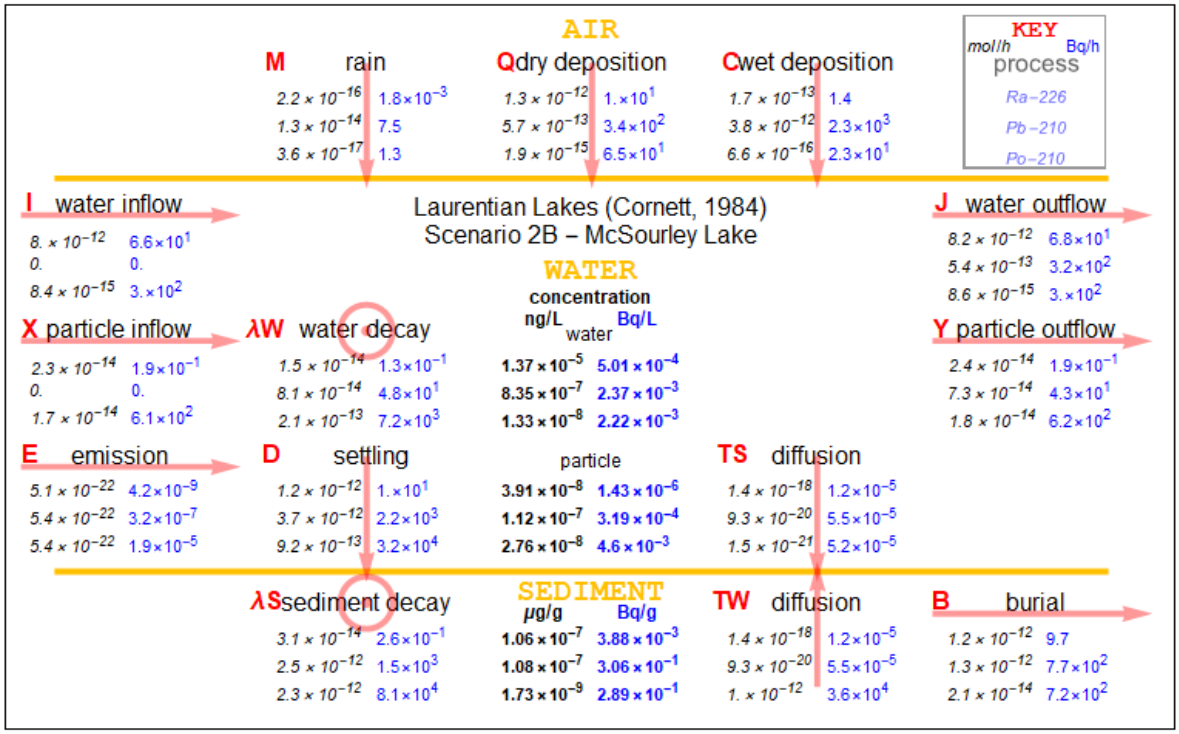

Figure I-4. Laurentian McSourley Lake case 2B

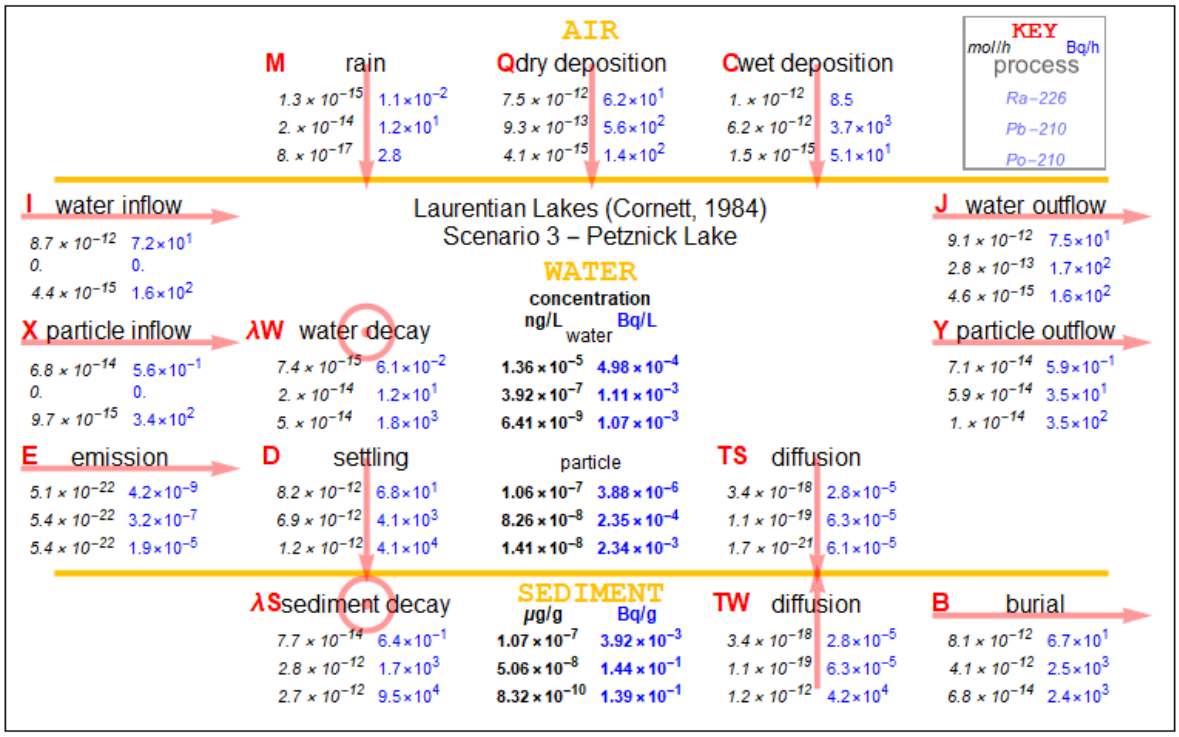

Figure I-5. Laurentian Petznick Lake case 3

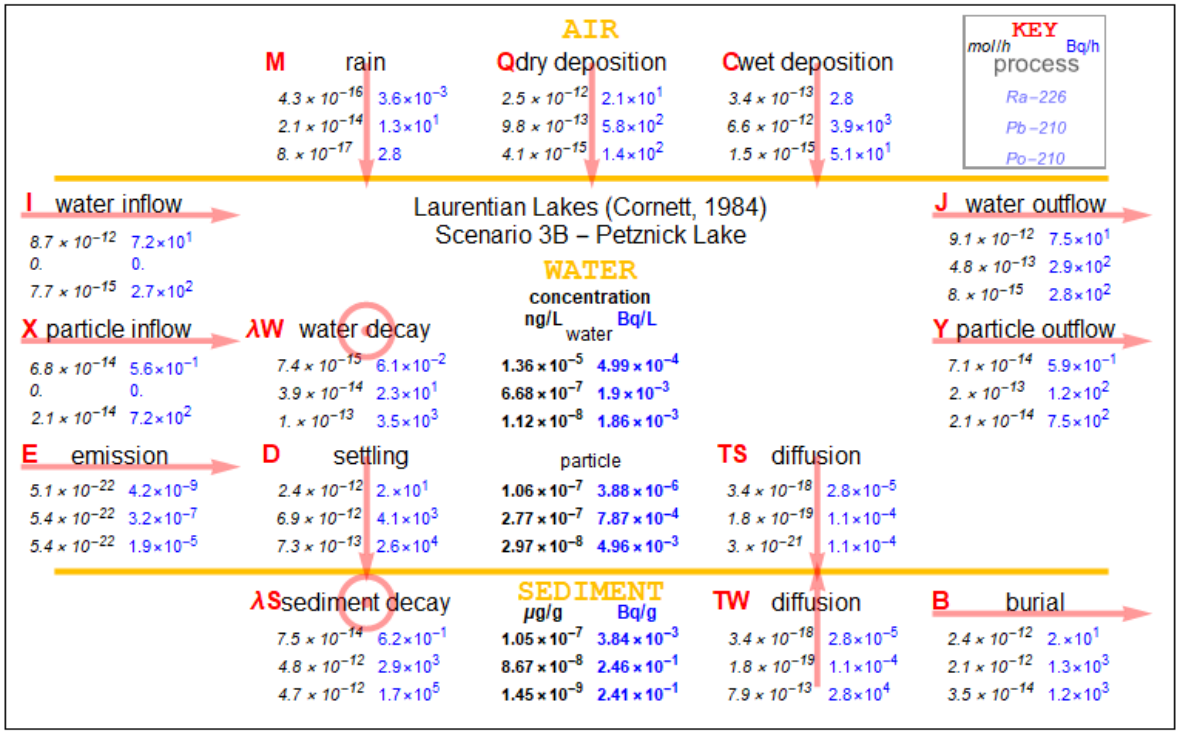

Figure I-6. Laurentian Petznick Lake case 3B

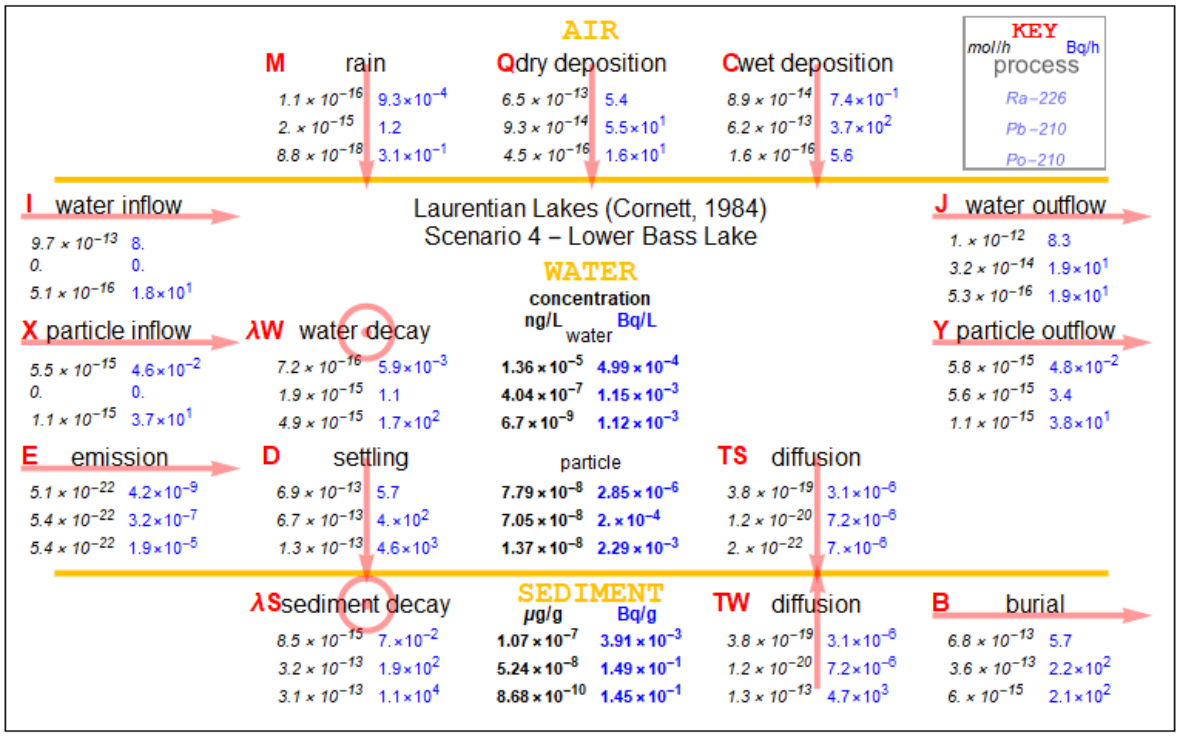

Figure I-7. Laurentian Lower Bass Lake case 4

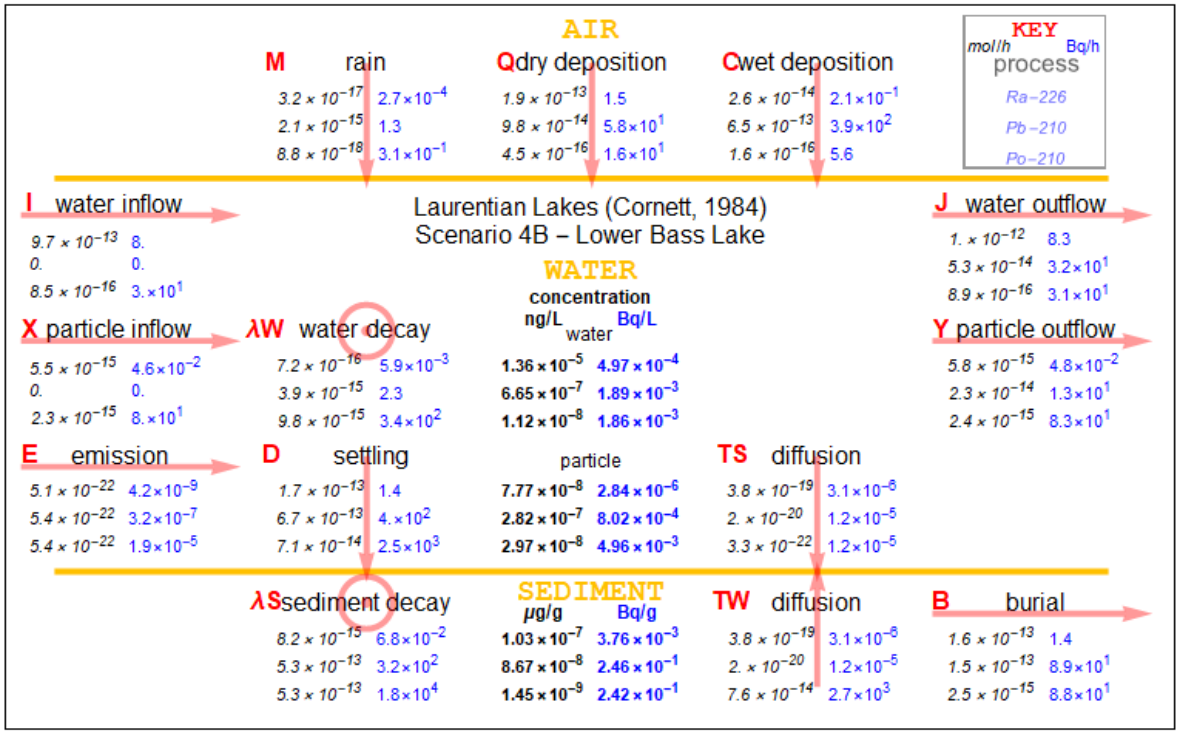

Figure I-8. Laurentian Lower Bass Lake case 4B

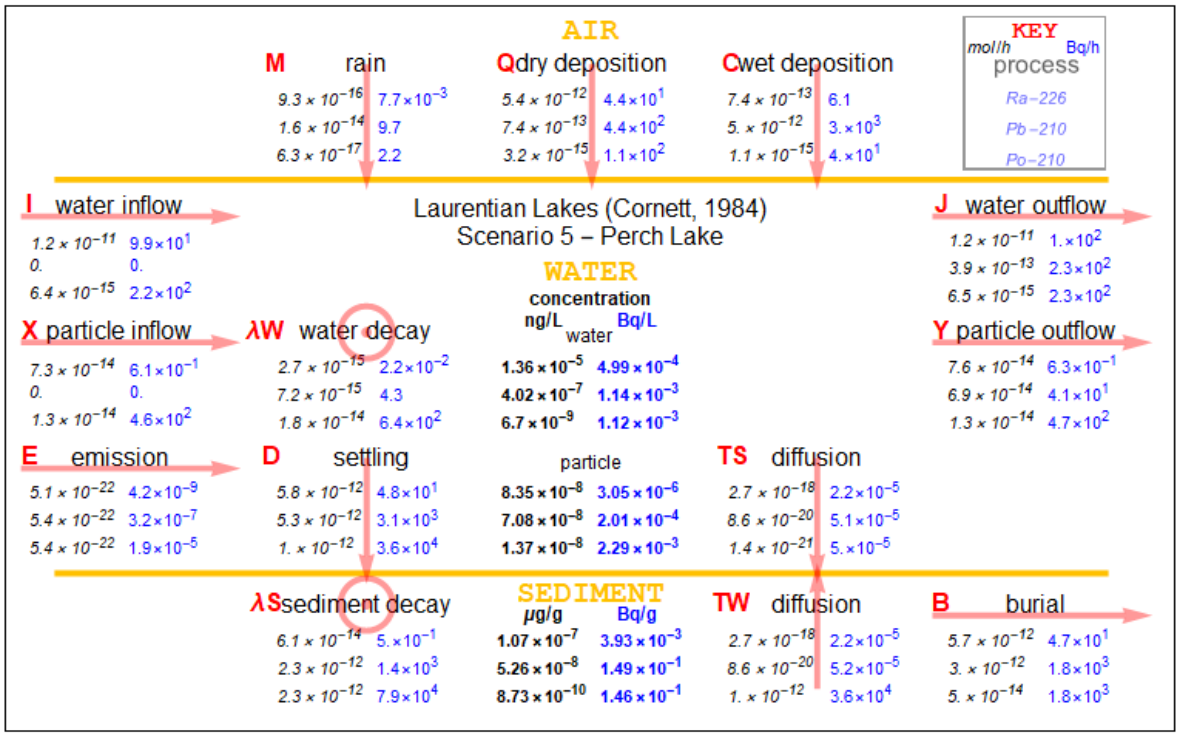

Figure I-9. Laurentian Perch Lake case 5

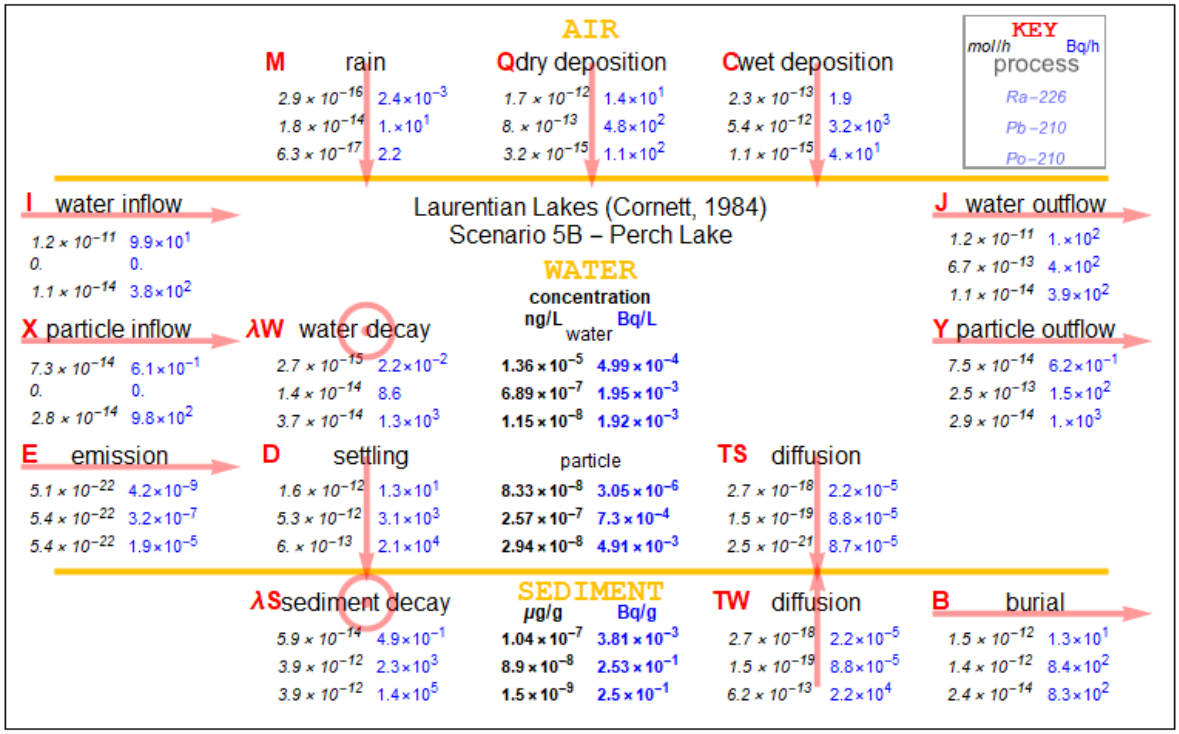

Figure I-10. Laurentian Perch Lake case 5B

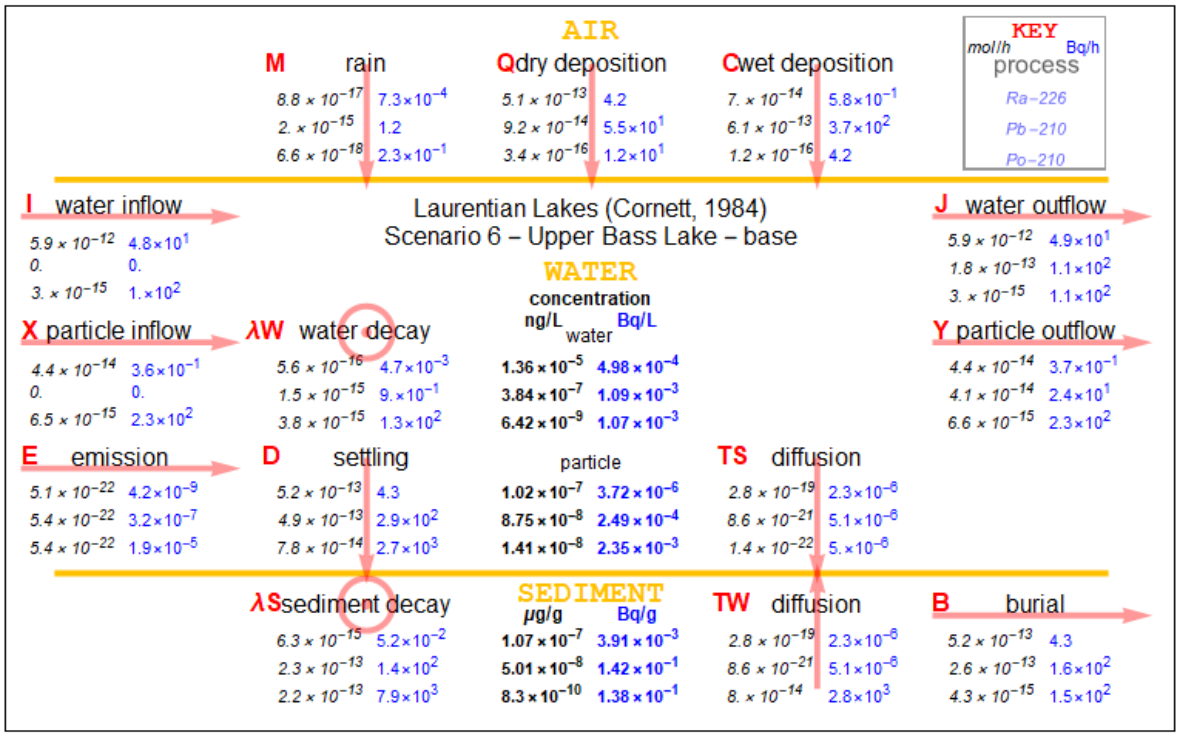

Figure I-11. Laurentian Upper Bass Lake case 6

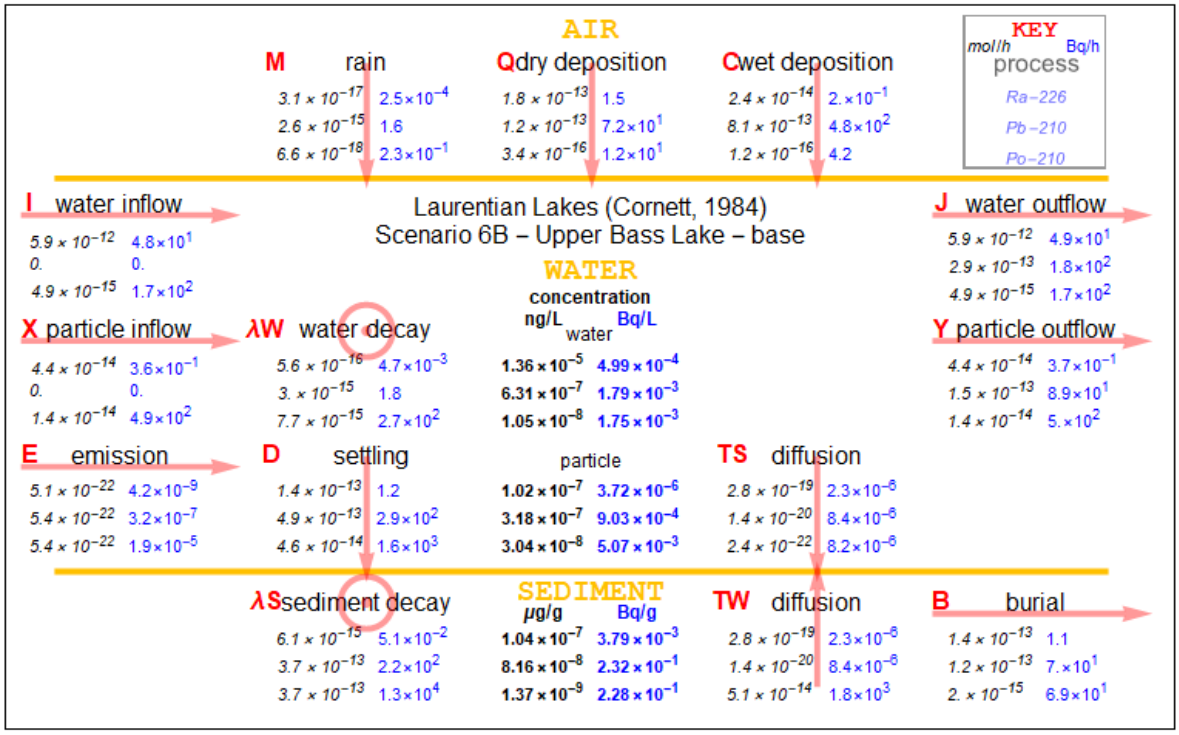

Figure I-12. Laurentian Upper Bass Lake case 6B

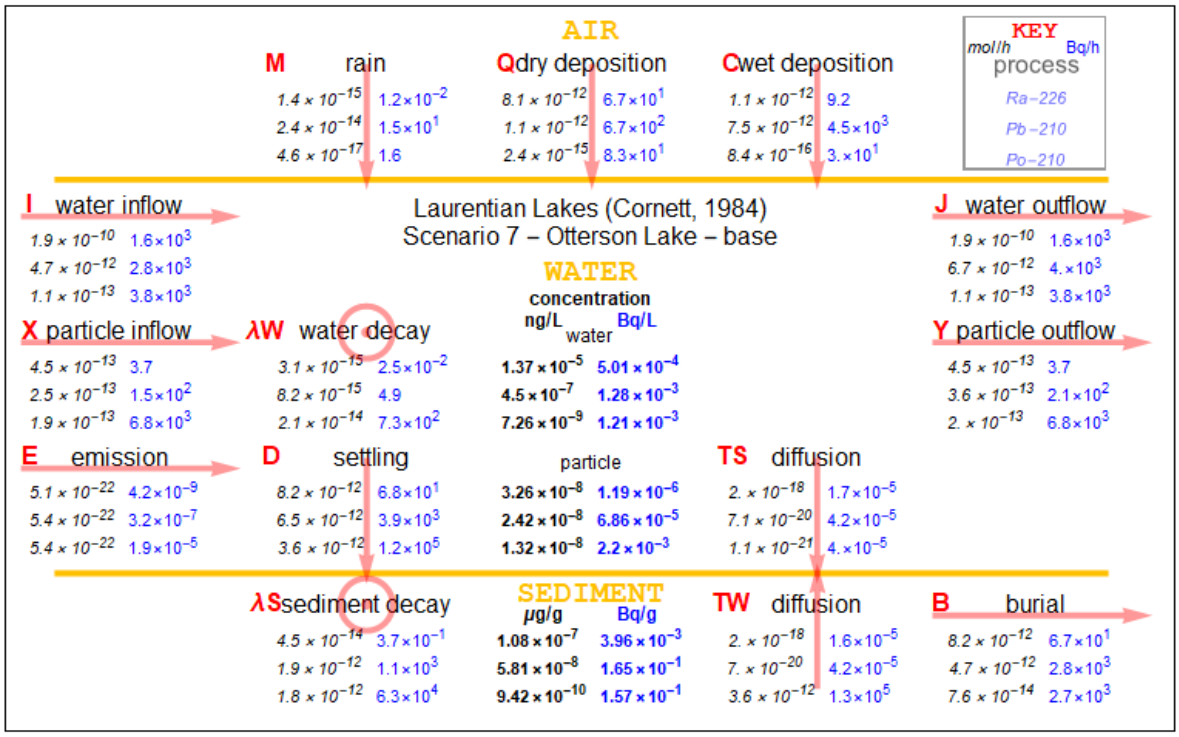

Figure I-13. Laurentian Otterson Lake case 7

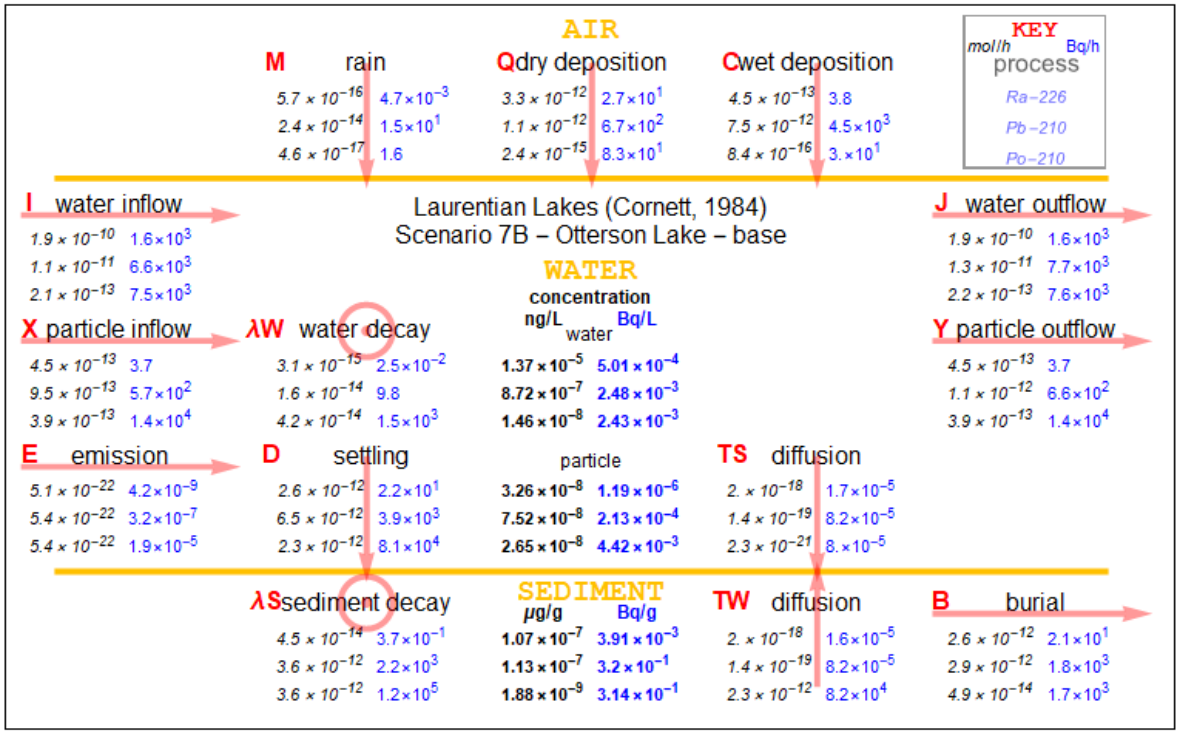

Figure I-14. Laurentian Otterson Lake case 7B

J Kiggavik

J.1 INPUT

Table J-1 lists properties for the Judge Sissons Lake, Nunavut.

Table J-1. Judge Sissons Lake properties

Property	Symbol	Value	Units
Depth of lake	d_{LA}	4.6[189]	m
Depth of sediment	d_{SE}	0.025[190]	m
Area of lake	A_{LA}	9.55E+07[189]	m^2
Area of sediment	A_{SE}	9.55E+07[189]	m^2
Density of SPM	ρ_w	2.4[191]	$g \cdot cm^{-3}$
Density of aerosol	ρ_A	1.5[191]	$g \cdot cm^{-3}$
Density of sediment	ρ_S	2.4[191]	$g \cdot cm^{-3}$
Concentration of water particulate	C_{PL}	0.35[192]	$mg \cdot L^{-1}$
Concentration of inflow particulate	C_{PI}	1.33[192]	$mg \cdot L^{-1}$
Concentration of aerosol	C_{PA}	15[193]	$\mu g \cdot m^{-3}$
Rate of rain	v_{RA}	0.273[194]	$m \cdot a^{-1}$
Volumetric rate of water inflow	Q_I	1.52E+04[195]	$m^3 \cdot h^{-1}$
Volumetric rate of water outflow	Q_J	1.82E+04[196]	$m^3 \cdot h^{-1}$
Volume fraction of sediment particles	f_{SV}	0.035[197]	-
Flux of particles, settling	F_S	0.042[198]	$g \cdot m^{-2} \cdot d^{-1}$
Flux of particles, resuspension	F_R	0	$g \cdot m^{-2} \cdot d^{-1}$
Flux of particles, burial	F_B	F_S[199]	$g \cdot m^{-2} \cdot d^{-1}$

Table J-2 lists the nuclide properties assumed for Kiggavik. Other default values are listed in Table F-2.

[189] From *Table 5.3-1* **(AREVA, 2011B)**
[190] From *section 5.4.4* depth / mass accumulation basis range 2-2.5 cm **(AREVA, 2011B)**
[191] From *Table 2* **(MACKAY, 1989)**
[192] From section J.2.2
[193] From *p.6755* **(TALBOT, 1983)**
[194] From *Baker Lake Stn* 1981-2010 http://climate.weather.gc.ca/climate_normals/
[195] From *section 5.1* Aniguq River unit area runoff 0.0062 $m^3 \cdot s^{-1} \cdot km^{-1}$, *Table 5.3-1* basin area 704.6 km^2 **(AREVA, 2011B)**
[196] From inlow[195] + precipitation[194], *Table 5.3-1* 9550 ha surface area **(AREVA, 2011B)**
[197] From *Table 5.4-2* average of depth accumulation at 11 m of 0.11 $mm \cdot a^{-1}$ & at 13 m of 0.26 $mm \cdot a^{-1}$ **(AREVA, 2011B)**, settling flux[198], & sediment particle density[191]
[198] From *Table 5.4-3* average of settling flux at 11 m of 11 $g \cdot m^{-2} \cdot a^{-1}$ & at 13 m of 20 $g \cdot m^{-2} \cdot a^{-1}$ **(AREVA, 2011B)**
[199] From F_R and particle balance (A.27); initial value, then fit according to section J.3

Table J-2. Kiggavik nuclide properties

Property			Ra-226	Pb-210	Po-210
Rain scavenging ratio	W_g	-	7.94E+05[200]	2.62E+05[201]	1.82E+04[202]
Deposition velocity	v_{AD}	$m \cdot h^{-1}$	568[203]	15.7[201]	5.01[203]
MTC water-sediment[204]	k_{TS}	$m \cdot h^{-1}$	fit	fit	fit
MTC sediment-water[204]	k_{TW}	$m \cdot h^{-1}$	fit	fit	fit

J.2 OPTIMIZATION

J.2.1 ATMOSPHERIC DEPOSITION

Pb-210 deposition data for many sites were compiled over decades of latitude. The 60-70°N latitude range is 3.7 ± 3.5 mBq $cm^{-2} \cdot a^{-1}$ **(BASKARAN, 2011)**, which corresponds to the Kiggavik site at about 64°N latitude. Following the method of section I.2 and the atmospheric concentration from Table J-9, the Pb-210 values were for the scavenging ratio:

$$W_g = 2.62E+05$$

and for the deposition velocity:

$$v_{AD} = 15.7 \ m \cdot h^{-1}$$

J.2.2 NUCLIDE CONCENTRATION ESTIMATES

A significant number of Kiggavik study area measurements of SPM and nuclide water were below detection limit, as well as the Pb-210 measurements of sediment concentration. The SPM, water concentration and sediment concentration were assumed to be lognormally distributed. Means of these distributions were estimated using the *elnormCensored* function with the *Quantile-Quantile regression* method from the *EnvStats* package for *R* **(MILLARD, 2013)**.

Table J-3 and Table J-4 contain tallies of the SPM measurements of stream inflow to Judge Sissons Lake and of Judge Sissons Lake itself (from *Attachment X.II*) **(AREVA, 2011c)**. There are only five inflow SPM measurements, two of which are below detection limit. Only three of the lake SPM measurements are above detection limit. The selected *R* method gave a mean inflow SPM concentration of 1.33 $mg \cdot L^{-1}$ and a lake SPM concentration of 0.35 $mg \cdot L^{-1}$.

[200] From section F.2.1.1 as Crystal Lake (Table F-2) and section G.2.1.1 as Bickford Pond (Table G-2)
[201] From section J.2.1
[202] From section G.2.1.2 as Bickford Pond (Table G-2)
[203] From section G.2.2 as Bickford Pond (Table G-2)
[204] MTC sediment-water k_{TW} was set for each nuclide

Table J-3. Judge Sissons Lake inflow stream SPM measurement tallies

value ($mg \cdot L^{-1}$)	<2	1	2
tally	2	1	2

Table J-4. Judge Sissons Lake SPM measurement tallies

value ($mg \cdot L^{-1}$)	<2	<1	1	1.1	2
tally	3	16	1	1	1

Table J-5 shows water concentration measurements for eight samples from locations of streams inflow to Judge Sissons Lake, and Table J-6 tallies of measurements from the balance of Kiggavik site sample locations (from *Attachment X.II*) **(AREVA, 2011c)**. Table J-7 shows mean nuclide inflow and lake water concentrations determined by the selected *R* method for these sets of the data.

Table J-5. Judge Sissons inflow stream water concentration measurements

	Ra-226	Pb-210	Po-210
DL ($Bq \cdot L^{-1}$)	0.005	0.02	0.005
WLISS-WQ001-P09	<0.005	<0.02	<0.005
WIJSS-WQ002-F09	0.007	<0.02	<0.005
WIJSS-001-P08	<0.005	<0.02	0.02
LWJSS-001-P08	<0.005	<0.02	0.008
CFJSS-001-P08	<0.005	<0.02	0.01
WIJSS-002-F08	<0.005	<0.02	<0.005
LWJSS-002-F08	<0.005	<0.02	<0.005
CFJSS-002-F08	0.005	<0.02	<0.005

Table J-6. Kiggavik study area water concentrations

tally	Ra-226	Pb-210	Po-210
DL ($Bq \cdot L^{-1}$)	0.005	0.02	0.005
<0.005	92		80
0.005	6		2
0.006	9		9
0.007	6		8
0.008	2		7
0.009	4		3
0.010	3		8
0.011	0	118	0
0.012	0		0
0.013	0		0
0.014	0		0
0.015	0		0
0.016	0		0
0.017	0		0
0.018	0		0
0.019	0		0
0.020	0	1	3
0.021	0	0	0
0.022	0	0	0
0.023	0	0	0
0.024	0	0	0
0.025	0	0	0
0.026	0	0	0
0.027	0	0	0
0.028	0	0	0
0.029	0	0	0
0.030	0	3	2
total >DL	30	4	42

Table J-7. Judge Sissons Lake water concentrations

$Bq \cdot L^{-1}$	Ra-226	Pb-210	Po-210
inflow	0.0031	0.0177	0.0048
lake	0.0049	0.0152	0.0059

Table J-8 shows the Kiggavik study area sediment samples concentration measurements. The *R EnvStats gofTest* function with the *Shapiro-Wilk* method showed that the data could be considered lognormally distributed. The *elnormCensored* function gave estimated mean sediment concentrations for Ra-226 of 0.032 $Bq \cdot g^{-1}$ and for Pb-210 of 0.050 $Bq \cdot g^{-1}$. Figure J-1 shows the *R EnvStats*

stripChart function charts of the sorted data giving a normal sample mean for Po-210 of 0.090 $Bq \cdot g^{-1}$, and also showing that the estimated mean concentration of Ra-226 in sediment samples from Judge Sissons Lake is 0.001-0.017 $Bq \cdot g^{-1}$ lower (95% confidence interval) than from the balance of Kiggavik site waterways **(MILLARD, 2013)**.

Table J-8. Judge Sissons sediment concentration measurements

$Bq \cdot g^{-1}$	Ra-226	Pb-210	Po-210
DL	0.01	0.02/0.04	0.005
JSL-001-F08	0.04	0.22	0.18
JSL-002-F08	0.03	0.09	0.08
JSL-006-F08	0.04	0.03	0.05
JSL-007-F08	0.03	<0.02	0.12
JSL-008-F08	0.03	0.09	0.12
JSL-SD001A-F09	0.05	0.06	0.11
JSL-SD001B-F09	0.04	0.09	0.19
SJL-SD001C-F09	0.04	0.07	0.09
SJL-SD001E-F09	0.07	0.11	0.08
SJL-SD001F-F09	0.04	0.11	0.08
JSL-SD002A-F09	0.03	0.09	0.12
JSL-SD002B-F09	0.03	0.09	0.11
JSL-SD002C-F09	0.05	0.18	0.28
JSL-SD002D-F09	0.04	0.19	0.15
JSL-SD002E-F09	0.03	0.06	0.08
JSL-SD006A-F09	0.03	<0.04	0.04
JSL-SD006B-F09	0.03	<0.04	0.06
JSL-SD006C-F09	<0.01	<0.04	0.05
JSL-SD006D-F09	0.02	0.07	0.11
JSL-SD006E-F09	0.03	<0.04	0.06
JSL-SD007A-F09	0.02	<0.04	0.04
JSL-SD007B-F09	0.03	<0.04	0.02
JSL-SD007C-F09	0.03	<0.04	0.09
JSL-SD007D-F09	0.03	<0.04	0.02
JSL-SD007E-F09	0.02	<0.04	0.04
JSL-SD008A-F09	0.03	<0.04	0.06
JSL-SD008B-F09	0.02	<0.04	0.07
JSL-SD008C-F09	0.02	<0.04	0.06
JSL-SD008D-F09	0.04	<0.04	0.07
JSL-SD008E-F09	0.04	<0.04	0.06

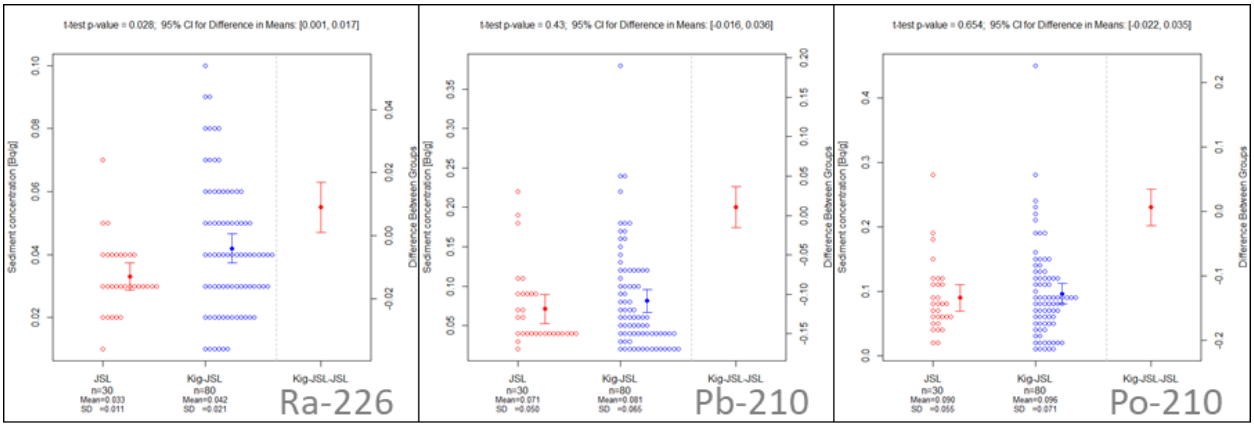

Figure J-1. Kiggavik and Judge Sissons Lake sediment concentration data

Table J-9 lists aerosol, inflow, rain, total water, and sediment concentrations.

Table J-9. Judge Sissons phase concentrations

Phase			Ra-226	Pb-210	Po-210
Air, aerosol[205]	C_{OA}	µg·m^{-3}	7.02E-11[206]	5.88E-11[206]	2.16E-13
Water inflow[207]	C_{OI}	ng·L^{-1}	8.34E-05	6.24E-06	2.86E-08
Rain	C_{OM}	µg·m^{-3}	1.59E-05[208]	2.64E-05[209]	1.86E-07[209]
Water	C_{OW}	ng·L^{-1}	fit	fit	fit
Water particles	C_{OP}	ng·L^{-1}	C_{OWP} - C_{OW}	C_{OWP} - C_{OW}	C_{OWP} - C_{OW}
Total water[210]	C_{OWP}	ng·L^{-1}	1.33E-04	5.35E-06	3.53E-08
Sediment solids[211]	C_{OS}	µg·g^{-1}	8.63E-07	1.76E-08	5.39E-10

The Table I-7 distribution coefficient limits were assumed for the Judge Sissons Lake.

[205] From *Table 5.1-1*: 2.57E-06, 1.67E-04, 3.60E-05 Bq·m^{-3} **(AREVA, 2011A)**
[206] Initial value, then fit according to section J.3
[207] From *Attachment X.II* tables for inflow to Judge Sissons Lake **(AREVA, 2011C)**
[208] From *Table 2* 0.035±0.020 dpm·L^{-1} (n=17) **(MOORE, 1976)**
[209] From *Table 1* Pb-210: 0.075 Bq·L^{-1}, Po-210: 0.031 Bq·L^{-1} **(THOMAS, 2000)**
[210] From *Attachment X.II* tables for Judge Sissons Lake **(AREVA, 2011C)**
[211] From *Attachment X.III* tables for Judge Sissons Lake **(AREVA, 2011C)**

J.3 PROCEDURE

The parameters adjusted to optimize the scenario were:

- C_{OW} observed water concentration of nuclides Table J-9
- C_{OA} observed concentration of aerosol nuclides Table J-9
- E_W emission to water
- k_{TW} diffusion coefficient for sediment-water Table J-2

The observed dissolved water concentrations C_{OW} of Ra-226, Pb-210 and Po-210 (C_{OW1}, C_{OW2} and C_{OW3}) were adjusted initially to set each sediment distribution coefficient K_d within the Table I-7 limits. Maintaining the sediment distribution coefficients Pb-210 K_{d2} and Po-210 K_{d3} at the minimum range values resulted in the SPM distribution coefficients of Pb-210 K_{p2} and of Po-210 K_{p3} being above the Table I-7 upper limits.

Table J-10 details the optimization process:

- Step 1: Ra-226 $C_{S1}/C_{OS1} = 1$ and $C_{W1}/C_{OW1} = 1$ by adjusting:
    - C_{OA1} Ra-226 observed concentration on aerosols Table J-9
    - k_{TW1} Ra-226 diffusion coefficient for sediment-water Table J-2
- Step 2: Pb-210 $C_{S2}/C_{OS2} = 1$ and $C_{W2}/C_{OW2} = 1$ by adjusting:
    - C_{OA2} Pb-210 observed concentration on aerosols Table J-9
    - k_{TW2} Pb-210 diffusion coefficient for sediment-water Table J-2
- Step 3: Po-210 $C_{S3}/C_{OS3} = 1$ and $C_{W3}/C_{OW3} = 1$ by adjusting:
    - k_{TW3} Po-210 diffusion coefficient for sediment-water Table J-2
    - E_{W3} Po-210 emission to water

Table J-10. Kiggavik Judge Sissons Lake optimization

par.	nuclide	units	target	initial	step 1	step 2	step 3
C_{OA}	Ra-226	$\mu g \cdot m^{-3}$	7.02E-11	7.02E-11	2.31E-11	2.31E-11	2.31E-11
C_{OA}	Pb-210	$\mu g \cdot m^{-3}$	5.88E-11	5.88E-11	5.88E-11	1.48E-11	1.48E-11
k_{TW}	Ra-226	$m \cdot h^{-1}$	NA	1.00E-10	1.07E-03	1.07E-03	1.07E-03
k_{TW}	Pb-210	$m \cdot h^{-1}$	NA	1.00E-10	1.00E-10	9.63E-02	9.63E-02
k_{TW}	Po-210	$m \cdot h^{-1}$	NA	1.00E-10	1.00E-10	1.00E-10	1.21E-02
E_W	Po-210	$kg \cdot a^{-1}$	NA	1.00E-18	1.00E-18	1.00E-18	4.39E-08
C_{OW}	Ra-226	$ng \cdot L^{-1}$	NA	1.00E-05	1.09E-04	1.09E-04	1.09E-04
C_{OW}	Pb-210	$ng \cdot L^{-1}$	NA	1.00E-06	2.63E-07	2.63E-07	2.63E-07
C_{OW}	Po-210	$ng \cdot L^{-1}$	NA	1.00E-08	4.16E-09	4.16E-09	4.16E-09
K_d low	Ra-226	$L \cdot kg^{-1}$	3.00E+02	-	-	-	-
K_d high	Ra-226	$L \cdot kg^{-1}$	7.90E+03	8.63E-04	7.92E+03	7.92E+03	7.92E+03
K_d low	Pb-210	$L \cdot kg^{-1}$	6.70E+04	1.76E+04	6.70E+04	6.70E+04	6.70E+04
K_d high	Pb-210	$L \cdot kg^{-1}$	1.30E+05	-	-	-	-
K_d low	Po-210	$L \cdot kg^{-1}$	1.30E+05	5.39E+04	1.30E+05	1.30E+05	1.30E+05
K_d high	Po-210	$L \cdot kg^{-1}$	3.80E+05	-	-	-	-
K_p low	Pb-210	$L \cdot kg^{-1}$	5.40E+05	-	-	-	-
K_p high	Pb-210	$L \cdot kg^{-1}$	5.60E+06	1.24E+07	5.52E+07	5.52E+07	5.52E+07
K_p low	Po-210	$L \cdot kg^{-1}$	6.80E+05	-	-	-	-
K_p high	Po-210	$L \cdot kg^{-1}$	6.10E+06	7.22E+06	2.14E+07	2.14E+07	2.14E+07
C_W/C_{OW}	Ra-226	-	1.00E+00	8.61E-02	1.00E+00	1.00E+00	1.00E+00
C_S/C_{OS}	Ra-226	-	1.00E+00	3.30E+01	1.00E+00	1.00E+00	1.00E+00
C_W/C_{OW}	Pb-210	-	1.00E+00	7.32E-02	6.40E-02	1.00E+00	1.00E+00
C_S/C_{OS}	Pb-210	-	1.00E+00	2.66E+01	1.05E+01	1.00E+00	1.00E+00
C_W/C_{OW}	Po-210	-	1.00E+00	7.30E-02	5.80E-02	4.78E-01	1.00E+00
C_S/C_{OS}	Po-210	-	1.00E+00	1.48E+01	5.85E+00	8.69E-01	1.00E+00

K Laboratory Calculations

K.1 MASS SPECTROMETRY

K.1.1 QUANTIFICATION LIMIT

The limit of detection concentration C_L was calculated from the standard deviation of blanks σ_0, confidence level t and the sensitivity or slope of the calibration plot m **(WANG, 2011)**:

$$C_L = \frac{t \cdot \sigma_0}{m} \tag{K-1}$$

The International Union of Pure and Applied Chemistry has recommended 3σ detection limits ($t = 3$) corresponding to a 98% confidence level. The limit of quantification concentration C_Q is 10 standard deviations of the blank **(THOMSEN, 2003)**:

$$C_Q = 3.3 C_{L(t=3)} \tag{K-2}$$

Table K-1 shows the Bruker Aurora M90 **(WANG, 2011)** Inductively-Coupled Plasma Source Mass Spectrometry (ICP-MS) **(PORCELLI, 2011)** calibration counts on August 12, 2016 of sub-samples from the original filtered samples diluted 2:1 with 2% HNO_3 solution and spiked with two separate standard solutions that included the species shown. Counts of Mg-24 and Fe-56 were not distinguished from background and the calibration curve of Th-232 was poorly resolved.

Table K-1. Aurora M90 ICP-MS calibration counts

std. (ppb)	Counts								
	Mg-24	Mn-55	Fe-56	Sr-88	Cs-133	Ba-137	Pb-208	Th-232	U-238
0	6528906	31870	5393542	6209	1051	844	1775	833	144
2.5	6842500	142213	5746376	128348	117083	15478	55296	127779	79562
0	6376309	31098	5252132	6794	1022	996	1775	600	154
2.5	6392376	136986	5432583	126070	112623	15748	53441	99292	77837
0	6535653	31903	5368667	7124	1014	1089	1700	478	143
2.5	6580318	136306	5568295	123609	113297	15975	54149	66326	78463
0	6157100	30371	5157887	6683	953	852	1670	515	142
2.5	6377339	133227	5448733	124292	111200	14951	51644	48636	74895
0	6438911	31688	5406294	6879	17897	1059	1729	522	157
2.5	6512555	132822	5550103	124246	111510	14963	52607	43176	74333
5	6543862	253155	5621115	256026	239332	32395	109586	140809	159032
10	6707744	498066	5918987	529197	500051	66679	227701	126487	332323

Table K-2 shows the diluted concentrations of the remaining species prepared from the stock solutions. Table K-3 gives the regression slopes m of the Table K-1 counts paired with the Table K-2 standard concentrations, the standard deviation of

the Table K-1 blank counts σ_0, the limit of detection concentration C_L from Equation K-1, the dilution-corrected C_L, and the limit of quantification from Equation K-2.

Table K-2. ICP-MS standard concentrations

std. (ppb)	Mn-55	Sr-88	Cs-133	Ba-137	Pb-208	U-238
0	0	0	0	0	0	0
2.5	2.522	2.522	2.355	2.522	2.522	2.438
5	5.170	5.170	4.827	5.170	5.170	4.998
10	10.234	10.234	9.555	10.234	10.234	9.894

Table K-3. ICP-MS quantification limit parameters

species	m (#/ppb)	σ_0 (#)	C_L (ppb)	undiluted C_L (ppb)	C_Q (ppb)
Mn-55	45099	116	0.0077	0.0154	0.0509
Sr-88	50529	474	0.0281	0.0563	0.1857
Cs-133	51257	9737	0.5699	1.1398	3.7612
Ba-137	6353	133	0.0630	0.1260	0.4158
Pb-208	21859	38	0.0051	0.0103	0.0340
U-238	33258	8	0.0007	0.0014	0.0046

K.1.2 CALIBRATION

The first two standards were designated for calibration by the Aurora M90 sample processing software, marking counts at 0 and 2.5 ppb for each species. These counts are indicated in the first two rows of Table K-1. In-115 is injected into the sample stream to indicated stability of the argon carrier gas. Figure K-1 shows the In-115 counts corresponding to the entire sampling sequence of the run.

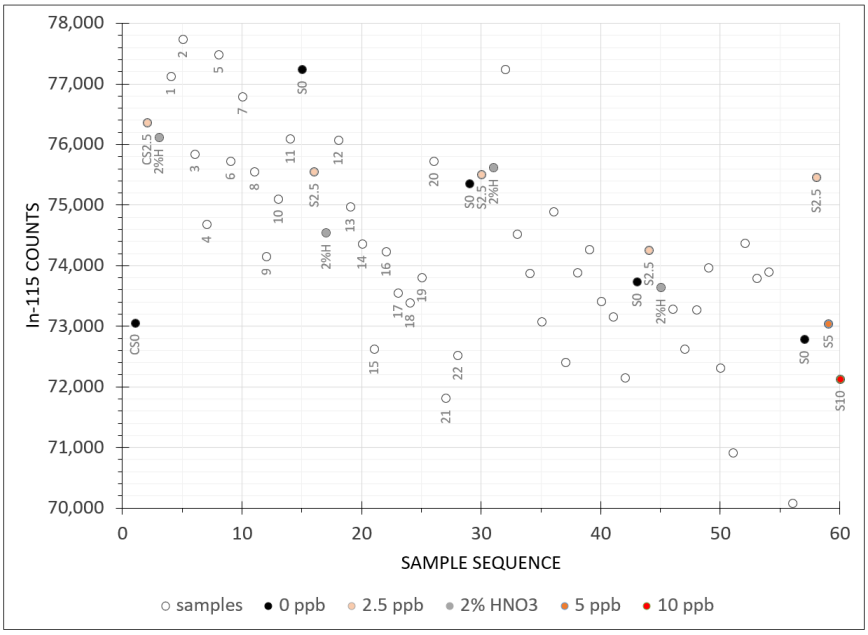

Figure K-1. ICP-MS counts of In-115

The result of a regression of the In-115 counts with the sample sequence number $\mathfrak{S}$ was $\mathfrak{N}_{S.In115}$:

$$\mathfrak{N}'_{S.In115} = (76250 \pm 360) - (65.8 \pm 10.3)\mathfrak{S} \qquad \text{(K-3)}$$

The trend in In-115 suggests a weakening in the carrier signal over the duration of the sample run, although the magnitude of the trend was small relative to the count uncertainty (r^2 = 0.41). The trend was assumed to apply to each of the measurement species over the sample sequence. Among the resolved species, as indicated by Table K-1, the counts of the 2.5 ppb standard samples was at most twice the counts of the In-115 samples (Mn-55, Sr-88 and Cs-133). The magnitude of uncertainty in the number of counts of In-115 relative to each of these species would be $\sqrt{2}$ according to a Poisson distribution **(MOOD, 1973)**. The extra uncertainty introduced by correcting for signal bias using the In-115 count trend was ignored. The resulting underestimate in concentration uncertainty was considered small relative to other unaccounted sources of measurement error.

K.1.3 CONCENTRATION

Table K-4 contains the instrument counts of each species and sample.

Table K-4. Aurora M90 ICP-MS species counts

Sequence	Sample	Counts					
		Mn-55	Sr-88	Cs-133	Ba-137	Pb-208	U-238
4	1	579221	634213	1249	22564	2447	482
5	2	502510	629704	1246	21714	2269	536
6	3	861202	6322946	2167	94700	4183	11375
7	4	739547	6054724	1890	85068	3582	10732
8	5	1006754	3200355	1074	330842	1568	2407
9	6	991503	3148160	1051	325872	2467	2397
10	7	496357	804328	1302	45441	1712	467
11	8	496201	780931	1318	42132	1484	484
12	9	1805827	1855549	1342	127785	2043	2758
13	10	1308058	1820260	1272	122797	2151	2751
14	11	587877	1373842	1521	88379	2327	4002
18	12	593902	1369765	1403	86619	1730	4075
19	13	218005	645587	1043	35008	1943	238
20	14	228253	646026	1077	35112	1877	249
21	15	819546	944566	1072	37068	2871	451
22	16	801639	936510	1027	35854	2885	439
23	17	506087	21690618	1131	134699	1736	7590
24	18	248047	22146107	1136	133849	1290	7866
25	19	2593123	10858510	1193	141668	4385	1003
26	20	1916537	10808318	1137	133637	2288	905
27	21	10864122	7278073	1426	400451	5126	17999
28	22	10597517	7038578	1391	387509	4263	18578

For each species *X* and sample sequence *S*, the Table K-4 instrument counts $\mathfrak{N}_{\mathfrak{S}.X}$ were corrected by scaling by the ratio of the Equation K-3 regression to the In-115 counts $\mathfrak{N}_{\mathfrak{S}.In115}$:

$$\mathfrak{N}'_{\mathfrak{S}.X} = \frac{\mathfrak{N}'_{\mathfrak{S}.In115}}{\mathfrak{N}_{\mathfrak{S}.In115}} \mathfrak{N}_{\mathfrak{S}.X} \qquad \text{(K-4)}$$

Table K-5 shows the counts for the standard samples corrected by the Equation K-3 In-115 regression for signal trend according to Equation K-4.

Table K-5. Standard counts corrected by In-115 regression

std. (ppb)	Counts					
	Mn-55	Sr-88	Cs-133	Ba-137	Pb-208	U-238
0	33230	6474	1096	881	1851	150
2.5	141732	127914	116687	15426	55109	79293
0	30299	6619	996	971	1730	150
2.5	136325	125463	112080	15673	53183	77462
0	31472	7028	1000	1074	1677	141
2.5	134060	121573	111430	15711	53257	77171
0	30239	6654	949	848	1663	142
2.5	131600	122774	109842	14769	51013	73980
0	31559	6851	17824	1055	1722	156
2.5	127484	119252	107029	14361	50492	71346
5	250772	253616	237079	32090	108555	157535
10	499224	530427	501213	66834	228230	333096

A linear regression was conducted for each species using the Table K-2 prepared standard concentrations and the dependent variable and the Table K-5 corrected counts as the independent variable. Table K-6 shows the results (all $r^2 > 0.99$) used to calculate the sub-sample concentrations.

Table K-6. Standard concentration – corrected count linear regressions

species	intercept $C_{0.X}$ (ppb)	slope $m_{\in.X}$ (ppb / counts)
Mn-55	-5.72E-01	2.21E-05
Sr-88	-2.57E-02	1.97E-05
Cs-133	4.81E-02	1.94E-05
Ba-137	-1.42E-02	1.57E-04
Pb-208	2.02E-02	4.56E-05
U-238	8.00E-02	3.00E-05

The concentrations of each species were calculated using the corrected counts from Equation K-4 predicted from the regression parameters in Table K-6:

$$C_{\in.X} = N'_{\in.X} \cdot \mathfrak{m}_{\in.X} + C_{0.X} \qquad \text{(K-5)}$$

The predicted sub-sample concentrations were corrected for the 2:1 dilution with 2% HNO_3 by $d_V = 2$ to give the original sample concentrations:

$$C'_{\in.X} = d_V C_{\in.X} \qquad \text{(K-6)}$$

The results of Equation K-6 are shown in Table K-7.

Table K-7. ICP-MS species calculated concentrations

Sample	Concentration (ppb)					
	Mn-55	Sr-88	Cs-133	Ba-137	Pb-208	U-238
1	24.1	24.6	0.144	6.94	0.261	0.188
2	20.5	24.2	0.143	6.62	0.243	0.191
3	36.9	250	0.180	29.7	0.422	0.843
4	32.0	243	0.171	27.0	0.372	0.813
5	42.3	123	0.137	101	0.180	0.301
6	42.6	124	0.137	102	0.265	0.304
7	20.5	31.2	0.146	14.0	0.194	0.188
8	20.8	30.8	0.147	13.2	0.176	0.189
9	80.1	74.5	0.149	40.8	0.230	0.328
10	56.9	72.1	0.146	38.6	0.238	0.326
11	24.6	53.6	0.155	27.4	0.251	0.398
12	24.8	53.3	0.150	26.8	0.196	0.401
13	8.50	25.4	0.137	11.0	0.218	0.174
14	9.02	25.6	0.138	11.1	0.213	0.175
15	36.2	38.4	0.139	12.0	0.311	0.188
16	34.6	37.2	0.136	11.3	0.306	0.186
17	21.6	870	0.141	42.9	0.202	0.623
18	10.0	890	0.141	42.7	0.160	0.640
19	114.7	433	0.143	44.9	0.445	0.221
20	82.2	420	0.140	41.2	0.246	0.213
21	497	298	0.154	130	0.526	1.280
22	479	285	0.152	125	0.440	1.303

Table K-8 shows the relative standard deviations of species counts reported by the Aurora M90 ICP-MS instrument software.

Table K-8. Aurora M90 ICP-MS species count error

Sample	Relative standard deviation (%)					
	Mn-55	Sr-88	Cs-133	Ba-137	Pb-208	U-238
1	0.77	2.11	4.85	1.85	1.74	0.97
2	2.54	1.00	1.01	1.93	3.01	5.24
3	1.21	0.43	1.05	0.22	0.80	0.73
4	0.61	2.64	1.23	0.31	1.88	1.07
5	1.15	1.88	2.86	0.64	2.57	2.83
6	1.53	1.52	2.72	0.97	2.02	3.09
7	1.73	1.41	3.03	1.87	3.54	5.89
8	1.96	2.32	4.91	1.82	1.71	2.13
9	4.23	1.29	3.11	0.36	1.12	3.85
10	1.48	1.23	3.49	2.45	1.52	3.21
11	0.27	0.65	1.32	1.41	3.63	2.83
12	0.80	2.42	4.20	1.69	3.77	1.36
13	0.53	1.46	1.54	1.95	3.88	11.70
14	2.11	3.32	1.49	2.68	0.35	8.45
15	0.50	1.81	5.10	2.75	1.69	6.43
16	1.47	1.44	3.67	1.18	1.49	2.48
17	0.62	1.79	1.17	0.69	0.73	0.85
18	0.81	0.99	4.27	1.29	2.27	0.45
19	1.92	1.40	1.55	2.06	0.63	7.71
20	2.47	1.03	3.93	0.68	1.99	2.09
21	0.89	1.02	2.85	1.72	1.04	1.05
22	0.97	1.75	3.97	1.66	1.31	2.96

K.2 ALPHA SPECTROMETRY

The Po-209 detection rate for each sample was from Table K-9 and Table K-10:

$$A_{Po209D} = \frac{\Re_{Po209}}{t_C} \tag{K-7}$$

Stock Po-209 solution had been prepared to 1.86 Bq·mL^{-1} which was used to spike the samples prior to the preparations for plating, giving an activity A_{Po209X}:

- 0.186 Bq, by 100 μL added for the Po-210 plating
- 0.279 Bq, by 150 μL added for the Po-210 ingrowth from Pb-210 plating

The counting efficiency for each sample was from Table K-9 and Table K-10:

$$\mathfrak{E}_C = \frac{A_{Po209D}}{A_{Po209X}} \tag{K-8}$$

The Po-210 detection rate for each sample corrected for background was from Table K-9 and Table K-10:

$$A_{Po210D} = \frac{\mathfrak{N}_{Po210} - \mathfrak{N}_{Po210B}}{t_C} \tag{K-9}$$

The activity of Po-210 corrected for efficiency at the time of counting was from Equations K-8 and K-9 (assigned as $A_{Po210E1}$ from Table K-9 and $A_{Po210E2}$ from Table K-10):

$$A_{Po210E} = \frac{A_{Po210D}}{\mathfrak{E}_C} \tag{K-10}$$

The number of a radionuclide *N* initially N_0 is after time *t* due to decay **(BOURDON, 2003)**:

$$\mathrm{N} = N_0 e^{-\lambda t} \tag{K-11}$$

The activity or rate of change is a proportion of the decay constant $\lambda = \ln 2/t_{1/2}$ and the number of a radionuclide **(BOURDON, 2003)**:

$$\mathrm{A} = \frac{dN}{dt} = -\lambda N \tag{K-12}$$

The activity of a radionuclide *A* initially A_0 is after time *t* due to decay from Equations K-11 and K-12:

$$\mathrm{A} = A_0 e^{-\lambda t} \tag{K-13}$$

The activity of Po-210 corrected for decay from the first plating to the first counting was from Equation K-10, and Equation K-13 using A_{Po210E} calculated from Table K-9:

$$A_{Po210P1} = \frac{A_{Po210E1}}{e^{-\lambda_{Po210}(t_2 - t_1)}} \tag{K-14}$$

The activity of Po-210 corrected for decay from the second plating to the second counting was from Equation K-10, and Equation K-13 using A_{Po210E} calculated from Table K-10:

$$A_{Po210P2} = \frac{A_{Po210E2}}{e^{-\lambda_{Po210}(t_4 - t_3)}} \tag{K-15}$$

The number of a radionuclide N_2 initially N_{20} is after time t due to decay and ingrowth from the parent radionuclide having number initially N_{10} **(BOURDON, 2003)**:

$$N_2 = \frac{\lambda_1}{\lambda_2 - \lambda_1} N_{10}\left(e^{-\lambda_1 t} - e^{-\lambda_2 t}\right) + N_{20} e^{-\lambda_2 t} \quad \text{(K-16)}$$

The activity of a radionuclide A_2 initially A_{20} was after time t due to decay and ingrowth from the parent radionuclide having number initially A_{10} from Equations K-12 and K-16:

$$A_2 = \frac{\lambda_2}{\lambda_2 - \lambda_1} A_{10}\left(e^{-\lambda_1 t} - e^{-\lambda_2 t}\right) + A_{20} e^{-\lambda_2 t} \quad \text{(K-17)}$$

The activity of Pb-210 at the first plating when the activity of Po-210 was depleted to the second plating by ingrowth of Po-210 was from Equations K-15 and K-17:

$$A_{10} = \frac{(\lambda_2 - \lambda_1) A_2}{\lambda_2 (e^{-\lambda_1 t} - e^{-\lambda_2 t})} \quad \text{(K-18)}$$

$$A_{Pb210P1} = \frac{(\lambda_{Po210} - \lambda_{Pb210}) A_{Po210P2}}{\lambda_{Po210}\left(e^{-\lambda_{Pb210}(t_3 - t_1)} - e^{-\lambda_{Po210}(t_3 - t_1)}\right)} \quad \text{(K-19)}$$

The activity of Pb-210 at sampling to the first plating was from Equations K-13 and K-19:

$$A_{Pb210S} = \frac{A_{Pb210P1}}{e^{-\lambda_{Pb210}(t_1 - t_0)}} \quad \text{(K-20)}$$

The activity of Po-210 at sampling to the first plating by decay and ingrowth from Pb-210 was from Equations K-14, K-17 and K-20:

$$A_{20} = A_2 e^{\lambda_2 t} + \frac{\lambda_2}{\lambda_2 - \lambda_1} A_{10}\left(1 - e^{(\lambda_2 - \lambda_1)t}\right) \quad \text{(K-21)}$$

$$A_{Po210S} = A_{Po210P1} e^{\lambda_{Po210}(t_1 - t_0)} + \frac{\lambda_{Po210}}{\lambda_{Po210} - \lambda_{Pb210}} A_{Pb210S}\left(1 - e^{(\lambda_{Po210} - \lambda_{Pb210})(t_1 - t_0)}\right) \quad \text{(K-22)}$$

Table K-11 shows the results from Equations K-20 and K-22, the sample mass and the resulting concentrations of the original samples. The concentration uncertainty was calculated from the Poisson distribution expected value $\mathcal{E}[\mathrm{X}] = \lambda$ and variance $\mathrm{var}[\mathrm{X}] = \lambda$ **(MOOD, 1973)** as the standard deviation of counts $\sqrt{D}$ as a proportion of counts D.

Table K-9. Alpha counting of Po-210 – set 1

SAMPLE	SAMPLE	PLATE 1	COUNT 1	TIME (s)	COUNTS		
	t_0	t_1	t_2	t_C	$\mathcal{N}_{Po210B}$	$\mathcal{N}_{Po209}$	$\mathcal{N}_{Po210}$
1	2016-Jul-16	2016-Sep-15	2016-Sep-19	193,155	1	3286	595
2	2016-Jul-17	2016-Sep-15	2016-Sep-19	193,166	8	3491	822
3	2016-Jul-17	2016-Sep-15	2016-Sep-19	193,165	7	6086	507
4	2016-Jul-17	2016-Sep-15	2016-Sep-19	193,175	4	5712	454
5	2016-Jul-17	2016-Sep-15	2016-Sep-19	193,179	6	2917	245
6	2016-Jul-17	2016-Sep-15	2016-Sep-19	193,174	2	4218	459
7	2016-Jul-17	2016-Sep-15	2016-Sep-19	193,129	5	5230	895
8	2016-Jul-17	2016-Sep-15	2016-Sep-20	84,185	1	1410	263
9	2016-Jul-17	2016-Sep-15	2016-Sep-20	84,175	8	2260	437
10	2016-Jul-17	2016-Sep-15	2016-Sep-20	84,165	7	1828	368
11	2016-Jul-17	2016-Sep-15	2016-Sep-20	84,154	4	1366	148
12	2016-Jul-17	2016-Sep-15	2016-Sep-20	84,146	6	1294	174
13	2016-Jul-17	2016-Sep-15	2016-Sep-20	84,140	2	1955	434
14	2016-Jul-17	2016-Sep-15	2016-Sep-20	84,101	5	1905	364
17	2016-Jul-20	2016-Sep-15	2016-Sep-21	95,386	1	2514	193
18	2016-Jul-20	2016-Sep-15	2016-Sep-21	95,415	8	2006	119
19	2016-Jul-20	2016-Sep-15	2016-Sep-21	95,444	7	1430	214
20	2016-Jul-20	2016-Sep-15	2016-Sep-21	95,444	4	1136	110
21	2016-Jul-20	2016-Sep-15	2016-Sep-21	95,464	6	1656	396
22	2016-Jul-20	2016-Sep-15	2016-Sep-21	95,539	2	2030	440

Table K-10. Alpha counting of Po-210 by ingrowth from Pb-210 – set 1

SAMPLE	PLATE 2	COUNT 2	TIME (s)	COUNTS		
	t_3	t_4	t_C	$\mathcal{N}_{Po210B}$	$\mathcal{N}_{Po209}$	$\mathcal{N}_{Po210}$
1	2017-Jan-19	2017-Feb-08	126,973	1	5823	175
2	2017-Jan-19	2017-Feb-08	126,861	8	6123	215
3	2017-Jan-19	2017-Feb-08	126,863	7	7446	242
4	2017-Jan-19	2017-Feb-08	126,860	4	6461	197
5	2017-Jan-19	2017-Feb-08	126,861	6	5682	56
6	2017-Jan-19	2017-Feb-08	126,859	2	6711	164
7	2017-Jan-19	2017-Feb-08	126,858	5	6281	225
8	2017-Jan-19	2017-Feb-10	183,524	1	9443	196
9	2017-Jan-19	2017-Feb-10	183,528	8	10867	365
10	2017-Jan-19	2017-Feb-10	183,517	7	10568	435
11	2017-Jan-19	2017-Feb-10	183,514	4	8826	160
12	2017-Jan-19	2017-Feb-10	183,514	6	7102	113
13	2017-Jan-19	2017-Feb-10	183,497	2	8842	336
14	2017-Jan-19	2017-Feb-10	183,497	5	8565	294
17	2017-Jan-19	2017-Feb-12	159,730	1	8152	124
18	2017-Jan-19	2017-Feb-12	159,741	8	7735	54
19	2017-Jan-19	2017-Feb-12	159,736	7	8128	158
20	2017-Jan-19	2017-Feb-12	159,733	4	8256	71
21	2017-Jan-19	2017-Feb-12	159,730	6	6448	506
22	2017-Jan-19	2017-Feb-12	159,728	2	8044	582

Table K-11. Concentrations of Pb-210 and Po-210 – set 1

SAMPLE	ACTIVITY (mBq)		SAMPLE MASS (kg)	CONCENTRATION (mBq·L^{-1})	
	Pb-210	Po-210		Pb-210	Po-210
	Eq. K-20	Eq. K-22			
1	1.99	3.95	13.3	1.49±0.11	2.96±0.12
2	2.25	5.19	19.0	1.19±0.08	2.74±0.10
3	2.10	1.37	18.2	1.15±0.07	0.75±0.03
4	1.99	1.32	16.9	1.18±0.08	0.78±0.04
5	0.59	1.89	19.2	0.30±0.04	0.99±0.06
6	1.61	2.21	19.6	0.82±0.06	1.13±0.05
7	2.33	3.55	19.1	1.22±0.08	1.85±0.06
8	1.39	4.30	20.6	0.67±0.05	2.09±0.13
9	2.21	4.12	18.8	1.18±0.06	2.19±0.11
10	2.73	4.13	20.0	1.37±0.07	2.07±0.11
11	1.19	2.30	18.7	0.64±0.05	1.23±0.10
12	1.01	2.99	19.9	0.51±0.05	1.50±0.11
13	2.54	4.80	19.9	1.28±0.07	2.42±0.12
14	2.27	4.06	18.8	1.21±0.07	2.16±0.11
17	1.03	1.61	19.5	0.53±0.05	0.83±0.06
18	0.40	1.28	19.1	0.21±0.03	0.67±0.06
19	1.26	3.28	18.2	0.69±0.06	1.80±0.12
20	0.55	2.20	18.2	0.30±0.04	1.21±0.12
21	5.27	4.27	18.1	2.90±0.13	2.35±0.12
22	4.90	3.89	20.1	2.43±0.10	1.93±0.09

K.3 SUPPLEMENTARY DATA

Table K-2 shows all sample locations comprising sets 1, 2 and 3 detailed in Table 27 and Table K-12. Table K-13 indicates the sample dates and alpha counting statistics. No further processing of the results is presented due to the failure to obtain second plating results for determination of Pb-210 by ingrowth. The original Po-210 counts could not be corrected for the Pb-210 ingrowth contribution between first sampling and plating.

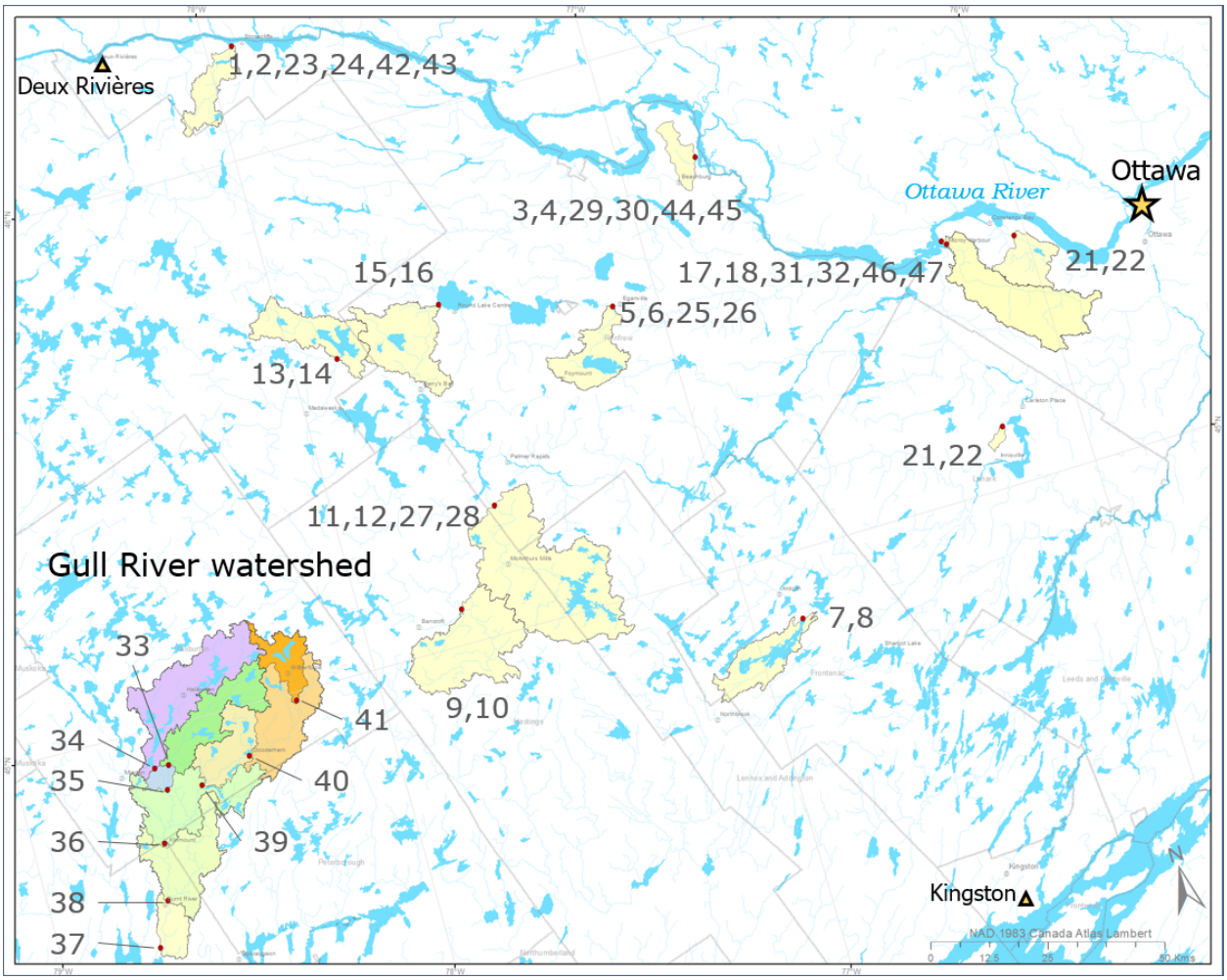

Figure K-2. Ottawa River and Gull River watershed sample locations

Table K-12. Ottawa River and Gull River sampling locations – sets 2, 3

sample	waterway	sampling location	
		latitude	longitude
23	Grant's Creek	46°12′41″	77°55′34″
24	Grant's Creek	46°12′41″	77°55′34″
25	Hurd's Creek	45°32′24″	77°07′18″
26	Hurd's Creek	45°32′24″	77°07′18″
27	Little Mississippi River	45°14′21″	77°34′24″
28	Little Mississippi River	45°14′21″	77°34′24″
29	Pleasant Valley Creek	45°46′08″	76°47′39″
30	Pleasant Valley Creek	45°46′08″	76°47′39″
31	Carp River	45°28′55″	76°13′19″
32	Carp River	45°28′55″	76°13′19″
33	Burnt River	44°55′43″	78°35′41″
34	Drag River	44°55′41″	78°37′59″
35	Burnt River	44°52′58″	78°36′51″
36	Burnt River	44°47′12″	78°39′27″
37	Burnt River	44°35′54″	78°44′18″
38	Burnt River	44°40′52″	78°41′15″
39	Irondale River	44°52′30″	78°31′18″
40	Irondale River	44°54′20″	78°22′48″
41	Irondale River	44°59′02″	78°13′13″
42	Grant's Creek	46°12′41″	77°55′34″
43	Grant's Creek	46°12′41″	77°55′34″
44	Pleasant Valley Creek	45°46′08″	76°47′39″
45	Pleasant Valley Creek	45°46′08″	76°47′39″
46	Carp River	45°28′55″	76°13′19″
47	Carp River	45°28′55″	76°13′19″

Table K-13. Alpha counting of Po-210 – sets 2, 3

SAMPLE	SAMPLE	PLATE 1	COUNT 1	TIME (s)	COUNTS		
	t_0	t_1	t_2	t_C	$\mathcal{N}_{Po210B}$	$\mathcal{N}_{Po209}$	$\mathcal{N}_{Po210}$
23	2016-Sep-24	2017-Jan-06	2017-Jan-10	114,835	1	283	66
24	2016-Sep-24	2017-Jan-06	2017-Jan-10	114,771	8	157	43
25	2016-Sep-24	2017-Jan-06	2017-Jan-17	80,330	6	837	60
26	2016-Sep-24	2017-Jan-06	2017-Jan-10	114,429	4	1530	106
27	2016-Sep-24	2017-Jan-06	2017-Jan-10	114,723	6	898	98
28	2016-Sep-24	2017-Jan-06	2017-Jan-10	114,709	2	1331	176
29	2016-Sep-24	2017-Jan-06	2017-Jan-10	114,694	5	1533	214
30	2016-Sep-24	2017-Jan-06	2017-Jan-14	174,366	1	1818	285
31	2016-Sep-27	2017-Jan-06	2017-Jan-14	174,383	8	2332	96
32	2016-Sep-27	2017-Jan-06	2017-Jan-14	174,398	7	1774	79
33	2016-Nov-19	2017-Jan-06	2017-Jan-14	174,417	4	1426	217
34	2016-Nov-19	2017-Jan-06	2017-Jan-14	174,424	6	1382	232
35	2016-Nov-19	2017-Jan-06	2017-Jan-14	174,456	2	1961	257
36	2016-Nov-19	2017-Jan-06	2017-Jan-14	174,465	5	2462	258
37	2016-Nov-19	2017-Jan-06	2017-Jan-16	165,922	1	2736	359
38	2016-Nov-19	2017-Jan-06	2017-Jan-16	165,932	8	2923	457
39	2016-Nov-19	2017-Jan-06	2017-Jan-16	165,923	7	2283	489
40	2016-Nov-19	2017-Jan-06	2017-Jan-16	165,914	4	2243	443
41	2016-Nov-19	2017-Jan-06	2017-Jan-16	165,909	6	2438	682
42	2016-Nov-20	2017-Jan-06	2017-Jan-16	165,908	2	360	98
43	2016-Nov-20	2017-Jan-06	2017-Jan-16	165,909	5	391	114
44	2016-Nov-20	2017-Jan-06	2017-Jan-17	80,355	1	802	215
45	2016-Nov-20	2017-Jan-06	2017-Jan-17	80,228	8	1133	357
46	2016-Nov-20	2017-Jan-06	2017-Jan-17	80,350	7	600	62
47	2016-Nov-20	2017-Jan-06	2017-Jan-17	80,339	4	1037	121

L Symbols

Table L-1. List of symbols

Symbol	Unit	Description
A_d	L^2	area of lake drainage (watershed)
A_{LA}	L^2	area of water body
$A_{Pb210P1}$	N	Pb-210 activity at first plating
A_{Pb210S}	N	Pb-210 activity at sampling
A_{Po209D}	N	Po-209 detection rate
A_{Po209X}	N	Po-209 stock spiked activity
A_{Po210D}	N	Po-210 detection rate above background
A_{Po210E}	N	Po-210 activity at counting
$A_{Po210P1}$	N	Po-210 activity at first plating
$A_{Po210P2}$	N	Po-210 activity at second plating
A_{Po210S}	N	Po-210 activity at sampling
A_{SE}	L^2	area of sediment
C_A	$N \cdot L^{-3}$	concentration in air on aerosol
C_{AB}	$N \cdot L^{-3}$	concentration in bulk air
C_E	$N \cdot L^{-3}$	concentration in epilimnion
C_H	$N \cdot L^{-3}$	concentration in hypolimnion
C_G	$N \cdot L^{-3}$	concentration in air as a gas
C_I	$N \cdot L^{-3}$	concentration in inflow, dissolved
C_L	$N \cdot L^{-3}$	concentration, limit of detection
C_M	$N \cdot L^{-3}$	concentration in rain
C_N	$N \cdot L^{-3}$	concentration in sediment, pore water
C_{OA}	$N \cdot L^{-3}$	concentration in air on aerosol - input (observed)
C_{OI}	$N \cdot L^{-3}$	concentration in inflow – input (observed)
C_{OM}	$N \cdot L^{-3}$	concentration in rain – input (observed)
C_{OP}	$N \cdot L^{-3}$	concentration in water, SPM – input (observed)
C_{OS}	$N \cdot L^{-3}$	concentration in sediment, solids – input (observed)
C_{OW}	$N \cdot L^{-3}$	concentration in water, dissolved – input (observed)
C_{OWP}	$N \cdot L^{-3}$	concentration in water, total – input (observed)
C_P	$N \cdot L^{-3}$	concentration in water, SPM
C_{PA}	$M \cdot L^{-3}$	concentration of aerosol
C_{PI}	$N \cdot L^{-3}$	concentration in inflow, SPM
C_{PL}	$M \cdot L^{-3}$	concentration of aerosol

Symbol	Unit	Description
C_{PLL}	$M \cdot L^{-3}$	concentration of inflow SPM, lake
C_Q	$N \cdot L^{-3}$	concentration, limit of quantification
C_S	$N \cdot L^{-3}$	concentration in sediment, solids
C_{SB}	$N \cdot L^{-3}$	concentration in bulk sediment
$C_{\in.X}$	$N \cdot L^{-3}$	Species *X* concentration from calibration
$C'_{\in.X}$	$N \cdot L^{-3}$	Species *X* concentration from calibration, undiluted
$C_{\in.0}$	$N \cdot L^{-3}$	Species *X* calibration intercept
C_W	$N \cdot L^{-3}$	concentration in water, dissolved
C_{WB}	$N \cdot L^{-3}$	concentration in bulk water
d_E	L	depth of epilimnion
d_H	L	depth of hypolimnion
d_{LA}	L	depth of harbour
d_{SE}	L	depth of sediment
d_V	unitless	dilution factor
D_B	$L^3 \cdot T^{-1}$	transport parameter, burial
D_C	$L^3 \cdot T^{-1}$	transport parameter, wet deposition
D_D	$L^3 \cdot T^{-1}$	transport parameter, SPM deposition
D_I	$L^3 \cdot T^{-1}$	transport parameter, inflow of water
D_J	$L^3 \cdot T^{-1}$	transport parameter, outflow of water
D_{EH}	$L^3 \cdot T^{-1}$	transport parameter, epilimnion/hypolimnion
D_{EHP}	$L^3 \cdot T^{-1}$	transport parameter, SPM epilimnion-hypolimnion
D_{HEP}	$L^3 \cdot T^{-1}$	transport parameter, SPM hypolimnion-epilimnion
D_{LEI}	$L^3 \cdot T^{-1}$	transport parameter, dissolved lake-epilimnion
D_{LEX}	$L^3 \cdot T^{-1}$	transport parameter, SPM lake-epilimnion
D_{LHI}	$L^3 \cdot T^{-1}$	transport parameter, dissolved lake-hypolimnion
D_{LHX}	$L^3 \cdot T^{-1}$	transport parameter, SPM lake-hypolimnion
D_M	$L^3 \cdot T^{-1}$	transport parameter, rain
D_Q	$L^3 \cdot T^{-1}$	transport parameter, dry deposition
D_R	$L^3 \cdot T^{-1}$	transport parameter, resuspension
D_T	$L^3 \cdot T^{-1}$	transport parameter, diffusion water/sediment
D_{TS}	$L^3 \cdot T^{-1}$	transport parameter, diffusion water-sediment
D_{TW}	$L^3 \cdot T^{-1}$	transport parameter, diffusion sediment-water
D_V	$L^3 \cdot T^{-1}$	transport parameter, volatilization water/air
D_X	$L^3 \cdot T^{-1}$	transport parameter, inflow of SPM
D_Y	$L^3 \cdot T^{-1}$	transport parameter, outflow of SPM

Symbol	Unit	Description
$D_{\lambda W}$	$L^3 \cdot T^{-1}$	transport parameter, decay in water
$D_{\lambda S}$	$L^3 \cdot T^{-1}$	transport parameter, decay in sediment
E_W	$M \cdot L^{-3}$	emission to water
f_{AV}	unitless	volume fraction of aerosol
f_C	unitless	fraction of watershed atm. dep. to lake
$f_{C.Po}$	unitless	Po-210 fraction of watershed atm. dep. to lake
f_{PW}	unitless	mol fraction adsorbed on SPM in water
f_{OS}	unitless	mass fraction dissolved in sediment (pore water)
f_{SV}	unitless	volume fraction of sediment particles
f_{WD}	unitless	mass fraction in water, dissolved
f_{WP}	unitless	mass fraction in water, adsorbed on SPM
f_{WV}	unitless	volume fraction of SPM
f_{WVL}	unitless	volume fraction of SPM, Lake Ontario
F_S	$M \cdot L^{-2} \cdot T^{-1}$	flux adsorbed on SPM, settling
F_R	$M \cdot L^{-2} \cdot T^{-1}$	flux adsorbed on SPM, resuspension
F_B	$M \cdot L^{-2} \cdot T^{-1}$	flux of sediment particles, burial
H	$L^2 \cdot T^{-2}$	Henry's Law (mass) solubility constant
I_C	$N\ L^{-2} \cdot T^{-1}$	flux of Pb-210 to lake from watershed
I_T	$N\ L^{-2} \cdot T^{-1}$	flux of Pb-210 to lake, total
I_W	N	watershed inventory
$I_{W.Pb}$	N	Pb-210 watershed inventory
$I_{W.Po}$	N	Po-210 watershed inventory
k_{HE}	$L \cdot T^{-1}$	mass transfer coefficient: thermocline
k_T	$L \cdot T^{-1}$	mass transfer coefficient: water/sediment
k_{TS}	$L \cdot T^{-1}$	mass transfer coefficient: water-sediment
k_{TW}	$L \cdot T^{-1}$	mass transfer coefficient: sediment-water
k_V	$L \cdot T^{-1}$	mass transfer coefficient: net air/water
k_{VA}	$L \cdot T^{-1}$	mass transfer coefficient: air-side
k_{VW}	$L \cdot T^{-1}$	mass transfer coefficient: water-side
K_d	$L^3 \cdot M^{-1}$	distribution coefficient, sediment
K_d'	$L^3 \cdot M^{-1}$	distribution coefficient, sediment (observed / input)
K_p	$L^3 \cdot M^{-1}$	distribution coefficient, SPM
$m_{WP.Pb}$	M	mass of Pb adsorbed on SPM
$m_{WD.Pb}$	M	mass of Pb dissolved in water
$m_{W.Pb}$	M	mass of Pb total in water

Symbol	Unit	Description
m_S	M	mass of sediment
$m_{S.Pb}$	M	mass of Pb total in sediment
$\dot{m}_{LEX}$	$M \cdot T^{-1}$	mass rate inflow lake-epilimnion
$\dot{m}_{LHX}$	$M \cdot T^{-1}$	mass rate inflow lake-hypolimnion
$\dot{m}_{HX}$	$M \cdot T^{-1}$	mass rate inflow land-harbour
$\dot{m}_{HLY}$	$M \cdot T^{-1}$	mass rate outflow epilimnion-lake
M	$M \cdot N^{-1}$	molar mass
n	N	mols
$\dot{n}_{IN}$	$N \cdot T^{-1}$	mol rate in
$\dot{n}_{OUT}$	$N \cdot T^{-1}$	mol rate out
P	$M \cdot L \cdot T^{-2}$	pressure
P_V	$M \cdot L^{-1} \cdot T^{-2}$	liquid vapour pressure
q_B	$N \cdot T^{-1}$	process rate, burial
q_C	$N \cdot T^{-1}$	process rate, wet deposition
q_D	$N \cdot T^{-1}$	process rate, SPM deposition
q_I	$N \cdot T^{-1}$	process rate, inflow of water
q_J	$N \cdot T^{-1}$	process rate, outflow of water
q_{EH}	$N \cdot T^{-1}$	process rate, epilimnion-hypolimnion
q_{HE}	$N \cdot T^{-1}$	process rate, hypolimnion-epilimnion
q_{EHP}	$N \cdot T^{-1}$	process rate, SPM epilimnion-hypolimnion
q_{HEP}	$N \cdot T^{-1}$	process rate, SPM hypolimnion-epilimnion
q_{LEI}	$N \cdot T^{-1}$	process rate, dissolved lake-epilimnion
q_{LEX}	$N \cdot T^{-1}$	process rate, SPM lake-epilimnion
q_{LHI}	$N \cdot T^{-1}$	process rate, dissolved lake-hypolimnion
q_{LHX}	$N \cdot T^{-1}$	process rate, SPM lake-hypolimnion
q_M	$N \cdot T^{-1}$	process rate, rain
q_Q	$N \cdot T^{-1}$	process rate, dry deposition
q_R	$N \cdot T^{-1}$	process rate, resuspension
q_{TS}	$N \cdot T^{-1}$	process rate, diffusion water-sediment
q_{TW}	$N \cdot T^{-1}$	process rate, burial sediment-water
q_{VA}	$N \cdot T^{-1}$	process rate, volatilization water-air
q_{VW}	$N \cdot T^{-1}$	process rate, volatilization air-water
q_X	$N \cdot T^{-1}$	process rate, inflow of SPM
q_Y	$N \cdot T^{-1}$	process rate, outflow of SPM
q_{WA}	$N \cdot T^{-1}$	atmospheric deposition to the watershed

Symbol	Unit	Description
$q_{WA.Po}$	$N \cdot T^{-1}$	Po-210 atmospheric deposition to the watershed
q_{WG}	$N \cdot T^{-1}$	input from geological source in watershed
$q_{\lambda W}$	$N \cdot T^{-1}$	process rate, decay in water
$q_{\lambda S}$	$N \cdot T^{-1}$	process rate, decay in sediment
Q_B	$L^3 \cdot T^{-1}$	volumetric rate, burial
Q_C	$L^3 \cdot T^{-1}$	volumetric rate, wet deposition
Q_D	$L^3 \cdot T^{-1}$	volumetric rate, SPM deposition
Q_I	$L^3 \cdot T^{-1}$	volumetric rate, inflow of water
Q_J	$L^3 \cdot T^{-1}$	volumetric rate, outflow of water
Q_{EH}	$L^3 \cdot T^{-1}$	volumetric rate, diffusion across thermocline
Q_{HE}	$L^3 \cdot T^{-1}$	volumetric rate, dissolved hypolimnion-epilimnion
Q_{HEP}	$L^3 \cdot T^{-1}$	volumetric rate, SPM hypolimnion-epilimnion
Q_{LEI}	$L^3 \cdot T^{-1}$	volumetric rate, dissolved lake-epilimnion
Q_{LEX}	$L^3 \cdot T^{-1}$	volumetric rate, SPM lake-epilimnion
Q_{LHI}	$L^3 \cdot T^{-1}$	volumetric rate, dissolved lake-hypolimnion
Q_{LHX}	$L^3 \cdot T^{-1}$	volumetric rate, SPM lake-hypolimnion
Q_M	$L^3 \cdot T^{-1}$	volumetric rate, rain
Q_Q	$L^3 \cdot T^{-1}$	volumetric rate, dry deposition
Q_R	$L^3 \cdot T^{-1}$	volumetric rate, resuspension
Q_{TS}	$L^3 \cdot T^{-1}$	volumetric rate, diffusion water-sediment
Q_{TW}	$L^3 \cdot T^{-1}$	volumetric rate, burial sediment-water
Q_V	$L^3 \cdot T^{-1}$	volumetric rate, volatilization water-air
Q_{VA}	$L^3 \cdot T^{-1}$	volumetric rate, volatilization water-air
Q_{VW}	$L^3 \cdot T^{-1}$	volumetric rate, volatilization air-water
Q_X	$L^3 \cdot T^{-1}$	volumetric rate, inflow of SPM
Q_Y	$L^3 \cdot T^{-1}$	volumetric rate, outflow of SPM
$Q_{\lambda W}$	$L^3 \cdot T^{-1}$	volumetric rate, decay in water
$Q_{\lambda S}$	$L^3 \cdot T^{-1}$	volumetric rate, decay in sediment
R	$M \cdot L^2 \cdot N^{-1} \cdot T^{-2} \cdot \theta^{-1}$	ideal gas law constant
S	$M \cdot L^{-3}$	chemical solubility
T_W	θ	temperature of water
v_{AD}	$L \cdot T^{-1}$	aerosol deposition rate
v_{RA}	$L \cdot T^{-1}$	rain rate
v_S	$L \cdot T^{-1}$	apparent settling velocity
V_{LA}	L^3	volume of lake

Symbol	Unit	Description
V_N	L^3	volume of sediment pore water
V_S	L^3	volume of sediment solids
V_W	L^3	volume of water
W_g	unitless	rain scavenging ratio
Z	$T^2 \cdot L^{-2}$	fugacity capacity
σ_I	unitless	standard deviation of input
σ_O	unitless	standard deviation of output
σ_0	unitless	standard deviation of blank counts
ρ_A	$M \cdot L^{-3}$	density of air
ρ_S	$M \cdot L^{-3}$	density of sediment
ρ_W	$M \cdot L^{-3}$	density of SPM
ρ_{WL}	$M \cdot L^{-3}$	density of SPM in Lake Ontario
λ	T^{-1}	radioactive decay constant
λ_h	T^{-1}	radioactive decay constant (hours)
λ_{Pb}	T^{-1}	Pb-210 radioactive decay constant
λ_{Po}	T^{-1}	Po-210 radioactive decay constant
τ_{TW}	T	removal residence time from water by sedimentation
τ_T	T	removal residence time from water by all processes
τ_W	T	watershed mean erosional residence time
$\tau_{W.Pb}$	T	watershed Pb-210 mean erosional residence time
$\tau_{W.Po}$	T	watershed Po-210 mean erosional residence time
$\mathfrak{E}_C$	unitless	Po-210 counting efficiency
$\mathcal{J}_A$	$N\ L^{-2} \cdot T^{-1}$	flux from atmospheric deposition
$\mathcal{J}_S$	$N\ L^{-2} \cdot T^{-1}$	flux to sediment from SPM deposition
$\mathcal{k}$	T^{-1}	sedimentation rate constant
$\mathcal{N}_{Po209}$	#	Po-209 sample counts
$\mathcal{N}_{Po210}$	#	Po-210 sample counts
$\mathcal{N}_{Po210B}$	#	Po-210 blank counts
$\mathcal{N}_{\mathcal{S}.In115}$	#	In-115 counts at sample sequence $\mathcal{S}$
$\mathcal{N}_{\mathcal{S}.In115}$	#	In-115 count regression prediction
$\mathcal{N}_{\mathcal{S}.X}$	#	Species *X* counts at sample sequence $\mathcal{S}$
$\mathcal{N}_{\mathcal{S}.X}$	#	Species *X* counts at sample sequence $\mathcal{S}$, corrected
$\mathcal{r}$	T^{-1}	hydraulic rate constant
$\mathcal{R}$	unitless	fraction of total water input retained in sediment
$\mathcal{S}$	unitless	sensitivity

Symbol	Unit	Description
f	$M \cdot L^{-1} \cdot T^{-2}$	fugacity
$\mathfrak{k}$	unitless	standard deviation of blank counts confidence level
m	$L^3 \cdot M^{-1}$	slope (sensitivity) of calibration plot
$m_{\mathfrak{S},X}$	$N \cdot L^{-3} \cdot \#^{-1}$	slope of species *X* standard concentration by counts
$\mathfrak{S}$	#	count sequence
$\mathbb{A}_A$	$M \cdot L^{-3}$	aquivalence, air
$\mathbb{A}_E$	$M \cdot L^{-3}$	aquivalence, epilimnion
$\mathbb{A}_H$	$M \cdot L^{-3}$	aquivalence, hypolimnion
$\mathbb{A}_S$	$M \cdot L^{-3}$	aquivalence, sediment
$\mathbb{A}_W$	$M \cdot L^{-3}$	aquivalence, water
$\mathbb{A}_{WI}$	$M \cdot L^{-3}$	aquivalence, water inflow
$\mathbb{A}_{WIL}$	$M \cdot L^{-3}$	aquivalence, water inflow, Lake Ontario
$\mathbb{Z}_A$	unitless	aquivalence capacity, air
$\mathbb{Z}_Q$	unitless	aquivalence capacity, aerosol
$\mathbb{Z}_P$	unitless	aquivalence capacity, SPM
$\mathbb{Z}_{PL}$	unitless	aquivalence capacity, SPM in Lake Ontario
$\mathbb{Z}_S$	unitless	aquivalence capacity, particles in sediment
$\mathbb{Z}_W$	unitless	aquivalence capacity, water
$\mathbb{Z}'_W$	unitless	aquivalence capacity, water (corrected)
$\mathbb{Z}_{AT}$	unitless	aquivalence capacity, bulk air
$\mathbb{Z}_{IT}$	unitless	aquivalence capacity, bulk inflow
$\mathbb{Z}_{ITL}$	unitless	aquivalence capacity, bulk inflow Lake Ontario
$\mathbb{Z}_{WT}$	unitless	aquivalence capacity, bulk water
$\mathbb{Z}_{ST}$	unitless	aquivalence capacity, bulk sediment

Bibliography

Al-Masri, M. S., Byrakdar, M. E., Mamish, S., & Al-Haleem, M. A. (2004). Determination of natural radioactivity in Euphrates river. *Journal of Radiological and Nuclear Chemistry*, *261*(2), 349–355. https://doi.org/10.1023/B:JRNC.0000034870.73873.8a

Alcock, C. B., Itkin, V. P., & Horrigan, M. K. (1984). Vapour pressure equations for the metallic elements: 298-2500K. *Canadian Metallurgical Quaterly*, *23*(3), 309–313. https://doi.org/10.1179/cmq.1984.23.3.309

Allen, Eric R. (1977). *Lake Ontario Atlas: Chemistry*. *NYSSGP-OA-77-010*. Springfield, VA. Retrieved from http://digitalcommons.brockport.edu/wr_misc/90/

Ansoborlo, Eric, Berard, Philippe, Den Auwer, Christophe, Leggett, Rich, Menetrier, Florence, Younes, Ali, … Moisy, Philippe. (2012). Review of chemical and radiotoxicological properties of polonium for internal contamination purposes. *Chemical Research in Toxicology*, *25*(8), 1551–1564. https://doi.org/10.1021/tx300072w

Appleby, P. G., & Oldfield, F. (1978). The calculation of lead-210 dates assuming a constant rate of supply of unsupported 210Pb to the sediment. *CATENA*, *5*(1), 1–8. https://doi.org/10.1016/S0341-8162(78)80002-2

AREVA. (2011a). *Tier 2 Volume 4 Atmospheric Environment Part A Air Quality*. *Kiggavik Project - Environmental Impact Statement*. Baker Lake, NU, Canada. Retrieved from http://kiggavik.ca/?attachment_id=4797#.WimTZzdrxaQ

AREVA. (2011b). *Tier 2 Volume 5 Aquatic Environment*. Baker Lake, NU, Canada. Retrieved from http://kiggavik.ca/?attachment_id=4799#.WiqxUTdrxaQ

AREVA. (2011c). *Tier 3 Technical Appendix 5C Aquatics Baseline (2 of 3)*. *Kiggavik Project - Environmental Impact Statement*. Baker Lake, NU, Canada.

Bacon, M. P., Spencer, D. W., & Brewer, P. G. (1976). 210Pb/226Ra and 210Po/210Pb disequilibria in seawater and suspended particulate matter. *Earth and Planetary Science Letters*, *32*(2), 277–296. https://doi.org/10.1016/0012-821X(76)90068-6

Bagnall, K. W. (1957). The chemistry of polonium. *Quaterly Reviews, Chemical Society*, *11*(1), 30–48. Retrieved from http://pubs.rsc.org/-/content/articlelanding/1957/qr/qr9571100030#!divAbstract

Bagnall, K. W. (1962). The chemistry of polonium. *Advances in Inorganic Chemistry and Radiochemistry*, *4*(C), 197–229. https://doi.org/10.1016/S0065-2792(08)60268-X

Bagnall, K. W. (1983). The chemistry of polonium. *Radiochimica Acta*, *32*, 153–161. https://doi.org/10.1524/ract.1983.32.13.153

Balistrieri, Laurie S., Murray, James W., & Paul, Barbara. (1995). The geochemical cycling of stable Pb, 210Pb, and 210Po in seasonally anoxic Lake Sammamish,

Washington, USA. *Geochimica et Cosmochimica Acta*, *59*(23), 4845–4861. https://doi.org/10.1016/0016-7037(95)00334-7

Barica, J., Poulton, D. J., Kohli, B., & Charlton, M. N. (1988). Water exchange between Lake Ontario and Hamilton Harbour: Water quality implications. *Water Pollution Research Journal of Canada*, *23*(2), 213–226. Retrieved from http://digital.library.mcgill.ca/page-turner-3/pageturner.php

Barry, P. J. (1975). Perch Lake. In P. J. Barry (Ed.), *Hydrological Studies on a Small Basin on the Canadian Shield* (pp. 93–130). Chalk River: Atomic Energy of Canada Ltd. Retrieved from https://www.library.yorku.ca/find/Record/393205

Baskaran, M. (2011). Po-210 and Pb-210 as atmospheric tracers and global atmospheric Pb-210 fallout: a review. *Journal of Environmental Radioactivity*, *102*(5), 500–513. https://doi.org/10.1016/j.jenvrad.2010.10.007

Beneš, P. (1982). Physico-chemical forms and migration in continental waters of radium from uranium mining and milling. In IAEA (Ed.), *Environmental migration of long-lived radionuclides : proceedings of an international symposium on migration in the terrestrial environment of long-lived radionuclides from the nuclear fuel cycle* (pp. 3–23). Vienna: International Atomic Energy Agency. Retrieved from https://inis.iaea.org/search/search.aspx?orig_q=RN:14717160

Beneš, P., & Strejc, P. (1986). Interaction of radium with freshwater sediments and their mineral components. *Journal of Radioanalytical and Nuclear Chemistry Articles*, *99*(2), 407–422. https://doi.org/10.1007/BF02037602

Benninger, Larry K. (1978). 210Pb balance in Long Island Sound. *Geochimica et Cosmochimica Acta*, *42*(8), 1165–1174. https://doi.org/10.1016/0016-7037(78)90111-4

Benoit, Gaboury, & Hemond, Harold F. (1987). A biogeochemical mass balance of 210Po and 210Pb in an oligotrophic lake with seasonally anoxic hypolimnion. *Geochimica et Cosmochimica Acta*, *51*(6), 1445–1456. https://doi.org/10.1016/0016-7037(87)90327-9

Benoit, Gaboury, & Hemond, Harold F. (1990). Polonium-210 and lead-210 remobilization from lake sediments in relation to iron and manganese cycling. *Environmental Science & Technology*, *24*(8), 1224–1234. https://doi.org/10.1021/es00078a010

Benoit, Gaboury, & Rozan, Tim F. (1999). The influence of size distribution on the particle concentration effect and trace metal partitioning in rivers. *Geochimica et Cosmochimica Acta*, *63*(1), 113–127. https://doi.org/10.1016/S0016-7037(98)00276-2

Binford, Michael W., Kahl, Jeffrey S., & Norton, Stephen A. (1993). Interpretation of210Pb profiles and verification of the CRS dating model in PIRLA project lake sediment cores. *Journal of Paleolimnology*, *9*(3), 275–296. https://doi.org/10.1007/BF00677218

Binford, MichaelW. (1990). Calculation and uncertainty analysis of 210Pb dates for PIRLA project lake sediment cores. *Journal of Paleolimnology*, *3*(3), 253–267. https://doi.org/10.1007/BF00219461

Blasco, M., Gazquez, M. J., Perez-Moreno, S. M., Grande, J. A., Valente, T., Santisteban, M., … Bolivar, J. P. (2016). Polonium behaviour in reservoirs potentially affected by acid mine drainage (AMD) in the Iberian Pyrite Belt (SW of Spain). *Journal of Environmental Radioactivity*, *152*, 60–69. https://doi.org/10.1016/j.jenvrad.2015.11.008

Boulange, Julien, Watanabe, Hirozumi, & Akai, Shinpei. (2017). A Markov Chain Monte Carlo technique for parameter estimation and inference in pesticide fate and transport modeling. *Ecological Modelling*, *360*, 270–278. https://doi.org/10.1016/j.ecolmodel.2017.07.011

Bourdon, B., Turner, Simon, Henderson, Gideon M., & Lundstrom, Craig C. (2003). Introduction to U-series Geochemistry. *Reviews in Mineralogy and Geochemistry*, *52*(1), 1–21. https://doi.org/10.2113/0520001

Brookins, Douglas G. (1988). *Eh-pH Diagrams for Geochemistry*. Springer Berlin Heidelberg. Retrieved from http://www.springer.com/gp/book/9783642730955

Brown, Richard, McTigue, Nancy, & Cornwell, David. (2015). *Controlling Lead in Drinking Water* (Web Report No. 4409). Newport News, VA. Retrieved from http://www.waterrf.org/Pages/Projects.aspx?PID=4409

Brunskill, G. J., & Wilkinson, P. (1987). Annual Supply of 238U, 234U, 230Th, 226Ra, 210Pb, 210Po, and 232Th to Lake 239 (Experimental Lakes Area , Ontario) from Terrestrial and Atmospheric Sources. *Canadian Journal of Fisheries and Aquatic Sciences*, *44*(S1), S215–S230. https://doi.org/10.1139/f87-297

Burton, W. M., & Stewart, N. G. (1960). Use of long-lived natural radioactivity as an atmospheric tracer. *Nature*, *186*(4725), 584–589. https://doi.org/doi:10.1038/186584a0

Campanha, Mariele B., Moreira, Altair B., & Bisinoti, Márcia Cristina. (2012). Metal fluxes at the sediment–water interface in rivers in the Turvo/Grande drainage basin, São Paulo State, Brazil. *Journal of Soils and Sediments*, *12*(10), 1508–1516. https://doi.org/10.1007/s11368-012-0591-0

Chai, Yingtao, & Urban, Noel R. (2004). 210Po and 210 Pb distributions and residence times in the nearshore region of Lake Superior. *Journal of Geophysical Research*, *109*(C10), 1–16. https://doi.org/10.1029/2003JC002081

Chamberlain, & A.C. (1960). Aspects of the deposition of radioactive and other gases and particles. *Int. J. Air Pollut.; (United States)*, *3*. Retrieved from https://www.osti.gov/biblio/5429192

Chau, N. D., Chwiej, T., & Chrusciel, E. (2001). 226Ra, 228Ra and 210Pb isotopes in some water samples of mines. *Journal of Radioanalytical and Nuclear*

Chemistry, *250*(2), 387–390. https://doi.org/10.1023/A:1017936705282

Cherrier, Jennifer, Burnett, William C., & LaRock, Paul A. (1995). Uptake of Polonium and Sulfur by Bacteria. *Geomicrobiology Journal*, *13*(2), 103–115. https://doi.org/10.1080/01490459509378009

Ciffroy, P., Durrieu, G., & Garnier, J. M. (2009). Probabilistic distribution coefficients (Kds) in freshwater for radioisotopes of Ag, Am, Ba, Be, Ce, Co, Cs, I, Mn, Pu, Ra, Ru, Sb, Sr and Th – implications for uncertainty analysis of models simulating the transport of radionuclides in rivers. *Journal of Environmental Radioactivity*, *100*(9), 785–794. https://doi.org/10.1016/J.JENVRAD.2008.10.019

Clulow, F. V, Dave, N. K., Lim, T. P., & Avadhanula, R. (1998a). Radionuclides (lead-210, polonium-210, thorium-230, and -232) and thorium and uranium in water, sediments, and fish from lakes near the city of Elliot Lake, Ontario, Canada. *Environmental Pollution*, *99*(2), 199–213. https://doi.org/10.1016/S0269-7491(97)00187-5

Clulow, F. V, Dave, N. K., Lim, T. P., & Avadhanula, R. (1998b). Radium-226 in water, sediments, and fish from lakes near the city of Elliot Lake, Ontario, Canada. *Environmental Pollution*, *99*(1), 13–28. https://doi.org/10.1016/S0269-7491(97)00176-0

Coale, Kenneth H., & Flegal, A. Russel. (1989). Copper, zinc, cadmium and lead in surface waters of Lakes Erie and Ontario. *Science of The Total Environment*, *87–88*, 297–304. https://doi.org/10.1016/0048-9697(89)90243-X

Cornett, Jack, Chant, Lorna, & Risto, Bert. (1992). Arsenic transport between water and sediments. *Sediment/Water Interactions*, 533–544. https://doi.org/10.1007/978-94-011-2783-7_46

Cornett, R. J., Chant, L., & Link, D. (1984). Sedimentation of Pb-210 in Laurentian Shield lakes. *Water Poll. J. Can.*, *19*(2), 97–109. Retrieved from http://digital.library.mcgill.ca/page-turner-3/pageturner.php

CSA. (2014). *Guidelines for calculating derived release limits for radioactive material in airborne and liquid effluents for normal operation of nuclear facilities*. *N288.1-14*. Mississauga, ON. Retrieved from http://shop.csa.ca/en/canada/nuclear/n2881-14/invt/27011562014

Diamond, M. L. (1999). Development of a fugacity/aquivalence model of mercury dynamics in lakes. *Water, Air, & Soil Pollution*, *111*(1), 337–357. https://doi.org/10.1023/A:1005062316518

Diamond, M. L., Mackay, D., & Welbourn, P. M. (1992). Models of multi-media partitioning of multi-species chemicals: The fugacity/aquivalence approach. *Chemosphere*, *25*(12), 1907–1921. https://doi.org/10.1016/0045-6535(92)90030-U

Diamond, Miriam L., & Ling-Lamprecht, Helen W. (1996). Loadings, dynamics and response time of seven metals in Hamilton Harbour: Results of a mass balance

study. *Water Quality Research Journal of Canada*, *31*(3), 623–641. Retrieved from http://digital.library.mcgill.ca/wqrj/search/issue.php?issue=WQRJ_Vol_31_No_3

Diamond, Miriam L., Mackay, Donald, Cornett, R. Jack, & Chant, Lorna A. (1990). A model of the exchange of inorganic chemicals between water and sediments. *Environmental Science & Technology*, *24*(5), 713–722. https://doi.org/10.1021/es00075a016

Dillon, P. J., & Evans, R. D. (1982). Whole-lake lead burdens in sediments of lakes in southern Ontario, Canada. *Hydrobiologia*, *91–92*(1), 121–130. https://doi.org/10.1007/BF02391927

Dominik, J., Burrus, D., & Vernet, J. P. (1987). Transport of the environmental radionuclides in an alpine watershed. *Earth and Planetary Science Letters*, *84*(2–3), 165–180. https://doi.org/10.1016/0012-821X(87)90083-5

Edgington, David N., & Robbins, John A. (1976). Records of lead deposition in Lake Michigan sediments since 1800. *Environmental Science & Technology*, *10*(3), 266–274. https://doi.org/10.1021/es60114a007

Eichler, B. (2002). *Die flüchtigkeitseigenschaften des poloniums*. *PSI-Report 02-12*. Villigen. Retrieved from http://www.iaea.org/inis/collection/NCLCollectionStore/_Public/33/045/33045410.pdf

El-Daoushy, F. (1988). A summary on the lead-210 cycle in nature and related applications in Scandinavia. *Environment International*, *14*(4), 305–319. https://doi.org/10.1016/0160-4120(88)90008-6

Elliott, S. E. M., Burns-Flett, C., Hesslein, R. H., Brunskill, G. J., & Lutz, A. (1981). *Cesium-137, Radium-226, Potassium-40 and Selected Stable Elements in Fish Populations from Great Slave Lake (NWT), Louis Lake (Saskatchewan), Lake Winnipeg (Manitoba), and Experimental Lakes Area (Northwestern Ontario)*. Winnipeg, MB. Retrieved from http://publications.gc.ca/pub?id=9.576361&sl=0

Encinas, D., Calzada, I., & Casado, H. (2004). Scavenging Ratios in an Urban Area in the Spanish Basque Country. *Aerosol Science and Technology*, *38*(7), 685–691. https://doi.org/10.1080/02786820490460716

Engelmann, Rudolf J. (1971). Scavenging Prediction Using Ratios of Concentrations in Air and Precipitation. *Journal of Applied Meteorology*, *10*(3), 493–497. https://doi.org/10.1175/1520-0450(1971)010<0493:SPUROC>2.0.CO;2

Ethier, A. L. M., Mackay, D., Toose-Reid, L. K., O'Driscoll, N. J., Scheuhammer, A. M., & Lean, D. R. S. (2008). The development and application of a mass balance model for mercury (total, elemental and methyl) using data from a remote lake (Big Dam West, Nova Scotia, Canada) and the multi-species multiplier method. *Applied Geochemistry*, *23*(3), 467–481. https://doi.org/10.1016/j.apgeochem.2007.12.015

Ethier, Adrienne. (2009). *HERMES: A modelling tool for predicting mercury concentrations and fluxes in lakes*. University of Ottawa. Retrieved from https://ruor.uottawa.ca/handle/10393/29777

Ethier, Adrienne L. M., Atkinson, Joseph F., Depinto, Joseph V., & Lean, David R. S. (2012). Estimating mercury concentrations and fluxes in the water column and sediment of Lake Ontario with HERMES model. *Environmental Pollution*, *161*(February), 335–342. https://doi.org/10.1016/j.envpol.2011.06.002

Evans, H. E., Dillon, P. J., Scholer, P. J., & Evans, R. D. (1986). The use of Pb/210Pb ratios in lake sediments for estimating atmospheric fallout of stable lead in South-Central Ontario, Canada. *Science of The Total Environment*, *54*, 77–93. https://doi.org/10.1016/0048-9697(86)90257-3

Evans, R. Douglas, & Rigler, Frank H. (1980). Calculation of the Total Anthropogenic Lead in the Sediments of a Rural Ontario Lake. *Environmental Science & Technology*, *14*(2), 216–218. https://doi.org/10.1021/es60162a009

Figgins, P. E. (1961). *The Radiochemistry of Polonium*. Washington, DC. Retrieved from http://library.lanl.gov/cgi-bin/getfile?rc000006.pdf

Gaillardet, J., Viers, J., & Dupré, B. (2014). Trace Elements in River Waters. In Karl Turekian & Heinrich Holland (Eds.), *Treatise on Geochemistry* (2nd ed., pp. 195–235). Elsevier. https://doi.org/10.1016/B978-0-08-095975-7.00507-6

Gavini, M. B., Beck, J. N., & Kuroda, P. K. (1974). Mean Residence Times of the Long-Lived Radon Daughters in the Atmosphere. *Journal of Geophysical Research*, *79*(30), 4447–4452. https://doi.org/10.1029/JC079i030p04447

Gibson, Walter Maxwell (Bell Telephone Laboratories). (1961). *The radiochemistry of lead*. Washington, DC. Retrieved from https://www.osti.gov/scitech/biblio/4843041-radiochemistry-lead

Goldberg, E. G. (1963). Geochronology with 210Pb. In International Atomic Energy Agency (Ed.), *Radioactive Dating* (pp. 121–131). Vienna: International Atomic Energy Agency. Retrieved from https://www-pub.iaea.org/books/IAEABooks/2003/Radioactive-Dating-Athens-19-23-Nov-1962

Grasty, R. L. (1994). Summer outdoor radon variations in Canada and their relation to soil moisture. *Health Physics*, *66*(2), 185–193. Retrieved from http://journals.lww.com/health-physics/Abstract/1994/02000/Summer_Outdoor_Radon_Variations_in_Canada_and.9.aspx

Guerin, Frederic. (2012). *Kiggavik Project Environmental Impact Statement Tier 1 Volume 1 Main Document* (Vol. Tier 1 Vol). Retrieved from http://kiggavik.ca/?attachment_id=4800#.WaSX79GQxaQ

Hamilton-Taylor, John. (1979). Enrichments of zinc, lead, and copper in recent sediments of Windermere, England. *Environmental Science & Technology*, *13*(6), 693–697. https://doi.org/10.1021/es60154a008

Harada, Koh, Burnett, William C., LaRock, Paul A., & Cowart, James B. (1989). Polonium in Florida groundwater and its possible relationship to the sulfur cycle and bacteria. *Geochimica et Cosmochimica Acta*, *53*(1), 143–150. https://doi.org/10.1016/0016-7037(89)90281-0

Hart, Donald R. (2011). *Special Investigations 2009 - Implications for Radiological Dose and Risk Calculations*. *Serpent River Watershed State of the Environment Report, Appendix F*. Mississauga, ON. Retrieved from https://www.denisonenvironmental.com/our-work/reports-and-presentations

Hem, J. D. (1976a). Inorganic Chemistry of Lead in Water. In T. G. Lovering (Ed.), *Geological Survey Professional Paper 957* (pp. 5–11). Washington, DC: USGS. https://doi.org/10.1016/0013-9327(73)90048-7

Hem, J. D., & Durum, W. H. (1973). Solubility and Occurrence of Lead in Surface Water. *Journal (American Water Works Association)*. American Water Works Association. https://doi.org/10.2307/41267396

Hem, John D. (1976b). Geochemical controls on lead concentrations in stream water and sediments. *Geochimica et Cosmochimica Acta*, *40*(6), 599–609. https://doi.org/10.1016/0016-7037(76)90106-X

Hesslein, Raymond H., & Slavicek, E. (1984). Geochemical pathways and biological uptake of radium in small Canadian Shield Lakes. *Canadian Journal of Fisheries and Aquatic Sciences*, *41*(3), 459–468. https://doi.org/10.1139/f84-055

Hoff, R. M., Strachan, W. M. J., Sweet, C. W., Chan, C. H., Shackleton, M., Bidleman, T. F., … Schroeder, W. H. (1996). Atmospheric deposition of toxic chemicals to the great lakes: a review of data through 1994. *Atmospheric Environment*, *30*(20), 3505–3527. https://doi.org/10.1016/1352-2310(96)00046-5

Hoffman, F. Owen, & Hammonds, Jana S. (1994). Propagation of Uncertainty in Risk Assessments: The Need to Distinguish Between Uncertainty Due to Lack of Knowledge and Uncertainty Due to Variability. *Risk Analysis*, *14*(5), 707–712. https://doi.org/10.1111/j.1539-6924.1994.tb00281.x

Hussain, N., Church, T. M., Veron, Alain J., & Larson, R. E. (1998). Radon daughter disequilibria and lead systematice in the western North Atlantic. *Journal of Geophysical Research*, *103*(D13), 16059–16071. https://doi.org/10.1029/98JD01367

Hussain, N., Ferdelman, T. G., Church, T. M., & Luther, George W. (1995). Bio-volatilization of polonium: Results from laboratory analyses. *Aquatic Geochemistry*, *1*(2), 175–188. https://doi.org/10.1007/BF00702890

IAEA. (1963). *A Basic Toxicity Classification of Radionuclides*. Vienna: International Atomic Energy Agency. Retrieved from https://www-pub.iaea.org/books/IAEABooks/1110/A-Basic-Toxicity-Classification-of-Radionuclides

IAEA. (1990). *The environmental behaviour of radium*. *TRS-310*. Vienna. Retrieved

from http://www-pub.iaea.org/books/IAEABooks/1414/The-Environmental-Behaviour-of-Radium

IAEA. (2001). *Generic models for use in assessing the impact of discharges of radioactive substances to the environment*. *SRS-19*. Vienna. Retrieved from http://www-pub.iaea.org/books/IAEABooks/6024/Generic-Models-for-Use-in-Assessing-the-Impact-of-Discharges-of-Radioactive-Substances-to-the-Environment

IAEA. (2003). *Extent of environmental contamination by naturally occurring radioactive material (norm) and technological options for mitigation*. *TRS-419*. Vienna. Retrieved from http://www-pub.iaea.org/books/IAEABooks/6789/Extent-of-Environmental-Contamination-by-Naturally-Occurring-Radioactive-Material-NORM-and-Technological-Options-for-Mitigation

IAEA. (2009a). *A Procedure for the Determination of Po-210 in Water Samples by Alpha Spectrometry*. *IAEA/AQ/12*. Vienna. Retrieved from http://www-pub.iaea.org/MTCD/publications/PDF/IAEA-AQ-12_web.pdf

IAEA. (2009b). *Quantification of radionuclide transfer in terrestrial and freshwater environments for radiological assessments. IAEA-TECDOC-1616*. Vienna: International Atomic Energy Agency. Retrieved from http://www-pub.iaea.org/books/IAEABooks/8103/Quantification-of-Radionuclide-Transfer-in-Terrestrial-and-Freshwater-Environments-for-Radiological-Assessments

IAEA. (2014). *The Environmental Behaviour of Radium: Revised Edition*. *TRS-476*. Vienna. Retrieved from http://www-pub.iaea.org/books/IAEABooks/10478/The-Environmental-Behaviour-of-Radium-Revised-Edition

IAEA. (2017). *The Environmental Behaviour of Polonium*. (Fernando P. Carvalho, Ed.). Vienna: IAEA. Retrieved from https://www-pub.iaea.org/books/IAEABooks/10845/The-Environmental-Behaviour-of-Polonium

Iman, Ronald L., & Helton, Jon C. (1988). An investigation of uncertainty and sensitivity analysis techniques for computer models. *Risk Analysis 8*, *8*(1), 71–90. https://doi.org/10.1111/j.1539-6924.1988.tb01155.x

Israel, H. (1951). Radioactivity of the Atmosphere. In Thomas F. Malone (Ed.), *Compendium of meteorology* (pp. 155–161). Baltimore, MD: American Meteorological Society. Retrieved from https://link.springer.com/chapter/10.1007/978-1-940033-70-9_13

Jacobi, W., & André, K. (1963). The vertical distribution of radon 222, radon 220 and their decay products in the atmosphere. *Journal of Geophysical Research*, *68*(13), 3799–3814. https://doi.org/10.1029/JZ068i013p03799

Jaworowski, Z., & Kownacka, L. (1976). Lead and radium in the lower stratosphere. *Nature*, *263*(5575), 303–304. https://doi.org/10.1038/263303a0

Joshi, S. R., McCrea, R. C., Shukla, B. S., & Roy, J. C. (1990). Partitioning and

transport of lead-210 in the ottawa river watershed. *Water, Air, & Soil Pollution*, *59*(3–4), 311–320. https://doi.org/10.1007/BF00211839

Kada, J., & Heit, M. (1992). The inventories of anthropogenic Ph, Zn, As, Cd, and the radionuclides 137Cs and excess 210Pb in lake sediments of the Adirondack region, USA. *Hydrobiologia*, *246*(3), 231–241. https://doi.org/10.1007/BF00005700

Kalnejais, Linda H., Martin, W. R., & Bothner, Michael H. (2015). Porewater dynamics of silver, lead and copper in coastal sediments and implications for benthic metal fluxes. *Science of The Total Environment*, *517*, 178–194. https://doi.org/10.1016/J.SCITOTENV.2015.02.011

Kemp, A. L. W., & Thomas, R. L. (1976). Impact of man's activities on the chemical composition in the sediments of Lakes Ontario, Erie and Huron. *Water, Air, and Soil Pollution*, *5*(4), 469–490. https://doi.org/10.1007/BF00280847

Kim, Guebuem, Kim, Su-Jin, Schultz, Michael K., & Burnett, William C. (2005). Enrichment of excess 210Po in anoxic ponds. *Environmental Science & Technology*, *39*(13), 4894–4899. https://doi.org/10.1021/es0482334

Kim, Guebuem, Kim, Tae-Hoon, & Church, Thomas M. (2011). Po-210 in the Environment: Biogeochemical Cycling and Bioavailability. In M. Baskaran (Ed.), *Handbook of Environmental Isotope Geochemistry* (Volume 1, pp. 271–284). Berlin: Springer-Verlag. https://doi.org/10.1007/978-3-642-10637-8

Kirby, Harold W. (Mound Laboratory), & Salutsky, Murrell Leon (WR Grace &. Co). (1964). *The radiochemistry of radium*. Clarksville, MD. Retrieved from http://www.radiochemistry.org/periodictable/pdf_books/pdf/rc000041.pdf

Kirkwood, Thomas B. L. (1979). Geometric Means and Measures of Dispersion. *Biometrics*, *35*(4), 908–909. Retrieved from https://www.jstor.org/stable/2530139

Klapwijk, Abraham, & Snodgrass, William J. (1985). Model for Lake-Bay Exchange Flow. *Journal of Great Lakes Research*, *11*(1), 43–52. https://doi.org/10.1016/S0380-1330(85)71742-X

Kneip, Theo J., Eisenbud, Merril, Strehlow, Clifford D., & Freudenthal, Peter C. (1970). Airborne Particulates in New York City. *Journal of the Air Pollution Control Association*, *20*(3), 144–149. https://doi.org/10.1080/00022470.1970.10469385

Kownacka, Ludwika, Jaworowski, Zbigniew, & Suplinska, Maria. (1990). Vertical distribution and flows of lead and natural radionuclides in the atmosphere. *Science of The Total Environment*, *91*, 199–221. https://doi.org/10.1016/0048-9697(90)90299-A

Krishnaswamy, S., Lal, D., Martin, J. M., & Meybeck, M. (1971). Geochronology of lake sediments. *Earth and Planetary Science Letters*, *11*(1–5), 407–414. https://doi.org/10.1016/0012-821X(71)90202-0

Langmuir, Irving. (1918). The adsorption of gases on plane surfaces of glass, mica

and platinum. *Journal of the American Chemical Society*, *40*(9), 1361–1403. https://doi.org/10.1021/ja02242a004

Lehmann, L., & Sittkus, A. (1959). Bestimmung von Aerosolverweilzeiten aus dem RaD- und RaF-Gehalt der atmosphärischen Luft und des Niederschlags. *Die Naturwissenschaften*, *46*(1), 9–10. https://doi.org/10.1007/BF00621355

Lei, Pei, Zhang, Hong, Shan, Baoqing, & Zhang, Bozheng. (2016). Distribution, diffusive fluxes, and toxicity of heavy metals and PAHs in pore water profiles from the northern bays of Taihu Lake. *Environmental Science and Pollution Research*, *23*(21), 22072–22083. https://doi.org/10.1007/s11356-016-7467-6

Lerman, A. (1979). *Geochemical processes. Water and sediment environments. Geochemical processes. Water and sediment environments.* New York: John Wiley and Sons, Inc. Retrieved from https://www.cabdirect.org/cabdirect/abstract/19831974672

Lewis, Dale M. (1977). The use of 210Pb as a heavy metal tracer in the Susquehanna River system. *Geochimica et Cosmochimica Acta*, *41*(11), 1557–1564. https://doi.org/10.1016/0016-7037(77)90167-3

Lewis, Gilbert Newton. (1901). The law of physico-chemical change. *Proceedings of the American Academy of Arts and Sciences*, *37*(3), 49–69. https://doi.org/10.2307/20021635

Limpert, Eckhard, Stahel, Werner A., & Abbt, Markus. (2001). Log-normal Distributions across the Sciences: Keys and Clues. *BioScience*, *51*(5), 341–352. https://doi.org/10.1641/0006-3568(2001)051[0341:lndats]2.0.co;2

Ling, Helen, Diamond, Miriam, & Mackay, Donald. (1993). Application of the QWASI Fugacity/Aquivalence Model to Assessing Sources and Fate of Contaminants in Hamilton Harbour. *Journal of Great Lakes Research*, *19*(3), 582–602. https://doi.org/10.1016/S0380-1330(93)71243-5

Macdonald, C. R., Ewing, L. L., Elkin, B. T., & Wiewel, A. M. (1996). Regional variation in radionuclide concentrations and radiation dose in caribou (Rangifer tarandus) in the Canadian Arctic; 1992-1994. *The Science of the Total Environment*, *182*(1–3), 53–73. https://doi.org/10.1016/0048-9697(95)05037-X

Mackay, D., & Paterson, S. (1982). Fugacity revisited. *Environmental Science & Technology*, *16*(12), 654A–660A. https://doi.org/10.1021/es00106a724

Mackay, Donald. (1979). Finding Fugacity Feasible. *Environmental Science & Technology*, *13*(10), 1218–1223. https://doi.org/10.1021/es60158a003

Mackay, Donald. (2001). *Multimedia environmental models : the fugacity approach* (2nd ed.). Boca Raton, FL: CRC Press. Retrieved from https://www.crcpress.com/Multimedia-Environmental-Models-The-Fugacity-Approach-Second-Edition/Mackay/p/book/9781566705424

Mackay, Donald, & Diamond, Miriam. (1989). Application of the qwasi (quantitative water air sediment interaction) fugacity model to the dynamics of organic and

inorganic chemicals in lakes. *Chemosphere*, *18*(7–8), 1343–1365. https://doi.org/10.1016/0045-6535(89)90027-1

Mackay, Donald, Joy, Michael, & Paterson, Sally. (1983). A quantitative water, air, sediment interaction (qwasi) fugacity model for describing the fate of chemicals in lakes. *Chemosphere*, *12*(7–8), 981–997. https://doi.org/10.1016/0045-6535(83)90251-5

Mackay, Donald, Sang, Susan, Vlahos, Penny, Diamond, Miriam, Gobas, Frank, & Dolan, David. (1994). A Rate Constant Model of Chemical Dynamics in a Lake Ecosystem: PCBs in Lake Ontario. *Journal of Great Lakes Research*, *20*(4), 625–642. https://doi.org/10.1016/S0380-1330(94)71183-7

MacLeod, Matthew, Fraser, Alison J., & Mackay, Don. (2002). Evaluating and expressing the propagation of uncertainty in chemical fate and bioaccumulation models. *Environmental Toxicology and Chemistry*, *21*(4), 700–709. https://doi.org/10.1002/etc.5620210403

Marsden, Ernest. (1964). Incidence and possible significance of inhaled or ingested polonium. *Nature*, *203*(4942), 230–233. https://doi.org/doi:10.1038/203230a0

Martínez-Aguirre, A., Morón, M. C., & García-León, M. (1991). Measurements of U- and Ra-isotopes in rainwater samples. *Journal of Radioanalytical and Nuclear Chemistry Articles*, *152*(1), 37–46. https://doi.org/10.1007/BF02042139

Marvin, Chris, Charlton, Murray, Milne, Jacqui, Thiessen, Lina, Schachtschneider, Joanne, Sardella, Gino, & Sverko, Ed. (2007). Metals Associated with Suspended Sediments in Lakes Erie and Ontario, 2000–2002. *Environmental Monitoring and Assessment*, *130*(1–3), 149–161. https://doi.org/10.1007/s10661-006-9385-4

Marvin, Christopher H., Charlton, Murray N., Stern, Gary A., Braekevelt, Eric, Reiner, Eric J., & Painter, Scott. (2003). Spatial and Temporal Trends in Sediment Contamination in Lake Ontario. *Journal of Great Lakes Research*, *29*(2), 317–331. https://doi.org/10.1016/S0380-1330(03)70437-7

Maugeri, Emilio Andrea, Neuhausen, Jorg, Eichler, Robert, Piguet, David, Mendonca, Tania Melo, Stora, Thierry, & Schumann, Dorothea. (2014). Thermochromatography study of volatile polonium species in various gas atmospheres. *Journal of Nuclear Materials*, *450*(1–3), 292–298. https://doi.org/10.1016/J.JNUCMAT.2013.11.024

Mayer, Tatiana, & Manning, Philip G. (1990). Inorganic Contaminants in Suspended Solids from Hamilton Harbour. *Journal of Great Lakes Research*, *16*(2), 299–318. https://doi.org/10.1016/S0380-1330(90)71423-2

McKee, P. M., Snodgrass, W. J., Hart, D. R., Duthie, H. C., McAndrews, J. H., & Keller, W. (1987). Sedimentation Rates and Sediment Core Profiles of 238 U and 232 Th Decay Chain Radionuclides in a Lake Affected by Uranium Mining and Milling. *Canadian Journal of Fisheries and Aquatic Sciences*, *44*(2), 390–398. https://doi.org/10.1139/f87-048

McKone, Thomas E. (1996). Alternative modeling approaches for contaminant fate in soils: uncertainty, variability, and reliability. *Reliability Engineering and System Safety1*, *54*(2–3), 165–181. https://doi.org/10.1016/S0951-8320(96)00073-7

Meija, Juris, Coplen, Tyler B., Berglund, Michael, Brand, Willi A., De Bièvre, Paul, Gröning, Manfred, … Prohaska, Thomas. (2016). Isotopic compositions of the elements 2013 (IUPAC Technical Report). *Pure and Applied Chemistry*, *88*(3), 293–306. https://doi.org/10.1515/pac-2015-0503

Millard, Steven P. (2013). *EnvStats : An R Package for Environmental Statistics*. New York: Springer. Retrieved from http://www.springer.com/us/book/9781461484554

Mljač, Liljana, & Križman, Milko. (1996). Radioactive contamination of surface waters from a fly-ash depository at Velenje (Solvenia). *Environment International*, *22*, 339–345. https://doi.org/10.1016/S0160-4120(96)00128-6

Momoshima, N., Song, Li X., Osaki, S., & Maeda, Y. (2002). Biologically induced Po emission from fresh water. *Journal of Environmental Radioactivity*, *63*(2), 187–197. https://doi.org/10.1016/S0265-931X(02)00028-0

Momoshima, Noriyuki, Song, L. I. Xiang, Osaki, Susumu, & Maeda, Yonezo. (2001). Formation and emission of volatile polonium compound by microbial activity and polonium methylation with methylcobalamin. *Environmental Science and Technology*, *35*(14), 2956–2960. https://doi.org/10.1021/es001730+

Mood, Alexander M., Graybill, Franklin A., & Boes, Duane C. (1973). *Introduction to the theory of statistics* (3d ed.). New York: McGraw-Hill. Retrieved from https://www.worldcat.org/title/introduction-to-the-theory-of-statistics/oclc/9602461

Moore, H. E., & Poet, S. E. (1976). Background levels of 226Ra in the lower troposphere. *Atmospheric Environment (1967)*, *10*(5), 381–383. https://doi.org/10.1016/0004-6981(76)90006-8

Moore, H. E., Poet, S. E., & Martell, E. A. (1973). 222Rn, 210Pb, 210Bi, and 210Po Profiles and Aerosol Residence Times versus Altitude. *Journal of Geophysical Research*, *78*(30), 7065–7075. https://doi.org/10.1029/JC078i030p07065

Moyer, Harvey V, Gngney, Lloyd B., & Rogers, Adrian J. (1956). *Polonium*. *TID-5221*. Oak Ridge, TN. https://doi.org/10.2172/4367751

Mudbidre, R., Baskaran, M., & Schweitzer, L. (2014). Investigations of the partitioning and residence times of Po-210 and Pb-210 in a riverine system in Southeast Michigan, USA. *Journal of Environmental Radioactivity*, *138*, 375–383. https://doi.org/10.1016/j.jenvrad.2014.01.007

Mudroch, Alena, & Mudroch, Paul. (1992). Geochemical Composition of the Nepheloid Layer in Lake Ontario. *Journal of Great Lakes Research*, *18*(1), 132–153. https://doi.org/10.1016/S0380-1330(92)71281-7

Mudroch, Alena, Sarazin, Laurie, & Lomas, Tammy. (1988). Summary of Surface

and Background Concentrations of Selected Elements in the Great Lakes Sediments. *Journal of Great Lakes Research*, *14*(2), 241–251. https://doi.org/10.1016/S0380-1330(88)71553-1

Natural Resources Canada. (2000). Canadian Land Cover. Retrieved May 4, 2018, from https://open.canada.ca/data/en/dataset/97126362-5a85-4fe0-9dc2-915464cfdbb7

Nelson, A. W., Eitrheim, E. S., Knight, A. W., May, D., Wichman, M. D., Forbes, T. Z., & Schultz, M. K. (2017). Polonium-210 accumulates in a lake receiving coal mine discharges—anthropogenic or natural? *Journal of Environmental Radioactivity*, *167*, 211–221. https://doi.org/10.1016/j.jenvrad.2016.10.023

NNDC. (2018). Interactive Chart of Nuclides. Retrieved May 19, 2018, from http://www.nndc.bnl.gov/chart/reCenter.jsp?z=82&n=128

Nriagu, J. O., Wong, H. K. T., & Coker, R. D. (1981). Particulate and dissolved trace metals in Lake Ontario. *Water Research*, *15*(1), 91–96. https://doi.org/10.1016/0043-1354(81)90188-3

Nriagu, Jerome O., Lawson, Greg, Wong, Henry K. T., & Cheam, Ven. (1996). Dissolved Trace Metals in Lakes Superior, Erie, and Ontario. *Environmental Science & Technology*, *30*(1), 178–187. https://doi.org/10.1021/es950221i

Nriagu, Jerome O., Wong, Henry K. t, & Snodgrass, William J. (1983). Historical Records of Metal Pollution in Sediments of Toronto and Hamilton Harbours. *Journal of Great Lakes Research*, *9*(3), 365–373. https://doi.org/10.1016/S0380-1330(83)71908-8

O'Connor, Donald J., & Connolly, John P. (1980). The effect of concentration of adsorbing solids on the partition coefficient. *Water Research*, *14*(1972), 1517–1523. https://doi.org/10.1016/0043-1354(80)90018-4

OME. (1992a). *Remedial Action Plan for Hamilton Harbour Stage I Report*. *2nd Edition*. Retrieved from https://archive.org/details/IREMEDIALACTIONPL00SNSN20258.ome

OME. (1992b). *The In-place pollutants program Volume VII Part 1*. Retrieved from https://archive.org/details/p1inplacepolluta07torouoft

OME. (1992c). *The In-place pollutants program Volume VII Part 2*. Retrieved from https://archive.org/details/p2inplacepolluta07torouoft/

Peirrard, Jean-Claude, Rimbault, Jean, & Aplincourt, Michel. (2002). Experimental study and modelling of lead solubility as a function of pH in mixtures of ground waters and cement waters. *Water Research*, *36*(4), 879–890. https://doi.org/10.1016/S0043-1354(01)00307-4

Peirson, D. H., Cambray, R. S., & Spicer, G. S. (1966). Lead-210 and polonium-210 in the atmosphere. *Tellus*, *18*(2–3), 427–433. https://doi.org/10.1111/j.2153-3490.1966.tb00254.x

Persson, Bertil R. R., & Holm, Elis. (2011). Polonium-210 and lead-210 in the

terrestrial environment: a historical review. *Journal of Environmental Radioactivity*, *102*(5), 420–429. https://doi.org/10.1016/j.jenvrad.2011.01.005

Peterson, John, MacDonell, Margaret, Haroun, Lynne, & Monette, Fred. (2007). *Radiological and Chemical Fact Sheets to Support Health Risk Analyses for Contaminated Areas*. Chicago. Retrieved from https://www.remm.nlm.gov/ANL_ContaminantFactSheets_All_070418.pdf

Petit, D., Mennessier, J. P., & Lamberts, L. (1984). Stable lead isotopes in pond sediments as tracer of past and present atmospheric lead pollution in Belgium. *Atmospheric Environment (1967)*, *18*(6), 1189–1193. https://doi.org/10.1016/0004-6981(84)90150-1

Pettersson, H. B. L., & Koperski, J. (1991). Investigation of Aerial Dispersion of Radioactive Dust from an Open-pit Uranium Mine by Passive Vinyl Collectors. *Health Physics*, *60*(5), 681–690. Retrieved from http://journals.lww.com/health-physics/Abstract/1991/05000/Investigation_of_Aerial_Dispersion_of_Radioactive.7.aspx

Pillai, P. M. B., Paul, A. C., Komalan, Nair S., & Pillai, K. C. (1988). Distribution of pollutants in rain water in an industrial area. *Indian Journal of Environmental Health*, *30*(3), 253–261. Retrieved from http://www.refdoc.fr/Detailnotice?idarticle

Poet, S. E., Moore, H. E., & Martell, E. A. (1972). Lead 210, Bismuth 210 , and Polonium 210 in the Atmosphere: Accurate Ratio Measurement and Application to Aerosol Residence Time Determination. *Journal of Geophysical Research*, *77*(33), 6515–6527. https://doi.org/10.1029/JC077i033p06515

Porcelli, D., & Baskaran, M. (2011). An Overview of Isotope Geochemistry in Environmental Studies. In Mark Baskaran (Ed.), *Handbook of Environmental Isotope Geochemistry* (Volume 1, pp. 11–32). Berlin: Springer. https://doi.org/10.1007/978-3-642-10637-8

Preiss, Nicolas, Mélières, Marie-Antoinette, & Pourchet, Michel. (1996). A compilation of data on lead 210 concentration in surface air and fluxes at the air-surface and water-sediment interfaces. *Journal of Geophysical Research: Atmospheres*, *101*(D22), 28847–28862. https://doi.org/10.1029/96JD01836

Rama, Koide, Minoru, & Goldberg, Edward D. (1961). Lead-210 in Natural Waters. *Science*, *134*(3472), 98–99. https://doi.org/10.1126/science.134.3472.98

Robbins, John A., & Edgington, D. N. (1975). Determination of recent sedimentation rates in Lake Michigan using Pb-210 and Cs-137. *Geochimica et Cosmochimica Acta*, *39*(3), 285–304. https://doi.org/10.1016/0016-7037(75)90198-2

Rossmann, Ronald, & Barres, James. (1988). Trace Element Concentrations in Near-Surface Waters of the Great Lakes and Methods of Collection, Storage, and Analysis. *Journal of Great Lakes Research*, *14*(2), 188–204. https://doi.org/10.1016/S0380-1330(88)71548-8

RPB. (2011). *Canadian Guidelines for the Management of Naturally Occurring Radioactive Materials (NORM)*. Ottawa, ON. Retrieved from https://www.canada.ca/en/health-canada/services/environmental-workplace-health/reports-publications/environmental-contaminants/canadian-guidelines-management-naturally-occurring-radioactive-materials-norm-health-canada-2000.html

RPB. (2017). The Canadian Radiological Monitoring Network – Airborne Radioactivity. Ottawa, ON: Health Canada Radiation Protection Bureau. Retrieved from vhttp://open.canada.ca/data/en/dataset/21b821cf-0f1c-40ee-8925-eab12d357668

Rudnick, R. L., & Gao, S. (2014). Composition of the Continental Crust. *Treatise on Geochemistry*, *4*, 1–51. https://doi.org/10.1016/B978-0-08-095975-7.00301-6

Russel, Cynthia, & Orr, Patti. (2011). *Serpent River Watershed State of the Environment Report*. Georgetown, ON. Retrieved from https://www.denisonenvironmental.com/our-work/reports-and-presentations

Sanchez, F., & Rodriguez-Alvarez, M. J. (1999). Effect of pH, temperature, conductivity and sediment size on thorium and radium activities along Jucar River (Spain). *Journal of Radioanalytical and Nuclear Chemistry*, *242*(3), 671–681. https://doi.org/10.1007/BF02347378

Sauvé, Sébastien, McBride, Murray, & Hendershot, William. (1998). Lead Phosphate Solubility in Water and Soil Suspensions. *Environmental Science & Technology*, *32*(3), 388–393. https://doi.org/10.1021/ES970245K

Sethy, N. K., Sutar, A. K., Rath, P., Jha, V. N., Ravi, P. M., & Tripathi, R. M. (2015). A review of radio chemical analysis and estimation of 210Po in soil matrices. *Journal of Radiation Research and Applied Sciences*, *8*(4), 590–596. https://doi.org/10.1016/j.jrras.2015.07.001

Settle, D. M., Patterson, C. C., Turekian, K. K., & Cochran, J. K. (1982). Lead precipitation fluxes at tropical oceanic sites determined from 210 Pb measurements. *Journal of Geophysical Research*, *87*(C2), 1239. https://doi.org/10.1029/JC087iC02p01239

Skwarzec, Bogdan, & Tuszkowska, Agnieszka. (2008). Inflow of 210Po from the Odra River Catchment Area to the Baltic Sea. *Chemia Analityczna*, *53*(6), 809–820. Retrieved from http://beta.chem.uw.edu.pl/chemanal/PDFs/2008/CHAN2008V53P00809.pdf

Slob, Wout. (1994). Uncertainty Analysis in Multiplicative Models. *Risk Analysis*, *14*(4), 571–576. https://doi.org/10.1111/j.1539-6924.1994.tb00271.x

Southwood, Jeanette M., Harris, Reed C., & MacKay, Don. (1989). Modeling the fate of chemicals in an aquatic environment: The use of computer spreadsheet and graphics software. *Environmental Toxicology and Chemistry*, *8*(11), 987–996. https://doi.org/10.1002/etc.5620081104

Strachan, William, & Eisenreich, Steven. (1988). Mass Balancing of Toxic Chemicals

in the Great Lakes: The Role of Atmospheric Deposition. In *International Joint Commission (IJC) Digital Archive*. Scarborough, ON: International Joint Commission. Retrieved from http://scholar.uwindsor.ca/ijcarchive/374

Strachan, William M. J., & Eisenreich, Steven J. (1987). Mass balance accounting of PCBs and lead in the aquatic environment. In Peter Meyboom & E. Lawder (Eds.), *Oceans '87* (pp. 1765–1770). Halifax, NS: IEEE Ocean Engineering Society. Retrieved from http://ieeexplore.ieee.org/xpl/mostRecentIssue.jsp?punumber=5451199

Sztanyik, L. B., Csepregi, T., Holland, E., Kerekes, A., Kurcz-Csiky, I., Kurtacs, E., … Szabo, Z. (1984). *Activity concentrations of radionuclides in the Hungarian reach of the Danube River and their public health implications*. *IAEA-TECDOC-311*. Vienna. Retrieved from https://inis.iaea.org/search/search.aspx?orig_q=RN:16001849

Talbot, R. W., & Andren, A. W. (1983). Relationships between Pb and 210Pb in aerosol and precipitation at a Semiremote Site in northern Wisconsin. *Journal of Geophysical Research*, *88*(C11), 6752–6760. https://doi.org/10.1029/JC088iC11p06752

Talbot, R. W., & Andren, A. W. (1984). Seasonal variations of 210Pb and 210Po concentrations in an oligotrophic lake. *Geochimica et Cosmochimica Acta*, *48*(10), 2053–2063. https://doi.org/10.1016/0016-7037(84)90386-7

Tanaka, Noriyuki, Takeda, Yoichiro, & Tsunogai, Shizuo. (1983). Biological effect on removal of Th-234, Po-210 and Pb-210 from surface water in Funka Bay, Japan. *Geochimica et Cosmochimica Acta*, *47*(10), 1783–1790. https://doi.org/10.1016/0016-7037(83)90026-1

Theng, Tee Lee, & Mohamed, Che Abd. Rahim. (2005). Activities of 210Po and 210Pb in the water column at Kuala Selango , Malaysia. *Journal of Environmental Radioactivity*, *80*(3), 273–286. https://doi.org/10.1016/j.jenvrad.2004.10.004

Thomas, P. A. (2000). Radionuclides in the terrestrial ecosystem near a canadian uranium mill—part iii: atmospheric deposition rates (pilot test). *Health Physics*, *78*(6), 633–640. Retrieved from http://journals.lww.com/health-physics/Abstract/2000/06000/RADIONUCLIDES_IN_THE_TERRESTRIAL_ECOSYSTEM_NEAR_A.5.aspx

Thompson, Shirley, Mackay, Donald, & MacLeod, Matthew. (1999). A Modeling Strategy for Planning the Virtual Elimination of Persistent Toxic Chemicals from the Great Lakes: An Illustration of Four Contaminants in Lake Ontario. *Journal of Great Lakes Research*, *25*(4), 814–827. https://doi.org/http://dx.doi.org/10.1016/S0380-1330(99)70779-3

Thomsen, Volker, Mercuro, David, & Schatzlein, Debbie. (2003). Limits of Detection in Spectroscopy. *Spectroscopy*, *18*(12), 112–114. Retrieved from http://www.spectroscopyonline.com/node/243198

Toose, Liisa K., & Mackay, Donald. (2004). Adaptation of fugacity models to treat

speciating chemicals with constant species concentration ratios. *Environmental Science and Technology*, *38*(17), 4619–4626. https://doi.org/10.1021/es049957i

Turekian, K. K., & Graustein, W. C. (2014). Natural Radionuclides in the Atmosphere. In Karl Turekian & Heinrich Holland (Eds.), *Treatise on Geochemistry* (2nd ed., pp. 273–289). Elsevier. https://doi.org/10.1016/B978-0-08-095975-7.00410-1

Turekian, Karl K., Nozaki, Y., & Benninger, Larry Y. (1977). Geocehmistry of atmospheric radon and radon products. *Annual Review of Earth and Planetary Sciences*, *5*, 227–255. https://doi.org/10.1146/annurev.ea.05.050177.001303

UNSCEAR. (1988). *Sources, Effects and Risks of Ionizing Radiation*. *UNSCEAR 1988 Report*. New York. Retrieved from http://www.unscear.org/unscear/en/publications/1988.html

UNSCEAR. (1993). *Sources and Effects of Ionizing Radiation*. *United Nations Scientific Committee on the Effects of Atomic Radiation*. New York. Retrieved from http://www.unscear.org/unscear/en/publications/1993.html

UNSCEAR. (2000). *Sources and Effects of Ionizing Radiation, United Nations Scientific Committee on the Effects of Atomic Radiation UNSCEAR 2000 Report to the General Assembly, with Scientific Annexes*. *Sources; Annex A, B, C, D, E* (Vol. I). New York. Retrieved from http://www.unscear.org/docs/publications/2000/UNSCEAR_2000_Report_Vol.I.pdf

USGS. (2013). *Water-resources data for the United States,Water-Data Report WDR-US-2013, site 04165500, Clinton River at Mount Clemens, MI*. *Water-resources data for the United States*. Washington, DC. Retrieved from https://wdr.water.usgs.gov/wy2013/pdfs/04165500.2013.pdf

USNRC. (1980). *Final Generic Environmental Impact Statement on uranium milling*. *Appendices G-V*. Washington, DC. Retrieved from http://web.ead.anl.gov/mildos/documents/NUREG_0706_Vol3_ML032751669.pdf

Wang, K., & Cornett, R. J. (1993). Distribution coefficients of 210Pb and 210Po in laboratory and natural aquatic systems. *Journal of Paleolimnology*, *9*(2), 179–188. https://doi.org/10.1007/BF00677519

Wang, XueDong, & Elliott, Shane. (2011). *Typical Detection Limits for the aurora M90 ICP-MS in Normal Sensitivity Mode*. *Application Note # CA-270689*.

Watmough, Shaun A. (2017). Historical and contemporary metal budgets for a boreal shield lake. *Science of The Total Environment*, *598*, 49–57. https://doi.org/10.1016/J.SCITOTENV.2017.04.077

Wei, Ching Ling, & Murray, James W. (1994). The behavior of scavenged isotopes in marine anoxic environments: 210Pb and 210Po in the water column of the Black Sea. *Geochimica et Cosmochimica Acta*, *58*(7), 1795–1811.

https://doi.org/10.1016/0016-7037(94)90537-1

Wilhelm, Ronald G. (2004). *Understanding variation in partition coefficient Kd values: Review of Geochemistry and Available Kd Values for Americium, Arsenic, Curium, Iodine, Neptunium, Radium, and Technetium* (Vol. III). Washington, DC. Retrieved from https://nepis.epa.gov

Zhang, Weihua, Chen, Jing, Ungar, Kurt, & Cooke, Michael. (2015). Estimation of the Arctic aerosols from local and long-range transport using relationships between 210Pb and 212Pb atmospheric activity concentrations. *Journal of Environmental Radioactivity*, *141*, 123–129. https://doi.org/10.1016/j.jenvrad.2014.12.008

Zhu, Xiaolei, Shan, Baoqing, Tang, Wenzhong, Li, Shanshan, & Rong, Nan. (2016). Distributions, fluxes, and toxicities of heavy metals in sediment pore water from tributaries of the Ziya River system, northern China. *Environmental Science and Pollution Research*, *23*(6), 5516–5526. https://doi.org/10.1007/s11356-015-5709-7